Towards Development of Spherical Geographic Automata Modelling Approaches for Global Land-Use/Land-Cover Change

by

Bright Addae

M.Sc., Christian-Albrechts-Universität zu Kiel, 2018

B.A., University of Ghana, 2014

Thesis Submitted in Partial Fulfillment of the

Requirements for the Degree of

Doctor Philosophy

in the

Department of Geography

Faculty of Environment

© Bright Addae 2024

SIMON FRASER UNIVERSITY

Spring 2024

Declaration of Committee

Name:	**Bright Addae**
Degree:	**Doctor of Philosophy**
Title:	**Towards Development of Spherical Geographic Automata Modelling Approaches for Global Land-Use/Land-Cover Change**

Examining Committee: **Chair: Eugene McCann**
Professor, Geography

Suzana Dragicevic
Supervisor
Professor

Kirsten Zickfeld
Committee Member
Professor, Geography

Peter Hall
Committee Member
Professor, Urban Studies

Bing Lu
Examiner
Assistant Professor, Geography

Eric Vaz
External Examiner
Professor, Geography and Environmental Studies
Toronto Metropolitan University

Abstract

Approaches of geographic automata grounded in the theories of complex spatial systems and geographic information science (GISc) have been utilized in many geospatial applications to analyze and simulate spatio-temporal processes including land-use/land-cover (LULC) change. Given the increasing interactions in human-environment systems and their significant impact on global sustainability issues, there is a need for new modelling methodologies for characterizing LULC change processes at the global level. However, current geosimulation modelling approaches are based on conventional geospatial data and two-dimensional planar representations which omit effects of the curvature of the Earth's surface. Such models when applied to LULC change can result in spatial and computational errors emanating from distortions. Therefore, the primary objective of this dissertation is to develop a suite of novel spherical geographic automata modelling approaches for simulating complex spatial systems at the global level and considering the curved surface of the Earth. The dissertation integrates spherical geodesic grids, geosimulation modelling approaches, theories of GISc, and complex systems to leverage the capabilities of these fields for better representation of different land systems at the global level. The proposed methodology is implemented to simulate LULC change as a complex spatial dynamic system operating on a sphere. Results from the models' implementations indicate the methodology offers a realistic and consistent framework for representing, simulating, analysing, and visualizing LULC change, particularly urbanization and deforestation, on a spherical surface. Moreover, the presentation of modelling results in the context of LULC change processes contribute to the enhancement of decision-making processes at the global level by providing tools that can be utilized for forecasting, scenario testing and policy formulation. This dissertation contributes new methodological frameworks to the fields of geographic information science, specifically geographic automata modelling, and land use science.

Keywords: geographic information science; geographic information systems; complex systems models; spherical geographic automata models; discrete global grid system; global land-use/land-cover (LULC) change; global urbanization; global deforestation

This is thesis is dedicated to my family for their support and encouragement.

Acknowledgements

I would like to express my deepest gratitude to those who have supported me throughout the journey of my doctoral studies and the completion of this dissertation. First and foremost, I am immensely thankful to my primary advisor and supervisor, Professor Suzana Dragićević, whose guidance, patience, and unwavering support have been pivotal to my academic growth and professional development. I am also grateful to my supervisory committee members, Prof. Kirsten Zickfeld and Prof. Peter Hall, whose insightful comments and constructive feedback inspired and enriched my research.

I extend my appreciation to the Natural Sciences and Engineering Research Council (NSERC) of Canada Discovery Grant awarded to Dr. Suzana Dragicevic which supported my research activities and enabled me to attend important conferences and workshops that significantly contributed to this research and my professional development. In addition, I am very grateful to Simon Fraser University and the Department of Geography for providing me with the opportunity to obtain several scholarships including the Graduate Deans Entrance Scholarship (GDES), the Micheal Geller Graduate Scholarship in Urban Development, Graduate Fellowships (GF), and Travel and Minor Research Awards (TMRA).

I am also indebted to my lab colleagues at the spatial analysis and modeling (SAM) Laboratory as well as other colleagues within and outside of the Department of Geography for their camaraderie, stimulating discussions, and for the countless times they lent me a helping hand. The collaborative and encouraging environment among lab members has been instrumental in the success of my research. I must also acknowledge the broader Geography community at SFU, and the valuable insights and support I received from fellow researchers, faculty members, and administrative staff.

Lastly, I would like to express my heartfelt gratitude to my family and friends, who have been my greatest source of strength and support. Their love, patience, and understanding have sustained me through the ups and downs of this challenging journey. This dissertation stands as a testament to the collective effort and support of all those mentioned above, and to many others who have contributed directly or indirectly to my academic journey. I am profoundly grateful for all the support I have received and for the opportunities that have been afforded to me.

Table of Contents

List of Tables

List of Figures

Chapter 1.

Introduction

Changes to the Earth's land surface through anthropogenic activities have significant implications for the structure and functioning of the Earth's systems as well as several consequences for human well-being (Turner et al., 2007). Although the Earth's land surface has been modified through human and natural environment interactions for centuries, the rate and extent of change in recent decades has intensified leading to unprecedented changes in ecosystems and environmental processes at the local, regional, and global scales (Ellis, 2011). Indeed, the cumulative effects of human activities on the Earth's systems have led some scientists and scholars to propose and define a new geological epoch, termed, the "Anthropocene" (Crutzen, 2002; Zalasiewicz et al., 2011). Over the last six decades, almost a third (32%) of the global land surface has been affected by anthropogenic activities such as urbanization, deforestation, agriculture intensification, and desertification (Winkler et al., 2021). The rate of change in the Earth's surface is expected to continue in the coming decades and land-based activities are likely to expand and further intensify in response to increasing demands for food, shelter, energy, raw materials, etc. (Hurtt et al., 2020).

The modification of the terrestrial Earth's surface through anthropogenic activities is termed land-use/land-cover (LULC) change (Lambin et al., 2006). LULC changes may result from either the conversion of one land-cover type to another or modification of its structure or function. Transformation of the Earth's surface affects soil properties, water, biota, and the atmosphere, which can ultimately result in reduced land productivity, biodiversity loss, altered biogeochemical cycles, and climate variability and change (Ellis, 2021; Foley et al., 2005). Although the term land-use and land-cover are often used interchangeably in the Land use science (LUS) literature, they mean different things. Land-cover is defined as the physical, or biophysical characteristics of the Earth's surface. The term is often used to describe vegetation and man-made features such as impervious surfaces, agricultural areas, forest, wetlands, water bodies, etc. Land-use is related to the functional or socio-economic purpose associated with the land. Land-use is characterized by the arrangements, activities and inputs people undertake on a certain land-cover type to produce, change, or maintain it (Jansen & Gregorio, 2002). This

includes uses such as residential, agriculture, forestry, recreational, among others. Land-use and land-cover are inherently coupled because changes in land-use practices can change land-cover and land cover determines specific land uses (Sleeter et al., 2018).

Research and studies on LULC change and its modelling has increased over the last decades due to the heightened awareness of the impact of land systems on environmental change and sustainability (Rounsevell et al., 2012). Land-use science has thus emerged as a primary component of global environmental change and sustainability research, giving rise to advanced Earth observation data collection, integrated research, and improved modelling approaches (Chang et al., 2018; Li et al., 2023; Turner et al., 2007). LULC change modelling entails methodological approaches used for examining the spatial and temporal dynamics of LULC change in order to better understand the functioning of the land system and to support land-use planning and policy (Verburg et al., 2004). LULC change models are analytical and decision-making tools used for analyzing, forecasting, and simulating past, present, and possible future LULC change conditions at different spatial scales (National Research Council, 2014). Models are useful for understanding the complex relationships between the socio-economic and biophysical drivers that influence the rate and spatial pattern of LULC change as well as assessing the consequences of changes in land-use and land-cover. LULC change models also enable the exploration of different potential future land system dynamics and alternative trajectories via "what-if" scenarios, assisting stakeholders anticipate and plan for changes in LULC patterns due to demographic shifts, technological advancements, institutional arrangements, and environmental conditions. LULC change models can likewise be applied by stakeholders as decision support systems to make informed policy and management decisions related to different environmental systems (Ellis, 2011). Given the implications of LULC change for climate and environmental change at the local and global scales, decisions and policies related to land systems can serve as strategies for mitigating and adapting to these changes and to reaching a more sustainable world (National Research Council, 2014). These models are particularly useful for exploring conditions that presently do not exist and thus cannot be observed by conducting experiments that test our understanding of key processes (Filatova et al., 2016).

1.1. Modelling Global Land-use/Land-cover Change

Global land-use change models have gained significance over the last decades for a variety of reasons. Addressing the numerous environmental and sustainability challenges requires a global perspective and approach. However, implementing such models require higher computational power to process larger spatial extent with large volumes of data. Earth and other environmental systems function at the global scale and land systems are increasingly impacted by drivers operating at these scales (Brenner & Schmid, 2012; Verburg et al., 2015). The emergence of global environmental and climate change issues over the last decades has also necessitated the need for decision-making and policy actions across multiple geographic scales and ecological dimensions (Foley et al., 2005). With regards to this, global LULC change models provide a useful toolkit for simulating scenarios, performing environmental assessments, and providing spatial information to assist the science, policy, and decision-support communities (Ren et al., 2019; Stehfest et al., 2019).

The key drivers of LULC change are related to demographic changes due to population increase and migration, but also include forces of globalization, international politics, and development of technology operate at large spatial scales of influence (Meyfroidt et al., 2018). Global and local forces operate concurrently and interactively to shape LULC change across the globe (Taylor & Rising, 2021). Substantial feedback also exists between land systems at different scales. Addressing the feedback between land and other biophysical and socioeconomic systems and the forces that influence LULC change requires a globally consistent framework.

Land-use/land-cover change has also become a central theme in several global policy organizations and intergovernmental bodies. Global LULC change models are valuable tools for scenario building and provide insightful information for the assessment of the processes and impacts of global environmental change. This is typified by the special reports of the Intergovernmental Panel on Climate Change (IPCC) on Climate Change and Land Use (IPCC, 2019) as well as the Land Degradation and Restoration Thematic Assessment report from the Intergovernmental Science–Policy Platform on Biodiversity and Ecosystem Services (IPBES, 2019). Also, land systems play an important role in several of the United Nations (UN) sustainable development goals (SDGs) such as No poverty (goal 1), Affordable and clean energy (goal 7), Sustainable

cities and communities (goal 11), Climate action (goal 13), and Life on land (goal 15) are directly and indirectly related to land systems (Munroe & Müller, 2020; Stehfest et al., 2019).

Earth systems models (ESM) and integrated assessment models (IAM) often require datasets on LULC change as key input to accurately simulate Earth system dynamics and examine the combined effects of human activities on the climate system. For instance, the Land Use Model Intercomparison Project (LUMIP) was recently initiated as part of the Coupled Model Intercomparison Project phase 6 (CMIP6) (Eyring et al., 2016). LUMIP aims to advance understanding of the impacts of LULC change on climate through the development of historical and future LULC datasets (Lawrence et al., 2016). Land use change datasets have also been applied to analyze land-use and land-cover feedback to the climate system and sources and sinks of carbon.

1.2. Overview of Land-use/Land-cover Change Modelling Approaches

The process of LULC change is generally influenced by interactions between biophysical factors, human factors and institutional policies which operate across different space and time (Veldkamp et al., 2001). Land systems consist of various interrelated and interacting components encompassing biological, ecological, social, and economic elements. As such, land systems are conceptualized as complex systems under the framework of complex systems theory (Parker et al., 2003). Land systems are often characterized by multiple non-linear relationships, social and biophysical heterogeneity, feedback, interactions at the local level, and natural and human adaptation (Liu et al., 2007). These characteristics limit the capability of traditional statistical and system dynamic modelling approaches to effectively examine complex system outcomes in land systems (Rindfuss et al., 2008). The complexity of land systems results in variations in LULC change outcomes based on geographic location, ecosystem types, and socio-economic structures.

Geographic automata or geosimulation models developed under the complexity science and GISc methodological frameworks have thus become common approaches for modelling LULC change processes (Torrens & Benenson, 2005). Geosimulation models are based on cellular automata (CA) and agent-based modelling (ABM) methods

4

that adopt a bottom-up approach which allows them to capture non-linear interactions between system elements at the local level while generating emergent spatial patterns at much larger scales (Batty & Xie, 1994; White & Engelen, 2000). Geographic automata models explicitly use geographic data and are flexible with efficient framework that enable the construction of detailed, complex, and dynamic models which are well suited for handling geographic processes (Torrens & Benenson, 2005). Geographic automata are characterized by their ability to also incorporate the spatial and temporal components of complex systems. These modelling approaches are coupled with geographic information systems (GIS) to develop spatially explicit LULC change models and have been utilized for decades to simulate several real-world complex spatial systems including urban development (Falah et al., 2020; Feng & Tong, 2020), LULC change (Feng & Qi, 2018; Jahanishakib et al., 2018; Lu et al., 2019), deforestation (Hasan et al., 2020; Ménard & Marceau, 2007), and agriculture expansion (Hou et al., 2019; Navarro Cerrillo et al., 2020) mainly at the local and regional levels.

To address the need for global LULC change models and applications, a number of spatially explicit modelling methods and approaches have been adopted to simulate LULC change at the global level. These include cellular automata (CA) (Li et al., 2016), SLEUTH (Zhou et al., 2019), Future Land Use Simulation (FLUS) (G. Chen et al., 2020), and DEMETER (M. Chen et al., 2020). Hybrid modelling approaches which combine geographic automata with other techniques such as statistical and machine learning (ML) have also been implemented (Cao et al., 2021; Li et al., 2021).

Advancements in artificial intelligence (AI) particularly machine learning (ML) and deep learning (DL) techniques, have provided a new avenue for enhancing the accuracy and complexity of LULC change models. As a result, DL techniques have been integrated with larger and historical datasets to enhance simulation models, albeit with a focus primarily on applications at local scales and for smaller spatial extents (Xiao et al., 2022). Deep learning techniques, including convolutional neural networks (CNN), long short-term memory (LSTM), recurrent neural networks (RNN), and deep neural networks (DNN) have demonstrated proficiency in capturing spatial and temporal dependencies within geospatial data (Xing et al., 2020). This capability makes them well-suited for extracting meaningful features from diverse multi-source and historical spatial datasets. These techniques provide the capacity to automatically learn complex patterns and relationships, which can be used to inform the transition rules governing geosimulation

models (Wang et al., 2022). Typically, the DL component of the LULC change model is implemented to acquire transition probabilities for the rules of the geosimulation model. Given the abilities of ML and DL techniques to learn from data and identify patterns, their integration with geosimulation methods can lead to the development of data-driven complex spatial system models that better represent LULC change dynamics (Ye et al., 2019).

1.3. Challenges of Global Land-use/Land-cover Change Modelling

Modelling LULC change at the global level presents several challenges. While some of these issues are general to all LULC change models irrespective of scale, others are peculiar to global LUL change modelling. LULC change processes and the drivers that influence them are spatially heterogeneous across the globe. When modelling at the global level, it is imperative to represent the variability in driving factors and their spatial characteristics which can be challenging from a methodological perspective (Meiyappan et al., 2014). Also, the different factors that influence LULC change operate at different spatial scales and global-scale LULC change modelling approaches must appropriately incorporate these multi-scale dynamics and representations (Verburg et al., 2019). Further, there is lack of consistent spatial datasets with global coverage to represent LULC and the different spatial drivers of LULC change at finer resolution (Jokar Arsanjani et al., 2016; Li et al., 2022).

A major challenge of building LULC change models to operate on a global scale is the lack of appropriate spatial reference systems that span the entirety of the Earth (Lin et al., 2018). The problem of representing the three-dimensional (3D) Earth's surface on a flat plane has been a persistent challenge in the field of geographic information science (GIScience) (Goodchild, 2018). Despite the fact that the Earth is spherical, the software and technologies within GIScience continue to be based on two-dimensional planar maps, exemplified by the use of Cartesian coordinates (Chrisman, 2017). Traditional geospatial models which employ two-dimensional (2D) representation of the Earth produce varying forms of spatial distortions. Although these distortions are negligible at the local scale, they can result in spatial and computational inaccuracies in large scale applications (Hall et al., 2020). This is primarily due to the transformation of the curved Earth's surface onto a planar medium, rendering traditional models

unsuitable for spatial analysis and simulation applications with global coverage (Li et al., 2020).

The use of geographic coordinate system (GCS) for global spatial analysis and representation of datasets results in unequal grid cell area due to convergence of the meridians and coordinate singularity (Kelly & Šavrič, 2021). Consequently, square cells at the equator gradually diminish in size as they progress towards the poles, eventually transforming into triangles due to the Earth's curvature. In light of this issue, global LULC change models and applications commonly specify the spatial resolution using the cell dimensions at the equator (Chen et al., 2022; Li et al., 2021; Zhou et al., 2019). Although certain cartographic equal-area projections provide a better spatial representation of geographic features at the global level, they still exhibit area and shape distortions across the globe (de Sousa et al., 2019). Moreover, many of these equal-area projections are region-specific and often yield substantial areal distortions in higher latitude regions, and thus unsuitable for global applications (Nowak & Nowak Da Costa, 2022).

Global geosimulation modelling approaches are predominantly based on traditional planar spatial models, use of raster GIS data formats, thus are deemed inappropriate for simulations at the global level. This problem has been recognized in the land use science literature, with recommendations to adopt spherical geospatial models for implementing global LULC models (Cao et al., 2019; Li et al., 2017).

1.4. Spherical Geodesic Grids

Spherical geodesic grids, known in GIScience as discrete global grid systems (DGGS) are spatial reference systems that utilize a spherical surface to account for the Earth's curvature (Goodchild, 2018). The spherical grid framework is composed of equal-area cells which are used to partition the Earth's surface and are structured at multiple resolutions to create a spatial hierarchy of cells (Béjar et al., 2023). DGGS provides a discrete approach to spatial referencing, utilizing cells as the primary spatial units to partition the Earth's surface. The resolution of the DGGS is pre-determined and is defined by the subdivision of cells (Thompson et al., 2022). A DGGS is comprised of four essential components: base polyhedron, cell type, method for hierarchical partitioning or refinement and cell indexing (Barnes, 2020).

1.4.1. Base Polyhedron

Due to the Earth's approximately spherical shape and curvature, projecting its surface onto a planar space inevitably introduces distortions. In the context of a grid-based spatial referencing system for the Earth, achieving equal-area cell coverage is a desirable property. To maintain as much as possible the area and shape properties of geographic features on a global scale, a spherical approximation of the Earth can be modelled using a Platonic solid (Bondaruk et al., 2020). There are only five Platonic solids or polyhedrons that are defined on three- dimensional geometric solids constructed with a single type of regular cell (Lei et al., 2020). Polyhedrons with smaller faces reduce the distortion introduced when transforming between a face of the Platonic solid and the corresponding spherical surface (White et al., 1998). The five polyhedrons used for implementing DGGS are tetrahedrons, cubes, octahedrons, dodecahedrons, and icosahedrons and are presented in Figure 1.1.
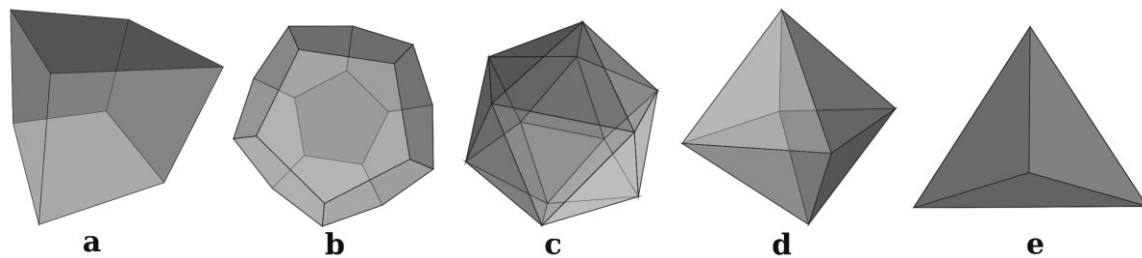
Figure 1.1.   **Five base polyhedrons for implementing DGGS: (a) cube; (b) dodecahedron; (c) icosahedron; (d) octahedron; (e) tetrahedron.**

1.4.2. Cell Types

The fundamental component of any DGGS is its cell structure that are used to cover the spherical surface of the Earth (Mahdavi-Amiri et al., 2015). Typically, three cell topologies are employed, squares, triangles, and hexagons (Figure 1.2). Each of these cell types have their own benefits and disadvantages and the choice of an appropriate type depends on the application. Essentially, squares are familiar, triangles are efficient for processing, and hexagons are the best fit.

Squares are very desirable due to their extensive applicability in remote sensing (RS) and raster GIS as well as compatibility with current hardware devices and software (Mahdavi-Amiri et al., 2015). However, their topology is not directly compatible with many Platonic solids. The neighbourhood relationship between square cells is also

complex as a square has four edge neighbouring cells and eight vertex neighbouring cells. Triangular shapes are a natural fit for the hierarchical partitioning of the Platonic solids (Wang et al., 2020). Triangles can also be efficiently rendered and are supported by numerous built-in graphic lattice functions (Peterson, 2017). However, the adjacency relationship for triangles is also complicated. A single triangle has 12 neighbours, with 3 of them having an edge neighbour and 9 of them containing a vertex connection (Sahr et al., 2003). Triangular tessellations are also composed of cells with different orientations.
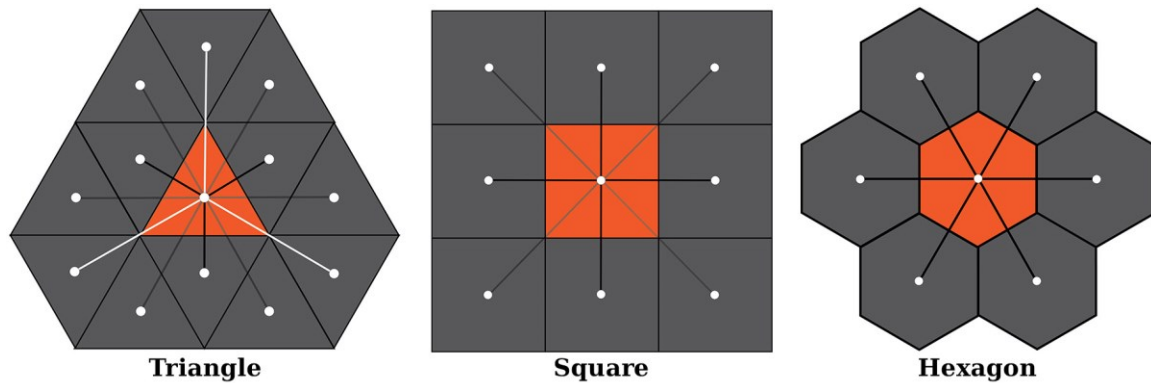
Figure 1.2.   Geometric properties and neighbourhood relationships for triangle, square, and hexagon.

Hexagonal cells have garnered significant attention in the scientific literature due to their numerous advantages. Among the three regular cells, hexagons are the most compact as they quantize the sphere with the smallest average error (Zhou et al., 2022). Hexagonal lattices also exhibit uniform and unambiguous geometric connectivity, where each cell has six neighbours with shared edges, and their centers are equidistant from one another; properties desirable for spatial analysis in GIS (Sahr et al., 2003). Furthermore, research indicate that hexagons have the highest sampling efficiency and angular resolution (Peterson, 2017). In addition to these advantages, hexagons are more effective for cartographic data visualization than square cells (Mechenich & Žliobaitė, 2023). Given the advantages and characteristics of hexagons as regular polygons, they are typically preferred for tessellating the spherical surface and are subsequently utilized throughout this dissertation research. In terms of disadvantages, hexagons are non-congruent and larger hexagonal cells cannot be evenly decomposed into smaller cells completely contained within the larger one (Robertson et al., 2020).

1.4.3. Refinement/Aperture

The multiresolution characteristic of a DGGS is achieved through refinement of cells from a coarse resolution to a finer resolution (Wang et al., 2020). Refinement methods are techniques that produce a set of fine resolution cells from a set of coarse cells in a uniform and systematic manner by reducing cell sizes (Ulmer et al., 2020). The ratio of the areas of cells at two successive resolutions is termed aperture. In the case of square cells, commonly employed refinements include one-to-four and one-to-nine, corresponding to apertures of 4 and 9, respectively. For triangle cells, one-to-four refinement is the most suitable. Hexagonal grids commonly utilize one-to-three, one-to-four and one-to-seven refinements, denoted as aperture 3, 4 and 7 respectively (Sahr, 2013). These three hexagonal refinement types are presented in Figure 1.3.
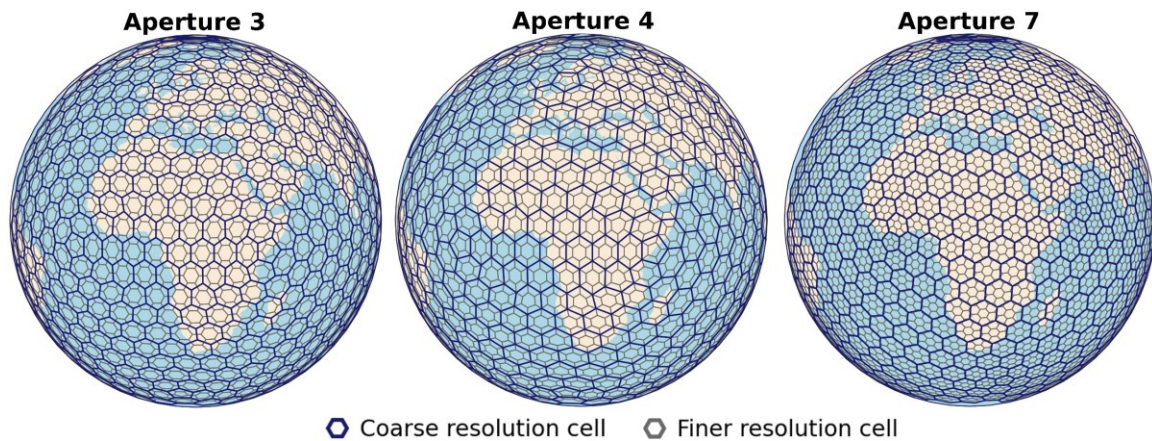
Figure 1.3.   Hexagonal hierarchical partitioning methods based on aperture 3, aperture 4, and aperture 7.

1.4.4. Cell Indexing

Within a DGGS, each cell is assigned a unique index or identifier to represent its location, and indexing of cells are usually performed through arithmetic techniques (Sahr, 2008). The cell's index may also denote a data structure or database utilized for retrieving associated data. The location index or code serve as an address for identifying and querying cells within the DGGS (Purss et al., 2019). Generally, there are three types of indexing techniques: hierarchy-based indexing, axis-based indexing (coordinate-based indexing) and space filling curve indexing (Alderson et al., 2020). Hierarchical indexing utilizes the hierarchical relationships between cells through the application of refinement starting from the base cell. Each cell is assigned an index at the initial

resolution, with subsequent indices of its children incorporating the parent cell's index as a prefix (Zhou et al., 2020). This indexing technique facilitates efficient spatial indexing and enables scalable representations of geographic features at different levels of detail.

Axis or coordinate based indexing in DGGS implementation is similar to Cartesian coordinate and the location of cells are specified as an offset along a set of axes (Sahr, 2019). This technique is valuable for its simplicity and ease of implementation. Coordinate based indexing is particularly useful when a uniform distribution of cells is desired, and it can be applied to both regular and irregular grids (Vince, 2006). For space-filling curves, a curve is passed over the domain of the cells, and the cells are indexed in the order that the curve intersects them (Alderson et al., 2020). Often, the curve can be refined to index more fine resolutions of the cells. The advantage of these method is that the curve can be defined to give neighbouring cells similar indices, allowing for efficient neighbourhood queries (Hall et al., 2020).

Despite the theoretical advantages of spherical geodesic grids for conducting spatial analysis and simulations at the global scale, their use and integration with other GIScience approaches and techniques remains limited (Hojati et al., 2022). In the context of complex systems modelling, spherical geographic grids and geographic automata can be integrated to create a novel theoretical framework that capitalizes on the capabilities of geographic automata modelling approaches in capturing the local interactions and spatial dynamics inherent in complex spatial systems and geodesic grids for accurate representation of spherical surfaces. The resulting model can provide a coherent modelling framework for simulating complex spatial processes at the global level. Essentially, this approach circumvents problems associated with spatial distortions emanating from the use of traditional spatial models. The discrete spatial tessellations of spherical geodesic grids and data integration characteristics provide a robust foundation for implementing geographic automata modelling approaches including cellular automata and agent-based models. Additionally, the multi-resolution grid structure of spherical geodesic grids offers a consistent framework for representing spatial data and complex spatial systems at different scales within the same modelling environment. Such an integrative modelling approach facilitates the simulation, analysis, and visualization of complex spatial systems on a spherical surface.

1.5. Research Questions and Objectives

The primary goal of this dissertation research is to integrate and leverage the potentials of geographic automata and spherical geodesic grids to effectively model, at the global scale, LULC change as a complex dynamic spatial system. This integration would enable the representation, analysis, and visualization of complex dynamic systems at the global level. The dissertation research aims to provide a comprehensive theoretical framework and practical implementations that aids in improved modeling of the dynamics of different global LULC change processes and analysis of the emerging spatial patterns on the spherical Erath's surface. Specifically, this dissertation endeavours to answer the following research questions:

1. What is the theoretical framework that enables geosimulation models to operate on the spherical Earth's surface?

2. How can spherical geosimulation models be implemented with real world spatial data to represent global LULC change?

3. How can spherical geosimulation models be improved to represent different global LULC change processes?

To address the aforementioned research questions, this dissertation research develops and implements a suite of novel geosimulation modelling approaches by integrating the framework of geographic automata and spherical geodesic grid. This novel approach is specifically designed for the purpose of characterizing and simulating a variety of complex spatial systems at the global level. The main objectives of the dissertation can be summarized as follows:

1. Develop a novel spherical geographic automata (SGA) theoretical modelling framework to represent complex spatial systems at the global scale;

2. Implement the SGA theoretical framework to model urbanization process at the global level;

3. Improve the SGA modelling approach to incorporate multicriteria evaluation (MCE) method, and apply to two case studies of global urbanization and deforestation under different scenarios;

4. Integrate deep learning (DL) method into the SGA modelling approach for simulating multiple LULC change processes and considering the shared socioeconomic pathway (SSP) scenarios.

1.6. Dissertation Overview

The dissertation is organized into seven chapters, with the first five chapters following the Introduction aimed at addressing the objectives of this dissertation. Specifically, chapter 2 lays the groundwork for the dissertation by providing a comprehensive overview of spherical geodesic grids and establishing the conceptual foundation for their development. A comparison of data representation in spherical geodesic grids and traditional spatial reference systems is also presented. Furthermore, this chapter introduces and conceptualizes the novel modelling approach, spherical geographic automata (SGA), which is developed for simulating diverse complex spatial systems at the global scale. The model is applied as a proof-of-concept to characterize different complex systems including population change dynamics using the Game of Life (GoL) theoretical framework, global urbanization to represent expansion process and deforestation to exemplify a shrinking phenomenon.

Chapter 3 presents a model case study that demonstrates the implementation of the SGA model for a detailed characterization of a real-world complex spatial system, represented by global urbanization process. The SGA model is utilized to simulate urban expansion at the global level and for 235 different countries. Transition rules are implemented to characterize urban growth across different regions in order to account for the spatial heterogeneity of the spatial process. Moreover, various scenarios are designed to represent different possible future global urban expansion trajectories.

In the subsequent two chapters, the dissertation focuses on the integration of the multi-criteria evaluation (MCE) technique as a spatial decision support system to facilitate a systematic approach to decision-making and incorporate the complexity and multiplicity inherent in land-use planning. The enhanced SGA model is implemented to simulate global urbanization and deforestation in different case studies. The proposed MCE-SGA modelling approach is implemented with several spatial drivers and designs diverse "what-if" scenarios to characterize change processes under different possible future conditions. Given the global scope of the model applications and limited resources in this research, soliciting stakeholder opinions to determine MCE parameters was not feasible. Consequently, a statistical technique was employed to derive these parameters. In Chapter 4, the MCE-SGA model is developed to simulate urbanization process at the global level at a high spatial resolution. Additionally, a clustering algorithm

is integrated into the modelling framework to classify spatial regions with similar characteristics, thereby enhancing the model's ability to capture and simulate urban land-use change. Chapter 5 of the dissertation presents the MCE-SGA model to represent and simulate deforestation under three scenarios. The implemented scenarios demonstrate the usefulness of the proposed model in characterizing LULC change under different possible conservation policies at the global level.

Considering the previous versions and implementations of the proposed modelling approaches only simulate one LULC type at a time, there is the need to further extend the model to be capable of simulating multiple LULC change types at the global level. Chapter 6 thus focuses on improving different components of the model to better represent the dynamics of LULC change at the global level. The SGA modelling framework is extended to simulate multiple LULC change as well as the incorporation of a deep learning (DL) component to leverage the capabilities of DL techniques in learning patterns from the data and assisting in deriving transition rules for simulating LULC change. The proposed model is implemented to simulate multiple LULC change processes and considering the five shared socioeconomic pathways (SSP) scenarios at the global level between 2020 and 2100.

All models in this research study were coded using the Python programming language (Van Rossum & Drake, 2009), and utilizing several open-sourced libraries including Geopandas, Shapely, Geoplot, Matplotlib, Uber H3, DGGRID, and PyTorch. The large-scale global models were executed on a Digital Research Alliance of Canada computing facility for increased computational power. Maps of simulation results were generated in Python as well as ArcGIS software to facilitate visualization.

This dissertation concludes with Chapter 7 by providing overall summary of obtained results, then outlines the general limitations and advantages of the research, discusses possible future research avenues, and insight of general contributions of the thesis findings to the relevant scientific fields.

1.7. References

Alderson, T., Purss, M., Du, X., Mahdavi-Amiri, A., & Samavati, F. (2020). Digital Earth platforms. In *Manual of digital Earth*, (Eds.) H. Guo, M. F. Goodchild, & A. Annoni,(pp. 25-54). Singapore: Springer Singapore.

Barnes, R. (2020). Optimal orientations of discrete global grids and the Poles of Inaccessibility. *International Journal of Digital Earth, 13*, 803-816. doi:10.1080/17538947.2019.1576786

Batty, M., & Xie, Y. (1994). From cells to cities. *Environment & Planning B: Planning & Design, 21*, 531-548. doi:10.1068/b21s031

Béjar, R., Lacasta, J., Lopez-Pellicer, F. J., & Nogueras-Iso, J. (2023). Discrete global grid systems with quadrangular cells as reference frameworks for the current generation of Earth observation data cubes. *Environmental Modelling & Software, 162*, 105656. doi:10.1016/j.envsoft.2023.105656

Bondaruk, B., Roberts, S. A., & Robertson, C. (2020). Assessing the state of the art in discrete global grid systems: OGC criteria and present functionality. *Geomatica, 30*, 1-22. doi:10.1139/geomat-2019-0015

Brenner, N., & Schmid, C. (2012). Planetary urbanization. In *Urban Constellations*, (Eds.) M. Gandy,(pp. 10-13). Berlin: Jovis.

Cao, B., Yu, L., Li, X., Chen, M., Li, X., Hao, P., & Gong, P. (2021). A 1km global cropland dataset from 10000 BCE to 2100 CE. *Earth Syst. Sci. Data, 13*(11), 5403-5421. doi:10.5194/essd-13-5403-2021

Cao, M., Zhu, Y., Quan, J., Zhou, S., Lü, G., Chen, M., & Huang, M. (2019). Spatial sequential modeling and prediction of global land use and land cover changes by integrating a global change assessment model and cellular automata. *Earth's Future, 7*, 1102-1116. doi:10.1029/2019EF001228

Chang, Y., Hou, K., Li, X., Zhang, Y., & Chen, P. (2018). Review of land use and land cover change research progress. *IOP Conference Series: Earth and Environmental Science, 113*(1), 012087. doi:10.1088/1755-1315/113/1/012087

Chen, G., Li, X., & Liu, X. (2022). Global land projection based on plant functional types with a 1-km resolution under socio-climatic scenarios. *Scientific Data, 9*, 1-18. doi:10.1038/s41597-022-01208-6

Chen, G., Li, X., Liu, X., Chen, Y., Liang, X., Leng, J., Xu, X., Liao, W., Qiu, Y. a., Wu, Q., & Huang, K. (2020). Global projections of future urban land expansion under shared socioeconomic pathways. *Nature Communications, 11*, 537. doi:10.1038/s41467-020-14386-x

Chen, M., Vernon, C. R., Graham, N. T., Hejazi, M., Huang, M., Cheng, Y., & Calvin, K. (2020). Global land use for 2015–2100 at 0.05° resolution under diverse socioeconomic and climate scenarios. *Scientific Data, 7*(1), 320. doi:10.1038/s41597-020-00669-x

Chrisman, N. R. (2017). Calculating on a round planet. *International Journal of Geographical Information Science, 31*(4), 637-657. doi:10.1080/13658816.2016.1215466

Crutzen, P. J. (2002). Geology of mankind. *Nature, 415*(6867), 23-23. doi:10.1038/415023a

de Sousa, L. M., Poggio, L., & Kempen, B. (2019). Comparison of FOSS4G supported equal-area projections ssing discrete distortion indicatrices. *ISPRS International Journal of Geo-Information, 8*(8), 1-13. doi:10.3390/ijgi8080351

Ellis, E. (2011). Land-use and land-cover change. *Encyclopedia of earth*(1), 1-4.

Ellis, E. (2021). Land use and ecological change: a 12,000-year history. *Annual Review of Environment and Resources, 46*(1), 1-33. doi:10.1146/annurev-environ-012220-010822

Eyring, V., Bony, S., Meehl, G. A., Senior, C. A., Stevens, B., Stouffer, R. J., & Taylor, K. E. (2016). Overview of the coupled model intercomparison project phase 6 (CMIP6) experimental design and organization. *Geosci. Model Dev., 9*(5), 1937-1958. doi:10.5194/gmd-9-1937-2016

Falah, N., Karimi, A., & Harandi, A. T. (2020). Urban growth modeling using cellular automata model and AHP (case study: Qazvin city). *Modeling Earth Systems and Environment, 6*(1), 235-248. doi:10.1007/s40808-019-00674-z

Feng, Y., & Qi, Y. (2018). Modeling patterns of land use in Chinese cities using an integrated cellular automata model. *ISPRS International Journal of Geo-Information, 7*(10). doi:10.3390/ijgi7100403

Feng, Y., & Tong, X. (2020). A new cellular automata framework of urban growth modeling by incorporating statistical and heuristic methods. *International Journal of Geographical Information Science, 34*(1), 74-97. doi:10.1080/13658816.2019.1648813

Filatova, T., Polhill, J. G., & van Ewijk, S. (2016). Regime shifts in coupled socio-environmental systems: review of modelling challenges and approaches. *Environmental Modelling & Software, 75*, 333-347. doi:10.1016/j.envsoft.2015.04.003

Foley, J. A., DeFries, R., Asner, G. P., Barford, C., Bonan, G., Carpenter, S. R., Chapin, F. S., Coe, M. T., Daily, G. C., Gibbs, H. K., Helkowski, J. H., Holloway, T., Howard, E. A., Kucharik, C. J., Monfreda, C., Patz, J. A., Prentice, I. C., Ramankutty, N., & Snyder, P. K. (2005). Global consequences of land use. *Science, 309*(5734), 570-574. doi:10.1126/science.1111772

Goodchild, M. F. (2018). Reimagining the history of GIS. *Annals of GIS, 24*, 1-8. doi:10.1080/19475683.2018.1424737

Hall, J., Wecker, L., Ulmer, B., & Samavati, F. (2020). Disdyakis triacontahedron DGGS. *ISPRS International Journal of Geo-Information, 9*. doi:10.3390/ijgi9050315

Hasan, M. E., Nath, B., Sarker, A. H. M. R., Wang, Z., Zhang, L., Yang, X., Nobi, M. N., Røskaft, E., Chivers, D. J., & Suza, M. (2020). Applying multi-temporal Landsat satellite data and Markov-cellular automata to predict forest cover change and forest degradation of Sundarban reserve forest, Bangladesh. *Forests, 11*(9). doi:10.3390/f11091016

Hojati, M., Robertson, C., Roberts, S., & Chaudhuri, C. (2022). GIScience research challenges for realizing discrete global grid systems as a Digital Earth. *Big Earth Data, 6*(3), 358-379. doi:10.1080/20964471.2021.2012912

Hou, H., Wang, R., & Murayama, Y. (2019). Scenario-based modelling for urban sustainability focusing on changes in cropland under rapid urbanization: A case study of Hangzhou from 1990 to 2035. *Science of the Total Environment, 661*, 422-431. doi:10.1016/j.scitotenv.2019.01.208

Hurtt, G. C., Chini, L., Sahajpal, R., Frolking, S., Bodirsky, B. L., Calvin, K., Doelman, J. C., Fisk, J., Fujimori, S., Klein Goldewijk, K., Hasegawa, T., Havlik, P., Heinimann, A., Humpenöder, F., Jungclaus, J., Kaplan, J. O., Kennedy, J., Krisztin, T., Lawrence, D., Lawrence, P., Ma, L., Mertz, O., Pongratz, J., Popp, A., Poulter, B., Riahi, K., Shevliakova, E., Stehfest, E., Thornton, P., Tubiello, F. N., van Vuuren, D. P., & Zhang, X. (2020). Harmonization of global land use change and management for the period 850–2100 (LUH2) for CMIP6. *Geosci. Model Dev., 13*(11), 5425-5464. doi:10.5194/gmd-13-5425-2020

Intergovernmental Panel on Climate Change (IPCC). (2019). Summary for policymakers. In *Climate Change and Land: an IPCC special report on climate change, desertification, land degradation, sustainable land management, food security, and greenhouse gas fluxes in terrestrial ecosystems*, (Eds.) P. R. Shukla, J. Skea, E. Calvo Buendia, V. Masson-Delmotte, H. O. Pörtner, D. Roberts, P. Zhai, R. Slade, S. Connors, R. Van Diemen, M. Ferrat, E. Haughey, S. Luz, S. Neogi, M. Pathak, J. Petzold, J. Portugal Pereira, P. Vyas, E. Huntley, K. Kissick, M. Belkacemi, & J. Malley.

Intergovernmental Science–Policy Platform on Biodiversity and Ecosystem Services (IPBES). (2019). The IPBES assessment report on land degradation and restoration. In, (Eds.) L. Montanarella, R. Scholes, & A. Brainich. Bonn, Germany: Secretariat of the Intergovernmental Science-Policy Platform on Biodiversity and Ecosystem Services.

Jahanishakib, F., Mirkarimi, S. H., Salmanmahiny, A., & Poodat, F. (2018). Land use change modeling through scenario-based cellular automata Markov: improving spatial forecasting. *Environmental Monitoring and Assessment, 190*(6), 332. doi:10.1007/s10661-018-6709-0

Jansen, L. J. M., & Gregorio, A. D. (2002). Parametric land cover and land-use classifications as tools for environmental change detection. *Agriculture, Ecosystems & Environment, 91*(1), 89-100. doi:10.1016/S0167-8809(01)00243-2

Jokar Arsanjani, J., Tayyebi, A., & Vaz, E. (2016). GlobeLand30 as an alternative fine-scale global land cover map: Challenges, possibilities, and implications for developing countries. *Habitat International, 55*, 25-31. doi:10.1016/j.habitatint.2016.02.003

Kelly, K., & Šavrič, B. (2021). Area and volume computation of longitude–latitude grids and three-dimensional meshes. *Transactions in GIS, 25*(1), 6-24. doi:10.1111/tgis.12636

Lambin, E. F., Geist, H., & Rindfuss, R. R. (2006). Introduction: Local processes with global impacts. In *Land-Use and Land-Cover Change: Local Processes and Global Impacts*, (Eds.) E. F. Lambin & H. Geist,(pp. 1-8). Berlin, Heidelberg: Springer Berlin Heidelberg.

Lawrence, D. M., Hurtt, G. C., Arneth, A., Brovkin, V., Calvin, K. V., Jones, A. D., Jones, C. D., Lawrence, P. J., de Noblet-Ducoudré, N., Pongratz, J., Seneviratne, S. I., & Shevliakova, E. (2016). The land use Model intercomparison project (LUMIP) contribution to CMIP6: rationale and experimental design. *Geosci. Model Dev., 9*(9), 2973-2998. doi:10.5194/gmd-9-2973-2016

Lei, K., Qi, D., & Tian, X. (2020). A new coordinate system for constructing spherical grid systems. *Applied Sciences (Switzerland), 10*. doi:10.3390/app10020655

Li, X., Chen, G., Liu, X., Liang, X., Wang, S., Chen, Y., Pei, F., & Xu, X. (2017). A new global Land-use and land-cover change product at a 1-km resolution for 2010 to 2100 based on human–environment interactions. *Annals of the American Association of Geographers, 107*, 1040-1059. doi:10.1080/24694452.2017.1303357

Li, X., Chen, G., Zhang, Y., Yu, L., Du, Z., Hu, G., & Liu, X. (2022). The impacts of spatial resolutions on global urban-related change analyses and modeling. *iScience, 25*(12), 105660. doi:10.1016/j.isci.2022.105660

Li, X., Tian, H., Lu, C., & Pan, S. (2023). Four-century history of land transformation by humans in the United States (1630–2020): annual and 1 km grid data for the HIStory of LAND changes (HISLAND-US). *Earth Syst. Sci. Data, 15*(2), 1005-1035. doi:10.5194/essd-15-1005-2023

Li, X., Yu, L., Sohl, T., Clinton, N., Li, W., Zhu, Z., Liu, X., & Gong, P. (2016). A cellular automata downscaling based 1 km global land use datasets (2010–2100). *Science Bulletin, 61*, 1651-1661. doi:10.1007/s11434-016-1148-1

Li, X., Zhou, Y., Hejazi, M., Wise, M., Vernon, C., Iyer, G., & Chen, W. (2021). Global urban growth between 1870 and 2100 from integrated high resolution mapped data and urban dynamic modeling. *Communications Earth & Environment, 2*(201), 1-10. doi:10.1038/s43247-021-00273-w

Li, Z., Gui, Z., Hofer, B., Li, Y., Scheider, S., & Shekhar, S. (2020). Geospatial information processing technologies. In *Manual of Digital Earth*, (Eds.) H. Guo, M. F. Goodchild, & A. Annoni,(pp. 191-227). Singapore: Springer Singapore.

Lin, B., Zhou, L., Xu, D., Zhu, A. X., & Lu, G. (2018). A discrete global grid system for earth system modeling. *International Journal of Geographical Information Science, 32*, 711-737. doi:10.1080/13658816.2017.1391389

Liu, J., Dietz, T., Carpenter, S. R., Alberti, M., Folke, C., Moran, E., Pell, A. N., Deadman, P., Kratz, T., Lubchenco, J., Ostrom, E., Ouyang, Z., Provencher, W., Redman, C. L., Schneider, S. H., & Taylor, W. W. (2007). Complexity of coupled human and natural systems. *Science, 317*(5844), 1513-1516. doi:10.1126/science.1144004

Lu, Y., Laffan, S., Pettit, C., & Cao, M. (2019). Land use change simulation and analysis using a vector cellular automata (CA) model: A case study of Ipswich City, Queensland, Australia. *Environment and Planning B: Urban Analytics and City Science, 47*(9), 1605-1621. doi:10.1177/2399808319830971

Mahdavi-Amiri, A., Samavati, F., & Peterson, P. (2015). Categorization and conversions for indexing methods of discrete global grid systems. *ISPRS International Journal of Geo-Information, 4*, 320-336. doi:10.3390/ijgi4010320

Mechenich, M. F., & Žliobaitė, I. (2023). Eco-ISEA3H, a machine learning ready spatial database for ecometric and species distribution modeling. *Scientific Data, 10*(1), 77. doi:10.1038/s41597-023-01966-x

Meiyappan, P., Dalton, M., O'Neill, B. C., & Jain, A. K. (2014). Spatial modeling of agricultural land use change at global scale. *Ecological Modelling, 291*, 152-174. doi:10.1016/j.ecolmodel.2014.07.027

Ménard, A., & Marceau, D. J. (2007). Simulating the impact of forest management scenarios in an agricultural landscape of southern Quebec, Canada, using a geographic cellular automata. *Landscape and Urban Planning, 79*(3), 253-265. doi:10.1016/j.landurbplan.2006.02.016

Meyfroidt, P., Roy Chowdhury, R., de Bremond, A., Ellis, E. C., Erb, K. H., Filatova, T., Garrett, R. D., Grove, J. M., Heinimann, A., Kuemmerle, T., Kull, C. A., Lambin, E. F., Landon, Y., le Polain de Waroux, Y., Messerli, P., Müller, D., Nielsen, J. Ø., Peterson, G. D., Rodriguez García, V., Schlüter, M., Turner, B. L., & Verburg, P. H. (2018). Middle-range theories of land system change. *Global Environmental Change, 53*, 52-67. doi:10.1016/j.gloenvcha.2018.08.006

Munroe, D. K., & Müller, D. (2020). Land-system science to support achieving the sustainable development goals. *Journal of Land Use Science, 15*(4), 477-481. doi:10.1080/1747423X.2020.1783085

National Research Council. (2014). *Advancing land change modeling: Opportunities and research requirements*. Washington, DC: The National Academies Press.

Navarro Cerrillo, R. M., Palacios Rodríguez, G., Clavero Rumbao, I., Lara, M. Á., Bonet, F. J., & Mesas-Carrascosa, F.-J. (2020). Modeling major rural land-use changes using the GIS-based cellular automata Metronamica model: The case of Andalusia (Southern Spain). *ISPRS International Journal of Geo-Information, 9*(7). doi:10.3390/ijgi9070458

Nowak, E., & Nowak Da Costa, J. (2022). Theory, strict formula derivation and algorithm development for the computation of a geodesic polygon area. *Journal of Geodesy, 96*(4), 20. doi:10.1007/s00190-022-01606-z

Parker, D. C., Manson, S. M., Janssen, M. A., Hoffmann, M. J., & Deadman, P. (2003). Multi-agent systems for the simulation of land-use and land-cover change: A review. *Annals of the Association of American Geographers, 93*, 314-337. doi:10.1111/1467-8306.9302004

Peterson, P. R. (2017). Discrete global grid systems. In *International Encyclopedia of Geography: People, the Earth, Environment and Technology*, (Eds.) D. C. Richardson, N. Goodchild, M.F. Kobayashi, A., W. Liu, & R. A. Marston,(pp. 1-10).

Purss, M. B. J., Peterson, P. R., Strobl, P., Dow, C., Sabeur, Z. A., Gibb, R. G., & Ben, J. (2019). DataCubes: a discrete global grid systems perspective. *Cartographica, 53*, 63-71. doi:10.3138/cart.54.1.2018-0017

Ren, Y., Lü, Y., Comber, A., Fu, B., Harris, P., & Wu, L. (2019). Spatially explicit simulation of land use/land cover changes: Current coverage and future prospects. *Earth-Science Reviews, 190*, 398-415. doi:10.1016/j.earscirev.2019.01.001

Rindfuss, R. R., Entwisle, B., Walsh, S. J., An, L., Badenoch, N., Brown, D. G., Deadman, P., Evans, T. P., Fox, J., Geoghegan, J., Gutmann, M., Kelly, M., Linderman, M., Liu, J., Malanson, G. P., Mena, C. F., Messina, J. P., Moran, E. F., Parker, D. C., Parton, W., Prasartkul, P., Robinson, D. T., Sawangdee, Y., Vanwey, L. K., & Verburg, P. H. (2008). Land use change: complexity and comparisons. *Journal of Land Use Science, 3*(1), 1-10. doi:10.1080/17474230802047955

Robertson, C., Chaudhuri, C., Hojati, M., & Roberts, S. A. (2020). An integrated environmental analytics system (IDEAS) based on a DGGS. *ISPRS Journal of Photogrammetry and Remote Sensing, 162*, 214-228. doi:10.1016/j.isprsjprs.2020.02.009

Rounsevell, M. D. A., Pedroli, B., Erb, K.-H., Gramberger, M., Busck, A. G., Haberl, H., Kristensen, S., Kuemmerle, T., Lavorel, S., Lindner, M., Lotze-Campen, H., Metzger, M. J., Murray-Rust, D., Popp, A., Pérez-Soba, M., Reenberg, A., Vadineanu, A., Verburg, P. H., & Wolfslehner, B. (2012). Challenges for land system science. *Land Use Policy, 29*(4), 899-910. doi:doi.org/10.1016/j.landusepol.2012.01.007

Sahr, K. (2008). Location coding on icosahedral aperture 3 hexagon discrete global grids. *Computers, Environment and Urban Systems, 32*, 174-187. doi:10.1016/j.compenvurbsys.2007.11.005

Sahr, K. (2013). On the optimal representation of vector location using fixed-width multi-precision quantizers. *International Archives of the Photogrammetry, Remote Sensing and Spatial Information Sciences - ISPRS Archives, 40*, 1-8. doi:10.5194/isprsarchives-XL-4-W2-1-2013

Sahr, K. (2019). Central place indexing: Hierarchical linear indexing systems for mixed-aperture hexagonal discrete global grid systems. *Cartographica: The International Journal for Geographic Information and Geovisualization, 53*(1), 16-29. doi:10.3138/cart.54.1.2018-0022

Sahr, K., White, D., & Kimerling, A. J. (2003). Geodesic discrete global grid systems. *Cartography and Geographic Information Science, 30*, 121-134. doi:10.1559/152304003100011090

Sleeter, B., Loveland, T. R., Domke, G. M., Herold, N., Wickham, J., & Wood, N. J. (2018). *Land cover and land use change*. Retrieved from Washington, DC, USA:

Stehfest, E., van Zeist, W.-J., Valin, H., Havlik, P., Popp, A., Kyle, P., Tabeau, A., Mason-D'Croz, D., Hasegawa, T., Bodirsky, B. L., Calvin, K., Doelman, J. C., Fujimori, S., Humpenöder, F., Lotze-Campen, H., van Meijl, H., & Wiebe, K. (2019). Key determinants of global land-use projections. *Nature Communications, 10*(1), 2166. doi:10.1038/s41467-019-09945-w

Taylor, C. A., & Rising, J. (2021). Tipping point dynamics in global land use. *Environmental Research Letters, 16*(12), 125012. doi:10.1088/1748-9326/ac3c6d

Thompson, J. A., Brodzik, M. J., Silverstein, K. A. T., Hurley, M. A., & Carlson, N. L. (2022). EASE-DGGS: A hybrid discrete global grid system for Earth sciences. *Big Earth Data, 6*(3), 340-357. doi:10.1080/20964471.2021.2017539

Torrens, P. M., & Benenson, I. (2005). Geographic automata systems. *International Journal of Geographical Information Science, 19*(4), 385-412. doi:10.1080/13658810512331325139

Turner, B. L., Lambin, E. F., & Reenberg, A. (2007). The emergence of land change science for global environmental change and sustainability. *Proceedings of the National Academy of Sciences, 104*(52), 20666-20671. doi:10.1073/pnas.0704119104

Ulmer, B., Hall, J., & Samavati, F. (2020). General method for extending discrete global grid systems to three dimensions. *ISPRS International Journal of Geo-Information, 9*(4), 233. doi:10.3390/ijgi9040233

Van Rossum, G., & Drake, F. (2009). Python 3 Reference Manual. Scotts Valley, CA: CreateSpace. Retrieved from https://www.python.org/

Veldkamp, A., Verburg, P. H., Kok, K., de Koning, G. H. J., Priess, J., & Bergsma, A. R. (2001). The need for scale sensitive approaches in spatially explicit land use change modeling. *Environmental Modeling & Assessment, 6*(2), 111-121. doi:10.1023/A:1011572301150

Verburg, P. H., Alexander, P., Evans, T., Magliocca, N. R., Malek, Z., Rounsevell, M. D., & van Vliet, J. (2019). Beyond land cover change: towards a new generation of land use models. *Current Opinion in Environmental Sustainability, 38*, 77-85. doi:10.1016/j.cosust.2019.05.002

Verburg, P. H., Crossman, N., Ellis, E. C., Heinimann, A., Hostert, P., Mertz, O., Nagendra, H., Sikor, T., Erb, K. H., Golubiewski, N., Grau, R., Grove, M., Konaté, S., Meyfroidt, P., Parker, D. C., Chowdhury, R. R., Shibata, H., Thomson, A., & Zhen, L. (2015). Land system science and sustainable development of the earth system: A global land project perspective. *Anthropocene, 12*, 29-41. doi:10.1016/j.ancene.2015.09.004

Verburg, P. H., Schot, P. P., Dijst, M. J., & Veldkamp, A. (2004). Land use change modelling: Current practice and research priorities. *GeoJournal, 61*, 309-324. doi:10.1007/s10708-004-4946-y

Vince, A. (2006). Indexing the aperture 3 hexagonal discrete global grid. *Journal of Visual Communication and Image Representation, 17*(6), 1227-1236. doi:10.1016/j.jvcir.2006.04.003

Wang, J., Bretz, M., Dewan, M. A. A., & Delavar, M. A. (2022). Machine learning in modelling land-use and land cover-change (LULCC): Current status, challenges and prospects. *Science of the Total Environment, 822*, 153559. doi:10.1016/j.scitotenv.2022.153559

Wang, R., Ben, J., Zhou, J., & Zheng, M. (2020). Indexing mixed aperture icosahedral hexagonal discrete global grid systems. *ISPRS International Journal of Geo-Information, 9*. doi:10.3390/ijgi9030171

White, D., Kimerling, A. J., Sahr, K., & Song, L. (1998). Comparing area and shape distortion on polyhedral-based recursive partitions of the sphere. *International Journal of Geographical Information Science, 12*, 805-827. doi:10.1080/136588198241518

White, R., & Engelen, G. (2000). High-resolution integrated modelling of the spatial dynamics of urban and regional systems. *Computers, Environment and Urban Systems, 24*, 383-400. doi:10.1016/S0198-9715(00)00012-0

Winkler, K., Fuchs, R., Rounsevell, M., & Herold, M. (2021). Global land use changes are four times greater than previously estimated. *Nature Communications, 12*(1), 1-10. doi:10.1038/s41467-021-22702-2

Xiao, B., Liu, J., Jiao, J., Li, Y., Liu, X., & Zhu, W. (2022). Modeling dynamic land use changes in the eastern portion of the hexi corridor, China by cnn-gru hybrid model. *GIScience & Remote Sensing, 59*(1), 501-519. doi:10.1080/15481603.2022.2037888

Xing, W., Qian, Y., Guan, X., Yang, T., & Wu, H. (2020). A novel cellular automata model integrated with deep learning for dynamic spatio-temporal land use change simulation. *Computers & Geosciences, 137*, 104430. doi:10.1016/j.cageo.2020.104430

Ye, L., Gao, L., Marcos-Martinez, R., Mallants, D., & Bryan, B. A. (2019). Projecting Australia's forest cover dynamics and exploring influential factors using deep learning. *Environmental Modelling & Software, 119*, 407-417. doi:10.1016/j.envsoft.2019.07.013

Zalasiewicz, J., Williams, M., Haywood, A., & Ellis, M. (2011). The Anthropocene: a new epoch of geological time? *Philosophical Transactions of the Royal Society A: Mathematical, Physical and Engineering Sciences, 369*(1938), 835-841. doi:10.1098/rsta.2010.0339

Zhou, J., Ben, J., Huang, X., Wang, R., Liang, X., Ding, J., & Liang, Q. (2022). Efficient cell navigation methods and applications of an aperture 4 hexagonal discrete global grid system. *International Journal of Geographical Information Science*, 1-21. doi:10.1080/13658816.2022.2125972

Zhou, J., Ben, J., Wang, R., Zheng, M., & Du, L. (2020). Lattice quad-tree indexing algorithm for a hexagonal discrete global grid system. *ISPRS International Journal of Geo-Information, 9*(2), 83. doi:10.3390/ijgi9020083

Zhou, Y., Varquez, A. C. G., & Kanda, M. (2019). High-resolution global urban growth projection based on multiple applications of the SLEUTH urban growth model. *Scientific Data, 6*, 1-10. doi:10.1038/s41597-019-0048-z

Chapter 2.

Enabling Geosimulations for Global Scale: Spherical Geographic Automata[1]

2.1. Abstract

Several complex dynamic spatial systems are operating on the global scale. Their representation with existing geosimulation models is limited to planar level and do not consider the curvature of the Earth's surface. Thus, the objective of this study is to propose and develop a spherical geographic automata (SGA) modelling approach to represent and simulate dynamic spatial processes at the global level. The proposed SGA model is implemented for three case studies including simulations of (1) Game of Life as population dynamics, (2) urban land-use growth, and (3) deforestation, all operating on the spherical Earth's surface. Simulation results indicate that the proposed SGA modelling approach can represent spatial processes such as expansion and shrinkage dynamics on the Earth's surface. The proposed approach has a potential to be adopted to represent different complex systems such as ecological, epidemiological, socio-economic, and Earth systems processes to support environmental management and policy making at global level.

2.2. Introduction

In recent decades, geospatial technological development and advancement are characterized by the collection of large volumes of multi-source and multi-temporal Earth observation data with global extent that have led to the new era of Big Earth Data (BED) (Guo et al., 2020). To overcome challenges associated with BED such as storage, integration, quality, multi-scale representation, processing, and visualization, new methodologies for spatio-temporal data analysis and modelling are needed (Yao et al., 2020). The efficient analysis and management of Big Earth Data requires a consistent spatial data framework that can integrate datasets from different sources and formats

---

[1] A version of this chapter is published: Addae, B., & Dragićević, S. (2023). Enabling geosimulations for global scale: Spherical geographic automata. *Transactions in GIS, 27*(3), 821–840.

and supports geospatial data at multiple resolutions at the global level (Alderson et al., 2020; Baumann, 2021). In addition to these challenges, traditional Geographic Information Systems (GIS) data models such as raster and vector data formats are primarily focused on small to medium scale applications and are based on two-dimensional (2D) representation of the real world. Transforming the curved Earth's surface onto a plane introduces various forms of spatial distortions which can cause inaccuracies in results obtained from spatial analysis and modelling (Chrisman, 2017). When addressing large-scale study areas with global datasets, distortions caused by the Earth's curvature cannot be neglected (Kelly & Šavrič, 2021; Mai et al., 2022). Thus, current spatial data models are seen as unsuitable for handling global Big Earth Data (Mahdavi-Amiri, Alderson, et al., 2015) Addressing the spherical component when representing dynamic spatial phenomena at large and global scales demand new generation of geosimulation models.

The limitations of planar map projections and conventional geospatial models has spurred the development of several spherical spatial models such as Lat-Long grid, Yin-Yang grid (Kageyama & Sato, 2004), Voronoi grid (Lukatela, 2002), and spherical geodesic grid (Carfora, 2007). The brief description and comparisons of common spherical spatial grids are presented in Table 2.1. The Lat-Long grid uses the latitudes and longitudes to partition the globe into tiles and is applied in numerous fields to represent spherical surfaces. They however have two numerical problems: coordinate singularity and convergence of the meridians (Williamson, 2007). The cells of the grid are unequal in area and shape where square cells at the equator degenerate into triangles at the poles; a challenge known in climate science as "the pole problem" (Heikes et al., 2013). The Yin-Yang is a type of composite grid based on the Lat-Long grid and constitute two separate grid components that partial intersect at the boundaries. The grid however requires extensive computational interpolation where the two grids overlap (Qaddouri & Lee, 2011). The grid spacing are also quasi-uniform with uneven size across the Earth's surface. The Voronoi grid tessellates the surface of an ellipsoid into spherical Voronoi cells with centroids generated from source data used in construction of the grid. The cells generated in the Voronoi grid are however irregular and unequal in size (Lukatela, 2002).

Table 2.1.   Common spherical grids showing key descriptions and properties.

Grid	Lat-Long	Yin-Yang	Voronoi	Spherical Geodesic
Description	Grid cell tessellation bounded by regularly spaced latitudes and longitudes	Two grid components based on the latitude and longitude grid that are combined and overlap at the edges	A global spatial indexing scheme based on Voronoi polygons constructed on a sphere	Multiresolution grid that partitions the Earth's surface into cells with regular shape and size
Grid spacing	Quasi uniform	Quasi uniform	Quasi uniform	Uniform grid spacing
Cell typology	Square	Square	Irregular polygons based on Voronoi diagram algorithm	Hexagons, triangles, squares
Advantages	Widely adopted for spatial data storage in several fields	Allows for parallel computation	The size of the grid can be easily adapted to the scale of the data	Equal area grid cells across the Earth's surface
Limitations	Unequal cell area due to convergence of the meridians	Unequal cell area and computationally intensive	Unequal cell area	Can be computationally intensive at finer scale
References	Santini *et al.* (2010); Williamson (2007)	Kageyama and Sato (2004); Qaddouri and Lee (2011)	Chen *et al.* (2003); Lukatela (2002)	Sahr *et al.* (2003); Mahdavi-Amiri, Samavati*, et al.* (2015)

Spherical geodesic grids, known in GIScience as discrete global grid systems (DGGSs) have been proposed as a new geospatial technology that utilizes a spherical grid framework to partition the globe and accommodate the curvature of the Earth's surface ('t Hart, 2022; Sahr et al., 2003). It addresses the curvature of the Earth's surface, avoiding the distortions caused by projecting the Earth onto a flat plane. DGGSs offer a discrete way for spatial referencing using cells as the smallest unit of its base rather than conventional coordinates (Hojati et al., 2022). The spherical grid framework is composed of equal-area cells that are organized at multiple resolutions or levels, forming a spatial hierarchy of cells. These properties make discrete global grid system (DGGS) suitable for efficient multi-source data processing, storage, visualization, parallel computation, analyses, and modelling (Gibb et al., 2022). Based on these characteristics, DGGSs have been adopted in several fields such as climate and Earth systems modelling (Randall et al., 2002), numerical weather predictions (Zängl et al., 2015), oceanography (Ringler et al., 2013), geophysics (Simpson et al., 2006), Earth

observation data collection (Talone et al., 2015), land-use science (Ellis et al., 2021), global gazetteers (Adams, 2017), among others.

As a geospatial data format, DGGS has several properties which make them desirable for spatio-temporal modelling especially cellular automata (CA) models (Gibb et al., 2022; Li & Stefanakis, 2020). The cell structure of DGGSs provide appropriate discrete spatial lattice for implementing geosimulation models. Additionally, the spherical grid offers a closed surface for simulating Earth's surface processes at the global level where boundary effects do not have to be considered unlike conventional geosimulation models (Goodchild, 2018). The multi-resolution grid structure also supports spatial hierarchical modelling capabilities where system components and processes can be represented and simulated at different levels and for large scale applications (Zhao et al., 2022).

Although there has been growing interest in DGGS development and applications in the last decade, its utilization and integration with spatio-temporal modelling techniques is still very limited. In the scientific literature, spatio-temporal models on curved surfaces based on cellular automata (CA) have been postulated for simulating glider dynamics (Ventrella, 2011) and multi-scale Game of Life (Kiester & Sahr, 2008). These studies integrated CA framework and spherical models to represent dynamic processes on a sphere. However, the proposed frameworks still remain proof-of concept models with no integration with actual geospatial data. They also lack model evaluation mechanisms and implementation to simulate real world spatio-temporal phenomena at the global scale. Though the advantages of utilizing DGGSs for implementing spatio-temporal models and global applications are documented in the GIScience literature, the development of spherical geosimulation models with real world simulation capabilities are still lacking.

For these reasons, the main objectives of this research study are (1) to propose and develop a novel modelling approach that operates on a sphere, specifically Spherical Geographic Automata (SGA) using DGGS and hexagonal spatial tessellation, and (2) to implement the proposed SGA model on three case studies to simulate different dynamic spatial processes at global level.

2.3. Theoretical Background of Geodesic Global Grid Systems

Discrete global grid systems can be constructed by specifying a number of mathematical properties such as base polyhedron, orientation of the polyhedron, cell type, refinement, and cell indexing (Zhou et al., 2020). Base polyhedrons or Platonic solids are three-dimensional (3D) geometric figures composed of regular polygons that are used to approximate the spherical Earth's surface. There are five polyhedrons including tetrahedron, cube, octahedron, dodecahedron, and icosahedron which are commonly used as the initial sphere for DGGSs as presented in Figure 2.1.
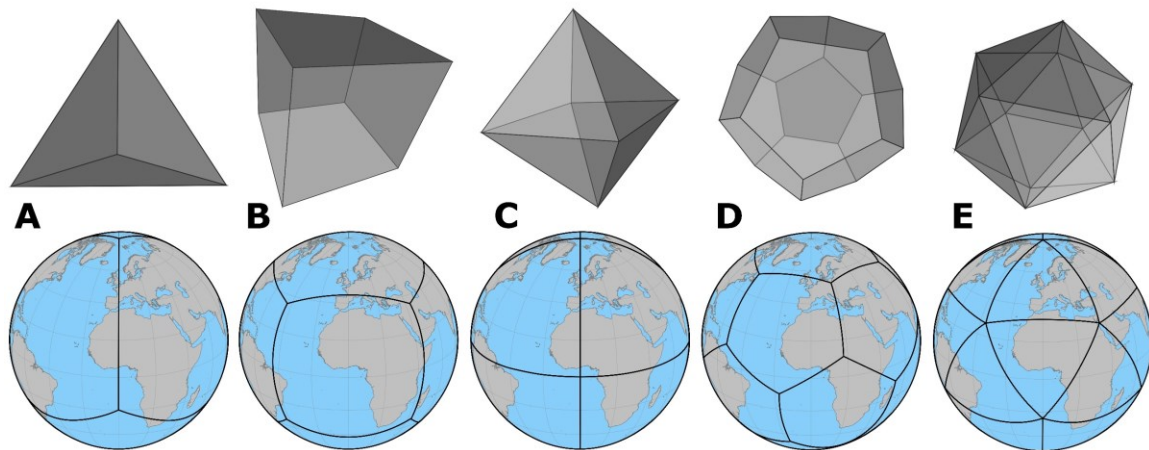
Figure 2.1.   Regular polyhedrons (top) and their corresponding spherical representations (bottom) for: a) Tetrahedron, b) Cube, c) Octahedron, d) Dodecahedron, and e) Icosahedron.

Polyhedrons with smaller and more faces provide a better representation of the Earth and cause less distortions when projecting between the base polyhedron and the corresponding spherical surface (Ulmer et al 2020). The icosahedron has 20 faces which can easily be packed into hexagons and is thus a popular design choice for constructing spherical models. Climate and Earth systems models such as the Model for Prediction Across Scales (MPAS), Non-hydrostatic Icosahedral Atmospheric Model (NICAM), Icosahedral Non-hydrostatic (ICON) global circulation model and Non-hydrostatic Icosahedral Model (NIM) are all based on the icosahedron (Ullrich & Jablonowski, 2012).

After defining the preferred base polyhedron, a fixed orientation relative to the actual surface of the Earth must be specified. The best choice of polyhedron orientation is often based on the intended DGGS application (Lei et al., 2020). A common

orientation of the icosahedron is to place a vertex at each of the poles and then align one of the edges of that vertex at the north pole with the prime meridian (Sahr et al., 2003). Similarly, Fuller's Dynamic Maximum tension (Dymaxion) orientation places all 12 of the spherical icosahedron vertices in the ocean so that the icosahedron vertices do not overlap with any landmass (Fuller, 1975). This characteristic makes the Fuller Dymaxion orientation a preferred choice when working with land areas at the global scale.

Different cell typologies are depicted in Figure 2.2 including triangles, quadrilaterals, and hexagons that can be used to tessellate the spherical polyhedron. Hexagonal cells are preferred in many DGGS implementations and applications due to its properties and advantages over traditional square grid cells used in raster GIS (Zhou et al., 2022). Compared with other regular cell types, hexagons are the most compact and tessellate the sphere with the least error (Robertson et al., 2020). Also, hexagons have uniform adjacency and neighbouring relationships in contrast to squares and triangles that have different edge and vertex neighbours (Randall et al., 2002). When used for spatial sampling, hexagons can accommodate 13% more area than square cells and also provide better approximation of circular regions (de Sousa & Leitão, 2018). These properties make hexagons suitable and desirable for spatial analyses and discrete spatial simulations (Peterson, 2017; Tong et al., 2013). Based on the merits and characteristics of hexagons as regular polygons, they are therefore used to tessellate the spherical surface and utilized henceforth throughout the research.
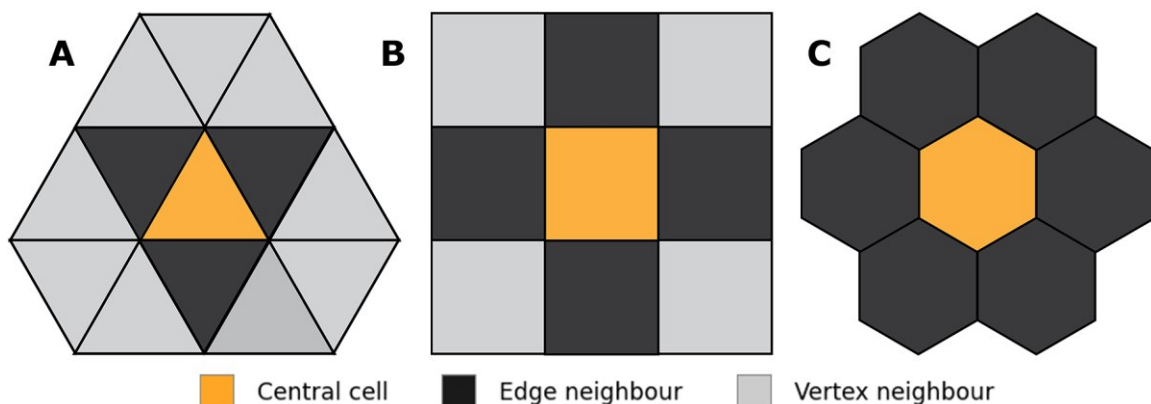
Figure 2.2.   Grid tessellations composed of a) triangle, b) square and c) hexagonal cells.

The resulting cells from the initial polyhedron are considered as the first resolution. To generate finer resolution cells, refinement techniques are applied to subdivide the initial polyhedron cells into a set of finer cells in a hierarchical and recursive manner (Adams, 2017). The ratio of the areas of cells at successive resolutions is termed aperture. DGGS based on hexagonal grids generally use 1-to-3, 1-to-4, and 1-to-7 refinements with aperture 3, 4, and 7 respectively (Zhao et al., 2022). In a hexagonal DGGS with aperture 4 for example, each successive resolution reduces the cell area by a factor of ¼. For each refinement, the coarse cell is referred to as the parent cell while the smaller cells partitioned from it are termed child cells. The choice of refinement or aperture determines the characteristics of the DGGS hexagonal cells. Figure 2.3 illustrates the structure and properties of cells at two resolutions for the three hexagonal refinements. Refinement 1-to-3 has the lowest aperture and capable of generating more grid resolutions among the three while refinement 1-to-4 produces rotation free tessellations at all resolutions which simplifies hierarchical analysis (Alderson et al., 2020; Vince, 2006). Child cells in 1-to-7 refinements cover the parent hexagonal cell space better and therefore provide a better congruency and simpler hierarchical relationship between successive resolutions. Unlike traditional raster datasets that can be resampled to arbitrary spatial resolutions, the resolution of DGGS cells are essentially fixed once the aperture is specified (Thompson et al., 2022).

Each discrete cell is assigned a unique identifier at each resolution and used as a data structure to represent its location (Sahr, 2008). Three techniques are primarily utilized to index cells in DGGSs: hierarchy-based indexing, axis or coordinate based indexing, and space filling curve indexing (Hall et al., 2020). For hexagonal DGGS, hierarchy-based indexing schemes are commonly used (Zhao et al., 2022). This technique uses the hierarchical relationship between cells through the application of refinement beginning with the base cell. An initial index is assigned to each cell at the first resolution and then using each cell's index as a prefix to the indices of its children (Zhou 2020). Mathematically, if a coarse cell *p* has index *G*, its children c_i, receive index *Gi* where *i* is a digit appended to *G* (Mahdavi-Amiri, Samavati, et al., 2015).
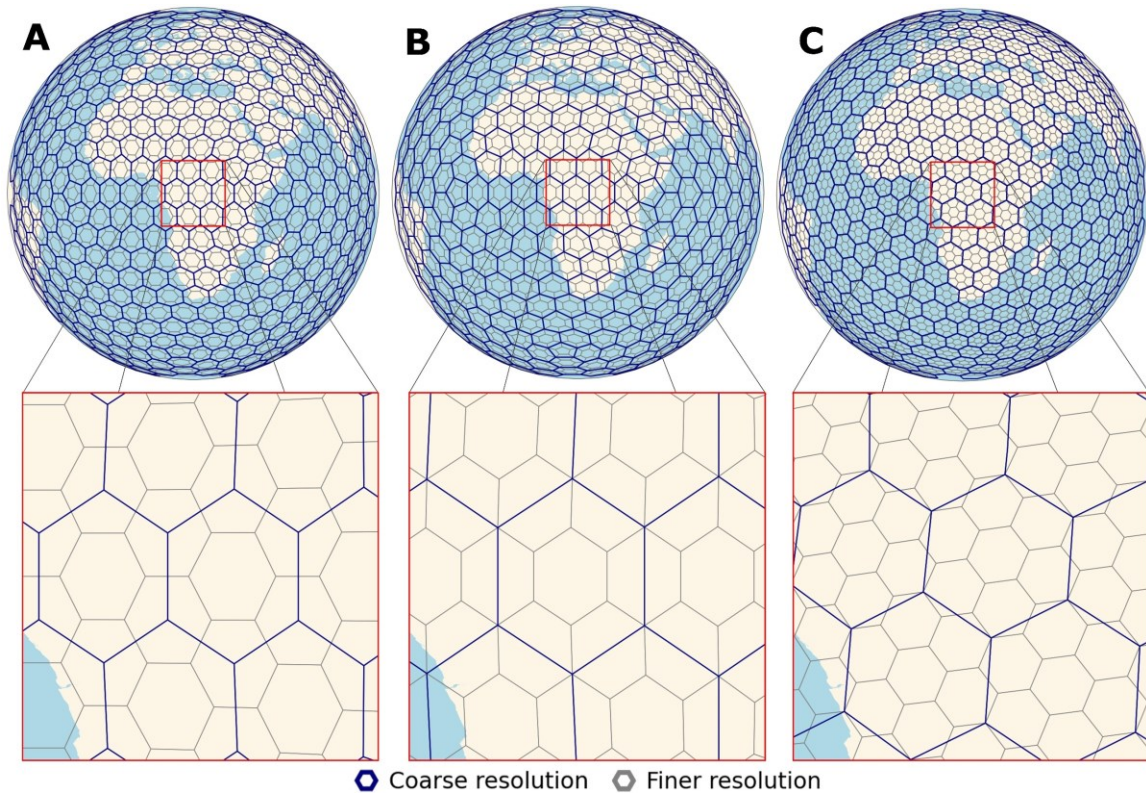
Figure 2.3. **Hierarchical partition of the spherical icosahedron using different hexagonal refinement methods: a) aperture 3, b) aperture 4, and c) aperture 7.**

2.3.1. Comparison of Geometric Distortions in Conventional GIS and DGGS

Global spatial datasets are primarily captured in geographic coordinate system (GCS). However, the representation of datasets in GCS produces unequal grid cell area due to convergence of the meridians (Kelly & Šavrič, 2021). For instance, square raster cells at the equator are transformed into triangles at the poles. Thus, it has become common for the spatial resolution of global raster datasets and spatial models to be defined using the cell dimension at the equator (Amatulli et al., 2022; Schaldach & Priess, 2008).

In Figure 2.4, global land-use/land-cover raster data with a spatial resolution of 111.59 km is compared with DGGS Icosahedral Snyder Equal Area (ISEA) aperture 4 hexagonal cells with an area of 12,452.77 km^2 and at different latitudes: latitude 0° (equator) and 75° N. From the comparative analysis, the ISEA DGGS hexagonal cells maintain their shape and size at both latitudes. On the contrary, the raster cells change

from squares at the equator to small rectangles at latitude 75° N. The rectangles eventually degenerate into triangles at the poles. These distortions can cause inaccurate spatial and statistical analyses especially in large-scale applications and sometimes produce misleading visualizations (Kazemi et al., 2022; Raposo et al., 2019).

For instance, using the ESA-CCI-LC dataset, Mousivand and Arsanjani (2019) calculated the total global urban extent in 2015 to be 908 thousand km^2. However, the ISEA DGGS framework used in this research study with the same ESA land-use/land-cover dataset computed the global urban extent to be 763 thousand km^2 for the year 2015, which is consistent with the results of Gong et al. (2020) who calculated the global urban land extent utilizing high resolution 30-meter land-use/land-cover datasets and partitioned the global land surface into 583 geographic grids. The difference between the two figures correspond to 19% of the global urban extent.

For global applications where areal statistics are important, equal-area map projections are better for preserving the areal properties of spatial features. However, when equal-area map projections are used, polygon segments are represented as straight lines instead of arcs of geodesics which can be an important source of error when computing surface area and distance at the global level (Santini et al., 2010). Moreover, many of these projections are designed for different regions and often exhibit large areal distortions in higher latitudes (Nowak & Nowak Da Costa, 2022).

To demonstrate areal distortions in existing equal-area projections, distortion indicators are calculated for cells in the Mollweide equal-area map projection and the ISEA DGGS at the global level following the method in de Sousa et al. (2019). The geodesic area for each polygon is calculated using the formula in Karney (2013) and available in the open source GeographicLib library (Karney, 2012). From the results, the Mollweide projection produces cells with unequal area across the globe with greater distortions at higher latitudes (Figure 2.5A). The ISEA DGGS hexagonal cells however show uniform distribution of cell area at the global level. As illustrated in Figure 2.5, existing equal-area map projections still exhibit areal distortions when used for large scale and global applications.
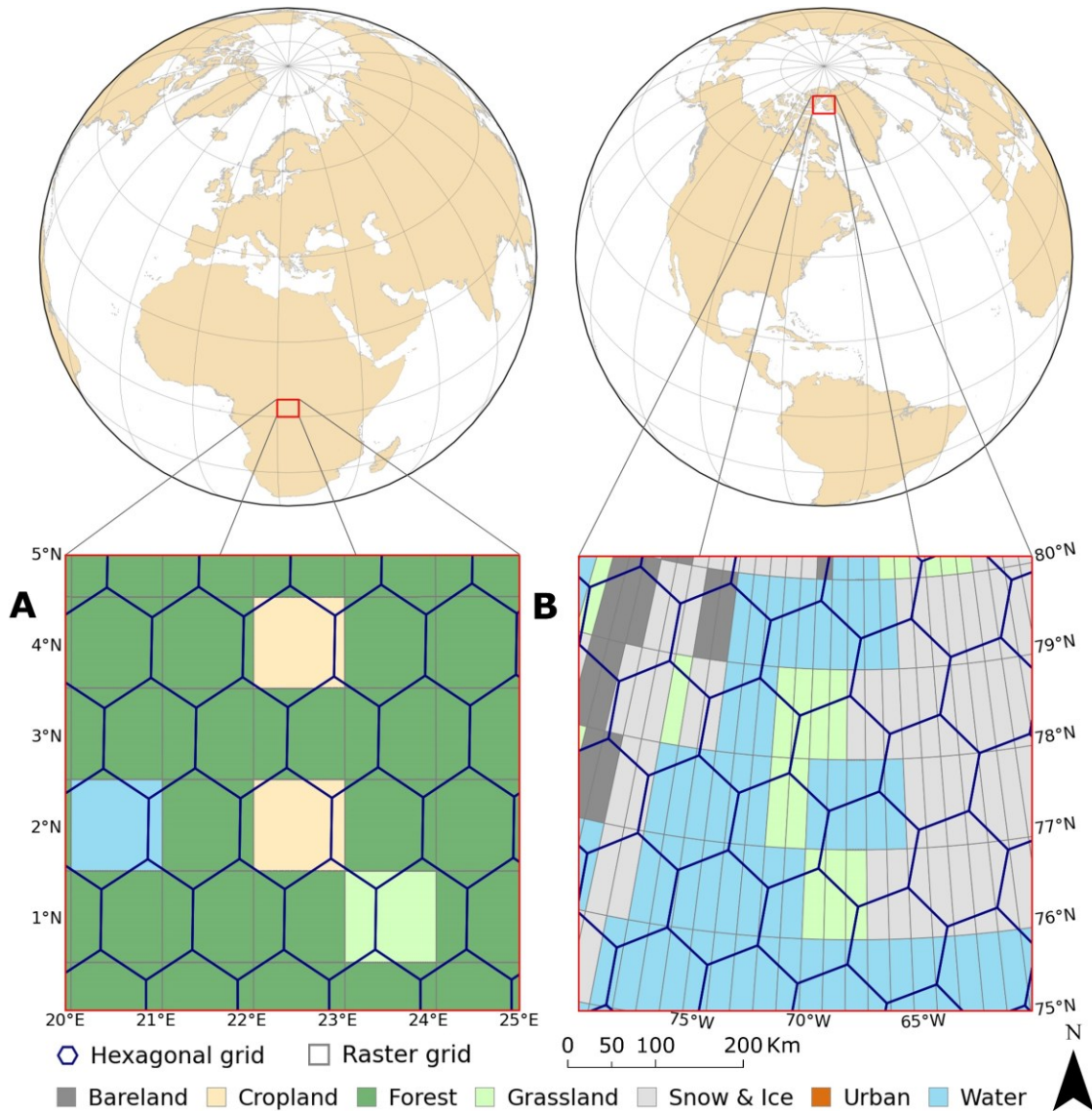
Figure 2.4. Comparison of raster square cells in geographic coordinate and DGGS ISEA 4 hexagonal cells at latitude a) 0° and b) 75° N.

For these reasons, this research study integrates DGGS and its abilities to tessellate spherical surface with the geographic automata systems, capable of simulating dynamics of complex spatial systems into a novel spherical geographic automata (SGA) modelling approach to represent global spatial processes.
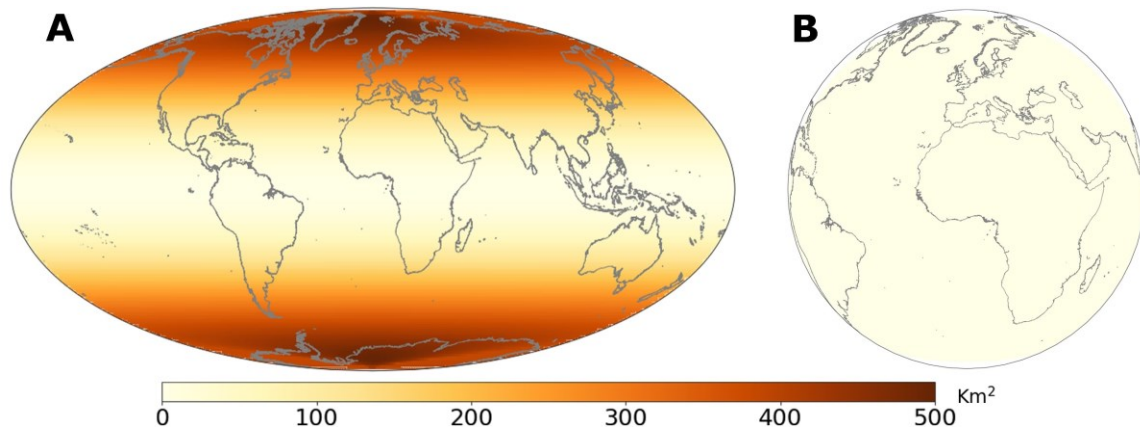
Figure 2.5. Global map of area distortions (in km^2) for a) Mollweide equal-area projection and b) ISEA DGGS.

2.4. Framework for Spherical Geographic Automata

Several real-world dynamic geographic phenomena can be described as complex spatial systems where interactions between system components occur at the local level and then give rise to spatial patterns at global level (Batty & Xie, 1994; Couclelis, 1985; Manson, 2001). A complex system is characterized by bottom-up non-linear interactions of system elements, space-time dynamics, emergence, evolution, self-organization, feedback loops, bifurcation, and path dependence. Complex spatial systems are often conceptualized as geographic automata systems (GAS) with two main mathematical methodologies; cellular automata (CA) and agent-based modeling (ABM) (Torrens & Benenson, 2005). GAS are discrete modelling systems based on arrangements of arrays of cells, where state of each cell is influenced by state of the cells in the neighborhood surrounding the central cell and is governed by the transition rules that represent the spatial process with discrete time steps (White & Engelen, 2000). In conventional GAS models, local effects are collected from the neighbouring cells or spatial adjacency that is defined using for example the Von Neumann neighbourhood (consist of four cells adjacent to the sides of the middle cell) or the Moore neighbourhood (eight adjacent cells). The grid space is typically composed of homogenous square cells thus making remote sensing (RS) and raster-based GIS data easy to incorporate into GAS models. Consequently, in the past decades, GAS modelling approaches have been applied widely to represent different dynamic geographic phenomena ranging from urban and regional growth, land-use and land-cover change, forest fires and insect disturbances, landslides, flooding, and other

physical processes, just to name a few. The assumption of homogenous square cells has however been extended to concept of non-homogeneous CA such as that operating on irregular polygons (Stevens & Dragićević, 2007). Recent advances have also represented system components and their interactions as network nodes and links with the conceptualization of GAS as network automata (Anderson & Dragićević, 2020). All these GAS approaches operate in a planar two-dimensional space, some work has also been completed to extend those into the three-dimensional space as voxel geographic automata (Jjumba & Dragićević, 2016).

When looking into representing geographical processes that are at the global scale, then spherical GAS models should be used. A spherical geographic automaton (SGA) is therefore proposed as a mathematical representation of a global complex dynamic spatial system that operates on a spherical surface and can be expressed as follows:

$$SGA = \{C^S, S, \Omega, f, \Delta T\} \tag{1}$$

where C^S is the spherical cell space that represents the landscape to be modelled and consisting of hexagonal cells, S denotes the hexagonal cell states, Ω is the spatial neighbourhood defined as a set of neighbouring cells that influence the evolution of the central hexagonal cell, f is the function of transition rules that determines changes in cell states, and ΔT is discrete increment of time.

The spherical cell space is constructed on the spherical geodesic grid which is based on the icosahedron and projected to the WGS84 ellipsoid using the icosahedral Snyder equal-area (ISEA) projection (Snyder, 1992). The cell space is thus composed of homogenous equal-area hexagonal cells. The cells are defined by their spatial properties including their geographic location on the spherical space as well as other non-spatial information based on the attributes of the complex spatial dynamic system being modelled. In the SGA modelling framework, each cell in the system has one of possible states. The state set Z is a collection of all possible hexagonal cell states and can be defined as $\{S_1, S_2, ..., S_k\}$ where k is a finite number.

The hexagonal neighbourhood Ω, in the SGA modelling framework is used to represent the localized region from which the central cell interacts. The neighbourhood

can be defined using adjacent cells around the central cell. For a hexagonal tessellation, each cell has six neighbouring cells that are equidistant from the central cell (Figure 2.2C). In a hexagonal grid, the neighbourhood of cells can be defined based on the grid resolution. The neighbourhood of a central cell (i,j) at an even resolution can be defined as:

$$\Omega = \{(i-1, j-1), (i-1, j), (i, j-1), (i, j+1), (i+1, j), (i+1, j+1)\} \tag{2}$$

and at odd resolution level as:

$$\Omega = \{(i+1, j-1), (i+1, j+2), (i-1, j-2), (i-1, j+1), (i+2, j+1), (i-2, j-1)\} \tag{3}$$

where (i, j) is the central cell's hexagonal coordinate and Ω is the neighbourhood of six cells around the central cell. As the spherical model has a closed surface, edge cells do not exist and boundary conditions are not defined in the proposed SGA modelling framework unlike conventional planar geosimulation models.

The function of transition rules f is used to represent the dynamic spatial system process being modelled on a spherical surface. The transition rules f, determine how the state of a cell $S_{(i,j)}$ changes through space and time in response to its current state and that of the cells in its spatial neighbourhood, Ω. In its basic form, the function is usually expressed as a set of "IF-THEN" statements that indicate specific conditions necessary for cell state change or otherwise. The time step ΔT, specifies the temporal dimension in which the system operates and is typically defined in a discrete manner. The time step starts from t_0 which is referred to as the initial state and increases by one at each iteration. The state of cells in the system are simultaneously updated at every iteration after the transitions rules are applied. The choice of time step normally depends on the spatial processes being modelled.

The proposed SGA modelling framework can be operationalized to simulate different spatio-temporal processes at the global scale by following the procedures outlined in Table 2.2.

Table 2.2.   **Description of steps for operationalizing SGA model for simulating complex dynamic spatial system.**

Steps	Descriptions
Complex system conceptualization	Identify the complex spatial dynamic system to be modelled and the components that make up the system. Identify the system properties and states that characterize the system. Determine the appropriate spatial extent at which the system should be represented.
Data acquisition and preprocessing	Data retrieval to represent properties of the system. Determine spatial and temporal resolution. Conversion of traditional spatial datasets to spherical format or use DGGS spherical data.
Define neighbourhood (Ω) and function of transition rules (f)	Determine the neighbourhood of each cell and their states. Develop transition rules that determine how the system evolves over time.
Implementation of SGA	Develop programming routines to represent different system mechanisms including neighbourhood, function of transition rules, and discrete time increment.
Model evaluation	Perform model evaluation including code verification, sensitivity analysis, model calibration and validation using actual datasets.
Scenarios	Design scenarios to represent different system conditions and possible what-if system trajectories.
SGA Model execution	Run simulations with appropriate parameters and time increment (ΔT).
Analysis of simulation results and visualization	Analyse obtained results from the SGA model to understand the process being modelled and how it evolves over time. Visualization of obtained results including statistics and maps.

2.5. SGA Implementation Case Studies and Simulation Results

To demonstrate the proposed modelling approach, the SGA modelling framework is used to implement several simplified spatial processes such as population dynamics, expansion, and shrinkage that are operating on a sphere. For the purpose of demonstrating the SGA modelling capabilities to represent these spatial processes, three case studies, have been developed to model: (1) Game of Life (GoL), (2) urban land-use growth, and (3) deforestation. The SGA model is implemented in the Python programming language (v3.8.5)(Van Rossum & Drake, 2009) using open-sourced DGGS library DGGRID (Sahr, 2022) and other geospatial libraries including gdal, geopandas, shapely, cartopy, rasterio, geodesy, and pyproj. The model is implemented

on a workstation with Intel(R) Xeon(R) Gold 6128 CPU @ 3.40GHz 3.39 GHz processor and 32 GB RAM with the processing time for each model iteration varying between 5 to 45 minutes.

2.5.1. SGA Game of Life (SGA_{GOL}) Model

The spherical geographic automata for Game of Life (SGA_{GOL}) represents automata with three states on a spherical surface, and rules for determining how their states changes over time. It extends the well-known Game of Life (Gardner, 1970) model representing theoretical complex system to operate on a sphere and in this case study to simulate the process of population dynamics at the global level. The SGA_{GOL} model is presented here to provide a simple proof-of-concept demonstration of the proposed framework so it can easily be implemented to simulate different real-world phenomena. Based on equation 1, SGA_{GOL} can be formulated as:

$$SGA_{GOL} = \{C^S, S_{GOL}, \Omega, f_{GOL}, \Delta T\} \qquad (4)$$

where C^S is the spherical surface with hexagonal spatial tessellation, S_{GOL} is the state of cells, Ω represents the hexagonal neighbourhood of six cells, f_{GOL} denotes transition rules and ΔT is the time step of the model. The SGA_{GOL} cell space consists of hexagonal cells located in spherical geographic space and with two primary cell states SGA_{GOL}: "dead" and "alive". The initial cell state is defined by randomly assigning "alive" to a given percentage of hexagonal cells on the spherical lattice. The model is initialized at time t_0 where 34% of the cells are selected as "alive". The "alive" cells are further categorized into two types, as "alive_1" or "alive_2" by random selection. For every iteration, the number of "alive" neighbours is calculated for each cell as well as the number of "alive_1" or "alive_2" cell types. The SGA_{GOL} model uses a set of transition rules f_{GOL} to simulate population growth, death, and survival across the globe based on each cell's current state and neighbourhood. An "alive" cell with two or three alive neighbours survives at the next time step. An "alive" cell with more than three or less than two alive neighbours becomes "dead" at the next time step. A "dead" cell with exactly two or three alive neighbours and at least one "alive_1" and "alive_2" cell becomes "alive" at the next time step. The new "alive" cell type is assigned based on the

minority in the neighbourhood or randomly assigned if the "alive" cell type is evenly distributed. If for example a "dead" cell has exactly three alive cells in its neighbourhood and two are "alive_1", the new cell would be assigned "alive_2". The SGA_{GOL} model is implemented with DGGS ISEA 3 grid with each hexagonal cell covering an area of 69,968 km^2. Model verification is performed to ensure the code used to define the concept and logic of the model is accurately implemented. The model is run for 10 iterations with each simulation representing one generation.

The simulation results of the SGA_{GOL} model output showing the evolution of cells on the sphere after five and ten iterations are presented in Figure 2.6. Based on the simulation outputs, all cells changed state at least once during the model run.
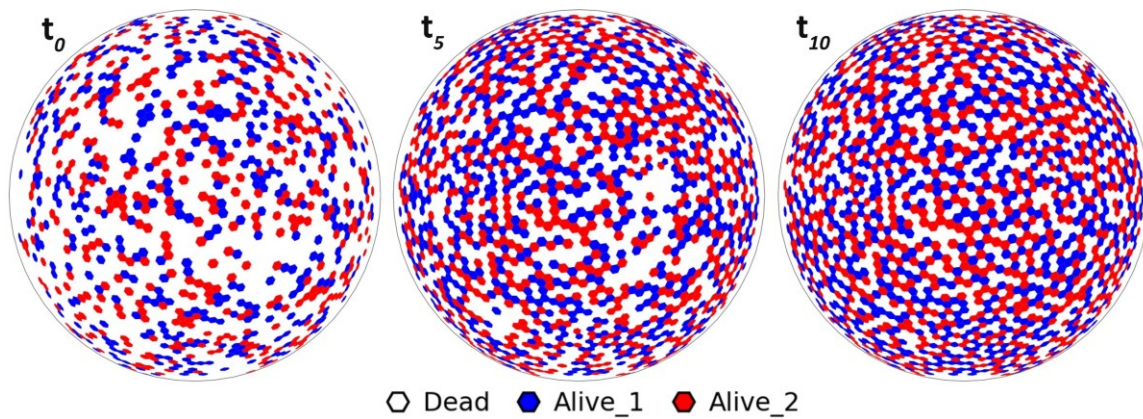
Figure 2.6. **Simulation results of SGA_{GOL} model showing the evolution of cell states over time on a spherical surface from initial state (t_0), after five (t_5), and ten (t_{10}) iterations.**

Common patterns observed in the conventional GoL model such as gliders and oscillators were not considered in this model application. The results also show a general trend of increasing population across the entire simulation run with the number of "alive" cells increases over the course of the simulation whisht "dead" cells decreases. At time t_0, 34% of the cell space was populated with "alive" cells and this proportion increases to 60% at time t_{10}. Also, the proportion of "alive_1" and "alive_2" cells remain in close equilibrium over the course of the simulation. This system dynamics can be attributed to the transition rules utilized in this study that maintains the balance between the number of "alive_1" and "alive_2" cell types over time.

2.5.2. SGA Global Urban Land-Use Growth (SGA_{GUL}) Model

The SGA global urban land-use growth SGA_{GUL} model is designed to simulate the spatial process of expansion as simplified by urban land-use growth across the globe using real-world geospatial datasets, and can be presented as:

$$SGA_{GUL} = \{C^S, S_{GUL}, \Omega, f_{GUL}, \Delta T\} \tag{5}$$

where C^S is composed of hexagonal spatial tessellation constructed using the spherical model, S_{GUL} is the state of cells based on simple binary class of "urban" and "non-urban", Ω represents the hexagonal neighbourhood of six cells around the central cell, f_{GUL} is the function of transition rules, and ΔT is time increment of the model. The initial state of cells at time t_0 = year 2000 has been derived using the European Space Agency (ESA) global land-use/land-cover dataset (ESA, 2017). Land-use datasets for the years 2000, 2010, and 2020 were used to implement and evaluate the SGA_{GUL} model. All spatial datasets are converted to DGGS ISEA 3 with each hexagon having an area of 287 km^2. The conversion of spatial datasets into hexagonal DGGS cells follows the methods described in Robertson et al. (2020) Transition rules f_{GUL} are designed to characterize the process of urban land-use growth to simulate urban development across the entire globe. Two scenarios: (a) Stalled Development and (b) Sustainable Development are implemented to represent different urban growth trajectories based on population increase projection data from the European Union Joint Research Centre (JRC) (Lutz et al., 2018). The Stalled Development scenario assumes global population with stagnated social development, low education levels, shorter life expectancy, and higher fertility rates resulting in higher population growth. The Sustainable Development scenario on the other hand assumes global population characterized by rapid social development, high education levels, longer life expectancy, and decreasing fertility, thus slower population growth.

Model calibration is performed using datasets for year 2000-2010 and validation with the 2010-2020 datasets. The simulation outputs are compared with actual land-use datasets using the Figure of Merit (*FoM*) index described in Pontius et al. (2008) and can be formulated as:

$$FoM = \frac{hits}{misses + hits + false\ alarms} \tag{6}$$

where hits are changed urban cells correctly simulated by the model, misses are changed urban cells the model was unable to simulate as changed cells, and false alarms are non-urban cells wrongly simulated as urban cells. In general terms, the hits equate to true positives, the misses denote false negatives and false alarms are the same as the false positives. The *FoM* value obtained for the SGA_{GUL} model in this study was 29.4% in the calibration phase and 25.1% during model validation. The low *FoM* values can be attributed to the simplified modelling parameters and less variables considered in the model design. The SGA_{GUL} model is constrained by urban demand at the national level and implemented to simulate urban land-use growth at the global scale for six iterations between 2020 (t_0) and 2080 (t_6) with a ten-year temporal interval.

The simulation results of urban growth in North America at each time step between 2020 and 2080 under the Stalled Development scenario are presented in Figure 2.7. Based on the simulation results, for example the total urban extent in North America increases by 76.5% under the Stalled Development scenario and 57.8% under the Sustainable Development scenario between 2020 and 2080. In addition, Figure 2.8 depicts the simulation outputs of urban land-use growth under the two scenarios by 2080 compared to the base year 2020 displayed for different parts of the globe and continents.

The simulation results indicate the global urban extent would increase from 793 thousand km^2 in 2020 to 1.7 million km^2 in 2080 under the Stalled Development scenario representing an urban growth of 118%. The total global urban extent under the Sustainable Development scenario however increases to 1.4 million km^2 in 2080 which corresponds to a growth of 77% between 2020 and 2080. The total global urban extents obtained from the model fall within the range found in the scientific literature with values varying between 1.1 million and 3.6 million km^2 based on different scenarios (Gao & O'Neill, 2020; Li et al., 2019; Li et al., 2021). The pattern of urban growth is similar under both scenarios although the urban extent is larger under the Stalled Development scenario as expected.
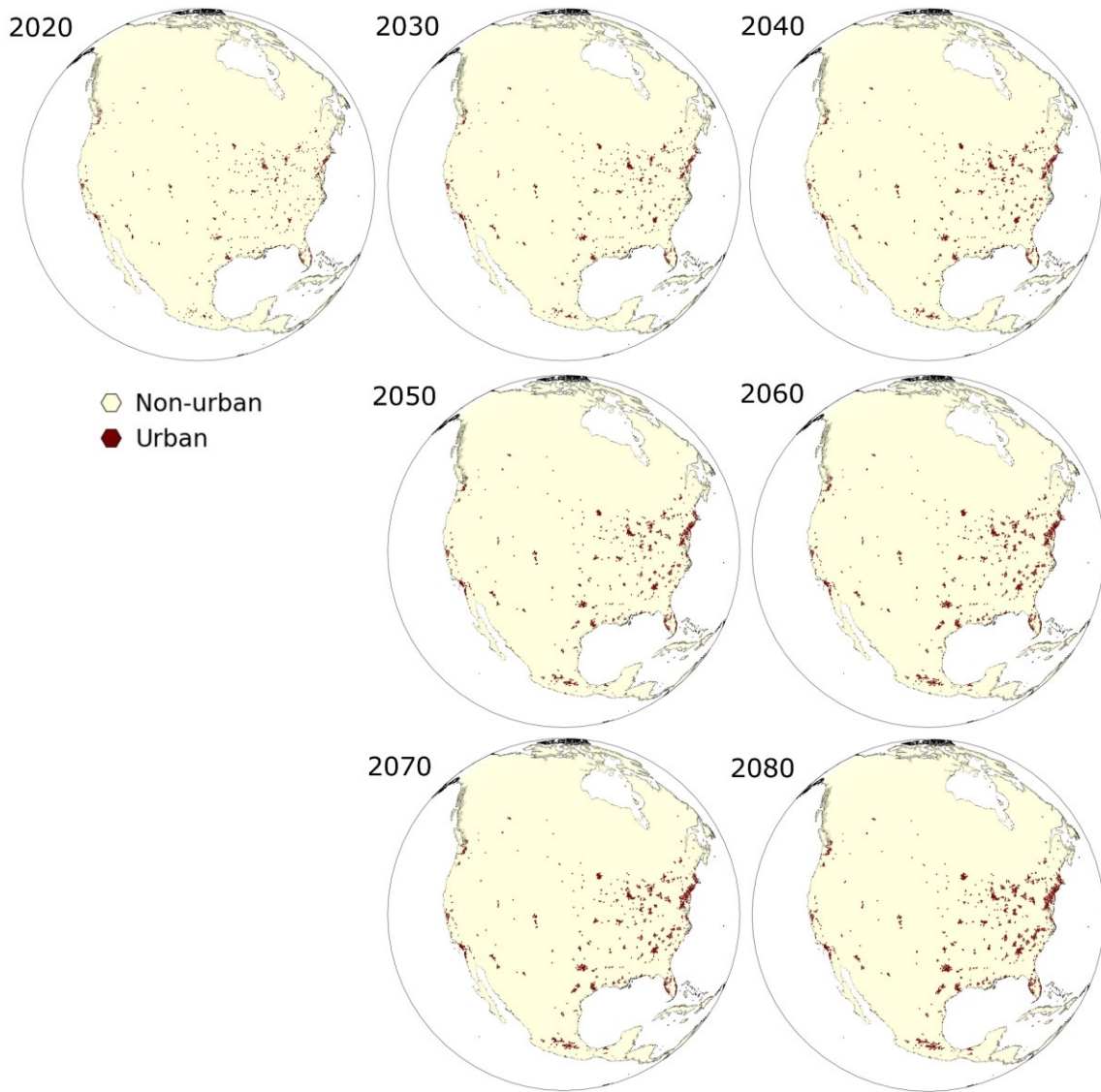
Figure 2.7.   Simulated urban extent between 2020 and 2080 with 10-year temporal increments for North America under the Stalled Development scenario.

The developed SGA_{GUL} model presents a simplified model for simulating urban growth process at the global scale and can be further refined to include more detailed datasets with finer spatial resolution and multiple datasets to represent the different factors that influence global urban land-use growth. The transition rules in the model can also be enhanced by incorporating multicriteria evaluation (MCE) techniques or machine learning to handle Big Earth Data and larger number of drivers.
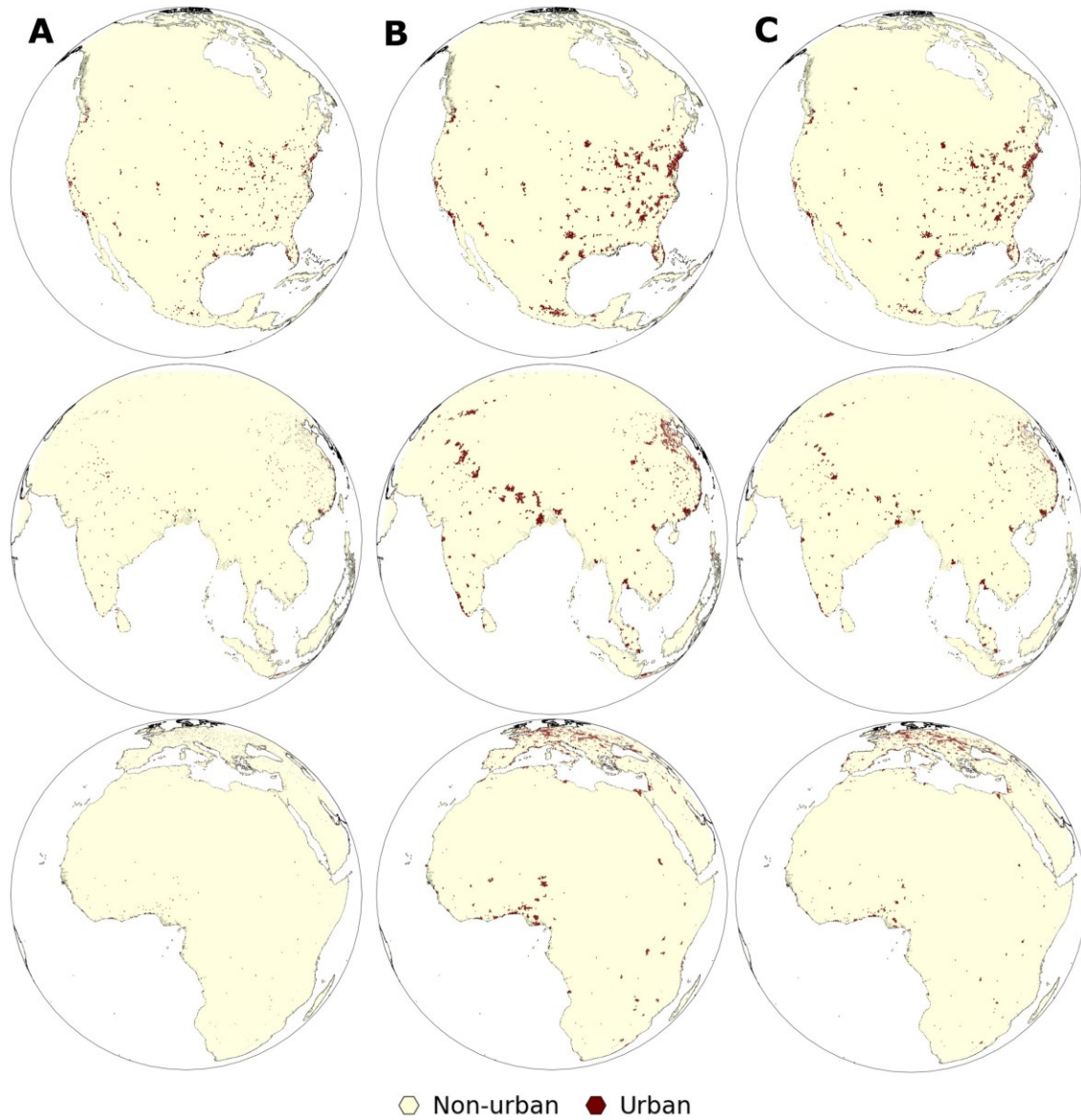
Figure 2.8. Comparison of a) initial year 2020 urban extent with obtained simulation results of urban growth in year 2080 under b) Stalled Development scenario, and c) Sustainable Development scenario for North America (top), Asia (middle), and Africa (bottom).

2.5.3. SGA Global Deforestation (SGA_{DEF}) Model

The proposed SGA framework is further implemented to simulate the spatial process of shrinking at the global scale, represented by deforestation, and can be formulated as follows:

$$SGA_{DEF} = \{C^S, S_{DEF}, \Omega, f_{DEF}, \Delta T\} \tag{7}$$

where S_{DEF} is the state of cells and f_{DEF} is the function of transition rules which determines how cell states change over time in the model. The cell states S_{DEF} are characterized as "forest" and "non-forest" and initialized at time t_0 using the ESA global land-use dataset for the year 2020. Transition rules f_{DEF} are designed to represent the processes of deforestation based on cell states and hexagonal neighbourhood Ω. At every iteration, if a "forest" cell has some specified neighbourhood conditions, the cell state is changed to "non-forest". Upon application of the transition rules, the cells are evaluated, and states updated simultaneously. The temporal resolution of the model is determined to be 10 years and each hexagonal cell encompasses an area of 287 km^2. The global deforestation model is however unconstrained, and change is determined only by the transition rules. To simulate forest change at the global level, a total of eight iterations are run to simulate the process of deforestation between 2020 (t_0) and 2100 (t_8).

The obtained simulation outputs of the global deforestation model for North America, South America, Africa, and the cumulative simulated forest loss between 2020 and 2100 are provided in Figure 2.9. In 2020, 48 million km^2 of the Earth's land surface was covered by forest. This however decreased to 30 million km^2 at the end of the 21st century which corresponds to a forest loss of 38%. The simulated forest loss obtained from the SGA_{DEF} model is consistent with other global land-use change model where global forest change varies between 25 million to 50 million km^2 by 2100 (Cao et al., 2019; Chen et al., 2020; Li et al., 2017). Despite the use of simple transition rules in the SGA_{DEF} case study, the simulation results indicate the pattern and process of deforestation can be well captured by the SGA model. No scenarios are however implemented in the S_{DEF} model and the rate of deforestation is only determined by the transition rules utilized.

Based on the simulation outputs, deforestation initially starts from the outskirt of large forest regions and shrinks into the interior. This can be explained whereby forest regions closer to disturbances, human activities, and have higher accessibility such as coastal areas and road networks are more prone to deforestation. Over time, regions with large forests become fragmented and replaced by small patches of trees. This change pattern is exemplified by the deforestation simulation outputs observed in North America in Figure 2.9 (top).
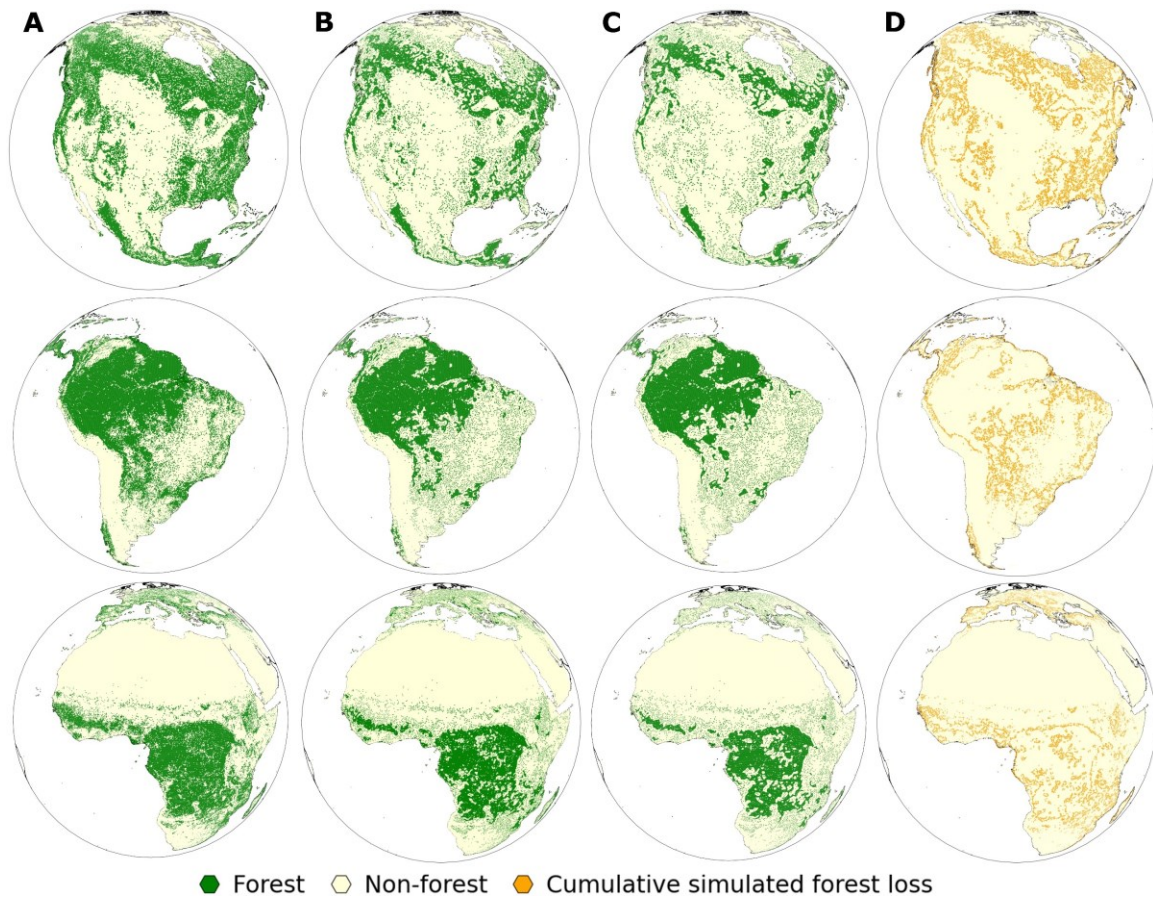
Figure 2.9.   Comparison of a) initial year 2020 forest cover with obtained simulation results of deforestation in year b) 2060, c) 2100 and d) the cumulative simulated forest loss for North America (top), South America (middle), and Africa (bottom).

While the S_{DEF} model presented in this study is capable of characterizing the process of deforestation, the simple binary states of "forest" and "non-forest" can be expanded to include several land-use/land-cover types and the array of factors that affect the change. The function of transition rules implemented in the model would thus need to be refined to correctly capture the conversion of forest and other land cover classes into the different land-use types, representing the effects of agricultural land expansion and urban land-use growth. Also, different deforestation scenarios can be implemented that portray possible future forest cover change pathways.

2.6.   Discussion and Conclusions

This research study presents the novel modelling approach of spherical geographic automata (SGA) that integrates cellular automata and spherical spatial

model to represent complex dynamic spatial processes on the Earth's curved surface. The model highlights the representation and modelling of spatio-temporal systems on a spherical surface unlike traditional geospatial models that are based on two-dimensional spatial technologies and constructed on flat maps. The SGA model differs from conventional geosimulation modelling approaches by utilizing new spherical geospatial models that address the curvature of the Earth's surface and hexagonal cells with equidistant neighbouring cells thus providing uniform spatial neighbourhood for application of transition rules. SGA presents an alternative modelling approach for spatial simulation and analyses at the global scale by providing equal-area cells that seamlessly cover the Earth's surface thereby avoiding spatial distortions and its associated effects that comes with projecting the spherical Earth onto a flat medium. In the era of Big Earth Data characterized by the availability of large volumes of geographic data from several sources at multiple spatial and temporal scales, the proposed spherical geographic automata (SGA) modelling approach provides a consistent geospatial framework for integrating spatial data from different sources, representing data at multiple levels, and performing advanced spatial analyses and simulations.

The novel SGA approach is implemented to successfully simulate different dynamic spatial phenomenon as demonstrated by the three case studies presented. The spherical Game of Life SGA_{GOL} model is implemented to simulate population change at the global level and on the sphere albeit using synthetic spatial data. This simple application provides a general demonstration of how dynamic spatial phenomena that evolve over space and time can be conceptualized and represented in the SGA model. Although the model is very generalized with simple transition rules, the results indicate complex system dynamics can still emerge. The global urban land-use growth as SGA_{GUL} model with two scenarios and the deforestation as SGA_{DEF} model are however implemented with real-world data using global land-use/land-cover datasets. This demonstrates the SGA model's capability for simulating full scale real-world spatio-temporal systems and applications for spatial decision making as well as executing possible what-if scenarios.

Although the proposed modelling approach can be used to represent different spatio-temporal processes on a spherical surface, the SGA model and applications have some caveats and limitations that can be improved. New components and mechanisms

can be integrated to enhance the SGA model's capability for handling complex processes that consist of several interactions and feedback such as modelling multiple land-use change processes at the global level consisting of urban growth, deforestation, desertification, and farmland conversion while also considering the effects and dynamics of climate change on the Earth's systems. Enhancement of the proposed model to represent the third dimension such as building height is also another area which needs further consideration. In order to properly represent and simulate real-world dynamic phenomena, spatio-temporal systems need to be conceptualized at finer scale which would require the use of detailed geospatial datasets. Such improvements necessitate the need for utilizing high performance computing (HPC) facilities dues to the increased computational demands that comes with improved spatial resolution of the system, number of datasets, and complexity of the system being modelled. Furthermore, the function of transition rules in the SGA model can be augmented by incorporating more comprehensive data and parameters (Addae & Dragićević, 2023), spatial decision-making methods such as spatial multi-criteria evaluation (MCE) (Addae & Dragićević, 2022) or machine learning techniques as well as considering multiple land-use changes and transition rules representing human-environment processes at different spatial scales. This can be especially useful when simulating spatio-temporal processes where human decision making is important, thus the SGA models can be used in policy planning and management at the global level.

In conclusion, this research study presents spherical geographic automata (SGA), a new geosimulation modelling approach for simulating spatio-temporal processes on a spherical surface with hexagonal spatial tessellation. In contrast to traditional space-time modelling frameworks that are based on two dimensional flat mediums, the novel SGA modelling approach provides a spherical spatial model for representing the Earth's curved surface, thus avoiding the effects of spatial distortions associated with planar map projections.

The three case studies presented in this research demonstrate the successful application of the proposed SGA modelling approach and provides a foundation for further development of spatio-temporal models that operate on spherical surfaces for representing dynamic spatial phenomena. The developed SGA modelling approach described in this research is flexible and can be extended to simulate different spatial

dynamic processes and systems on the global scale including ecological, socio-economic, biogeographical, climatology, and epidemiological systems.

2.7. References

't Hart, M. (2022). The projection point geodesic grid algorithm for meshing the sphere. *Journal of Computational Physics, 454*, 110993. doi:10.1016/j.jcp.2022.110993

Adams, B. (2017). Wāhi, a discrete global grid gazetteer built using linked open data. *International Journal of Digital Earth, 10*(5), 490-503. doi:10.1080/17538947.2016.1229819

Addae, B., & Dragićević, S. (2022). Integrating multi-criteria analysis and spherical cellular automata approach for modelling global urban land-use change. *Geocarto International*, 2152498. doi:10.1080/10106049.2022.2152498

Addae, B., & Dragićević, S. (2023). Modelling global urban land-use change process using spherical cellular automata. *GeoJournal, 88*, 2737–2754. doi:10.1007/s10708-022-10776-4

Alderson, T., Purss, M., Du, X., Mahdavi-Amiri, A., & Samavati, F. (2020). Digital Earth platforms. In *Manual of digital Earth*, (Eds.) H. Guo, M. F. Goodchild, & A. Annoni,(pp. 25-54). Singapore: Springer Singapore.

Amatulli, G., Garcia Marquez, J., Sethi, T., Kiesel, J., Grigoropoulou, A., Üblacker, M. M., Shen, L. Q., & Domisch, S. (2022). Hydrography90m: A new high-resolution global hydrographic dataset. *Earth Syst. Sci. Data, 14*(10), 4525-4550. doi:10.5194/essd-14-4525-2022

Anderson, T., & Dragićević, S. (2020). Representing Complex Evolving Spatial Networks: Geographic Network Automata. *ISPRS International Journal of Geo-Information, 9*(4). doi:10.3390/ijgi9040270

Batty, M., & Xie, Y. (1994). From cells to cities. *Environment & Planning B: Planning & Design, 21*, 531-548. doi:10.1068/b21s031

Baumann, P. (2021). A general conceptual framework for multi-dimensional spatio-temporal data sets. *Environmental Modelling and Software, 143*(June), 105096. doi:10.1016/j.envsoft.2021.105096

Cao, M., Zhu, Y., Quan, J., Zhou, S., Lü, G., Chen, M., & Huang, M. (2019). Spatial sequential modeling and prediction of global land use and land cover changes by integrating a global change assessment model and cellular automata. *Earth's Future, 7*, 1102-1116. doi:10.1029/2019EF001228

Carfora, M. F. (2007). Interpolation on spherical geodesic grids: A comparative study. *Journal of Computational and Applied Mathematics, 210*(1-2), 99-105. doi:10.1016/j.cam.2006.10.068

Chen, J., Zhao, X., & Li, Z. (2003). An algorithm for the generation of Voronoi diagrams on the sphere based on QTM. *Photogrammetric Engineering and Remote Sensing, 69*, 79-89. doi:10.14358/PERS.69.1.79

Chen, M., Vernon, C. R., Graham, N. T., Hejazi, M., Huang, M., Cheng, Y., & Calvin, K. (2020). Global land use for 2015–2100 at 0.05° resolution under diverse socioeconomic and climate scenarios. *Scientific Data, 7*(1), 320. doi:10.1038/s41597-020-00669-x

Chrisman, N. R. (2017). Calculating on a round planet. *International Journal of Geographical Information Science, 31*(4), 637-657. doi:10.1080/13658816.2016.1215466

Couclelis, H. (1985). Cellular Worlds: A Framework for Modeling Micro—Macro Dynamics. *Environment and Planning A: Economy and Space, 17*(5), 585-596. doi:10.1068/a170585

de Sousa, L. M., & Leitão, J. P. (2018). HexASCII: A file format for cartographical hexagonal rasters. *Transactions in GIS, 22*, 217-232. doi:10.1111/tgis.12304

de Sousa, L. M., Poggio, L., & Kempen, B. (2019). Comparison of FOSS4G supported equal-area projections ssing discrete distortion indicatrices. *ISPRS International Journal of Geo-Information, 8*(8), 1-13. doi:10.3390/ijgi8080351

Ellis, E. C., Gauthier, N., Klein Goldewijk, K., Bliege Bird, R., Boivin, N., Díaz, S., Fuller, D. Q., Gill, J. L., Kaplan, J. O., Kingston, N., Locke, H., McMichael, C. N. H., Ranco, D., Rick, T. C., Shaw, M. R., Stephens, L., Svenning, J.-C., & Watson, J. E. M. (2021). People have shaped most of terrestrial nature for at least 12,000 years. *Proceedings of the National Academy of Sciences, 118*(17), e2023483118. doi:doi:10.1073/pnas.2023483118

European Space Agency. (2022). *ESA CCI Land Cover map series 1992-2020*. Retrieved 15 November 2022 from: http://maps.elie.ucl.ac.be/CCI/viewer/index.php

Fuller, R. B. (1975). *Synergistics*. New York: MacMillan.

Gao, J., & O'Neill, B. C. (2020). Mapping global urban land for the 21st century with data-driven simulations and Shared Socioeconomic Pathways. *Nature Communications, 11*(1), 1-12. doi:10.1038/s41467-020-15788-7

Gardner, M. (1970). The fantastic combinations of John Conway's new solitaire game "life". *Scientific American, 223*(4), 120-123.

Gibb, R. G., Purss, M. B. J., Sabeur, Z., Strobl, P., & Qu, T. (2022). Global reference grids for big Earth data. *Big Earth Data, 6*(3), 251-255. doi:10.1080/20964471.2022.2113037

Goodchild, M. F. (2018). Reimagining the history of GIS. *Annals of GIS, 24*, 1-8. doi:10.1080/19475683.2018.1424737

Guo, H., Nativi, S., Liang, D., Craglia, M., Wang, L., Schade, S., Corban, C., He, G., Pesaresi, M., Li, J., Shirazi, Z., Liu, J., & Annoni, A. (2020). Big Earth data science: An information framework for a sustainable planet. *International Journal of Digital Earth, 13*(7), 743-767. doi:10.1080/17538947.2020.1743785

Hall, J., Wecker, L., Ulmer, B., & Samavati, F. (2020). Disdyakis triacontahedron DGGS. *ISPRS International Journal of Geo-Information, 9*. doi:10.3390/ijgi9050315

Heikes, R. P., Randall, D. A., & Konor, C. S. (2013). Optimized icosahedral grids: Performance of finite-difference operators and multigrid solver. *Monthly Weather Review, 141*(12), 4450-4469. doi:10.1175/MWR-D-12-00236.1

Hojati, M., Robertson, C., Roberts, S., & Chaudhuri, C. (2022). GIScience research challenges for realizing discrete global grid systems as a Digital Earth. *Big Earth Data, 6*(3), 358-379. doi:10.1080/20964471.2021.2012912

Jjumba, A., & Dragićević, S. (2016). Towards a voxel-based geographic automata for the simulation of geospatial processes. *ISPRS Journal of Photogrammetry and Remote Sensing, 117*, 206-216. doi:10.1016/j.isprsjprs.2016.01.017

Kageyama, A., & Sato, T. (2004). "Yin-Yang grid": An overset grid in spherical geometry. *Geochemistry, Geophysics, Geosystems, 5*(9). doi:10.1029/2004GC000734

Karney, C. F. F. (2012). GeographicLib (Version v 2.1.). Retrieved from https://geographiclib.sourceforge.io/

Karney, C. F. F. (2013). Algorithms for geodesics. *Journal of Geodesy, 87*(1), 43-55. doi:10.1007/s00190-012-0578-z

Kazemi, M., Wecker, L., & Samavati, F. (2022). Efficient calculation of distance transform on discrete global grid systems. *ISPRS International Journal of Geo-Information, 11*(6), 322. doi:10.3390/ijgi11060322

Kelly, K., & Šavrič, B. (2021). Area and volume computation of longitude–latitude grids and three-dimensional meshes. *Transactions in GIS, 25*(1), 6-24. doi:10.1111/tgis.12636

Kiester, A. R., & Sahr, K. (2008). Planar and spherical hierarchical, multi-resolution cellular automata. *Computers, Environment and Urban Systems, 32*, 204-213. doi:10.1016/j.compenvurbsys.2008.03.001

Lei, K., Qi, D., & Tian, X. (2020). A new coordinate system for constructing spherical grid systems. *Applied Sciences (Switzerland), 10*. doi:10.3390/app10020655

Li, M., & Stefanakis, E. (2020). Geospatial operations of discrete global grid systems — A comparison with traditional GIS. *Journal of Geovisualization and Spatial Analysis, 4*(26).

Li, X., Chen, G., Liu, X., Liang, X., Wang, S., Chen, Y., Pei, F., & Xu, X. (2017). A new global Land-use and land-cover change product at a 1-km resolution for 2010 to 2100 based on human–environment interactions. *Annals of the American Association of Geographers, 107*, 1040-1059. doi:10.1080/24694452.2017.1303357

Li, X., Zhou, Y., Eom, J., Yu, S., & Asrar, G. (2019). Projecting global urban area growth through 2100 based on historical time series data and future shared socioeconomic pathways. *Earth's Future, 7*(4), 351-362. doi:10.1029/2019EF001152

Li, X., Zhou, Y., Hejazi, M., Wise, M., Vernon, C., Iyer, G., & Chen, W. (2021). Global urban growth between 1870 and 2100 from integrated high resolution mapped data and urban dynamic modeling. *Communications Earth & Environment, 2*(201), 1-10. doi:10.1038/s43247-021-00273-w

Lukatela, H. (2002). A seamless global terrain model in the Hipparchus system. In *Discrete global grids: A web book*, (Eds.) M. F. Goodchild & A. J. Kimerling. University of California, Santa Barbara.

Lutz, W., Goujon, A., Kc, S., Stonawski, M., & Stilianakis, N. (2018). *Demographic and human capital scenarios for the 21st century: 2018 assessment for 201 countries*. Luxembourg: Publications Office of the European Union.

Mahdavi-Amiri, A., Alderson, T., & Samavati, F. (2015). A survey of digital Earth. *Computers & Graphics, 53*, 95-117. doi:10.1016/j.cag.2015.08.005

Mahdavi-Amiri, A., Samavati, F., & Peterson, P. (2015). Categorization and conversions for indexing methods of discrete global grid systems. *ISPRS International Journal of Geo-Information, 4*, 320-336. doi:10.3390/ijgi4010320

Mai, G., Janowicz, K., Hu, Y., Gao, S., Yan, B., Zhu, R., Cai, L., & Lao, N. (2022). A review of location encoding for GeoAI: Methods and applications. *International Journal of Geographical Information Science, 36*(4), 639-673. doi:10.1080/13658816.2021.2004602

Manson, S. M. (2001). Simplifying complexity: a review of complexity theory. *Geoforum, 32*(3), 405-414. doi:10.1016/S0016-7185(00)00035-X

Mousivand, A., & Arsanjani, J. J. (2019). Insights on the historical and emerging global land cover changes: The case of ESA-CCI-LC datasets. *Applied Geography, 106*(December 2018), 82-92. doi:10.1016/j.apgeog.2019.03.010

Nowak, E., & Nowak Da Costa, J. (2022). Theory, strict formula derivation and algorithm development for the computation of a geodesic polygon area. *Journal of Geodesy, 96*(4), 20. doi:10.1007/s00190-022-01606-z

Peterson, P. R. (2017). Discrete Global Grid Systems. In *International Encyclopedia of Geography*, (Eds.) D. Richardson, N. Castree, M.F. Goodchild, A. Kobayashi, W. Liu, & R.A. Marston,(pp. 1-10).

Pontius, R. G., Boersma, W., Castella, J.-C., Clarke, K., de Nijs, T., Dietzel, C., Duan, Z., Fotsing, E., Goldstein, N., Kok, K., Koomen, E., Lippitt, C. D., McConnell, W., Mohd Sood, A., Pijanowski, B., Pithadia, S., Sweeney, S., Trung, T. N., Veldkamp, A. T., & Verburg, P. H. (2008). Comparing the input, output, and validation maps for several models of land change. *The Annals of Regional Science, 42*(1), 11-37. doi:10.1007/s00168-007-0138-2

Qaddouri, A., & Lee, V. (2011). The Canadian global environmental multiscale model on the Yin-Yang grid system. *Quarterly Journal of the Royal Meteorological Society, 137*(660), 1913-1926. doi:10.1002/qj.873

Randall, D. A., Ringler, T. D., Heikes, R. P., Jones, P., & Baumgardner, J. (2002). Climate modeling with spherical geodesic grids. *Computing in Science & Engineering,, 4*(5), 32-41. doi:10.1109/MCISE.2002.1032427

Raposo, P., C. Robinson, A., & Brown, R. (2019). A virtual globe using a discrete global grid system to illustrate the modifiable areal unit problem. *Cartographica: The International Journal for Geographic Information and Geovisualization, 54*(1), 51-62. doi:10.3138/cart.54.1.2018-0015

Ringler, T., Petersen, M., Higdon, R. L., Jacobsen, D., Jones, P. W., & Maltrud, M. (2013). A multi-resolution approach to global ocean modeling. *Ocean Modelling, 69*, 211-232. doi:10.1016/j.ocemod.2013.04.010

Robertson, C., Chaudhuri, C., Hojati, M., & Roberts, S. A. (2020). An integrated environmental analytics system (IDEAS) based on a DGGS. *ISPRS Journal of Photogrammetry and Remote Sensing, 162*, 214-228. doi:10.1016/j.isprsjprs.2020.02.009

Sahr, K. (2008). Location coding on icosahedral aperture 3 hexagon discrete global grids. *Computers, Environment and Urban Systems, 32*, 174-187. doi:10.1016/j.compenvurbsys.2007.11.005

Sahr, K. (2022). DGGRID version 7.5. Retrieved March 2023 from https://github.com/sahrk/DGGRID

Sahr, K., White, D., & Kimerling, A. J. (2003). Geodesic discrete global grid systems. *Cartography and Geographic Information Science, 30*, 121-134. doi:10.1559/152304003100011090

Santini, M., Taramelli, A., & Sorichetta, A. (2010). ASPHAA: A GIS-based algorithm to calculate cell area on a latitude-longitude (Geographic) regular grid. *Transactions in GIS, 14*(3), 351-377. doi:10.1111/j.1467-9671.2010.01200.x

Schaldach, R., & Priess, J. A. (2008). Integrated models of the land system: A review of modelling approaches on the regional to global ccale. *Living Reviews in Landscape Research, 2*, 1-34. doi:10.12942/lrlr-2008-1

Simpson, J. J., Heikes, R. P., & Taflove, A. (2006). FDTD modeling of a novel ELF radar for major oil deposits using a three-dimensional geodesic grid of the Earth-ionosphere waveguide. *IEEE Transactions on Antennas and Propagation, 54*(6), 1734-1741. doi:10.1109/TAP.2006.875504

Snyder, J. P. (1992). An equal-area map projection for polyhedral globes. *Cartographica, 29*(1), 10-21. doi:10.3138/27H7-8K88-4882-1752

Stevens, D., & Dragićević, S. (2007). A GIS-Based Irregular Cellular Automata Model of Land-Use Change. *Environment and Planning B: Planning and Design, 34*(4), 708-724. doi:10.1068/b32098

Talone, M., Portabella, M., Martínez, J., & González-Gambau, V. (2015). About the optimal grid for SMOS level 1C and level 2 products. *IEEE Geoscience and Remote Sensing Letters, 12*(8), 1630-1634. doi:10.1109/LGRS.2015.2416920

Thompson, J. A., Brodzik, M. J., Silverstein, K. A. T., Hurley, M. A., & Carlson, N. L. (2022). EASE-DGGS: A hybrid discrete global grid system for Earth sciences. *Big Earth Data, 6*(3), 340-357. doi:10.1080/20964471.2021.2017539

Tong, X., Ben, J., Wang, Y., Zhang, Y., & Pei, T. (2013). Efficient encoding and spatial operation scheme for aperture 4 hexagonal discrete global grid system. *International Journal of Geographical Information Science, 27*(5), 898-921. doi:10.1080/13658816.2012.725474

Torrens, P. M., & Benenson, I. (2005). Geographic automata systems. *International Journal of Geographical Information Science, 19*(4), 385-412. doi:10.1080/13658810512331325139

Ullrich, P. A., & Jablonowski, C. (2012). MCore: A non-hydrostatic atmospheric dynamical core utilizing high-order finite-volume methods. *Journal of Computational Physics, 231*(15), 5078-5108. doi:10.1016/j.jcp.2012.04.024

Van Rossum, G., & Drake, F. (2009). Python 3 Reference Manual. Scotts Valley, CA: CreateSpace. Retrieved from https://www.python.org/

Ventrella, J. (2011). Glider dynamics on the sphere: Exploring cellular automata on geodesic grids. *Journal of Cellular Automata, 6*, 245-256.

Vince, A. (2006). Indexing the aperture 3 hexagonal discrete global grid. *Journal of Visual Communication and Image Representation, 17*(6), 1227-1236. doi:10.1016/j.jvcir.2006.04.003

White, R., & Engelen, G. (2000). High-resolution integrated modelling of the spatial dynamics of urban and regional systems. *Computers, Environment and Urban Systems, 24*, 383-400. doi:10.1016/S0198-9715(00)00012-0

Williamson, D. L. (2007). The evolution of dynamical cores for global atmospheric models. *Journal of the Meteorological Society of Japan. Ser. II, 85B*, 241-269. doi:10.2151/jmsj.85B.241

Yao, X., Li, G., Xia, J., Ben, J., Cao, Q., Zhao, L., Ma, Y., Zhang, L., & Zhu, D. (2020). Enabling the big earth observation data via cloud computing and DGGS: Opportunities and challenges. *Remote Sensing, 12*, 1-15. doi:10.3390/RS12010062

Zängl, G., Reinert, D., Rípodas, P., & Baldauf, M. (2015). The ICON (ICOsahedral Non-hydrostatic) modelling framework of DWD and MPI-M: Description of the non-hydrostatic dynamical core. *Quarterly Journal of the Royal Meteorological Society, 141*(687), 563-579. doi:10.1002/qj.2378

Zhao, L., Li, G., Yao, X., Ma, Y., & Cao, Q. (2022). An optimized hexagonal quadtree encoding and operation scheme for icosahedral hexagonal discrete global grid systems. *International Journal of Digital Earth, 15*(1), 975-1000. doi:10.1080/17538947.2022.2088871

Zhou, J., Ben, J., Huang, X., Wang, R., Liang, X., Ding, J., & Liang, Q. (2022). Efficient cell navigation methods and applications of an aperture 4 hexagonal discrete global grid system. *International Journal of Geographical Information Science*, 1-21. doi:10.1080/13658816.2022.2125972

Zhou, J., Ben, J., Wang, R., Zheng, M., & Du, L. (2020). Lattice quad-tree indexing algorithm for a hexagonal discrete global grid system. *ISPRS International Journal of Geo-Information, 9*(2), 83. doi:10.3390/ijgi9020083

Chapter 3.

Modelling Global Urban Land-use Change Process Using Spherical Cellular Automata[2]

3.1. Abstract

Urbanization process is one of the drivers of environmental and social changes across the globe entailing many environmental problems. Long term land-use change geosimulation models are useful tools to represent the complex human-environment interactions and evaluate the impacts of urbanization on the environment. However, many modelling approaches are not always fit to fully address this process at global scale and the issues of distortions related to Earths' curvature. Thus, the goal of this research study is to model and examine the long term global urban land-use change using spherical cellular automata approach. The developed model is implemented to simulate urban land-use change across 235 world countries and using two scenarios considering zero-migration and constant-fertility. The simulation results indicate that, between 2015 and 2095, the total global urban extent will double in size with the most extensive change in urban areas occurring in Africa and Asia. The proposed spherical model can be used to assist global urbanization policy making and environmental impact assessments.

3.2. Introduction

Over the last century, anthropogenic activities have transformed the land surface and atmospheric composition in numerous ways which are primarily manifested through processes such as deforestation, farmland conversion, mineral extraction and urbanization (Verburg et al., 2015). These processes are commonly referred to as land-use/land-cover change (LULCC) (Lambin et al., 2001). Land-use change (LUC) is regarded as one of the anthropogenic activities contributing to global climate change as well as biodiversity loss, soil water pollution, and altered hydrological cycle (Houghton,

---

2018; Sitch et al., 2005). Due to the diverse effects of land-use change on the environment, there is a need to advance analytical and modelling approaches to understand and analyse the LUC phenomenon and alleviate environmental impacts. Simulation models can represent spatial patterns of land-use change and provide possible scenarios that can be used for decision-making or policy building for environmental protection (Verburg et al., 2004). Spatially explicit modelling has become a part of procedures for environmental impact assessments, land-use policy and spatial decision making in general for wide range of land-use problems (Huang et al., 2019; Meiyappan et al., 2014).

One evident consequence of the spatial expansion of cities as urban lands is accompanied by the transformation of other land-use/land-cover features. A distinguishing feature of urbanization is the rise of extensive urban regions that have emerged from several smaller satellite urban areas into mega-urban units (Brenner & Schmid, 2012; Seto et al., 2017). This, coupled with other global impacts of urbanization, has necessitated the need to move from modelling urban land-use change on a local scale to much larger continental and global scales (Creutzig et al., 2019). Urban areas encompass less than 3% of the Earth's surface, yet the environmental impact of urbanization is global (Romero-Lankao et al., 2014). According to estimates, urban areas account for 75% of global carbon emissions and 60% of domestic water consumption (Acuto et al., 2018; Grimm et al., 2008). With the global urban population projected to increase from 56% in 2020 to 85% in 2100, urban land-use change and the process of urbanization are expected to influence global environmental change in the coming decades and until the end of the 21st century (OECD, 2015; UN-DESA, 2019).

To better comprehend the future of urbanization as well as the interaction between urbanization and other environmental systems, global urban land-use change models capable of forecasting long-term urban expansion are needed for several reasons (Acuto et al., 2018; Seto et al., 2012). Within the current world system, the factors that drive land-use change such as globalization, demographic change, economic growth, local and international political situations have no regional boundaries (Meyfroidt et al., 2013). Also, cities across the globe have become interconnected through the flow and mobility of people, capital, information, or labour to name a few (Geist et al., 2006; Sassen, 2005). Large-scale and local forces operate concurrently and interactively to shape urban landscapes across the globe (Verburg et al., 2019).

Further, the combined effects of urban land-use changes at the global level have considerable effects on biodiversity, agricultural productivity, water resources and ultimately on climate change. To represent the different factors and capture the complexities of land-use change process, geosimulation models (Torrens & Benenson, 2005) have been adopted in several land-use change studies (Schaldach & Priess, 2008). Such models reported in the scientific literature include GEONAMICA (Engelen et al., 1995), GEOMOD (Hall et al., 1995) and SLEUTH (Clarke et al., 1997) to name a few well known geosimulation approaches. However, these models are developed to simulate urban land-use change covering rather smaller spatial extents of metropolitan regions and are typically not designed to suit the needs of simulations to represent long term land-use process at the continental or global scale.

Geosimulation models of land-use change are often implemented with raster cells or equal square cells spatial tessellation and most studies rely on remote sensing or raster GIS data (Batty & Xie, 1994; White & Engelen, 2000). However, spatial modelling of land-use change at global scale including urban expansion presents the problem of distortions in shape and size of different regions, especially for large countries remains a challenge which is yet to be addressed in land-use science (Cao et al., 2019; Li et al., 2017). Although equal-area map projections are more convenient for preserving the surface of geographic features, distortion of spatial information still persist. Implementation and comparison of equal-area projections including the Goode Homolosine, Cylindrical Equal Area and Mollweide projections to represent global raster datasets indicate considerable differences in total land-use sizes at large spatial scales (Usery & Seong, 2001). In many global models, the dimensions of cells used to represent spatial data changes in size from the equator towards the south and north poles (Wang et al., 2020). Due to this problem, most global-scale land-use change models generally refer to the spatial resolution of their models by stating the resolution at the equator with the common phrase "*roughly 5 km at the equator*" (Chen et al., 2020; Gao & O'Neill, 2019; Zhou et al., 2019). This is not appropriate because of the spherical nature and curvature of the Earth which distorts the shape and size of grids. Such distortions are absent at the local scale but are however prominent when implemented on a larger scale (Ventrella, 2011).

In order to partition the globe, Discrete Global Grid System (DGGS) have been developed as an Earth reference system which utilizes a spherical tessellation of space

57

to accommodate the curvature of the Earth's surface (Yao et al., 2020). DGGS is a discrete approach for spatial referencing, based on cells as the smallest unit with multiple levels of resolution (Alderson et al., 2020). In addition to their equal-area characteristics, DGGS have also been proven to provide a more efficient data structure for storing geospatial data than traditional geographic information systems (GIS).

Therefore, the main objective of this research study is to model and analyse the long-term urban land use change process using the spherical cellular automata approach that operates at global spatial scale. The developed model is implemented with the data for 235 world countries and for the period from 1995 to 2015 to simulate the world urbanization process to 2095 with 10-year intervals.

3.3. Theoretical Background

The key component of any DGGS is its cell configuration that are used to cover the spherical Earth's surface (Mahdavi-Amiri et al., 2015). A DGGS framework is comprised of four main elements: base polyhedron, cell type, refinement and cell indexing (Barnes, 2020). Base polyhedron or platonic solid is a geometric solid which is used to represent the spherical approximation and curvature of the Earth (Bondaruk et al., 2020). Among the five spherical polyhedrons (i.e. tetrahedrons, cubes, octahedrons, dodecahedrons, and icosahedrons), those with more and smaller faces closely approximate the curved surface of the Earth that imply the least distortions (Hall et al., 2020). The spherical polyhedrons are partitioned into smaller cells consisting of polygons of the same size and shape such as triangles or hexagons, and containing the information on the location so they can be linked to spatial data (Wang et al., 2020). Hexagonal cells have gained considerable attention in recent scientific literature because of their uniform and unambiguous geometric connectivity, equidistant neighbourhood and smaller average error in quantizing the sphere (Robertson et al., 2020). In addition, research indicate hexagons have the capability to continuously cover the globe (Sahr, 2011) thus making them appropriate for spherical spatial analysis and modelling.

The surface area and spatial resolution of hexagonal cells in a DGGS framework are defined in a consistent process of hierarchical subdivisions of cells. These subdivisions are based on the ratio of the areas of cells at two different spatial

resolutions *k* and *k+1* and are termed as refinement or *aperture* (Mahdavi-Amiri et al., 2015). When working with hexagons, one-to-three, one-to-four and one-to-seven refinements are commonly used, with apertures of 3, 4 and 7 respectively (Bousquin, 2021). To support more resolutions, mixed aperture refinements such as 3 and 4 have also been developed and implemented (Wang et al., 2020). Each hexagonal cell is indexed with a unique identifier based on hierarchical or other indexing techniques. The identifier is used in the data structure to represent the location of the cell and to perform nearest neighbour and parent-child cell relationship functions (Alderson et al., 2020). Despite these characteristics, the application of DGGS with geospatial data is still underutilized, with majority of the existing studies focusing on simple spatial analyses including buffering and Boolean operations. However, geosimulation modelling techniques such as cellular automata (CA) have great potential to be integrated within DGGS to represent dynamic processes on the globe given their appropriate cell structure considering the spherical surface of the Earth (Li & Stefanakis, 2020).

Cellular automata are geosimulation modelling approaches that are used to represent and capture the spatial and temporal characteristics inherent in dynamic spatial phenomena (Torrens & Benenson, 2005). CA models are governed by main elements namely, the regular homogenous cells or grid partition and their states, spatial neighbourhood, function of transition rules, and discrete time steps (Batty et al., 1999; White & Engelen, 2000). The function of transition rules is the key component of a CA model as they govern the spatial process being modelled, using information at the local level based on cell states within the neighbourhood surrounding the central cell. Time is discrete in CA models with a synchronous updating of cell states following the transition rules applied to every cell in a single data layer. The choice of time step is often related to the nature of the dynamics of the phenomenon to be represented and the available temporal snapshots from datasets that determine the temporal resolution of the model.

Traditional CA models have generally been implemented with regular square grids although a few studies have been performed with hexagons. These applications include hexagonal CA models to study earth material movement (D'Ambrosio et al., 2003), forest fire (Trunfio, 2004) and dispersion of reagents in a chemical medium (Adamatzky et al., 2006). Using proof of concept models, Nugraha et al. (2020) also performed a comparative analysis of square and hexagonal CA for urban growth modelling. Although these studies have highlighted the advantages of implementing CA

models with hexagonal cells instead of square cells, hexagonal CA have not yet been widely applied to simulate urban land-use change using real-world land-use datasets. Iovine et al. (2005) indicate that hexagonal cells provide more homogenous CA neighbourhoods for transition rules when implementing CA models. In addition, they have also been shown to better preserve the areal properties of features when resampling land-use/land-cover datasets especially urban land-use type (Shoman et al., 2019).

Given the advantages of DGGS and hexagonal cells to accommodate for the spherical nature of the Earth's surface and the capability of cellular automata models in capturing the complexity of space-time dynamics of geospatial processes, this research study aims to integrate these approaches to effectively simulate and analyze the long-term urbanization process at global spatial scale.

3.4. Methodology

3.4.1. Study Area and Datasets

This research study encompasses 235 world countries as the study area, covering the entire landmass of the Earth, except for Antarctic and Greenland, including six continents: Africa (58 countries), Asia (51 countries), Europe (48 countries), North America (4 countries), South America (50 countries), and Australia/Oceania (24 countries). These world countries are further grouped into 20 sub-regions according to United Nations geographic region classification (UN-DESA, 2021).

The primary land-use datasets used in this research study were obtained from the European Space Agency Climate Change Initiative Land-Cover (ESA-CCI-LC) portal (ESA, 2017). This is the most comprehensive dataset for global land-use change studies as the data has finer spatial resolution of 300 meters and offers time series (from 1995) with a temporal resolution of one year (Radwan et al., 2021). The original 37 different land-cover types were reclassified into seven major categories: bare-land, cropland, grassland, forest, snow and permanent ice, urban and water bodies. The temporal resolution of the model was determined to be 10 years based on the time series of the available land-use dataset. Thus, land-use data for the years 1995, 2005 and 2015 were utilized in building and testing the model. Data representing protected areas including

parks and public lands, wildlife and biodiversity reserves, conservation sites, and marine protected zones collated by the International Union for the Conservation of Nature (IUCN) was also obtained from the World Database on Protected Areas (WDPA) online data catalogue (WDPA, 2020). Also, historical and projected population data between 1995 and 2100 were acquired from the United Nations Department of Economic and Social Affairs (UN-DESA) online data repository (UN-DESA, 2020). The global per capita urban land or urban land consumption (ULC) is described as the size of urban land per person (Gao & O'Neill, 2019), and calculated using the total urban land size derived from the ESA-CCI data for 2015 and population from the UN population dataset for the same year, the obtained global ULC value is 97 m^2.

The modelling procedures were accomplished using hexagonal cells covering the global Earth surface. The spatial datasets were converted into the DGGS framework (Figure 3.1) with the same spatial resolution of the available global spatial datasets, thus mixed aperture 3 and 4 hexagonal DGGS cells were chosen with each hexagonal cell covering an area of 4.5 km^2 with a side length of 1.3 km and long diagonal of 2.6 km.
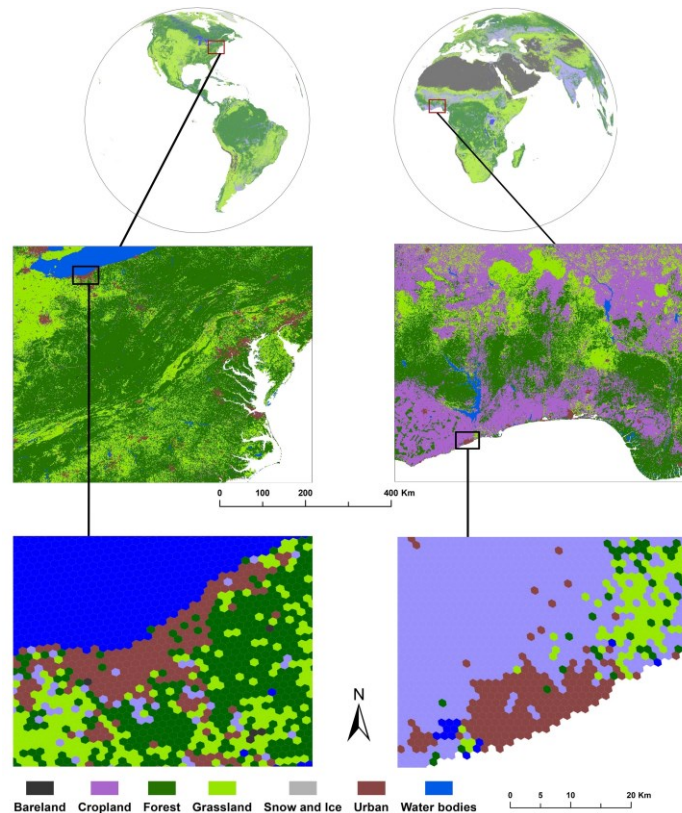
Figure 3.1.   Global land-use data for year 2015 resampled into DGGS framework where each hexagonal cells covers 4.5 km^2 surface area.

3.4.2. Spherical CA Model Overview

The proposed spherical CA model is composed of two sub-model components: a top-down Urban Demand Model (UDM) and a bottom-up Urban Growth Simulator (UGS). The overall workflow of the model is presented in Figure 3.2.
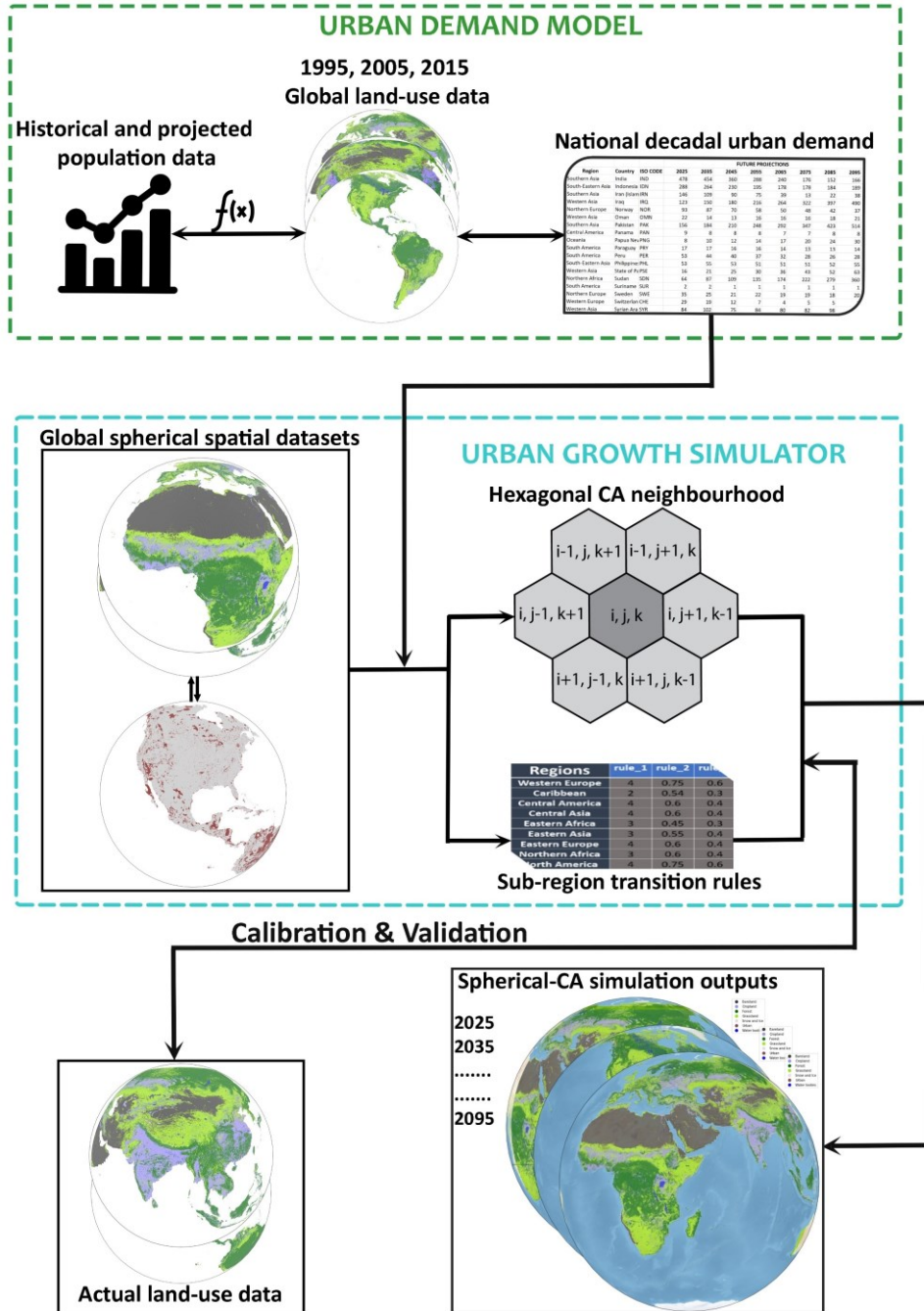
Figure 3.2.   **Conceptual framework of the spherical CA model for long-term simulation of global urbanization process.**

The UDM component computes the total urban land demand for all 235 world countries at a 10-year temporal resolution based on historical land-use data and population growth trends using a regression function. These national urban demand figures are used as input and constraint parameter for spatializing urban land-use change in the UGS model. Specifically, the model uses past population and urban land-use data to determine the relationship between urban expansion and population change and computes future urban demand based on projected population for each country.

The function of the UGS model component is to simulate the dynamics of urban development. The UGS component of the model is based on a spherical CA model that uses hexagonal spatial tessellation and can be formulated as:

$$S_{ijk}^{T_{i+1}} = f\ (S_{ijk}^{T_i}, H_{ijk}^{T_i}) \tag{1}$$

where *f* represents the function of transition rules that govern how the state of a hexagonal cell $S_{ijk}^{T_i}$ change from time T_i to a new state $S_{ijk}^{T_{i+1}}$ at the subsequent time step T_{i+1}, $H_{ijk}^{T_i}$ represents the hexagonal neighbourhood of six cells surrounding the central cell at time T_i at location (*i,j,k*). The location of each cell is determined using the hexagonal coordinate system which has three natural axes spaced 120° apart, denoted as *i*, *j* and *k*. The neighbourhood of each cell can be defined using the hexagonal coordinate system.

To represent the dynamics of urban development in different regions and countries, multiple transition rules were implemented. The UGS model contains sub-region transition rules which ensures that countries in the same region with similar population growth and urban land-use change trends have the same simulation parameters. Four different transition rules were selected based on the observed historical population change dynamics and urban land-use change rate, thus they influence the speed and the shape of urban development in a particular region. During each iteration, existing urban cells remain unchanged as well as those classified as snow, ice, and water bodies. The UGS model also incorporates the impact of urban development restrictions and constraints. For every iteration, the model verifies if the number of simulated cells has reached the urban demand for each country and updates

the land-use data representing new input for the subsequent iteration until the final simulation has been completed.

Based on the United Nations population projections (UN-DESA, 2020), two distinct population growth scenarios are developed to characterize global urban expansion under different population growth dynamics: scenario 1, zero-migration, and scenario 2, constant-fertility. Generally, zero-migration has a lower population growth trend than the constant-fertility scenario. The zero-migration scenario assumes no migration between countries with medium fertility and mortality rates. Under the constant-fertility scenario, fertility levels remain unchanged at the level estimated for the previous period with normal mortality and international migration rates.

3.4.3. Model Evaluation and Implementation

The spherical CA model was operationalized using DGGRID (Sahr, 2020) and Uber's H3 open-source DGGS library (Uber Technologies Inc, 2020) and code from the Python programming language (Van Rossum & Drake, 2009). DGGRID is an open-source library designed to generate multi-resolution spherical cells with hierarchical indexes and supports both the Icosahedral Snyder Equal Area (ISEA) projection and the R. Buckminster Fuller Icosahedral projection.

The developed model was evaluated by performing model calibration and validation. In this research study, datasets for the period 1995-2005 were used to calibrate and then 2005-2015 to validate the spherical CA model. Calibration was accomplished to obtaining appropriate transition rules by adjusting the simulation parameters after multiple runs of the model. To validate the model, the model was run to simulate urban land-use change between 2005 and 2015. After each iteration run, the simulated output is assessed against actual land-use data using standard simulation output comparison metrics such as the Figure of Merit (*FoM*) index (Varga *et al.*, 2019) that can be calculated as:

$$FoM = \frac{B}{A + B + C} \qquad (2)$$

where *A* is the number of actual changed cells simulated as non-changed cells; *B* is the number of actual changed cells simulated as changed cells; and *D* is the number of actual non-changed cells simulated as changed cells. In this research study, as only urban land-use change was modelled and urban cell states do not change during the simulations, the Figure of Merit index is composed of three components.

To enable model comparison, a raster grid CA was also implemented with the same model mechanism and parameters as the spherical CA model. All spatial datasets used in the raster CA model are reprojected into the Goode's Homolosine equal-area projection with a spatial resolution of 2.12 km, and consistent with the size of hexagonal cells in the spherical CA model. The global raster CA model was implemented with the Moore neighbourhood configuration.

The obtained values for *FoM* for the spherical CA model calibration and validation were 40.2% and 38.7% respectively. This is comparatively better than the *FoM* values computed for the raster CA model with 33.1% and 28.5% for calibration and validation respectively. The *FoM* values obtained from the spherical CA model were relatively better than the results of other global land-use change simulation models such as Cao et al. (2019), Chen et al. (2020), and Li et al. (2017) who obtained average *FoM* values of 28%, 24.4% and 19% respectively in these research studies.

3.5. Results

3.5.1. Simulation Results of Global Urbanization Process

Figure 3.3 presents the simulation results of urban land-use change at the global scale for 2095 under both scenarios and for selected geographic regions.
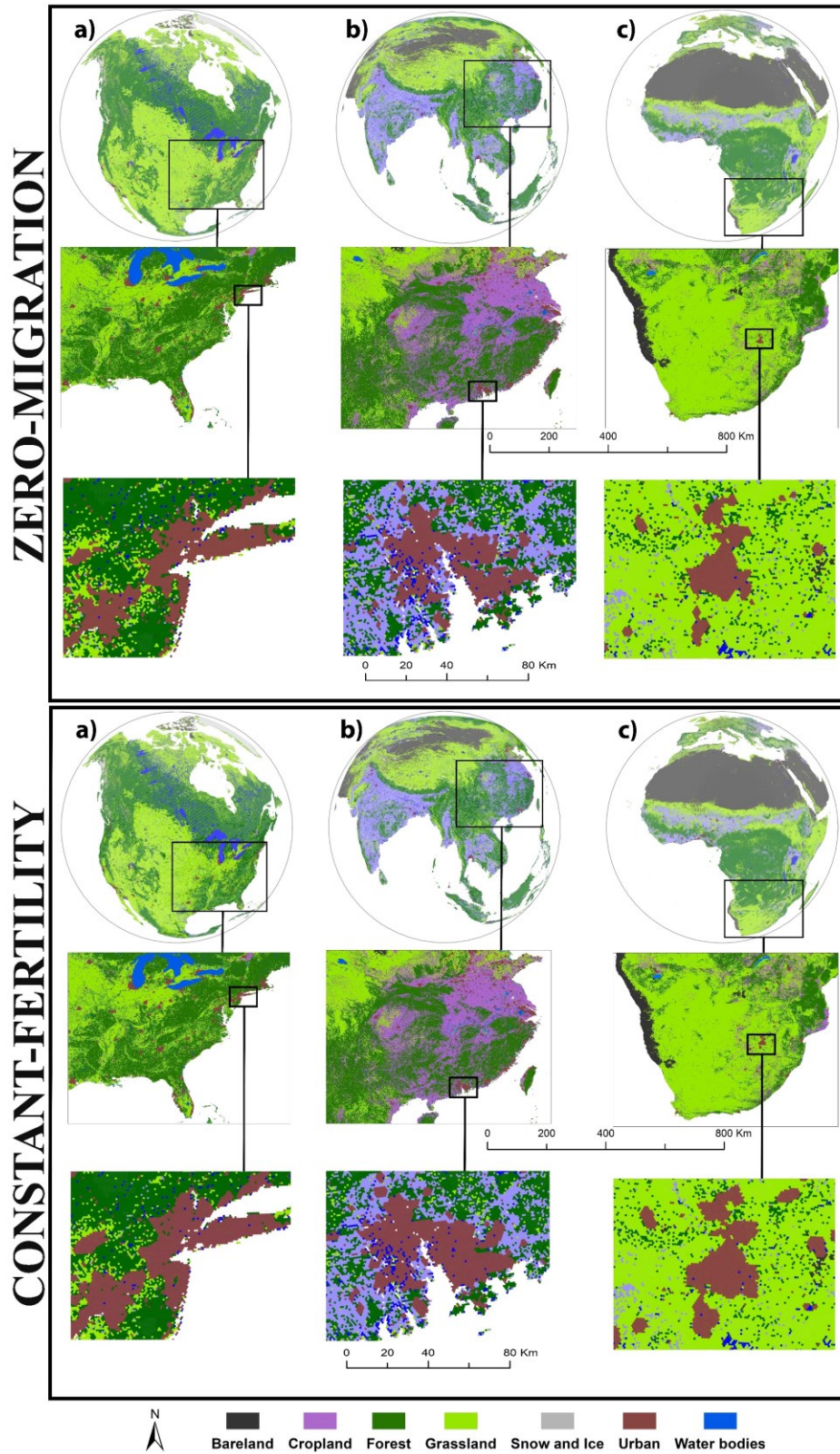
Figure 3.3. Generated simulation results showing urban growth at various scales for year 2095 in a) North America, b) Asia, and c) Africa, under zero-migration and constant-fertility scenarios.

Comparatively, the simulated urban growth was more extensive under the constant-fertility than the zero-migration scenario. The obtained simulation results from the spherical CA model indicate the total global urban extent by the year 2095 amounts to 1.24 million km^2 under the zero-migration scenario and 1.56 million km^2 for the constant-fertility scenario. Under zero-migration scenario, the total global urban extent simulated between 2015 and 2095 represents a growth of 0.47 million km^2, while the total urban area under the constant-fertility scenario increases by 0.78 million km^2 which corresponds to 62% and 105% urban expansion respectively. The global urban land consumption also rises from 97 m^2 in 2015 to 133 m^2 and 168 m^2 in 2095 under zero-migration and constant-fertility respectively, which represents an increase of 37% under the zero-migration scenario and 73% under constant-fertility.

Although the simulation results reveal urban expansion would occur in all regions across the globe, differences in urban expansion patterns can be observed and expressed in the urban land size values and rates of urban expansion. Figure 3.4a presents values obtained for continental contribution to total global urban expansion in the period from 2015 to 2095 while Figure 3.4b displays the rates of urban expansion under both scenarios. The rate of urban expansion has been derived as the change in urban extent between base year 2015 and last year 2095, compared to the base year and expressed as percentage. The total simulated urban area per continent in the period from 2015 to 2095 is also presented in Table 3.1.

According to the simulation results, Asia will continue to be the hot spot of urbanization, with nearly half of the global urban growth between 2015 and 2095 occurring in Asia (Figure 3.4a). In terms of urban land size, the results further indicate the total urban extent of cities in Asia will expand by 0.21 million km^2 under zero-migration and 0.32 million km^2 under the constant-fertility scenario. By the year 2095, the urban extent of Asia will account for 40% of the total global urban extent under the constant-fertility scenario. Simulation outputs from the model demonstrate that Africa will also contribute a significant amount of urban expansion to the total global urban extent, accounting for 27% of the total urban expansion that will occur between 2015 and 2095 under the constant-fertility scenario. Together, Asia and Africa will account for 65% of the global urban expansion simulated between 2015 and 2095 under zero-migration and 68% in the constant-fertility scenario. Although Asia will contribute the largest urban extent, cities in Africa are shown to have the highest rates of urban expansion. The

simulation outputs indicate that urban areas in Africa will expand by 210% under zero-migration and 470% in the constant-fertility scenario (Figure 3.4b).
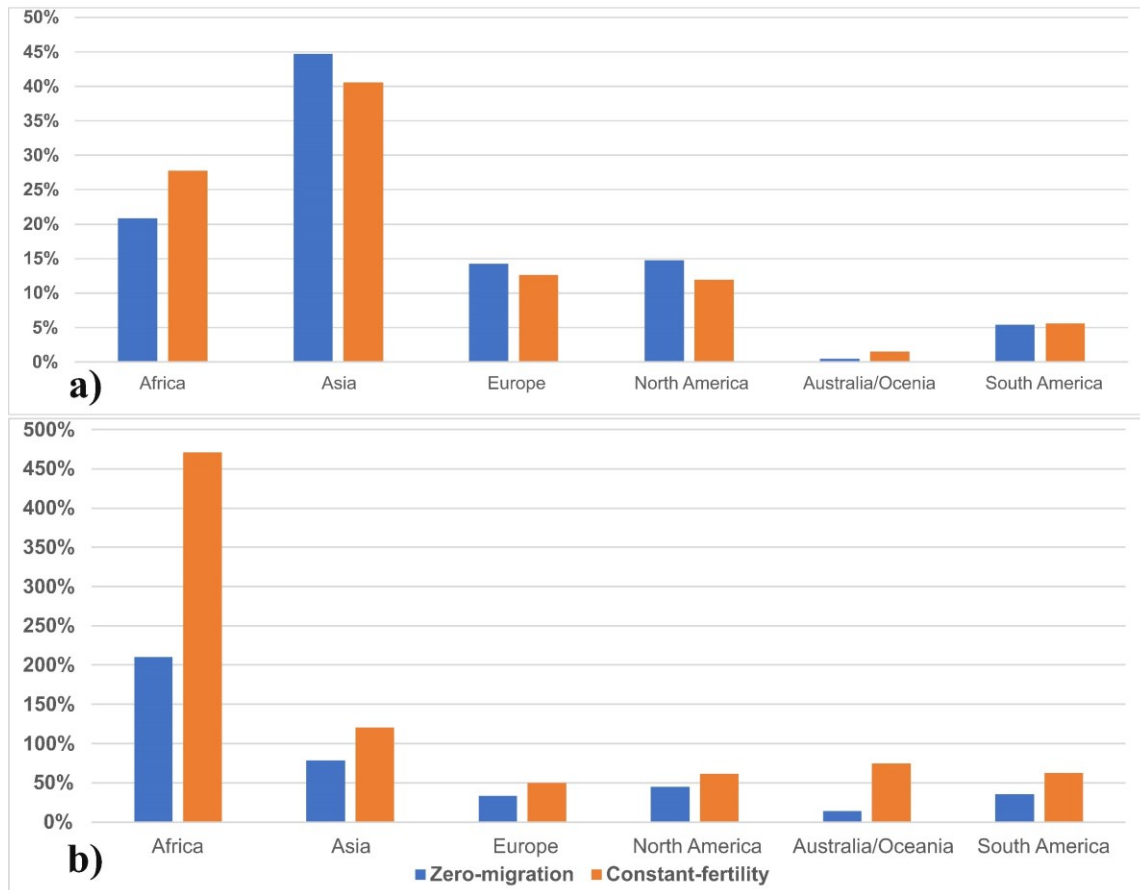
Figure 3.4.   Obtained values in (%) for continental (a) contribution to overall global urban expansion, and (b) rates of urban expansion between 2015 and 2095 under both scenarios.

Compared to Asia and Africa, developed regions like Europe and North America are indicated to have relatively lower rates of urbanization under both scenarios. Although the urban land-use growth in percentage terms is smaller than what simulation results show for Asia and Africa, the spatial extent of urban growth in developed regions is still significant. Under the constant-fertility scenario for example, the total urban area in Europe increases by 101 thousand km^2, whereas the total urban area of Africa expands by 222 thousand km^2 in the period from 2015 to 2095. However, the results indicate the rate of urban expansion in Africa will be 9 times more than that of Europe which is mainly due to the relatively small coverage of Africa's urban extent in 2015. For instance,

in 2015, the total urban extent of Europe (including Russia) was 202 thousand km^2 while Africa only had 47 thousand km^2 of urban land.

Table 3.1. **Simulated urban land-use growth (in thousand km^2) by continent between 2015 and 2095 under scenario 1 zero-migration, and scenario 2 constant-fertility.**

Continent	Scenario	2015	2025	2035	2045	2055	2065	2075	2085	2095
Africa	1	47.1	60	73.5	87.7	101.6	114.5	126.3	136.9	145.9
	2	47.1	60.2	76.6	96.9	121.9	151.3	185	224.3	268.7
Asia	1	269.1	323	368	403.5	430	448.5	462.4	473.2	481.6
	2	269.1	335.6	393.7	408.1	451.1	489.2	524.1	558.4	593.1
Europe	1	202.3	215.5	225.8	235.3	243.8	251.9	259.1	264.9	270
	2	202.3	221.6	236.8	250.7	263.6	275.5	286.2	295.2	303.1
North America	1	159.9	173.6	186.5	196.7	204.8	213.1	220.8	226.8	232.1
	2	159.9	178.6	196.1	209.9	221	232.3	243	251.4	258.8
Australia/ Oceania	1	16.3	17.7	18.2	18.4	18.5	18.5	18.5	18.5	18.5
	2	16.3	18.1	19.7	21.2	22.6	24.1	25.5	26.9	28.5
South America	1	66.5	75.1	81.9	86.1	88.5	89.6	90	90.1	90.1
	2	66.5	73.8	81	87.2	92.3	96.9	101	104.7	108.1

In terms of the relationship between population growth and urban development, the simulation outputs indicate that most regions would have increased urban land consumption values. Though population growth in developed countries is projected to stagnate in the coming decades with some regions experiencing negative population changes, reasonable urban development was still simulated. The ULC in Europe will increase from 272 m2 in 2015 to 447 m2 and 502 m2 in 2095 under zero-migration and the constant-fertility scenarios respectively. In contrast, Asia and Africa have the lowest levels of ULC in comparison to the other continents despite having the highest rates of urbanization. For the zero-migration scenario, the ULC of Asia increases from 61 m2 in 2015 to 102 m2 in 2095 whilst that of Africa increases from 40 m2 to 45 m2 within the same period. Compared to all regions, Asia will have the largest change in urban land consumption by the year 2095 under both scenarios.

3.5.2. Regional and Sub-regional Variations of Urban Land-use Growth

When looking further into the 20 world sub-regions, it has been noticed that different dynamics of urban land-use change has occurred. Figure 3.5a presents the graph with comparisons of total simulated urban land by 2095. The rates of urban expansion at the sub-regional level is also presented in Figure 3.5b. Simulation results indicate that Eastern Asia will have the most extensive growth of cities with the urban extent of this sub-region expanding by 116 thousand km^2 under zero-migration and 142 thousand km^2 under constant-fertility. Under the constant-fertility scenario, 56% of the total simulated urban expansion on the Asian continent will occur in Eastern Asia.
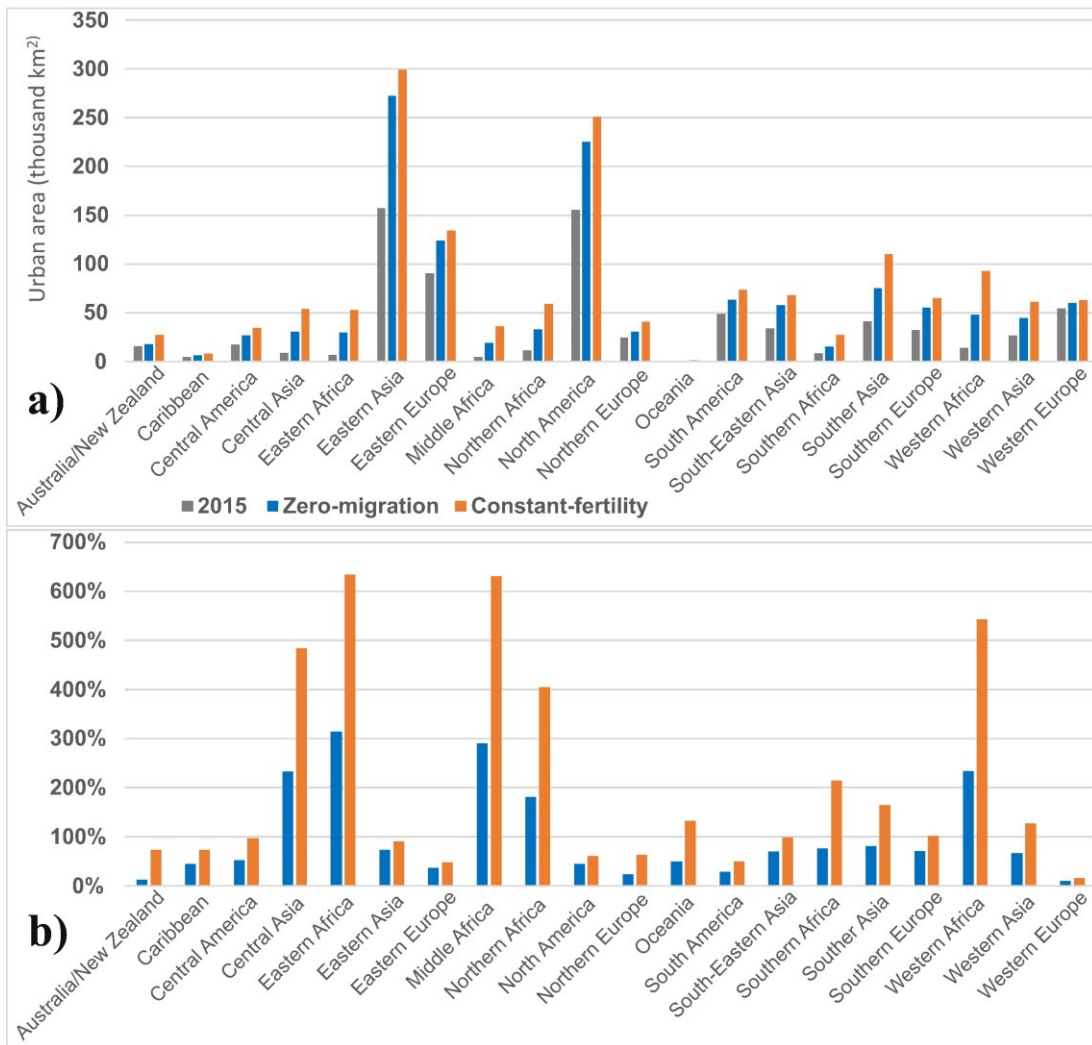
Figure 3.5.   Values for 20 world sub-regions (a) total simulated urban area between 2015 and 2095, and (b) rate of expansion at the sub-regional level under both scenarios.

3.5.3. Country Level Variation of Urbanization Growth

Figure 3.6 presents the values of urban growth change in countries with largest urban extent in each sub-region under both scenarios. At the country level, the simulation outputs demonstrate China, the United States, Russia, and India will have the largest urban extent globally by the year 2095. Under the constant-fertility scenario, the total urban extent of these four countries will account for 37% of the global urban extent by the year 2095. These countries are also indicated to contribute 32% of the global urban expansion that will occur between 2015 and the end of the century under the zero-migration scenario.
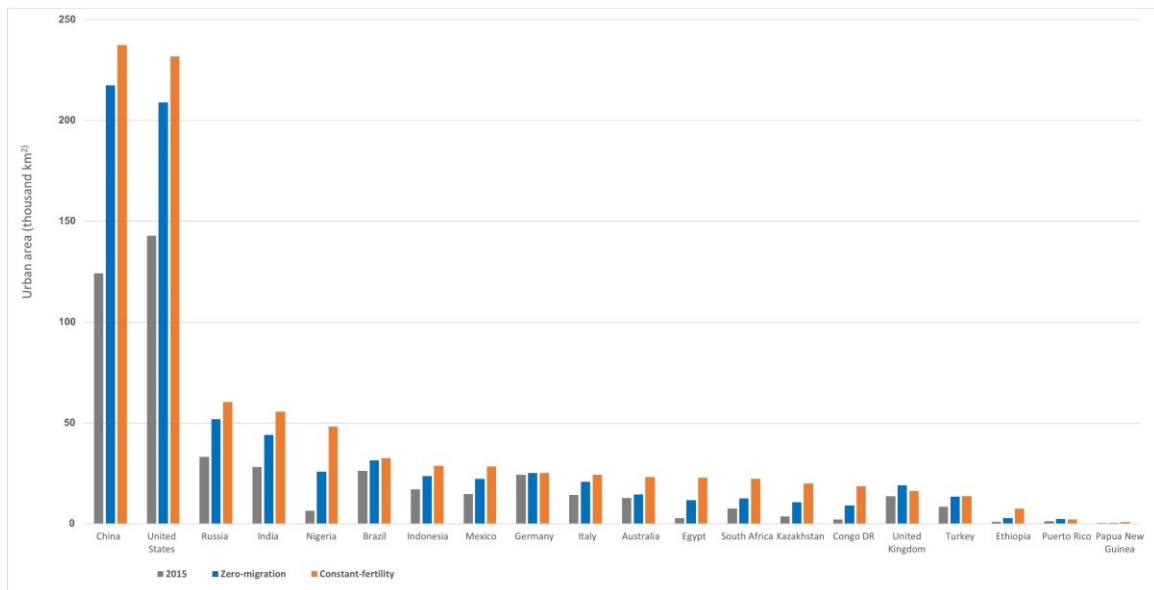
Figure 3.6.   **Obtained simulation values for countries with the largest urban size in each sub-region for the year 2095 compared with the base year 2015.**

Using the United States, China, and Nigeria as examples of countries with different dynamics of urbanization, distinct urban land-use growth patterns emerge. Urbanized countries like the United States have a relatively slow rate of urban expansion while urbanization in China continues at a steady rate. Using the constant-fertility scenario as an example, the rate of urban expansion of the USA and China will be 62% and 91% respectively. Also, the total urban extent of the United States is calculated to reach 232 thousand km^2 while that of China will expand to 238 thousand km^2 by the year 2095 under the constant-fertility scenario (Figure 3.6). On the other hand, the urban extent of Nigeria will continue to expand rapidly with the total urban area reaching 48

thousand km^2 by the year 2095. This increase represents an urban expansion rate of 644%.

In addition to the global, continental, and country level urban expansion simulation analysis, urban development trends at the metropolitan level were also evaluated. Figure 3.7 depicts maps with the simulated urban growth for specific metropolitan areas that exhibit different urbanization dynamics in the period from 2015 to 2095 under the two scenarios. In this research study, metropolitan areas are characterized as slow if its obtained urban expansion rates are lower than 100%, moderate if between 100% and 200%, and rapid if the obtained values are higher than 200%. Based on the obtained simulation results and rates of urban expansion at the metropolitan level, different cities can be classified as slow (e.g., Chicago, Paris, Sao Paulo, London), moderate, (e.g., New Delhi, Johannesburg, Moscow, Mexico City) and rapidly urbanizing (e.g., Beijing, Lagos, Cairo, Bangkok). Metropolitan areas of Chicago (Figure 3.7a), Beijing (Figure 3.7b), and New Delhi (Figure 3.7c) are used as examples of metropolitan regions with these distinct urbanization rates in the period from 2015 to 2095. The simulation results also indicate variations in the size of the extent of urban areas among the three classes of metropolitan regions. For slow urbanizing metropolitan regions like Chicago, London and Paris, there are no substantial growth in urban extent between 2015 and 2095. However, metropolitan areas labelled as rapid urbanization such as Beijing, Cairo, and Lagos experience significant increase in urban extent between the same period. Moderate urbanization regions like Johannesburg, Moscow and New Delhi also show considerable increase in urban extent although less than what is seen in rapid urbanization cities.
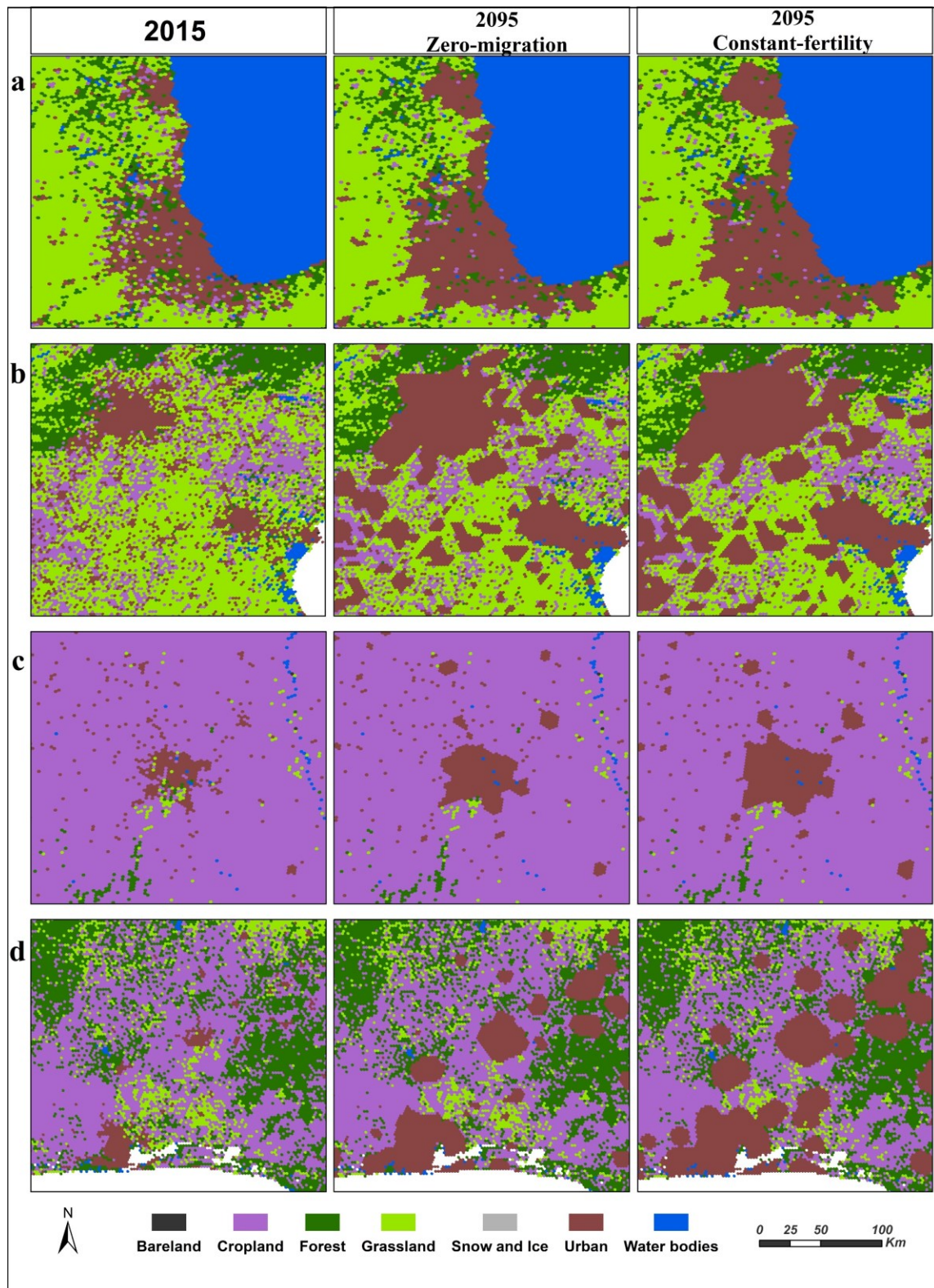
Figure 3.7. Simulated urban extent for year 2095 under zero-migration and constant-fertility scenarios in comparison with initial urban extent at year 2015 in selected metropolitan regions a) Chicago, USA, b) Beijing, China c) New Delhi, India, and d) Lagos/Ibadan

From Figure 3.7 it can be observed that smaller cities at the outskirt of the metropolitan core experience less urban growth under zero-migration while in the constant-fertility scenario, all metropolitan areas including the core and peripheries experience extensive urbanization. Moreover, the urban expansion rates of these metropolitan regions are faster than that of their respective countries' averages, especially under the constant-fertility scenario. As cities expand outward and towards each other, regions with multiple metropolitan cores are merging into larger continuous urban agglomerations or megapolis especially in regions with rapid urban expansion rates as can be seen in the Beijing-Tianjin-Hebei (Jing-Jin-Ji) and Lagos/Ibadan regions as depicted in Figures 3.7b and 3.7d respectively.

3.6. Discussion

This research study proposed and implemented a spherical cellular automata modelling approach to address global and long-term forecast of urban land-use change. The presented model is intended to provide a new and different spatial framework for representing and evaluating urbanization process while considering the global scale and Earth's curvature. Based on obtained results the model was capable of realistically representing the global urban land-use change and *FoM* values for model evaluation indicate the proposed model performs better than the corresponding raster CA model in simulating urban land-use change. The total global urban land size obtained from the spherical model for the year 2015 was 763 thousand km^2 and is commensurate with calculations of other scholars such as Kuang (2019) and Gong et al. (2020) who used finer 30-meter spatial resolution data and divided the Earth surface into 583 sub-grids to compute the global urban land size. The developed spherical CA model simulated a total global urban extent ranging between 1.24 and 1.56 million km^2 by the year 2095 for the two scenarios which is consistent with the study of Gao and O'Neill (2020) who projected a total global urban extent of 1.6 million km^2 close to the end of the 21st century. In addition, the total simulated urban extent of China and USA for the year 2095 is comparable to the simulation outputs obtained by Li et al. (2019). Obtained simulation results are also coherent with urban land-use change theories and research findings. For example, it is widely known that cities are becoming more expansive as the rate of urban growth is higher than the population change (Angel et al., 2011). Thus, the urban land

74

consumption for most countries based on the simulation outcomes increase over time which indicate unsustainable urban development.

The obtained simulation results are consistent with the literature and confirm that in the next few decades, the urbanization process in developing countries would be more extensive and rapid compared to that of developed countries (Seto *et al.*, 2012). Developing countries particularly in Africa and Asia will experience the most dramatic change in growth of cities and urbanization. For example, altogether, cities in China, India, Nigeria, Pakistan, Egypt, and Russia account for 33% of new urban areas by the year 2095 under the constant-fertility scenario, reaching almost an area about the size of the United Kingdom. In addition, more than two thirds of the global urban growth simulated between 2015 and 2095 will take place in Africa and Asia (Huang et al., 2019) which is coherent with the obtained results from this spherical modelling approach.

Given that developing countries are more at risk from environmental problems caused by urbanization and land-use change, and least able to remedy its consequences, the economic, social and environmental gaps between advanced and developing countries is likely to worsen. This means that the UN's Sustainable Development Goals (SDG) (UN-DESA, 2020) regarding urban development, environmental conservation, and reducing inequality between countries are unlikely to be achieved. There is however still a window of opportunity to formulate and implement sustainable urban policies and conservation schemes at global level to handle the negative impacts of rapid urbanization for this century. If these policies are well formulated and implemented, cities in developing countries could become engines of economic development. The comprehensive observation of the global urbanization process, predominantly in developing countries is important in attaining the UN's SDGs (Sun et al., 2020) and the proposed new spherical cellular automata model from this research study can contribute to the improved long-term planning at the global level.

3.7. Conclusions

Urbanization is often seen as a local phenomenon with most urban land-use geosimulation models implemented to simulate land-use change are designed to operate at the local and regional scales. However, the consequences of the urbanization process have several environmental impacts that also include the global scale. Existing

global urban land-use models mostly depend on the raster datasets from remote sensing and GIS data, thus do not consider the effects of geometric distortions due to the nature of Earth surface. This research study and proposed spherical automata model represents a first step towards developing the spherical modelling framework for representing long-term global urbanization process and considering the curved Earth's surface.

Although the simulation results from the proposed model are in agreement with results obtained from other global urban land-use studies, this research study has some limitations and can further be improved by using factors like population density, gross domestic product (GDP) and other drivers of urban land-use change or including multi-criteria evaluation to further guide transition rules. The estimation of the urban land demand using only population data is insufficient as urbanization is influenced by other factors such as economic growth, technology, political conditions, etc. This limitation could lead to underestimation of urban growth in some countries where urban development is not strongly associated with population growth. Additionally, the model could be enhanced if datasets containing wider number of land-use classes and finer spatial or temporal resolution such as for example Sentinel 2A global land-use/land-cover data, however assuming the global coverage is available, this would demand higher computational power to execute the model. In addition, the model can be amended by exploring multiple scenarios related to climate change, decrease of rainfall and sea level rise. It would be beneficial to include multiple indicators to estimate urban land demand as well as other scenarios such as the Shared Socioeconomic Pathways (SSP) and incorporating Earth systems model components with the S-CA to represent the feedback between urban land-use change and other natural systems.

The proposed spherical cellular automata approach implemented in this research study has the potential to be used as a tool to assess present and future global long term urbanization planning strategies, to evaluate possible challenges associated with environment and climate change due to anthropogenic effects and to explore ecological risks. The model outputs can also be an important source of information for global policy building for regional or intergovernmental bodies like the United Nations and its agencies.

3.8. References

Acuto, M., Parnell, S., & Seto, K. C. (2018). Building a global urban science. *Nature Sustainability, 1*, 2-4. doi:10.1038/s41893-017-0013-9

Adamatzky, A., Wuensche, A., & De Lacy Costello, B. (2006). Glider-based computing in reaction-diffusion hexagonal cellular automata. *Chaos, Solitons & Fractals, 27*(2), 287-295. doi:10.1016/j.chaos.2005.03.048

Alderson, T., Purss, M., Du, X., Mahdavi-Amiri, A., & Samavati, F. (2020). Digital Earth Platforms. In H. Guo, M. F. Goodchild, & A. Annoni (Eds.), *Manual of Digital Earth* (pp. 25-54). Singapore: Springer Singapore.

Angel, S., Parent, J., Civco, D. L., Blei, A., & Potere, D. (2011). The dimensions of global urban expansion: Estimates and projections for all countries, 2000-2050. *Progress in Planning, 75*, 53-107. doi:10.1016/j.progress.2011.04.001

Barnes, R. (2020). Optimal orientations of discrete global grids and the Poles of Inaccessibility. *International Journal of Digital Earth, 13*, 803-816. doi:10.1080/17538947.2019.1576786

Batty, M., & Xie, Y. (1994). From cells to cities. *Environment & Planning B: Planning & Design, 21*, 531-548. doi:10.1068/b21s031

Batty, M., Xie, Y., & Sun, Z. (1999). Modeling urban dynamics through GIS-based cellular automata. *Computers, Environment and Urban Systems, 23*(3), 205-233. doi:10.1016/S0198-9715(99)00015-0

Bondaruk, B., Roberts, S. A., & Robertson, C. (2020). Assessing the state of the art in Discrete Global Grid Systems: OGC criteria and present functionality. *Geomatica, 30*, 1-22. doi:10.1139/geomat-2019-0015

Bousquin, J. (2021). Discrete Global Grid Systems as scalable geospatial frameworks for characterizing coastal environments. *Environmental Modelling and Software, 146*, 105210. doi:10.1016/j.envsoft.2021.105210

Brenner, N., & Schmid, C. (2012). Planetary urbanization. In M. Gandy (Ed.), *Urban Constellations* (pp. 10-13). Berlin: Jovis.

Cao, M., Zhu, Y., Quan, J., Zhou, S., Lü, G., Chen, M., & Huang, M. (2019). Spatial sequential modeling and predication of global land use and land cover changes by integrating a global change assessment model and cellular automata. *Earth's Future, 7*, 1102-1116. doi:10.1029/2019EF001228

Chen, G., Li, X., Liu, X., Chen, Y., Liang, X., Leng, J., Xu, X., Liao, W., Qiu, Y. a., Wu, Q., & Huang, K. (2020). Global projections of future urban land expansion under shared socioeconomic pathways. *Nature Communications, 11*, 537. doi:10.1038/s41467-020-14386-x

Clarke, K. C., Hoppen, S., & Gaydos, L. (1997). A self-modifying cellular automaton model of historical urbanization in the San Francisco Bay area. *Environment and Planning B: Planning and Design, 24*(2), 247-261. doi:10.1068/b240247

Creutzig, F., Lohrey, S., Bai, X., Baklanov, A., Dawson, R., Dhakal, S., Lamb, W. F., McPhearson, T., Minx, J., Munoz, E., & Walsh, B. (2019). Upscaling urban data science for global climate solutions. *Global Sustainability, 2*. doi:10.1017/sus.2018.16

D'Ambrosio, D., Di Gregorio, S., & Iovine, G. (2003). Simulating debris flows through a hexagonal cellular automata model: SCIDDICA SCIDDICA S3–hex. *Nat. Hazards Earth Syst. Sci., 3*(6), 545-559. doi:10.5194/nhess-3-545-2003

Engelen, G., White, R., Uljee, I., & Drazan, P. (1995). Using cellular automata for integrated modelling of socio-environmental systems. *Environmental Monitoring and Assessment, 34*(2), 203-214. doi:10.1007/BF00546036

European Space Agency. (2017). *Land Cover CCI Product User Guide Version 2. Tech. Rep.* Retrieved 10 November 2019 from: http://maps.elie.ucl.ac.be/CCI/viewer/download/ESACCI-LC-Ph2-PUGv2_2.0.pdf

Gao, J., & O'Neill, B. C. (2019). Data-driven spatial modeling of global long-term urban land development: The SELECT model. *Environmental Modelling and Software, 119*, 458-471. doi:10.1016/j.envsoft.2019.06.015

Gao, J., & O'Neill, B. C. (2020). Mapping global urban land for the 21st century with data-driven simulations and Shared Socioeconomic Pathways. *Nature Communications, 11*(1), 1-12. doi:10.1038/s41467-020-15788-7

Geist, H., McConnell, W., Lambin, E. F., Moran, E., Alves, D., & Rudel, T. (2006). Causes and Trajectories of Land-Use/Cover Change. In E. F. Lambin & H. Geist (Eds.), *Land-Use and Land-Cover Change: Local Processes and Global Impacts* (pp. 41-70). Berlin, Heidelberg: Springer Berlin Heidelberg.

Gong, P., Li, X., Wang, J., Bai, Y., Chen, B., Hu, T., Liu, X., Xu, B., Yang, J., Zhang, W., & Zhou, Y. (2020). Annual maps of global artificial impervious area (GAIA) between 1985 and 2018. *Remote Sensing of Environment, 236*, 111510. doi:10.1016/j.rse.2019.111510

Grimm, N. B., Faeth, S. H., Golubiewski, N. E., Redman, C. L., Wu, J., Bai, X., & Briggs, J. M. (2008). Global change and the ecology of cities. *Science, 319*, 756-760. doi:10.1126/science.1150195

Hall, C. A. S., Tian, H., Qi, Y., Pontius, G., & Cornell, J. (1995). Modelling Spatial and Temporal Patterns of Tropical Land Use Change. *Journal of Biogeography, 22*(4/5), 753. doi:10.2307/2845977

Hall, J., Wecker, L., Ulmer, B., & Samavati, F. (2020). Disdyakis triacontahedron DGGS. *ISPRS International Journal of Geo-Information, 9*. doi:10.3390/ijgi9050315

Houghton, R. A. (2018). Interactions between land-use change and climate-carbon cycle feedbacks. *Current Climate Change Reports, 4*, 115-127. doi:10.1007/s40641-018-0099-9

Huang, K., Li, X., Liu, X., & Seto, K. C. (2019). Projecting global urban land expansion and heat island intensification through 2050. *Environmental Research Letters, 14*, 114037. doi:10.1088/1748-9326/ab4b71

Iovine, G., D'Ambrosio, D., & Di Gregorio, S. (2005). Applying genetic algorithms for calibrating a hexagonal cellular automata model for the simulation of debris flows characterised by strong inertial effects. *Geomorphology, 66*(1-4 SPEC. ISS.), 287-303. doi:10.1016/j.geomorph.2004.09.017

Kuang, W. (2019). Mapping global impervious surface area and green space within urban environments. *Science China Earth Sciences, 62*, 1591-1606. doi:10.1007/s11430-018-9342-3

Lambin, E. F., Turner, B. L., Geist, H. J., Agbola, S. B., Angelsen, A., Bruce, J. W., Coomes, O. T., Dirzo, R., Fischer, G., Folke, C., George, P. S., Homewood, K., Imbernon, J., Leemans, R., Li, X., Moran, E. F., Mortimore, M., Ramakrishnan, P. S., Richards, J. F., Skånes, H., Steffen, W., Stone, G. D., Svedin, U., Veldkamp, T. A., Vogel, C., & Xu, J. (2001). The causes of land-use and land-cover change: Moving beyond the myths. *Global Environmental Change, 11*, 261-269. doi:10.1016/S0959-3780(01)00007-3

Li, M., & Stefanakis, E. (2020). Geospatial Operations of Discrete Global Grid Systems — a Comparison with Traditional GIS. *Journal of Geovisualization and Spatial Analysis, 4*(26).

Li, X., Chen, G., Liu, X., Liang, X., Wang, S., Chen, Y., Pei, F., & Xu, X. (2017). A new global Land-use and land-Cover change product at a 1-km resolution for 2010 to 2100 based on human–environment interactions. *Annals of the American Association of Geographers, 107*, 1040-1059. doi:10.1080/24694452.2017.1303357

Li, X., Zhou, Y., Eom, J., Yu, S., & Asrar, G. R. (2019). Projecting global urban area growth through 2100 based on historical time series data and future shared socioeconomic pathways. *Earth's Future, 7*(4), 351-362. doi:10.1029/2019EF001152

Mahdavi-Amiri, A., Samavati, F., & Peterson, P. (2015). Categorization and conversions for indexing methods of discrete global grid systems. *ISPRS International Journal of Geo-Information, 4*, 320-336. doi:10.3390/ijgi4010320

Meiyappan, P., Dalton, M., O'Neill, B. C., & Jain, A. K. (2014). Spatial modeling of agricultural land use change at global scale. *Ecological Modelling, 291*, 152-174. doi:10.1016/j.ecolmodel.2014.07.027

Meyfroidt, P., Lambin, E. F., Erb, K.-H., & Hertel, T. W. (2013). Globalization of land use: distant drivers of land change and geographic displacement of land use. *Current Opinion in Environmental Sustainability, 5*(5), 438-444. doi:10.1016/j.cosust.2013.04.003

Nugraha, A. T., Waterson, B. J., Blainey, S. P., & Nash, F. J. (2020). On the consistency of urban cellular automata models based on hexagonal and square cells. *Environment and Planning B: Urban Analytics and City Science*, 1-15. doi:10.1177/2399808319898501

Organisation for Economic Co-operation and Development. (2015). *The Metropolitan Century: Understanding urbanization and its consequences*. Paris: OECD Publishing.

Radwan, T. M., Blackburn, G. A., Whyatt, J. D., & Atkinson, P. M. (2021). Global land cover trajectories and transitions. *Scientific Reports, 11*(1), 1-16. doi:10.1038/s41598-021-92256-2

Robertson, C., Chaudhuri, C., Hojati, M., & Roberts, S. A. (2020). An integrated environmental analytics system (IDEAS) based on a DGGS. *ISPRS Journal of Photogrammetry and Remote Sensing, 162*, 214-228. doi:10.1016/j.isprsjprs.2020.02.009

Romero-Lankao, P., Gurney, K. R., Seto, K. C., Chester, M., Duren, R. M., Hughes, S., Hutyra, L. R., Marcotullio, P., Baker, L., Grimm, N. B., Kennedy, C., Larson, E., Pincetl, S., Runfola, D., Sanchez, L., Shrestha, G., Feddema, J., Sarzynski, A., Sperling, J., & Stokes, E. (2014). A critical knowledge pathway to low-carbon, sustainable futures: Integrated understanding of urbanization, urban areas, and carbon. *Earth's Future, 2*, 515-532. doi:10.1002/2014ef000258

Sahr, K. (2011). Hexagonal discrete global GRID systems for geospatial computing. *Archives of Photogrammetry, Cartography and Remote Sensing, 22*, 363-376.

Sahr, K. (2020). DGGRID version 7.1. Retrieved August 2020 from https://github.com/sahrk/DGGRID

Sassen, S. (2005). The global city : Introduction concept. *Brown Journal of World Affair, 38*, 557-573.

Schaldach, R., & Priess, J. A. (2008). Integrated models of the land system: A review of modelling approaches on the regional to global ccale. *Living Reviews in Landscape Research, 2*, 1-34. doi:10.12942/lrlr-2008-1

Seto, K. C., Golden, J. S., Alberti, M., & Turner, B. L. (2017). Sustainability in an urbanizing planet. *Proceedings of the National Academy of Sciences of the United States of America, 114*(34), 8935-8938. doi:10.1073/pnas.1606037114

Seto, K. C., Güneralp, B., & Hutyra, L. R. (2012). Global forecasts of urban expansion to 2030 and direct impacts on biodiversity and carbon pools. *Proceedings of the National Academy of Sciences of the United States of America, 109*, 16083-16088. doi:10.1073/pnas.1211658109

Shoman, W., Alganci, U., & Demirel, H. (2019). A comparative analysis of gridding systems for point-based land cover/use analysis. *Geocarto International, 34*(8), 867-886. doi:10.1080/10106049.2018.1450449

Sitch, S., Brovkin, V., von Bloh, W., van Vuuren, D., Eickhout, B., & Ganopolski, A. (2005). Impacts of future land cover changes on atmospheric CO2 and climate. *Global Biogeochemical Cycles, 19*, 1-15. doi:10.1029/2004GB002311

Sun, L., Chen, J., Li, Q., & Huang, D. (2020). Dramatic uneven urbanization of large cities throughout the world in recent decades. *Nature Communications, 11*(1), 5366. doi:10.1038/s41467-020-19158-1

Torrens, P. M., & Benenson, I. (2005). Geographic automata systems. *International Journal of Geographical Information Science, 19*(4), 385-412. doi:10.1080/13658810512331325139

Trunfio, G. A. (2004, 2004//). *Predicting Wildfire Spreading Through a Hexagonal Cellular Automata Model.* Paper presented at the Cellular Automata, Berlin, Heidelberg.

Uber Technologies Inc. (2020). H3: Hexagonal hierarchical geospatial indexing system. Retrieved July 2020 from https://h3geo.org/

United Nations - Department of Economic and Social Affairs: Population Division. (2020). *World Population Prospects 2019*. Retrieved 9 November 2020 from: https://population.un.org/wpp/

United Nations - Department of Economic and Social Affairs: Statistics Division. (2019). *World urbanization prospects; The 2018 revison (ST/ESA/SER.A/420)*. New York: United Nations.

United Nations - Department of Economic and Social Affairs: Statistics Division. (2020). The 17 sustainable development goals. Retrieved 21 April from https://sdgs.un.org/goals/goal10

United Nations - Department of Economic and Social Affairs: Statistics Division. (2021). Standard country or area codes for statistical use (M49). Retrieved April from https://unstats.un.org/unsd/methodology/m49/

Usery, E. L., & Seong, J. C. (2001). All equal-area map projections are created equal, but some are more equal than others. *Cartography and Geographic Information Science, 28*, 183-193. doi:10.1559/152304001782153053

Van Rossum, G., & Drake, F. (2009). *Python 3 Reference Manual*. Scotts Valley, CA: CreateSpace.

Varga, O. G., Pontius, R. G., Singh, S. K., & Szabó, S. (2019). Intensity Analysis and the Figure of Merit's components for assessment of a Cellular Automata – Markov simulation model. *Ecological Indicators, 101*(June 2019), 933-942. doi:10.1016/j.ecolind.2019.01.057

Ventrella, J. (2011). Glider dynamics on the sphere: Exploring cellular automata on geodesic grids. *Journal of Cellular Automata, 6*, 245-256.

Verburg, P. H., Alexander, P., Evans, T., Magliocca, N. R., Malek, Z., Rounsevell, M. D., & van Vliet, J. (2019). Beyond land cover change: towards a new generation of land use models. *Current Opinion in Environmental Sustainability, 38*, 77-85. doi:10.1016/j.cosust.2019.05.002

Verburg, P. H., Crossman, N., Ellis, E. C., Heinimann, A., Hostert, P., Mertz, O., Nagendra, H., Sikor, T., Erb, K. H., Golubiewski, N., Grau, R., Grove, M., Konaté, S., Meyfroidt, P., Parker, D. C., Chowdhury, R. R., Shibata, H., Thomson, A., & Zhen, L. (2015). Land system science and sustainable development of the earth system: A global land project perspective. *Anthropocene, 12*, 29-41. doi:10.1016/j.ancene.2015.09.004

Verburg, P. H., Schot, P. P., Dijst, M. J., & Veldkamp, A. (2004). Land use change modelling: Current practice and research priorities. *GeoJournal, 61*, 309-324. doi:10.1007/s10708-004-4946-y

Wang, R., Ben, J., Zhou, J., & Zheng, M. (2020). Indexing mixed aperture icosahedral hexagonal discrete global grid systems. *ISPRS International Journal of Geo-Information, 9*. doi:10.3390/ijgi9030171

White, R., & Engelen, G. (2000). High-resolution integrated modelling of the spatial dynamics of urban and regional systems. *Computers, Environment and Urban Systems, 24*, 383-400. doi:10.1016/S0198-9715(00)00012-0

World Database on Protected Areas. (2020). *Global database on terrestrial and marine protected areas*. Retrieved 4 March 2020 from: https://www.protectedplanet.net/en/search-areas?filters%5Bdb_type%5D%5B%5D=wdpa&geo_type=region

Yao, X., Li, G., Xia, J., Ben, J., Cao, Q., Zhao, L., Ma, Y., Zhang, L., & Zhu, D. (2020). Enabling the big earth observation data via cloud computing and DGGS: Opportunities and challenges. *Remote Sensing, 12*, 1-15. doi:10.3390/RS12010062

Zhou, Y., Varquez, A. C. G., & Kanda, M. (2019). High-resolution global urban growth projection based on multiple applications of the SLEUTH urban growth model. *Scientific Data, 6*, 1-10. doi:10.1038/s41597-019-0048-z

Chapter 4.

Integrating Multi-criteria Analysis and Spherical Cellular Automata Approach for Modelling Global Urban Land-use Change[3]

4.1. Abstract

Existing geosimulation land-use change models are predominantly designed to operate at local or regional spatial scales. When these models are applied on data at the global level, they do not consider the effects of spatial distortions caused by the curvature of the Earth's surface and often lack some refinements related to land suitability analysis. Therefore, the main objective of this study is to integrate multi-criteria evaluation with spherical cellular automata, to develop a novel modelling approach for simulating global urban land-use change. The world region is clustered into sub-regions to improve the suitability analysis. The obtained results reveal differences in urban growth rate and the size of the extent across the four clusters. The 64% of the total global urbanization are occurring in urban region clusters characterized by high gross domestic product and population density, while urban regions in isolated locations have the lowest urban growth rate.

4.2. Introduction

Land-use and land-cover changes can be perceived as a complex dynamic spatial system that characterize the alteration of the Earth surface mainly through human activities thus having different consequences on the natural environment (Turner et al., 2021; Winkler et al., 2021). Urban land-use change research studies have become prominent in the past decades due to the several global sustainability problems and consequences associated with urban sprawl (Nuissl & Siedentop, 2021). To examine and model urban land-use dynamics, a number of spatially explicit land-use change models reported in the scientific literature were designed mainly for small scale

---

[3] A version of this chapter is published: Addae, B., & Dragićević, S. (2023). Integrating multi-criteria analysis and spherical cellular automata approach for modelling global urban land-use change. *Geocarto International, 38*(1).

applications. The utilization of these models for simulating urban land-use change patterns and possible future scenarios at larger spatial scales poses challenges that are peculiar to spatial modelling at the global scale.

Urban land-use models that represent the dynamics of change generally use geospatial data from remote sensing (RS) and geographic information systems (GIS) predominantly in raster GIS data format, thus they are implemented with traditional two-dimensional (2D) spatial tessellation. While such models are suitable to address dynamics of urban land-use change at the local or regional levels, this however is not suitable when addressing global modelling due to spatial distortions caused by the curvature of the Earth surface. Distortions are minimal at the local level but are however pronounced at larger spatial scales which incur errors in some spatial and statistical analyses especially at the global level (Ellis et al., 2021; Hall et al., 2020). For example, the shape and size of geospatial data represented in geographic coordinate system (GCS) change from square cells at the equator to triangles at the poles (Hojati et al., 2022; Zhai et al., 2010). Although equal-area projections such as Goode's Homolosine and Cylindrical equal-area are often used for large scale spatial analysis, global land-use change models implemented with these projections however produce spatial distortions (Cao et al., 2019; Li et al., 2017). Further, commonly used global equal-area projections still have area and shape distortions when used to represent global raster datasets (de Sousa et al., 2019). Discrete global grid systems (DGGS) have been developed as spatial referencing system which utilizes spherical tessellations to better represent the Earth's surface (Purss et al., 2019). DGGS provide a geospatial framework for global spatial analyses and modelling with equal surface area cells. DGGS also supports multiple cell typologies including hexagonal grids, which have been receiving considerable interest recently because of the advantages they offer over square and triangle cell types when used for geospatial operations. For instance, hexagonal cells have uniform adjacency and neighbouring relationships and can closely approximate circular regions (Sahr, 2011; Zhao et al., 2022). Among regular cells, hexagons are the most compact in tessellating the sphere (Robertson et al., 2020). When used to implement cellular automata (CA) models, hexagonal cells also provide unambiguous spatial neighbourhood and have been indicated to produce more accurate outputs compared to square cells (Iovine et al., 2005; Nugraha et al., 2020). Hexagonal DGGS as a geospatial data model can offer appropriate basis for spatial analysis and

simulation at the global level (Kiester & Sahr, 2008). Spherical CA also provide an suitable grid topology for modelling and understanding naturally closed systems at the global scale (Ventrella, 2011). In a hexagonal grid, the relative location and neighbourhood of cells can be defined using the hexagonal coordinate system which has three coordinate axes that are evenly spaced apart and are usually denoted as i, j, k. A central cell has six neighbouring cells that are equidistant from each other thus making the neighbourhood more compact. Measuring distance on the hexagonal grid can be expressed as the number of cell rings from the origin (Li & Stefanakis, 2020).

Existing global urban land-use change modelling approaches simulate urban change using mainly SLEUTH (Zhou et al., 2019), probabilistic (Seto et al., 2012), cellular automata (Li et al., 2016), statistical (Gao & O'Neill, 2019), and machine learning techniques (Chen et al., 2022). Although these modelling techniques are capable of representing the determinants of urban land-use change and simulating land-use patterns, the underlying techniques in these models have been criticized for lack of integration of decision-making capabilities (National Research Council, 2014; Verburg et al., 2015). Multicriteria evaluation (MCE) techniques have been developed and widely adopted as GIS-based decision-making approaches for solving spatial problems (Malczewski, 1996). MCE provides a collection of methods and procedures for structuring and solving decision problems involving multiple criteria and when integrated with GIS can assist in broad range of spatial and geographical applications (Malczewski & Jankowski, 2020). MCE can be utilized in characterizing decision-making processes of various stakeholders and subject experts to solicit their opinions in various stages from choice of criteria to weights. In addition, in land-use change modelling, MCE is often coupled with cellular automata (CA) to enhance the function of transition rules (Cao et al., 2014; Wu & Webster, 1998) that improves model capacity to forecast. There has been a significant number of studies that have incorporated MCE methods in CA models of urban land-use change to improve the simulation abilities (Masoudi et al., 2021; Mohamed & Worku, 2020; Rimal et al., 2018). However, these studies are conducted at smaller spatial extents with majority of them operationalized at the city or metropolitan region level. Currently, there are no available MCE-CA methods designed to simulate urban development at global scale.

Given the capabilities of cellular automata to capture local interactions and complexity of space-time dynamics of urban land-use process, the merit of MCE in

representing human decision-making for land suitability analysis, and DGGS hexagonal grids in tessellating spherical surfaces, the main objective of this research study is to develop and implement a novel global MCE spherical-CA (MCE-S-CA) model to simulate urban land-use change. The proposed model can be utilized by various stakeholders and interested parties to simulate possible future global scale urban growth scenarios and examining the causes and effects of urban land-use change on the environment.

4.3. Methodology

4.3.1. Datasets

Several geospatial datasets that allow for global Earth coverage have been used in this research study. Due to the unavailability of datasets originally captured in DGGS formats, the study utilized existing geospatial datasets in geographic coordinate system (GCS). Datasets for the years 1995, 2005 and 2015 were used to implement and evaluate the proposed MCE-S-CA model. Global land-use/land-cover data were acquired from the European Space Agency portal (ESA, 2017). Gridded population density dataset was obtained from LandScan (Rose et al., 2020) and gross domestic product (GDP) from National Centers for Environmental Information (NCEI) (Ghosh et al., 2011). Location of protected areas were obtained from the World Database on Protected Areas (WDPA) online data catalogue (WDPA, 2020). Global digital elevation model (DEM) was acquired from the United States Geological Survey (USGS) data portal (USGS, 2020). Also, global road dataset was obtained from the Global Road Inventory Project (Meijer J.R. et al., 2018). The proposed modelling framework utilizes data that are mapped to a specified DGGS consisting of hexagonal cells with each covering an area of 0.63 km^2 with edge and long diagonal dimensions of 0.49 km and 0.99 km respectively thus used as the spatial resolution of the model. The conversion of existing spatial datasets to DGG cells follows the techniques described in Robertson et al. (2020).

4.3.2. Model Overview

The systematic workflow of the proposed MCE-S-CA model is presented in Figure 4.1 and consists of four main steps. The first step entails creating geospatial

86

database and defining the decision problem which in this context involves finding suitable locations for urban development at the global scale and considering the spherical Earth surface. Subsequently, criteria that are relevant to urban development are identified within the urban science literature and corresponding suitability functions are developed for each of them.
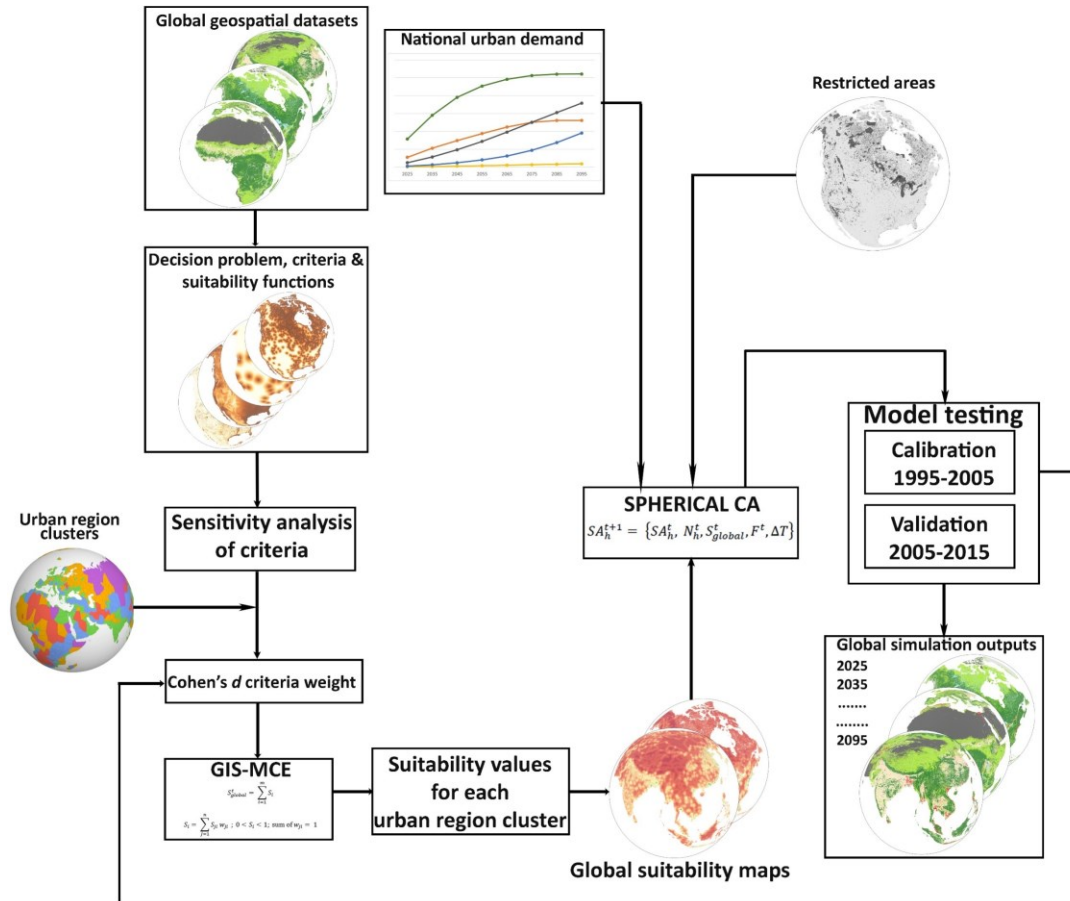
Figure 4.1. **Workflow of the MCE-S-CA modelling framework for simulation of the long-term urban growth dynamics at the global scale.**

The second step comprises sensitivity analysis of selected criteria and classification of urban regions into clusters based on their similarities. Sensitivity analysis was performed to evaluate the influence of the selected criteria on overall suitability analysis. Global urbanization is characterized by diverse dynamics of various regions represented by different criteria that need different preferences. The clustering was used to identify urban regions with similar characteristics and then grouped into urban region clusters to enhance the suitability analysis.

The third step involves implementing GIS-MCE by generating criteria weights which reflect the relative importance of each criterion in the decision-making process. Given that actual stakeholders were not involved in this process, Cohen's *d* criteria weight method has been applied to derive the values for the weights. Within the hexagonal data framework, criteria and weights were standardized to obtain the overall suitability values. The analysis is performed for each urban region cluster and combined to form the global suitability map which is then used as input to the spherical cellular automata (S-CA) model.

In the fourth step, the model is evaluated and then implemented to simulate urban land-use change. The temporal resolution of the model was determined to be 10 years based on the time interval of the available land-use datasets used in building and evaluating the model. This time period is also adequate to monitor and quantify the urban land-use change across the globe. Model evaluation comprises calibration using datasets for year 1995 and 2005 and validation using 2005 and 2015 data. For the period from 2015 to 2095 with each iteration corresponding to 10 years, the S-CA model generates the simulation outputs of urban land-use change based on obtained suitability values and considering national urban demand data and protected regions as constraints. The detailed description of each step of the proposed MCE-S-CA model is presented in the following sub sections.

4.3.3. Selection of Criteria and Suitability Functions

The identified criteria for this research study can be classified into three groups: socio-economic, biophysical, and proximity. Table 4.1 presents all selected criteria and their respective suitability functions in vertex notation and for GIS data layers with hexagonal cells. Suitability function values span from 0 to 1, where 1 indicate a full satisfaction for a criterion and 0 no satisfaction. Figure 4.2 was generated to present the spherical maps for all the criteria however depicted only for North America due to simplicity reasons. For each criterion, locations with maximum suitability are indicated in darker shades of brown while unsuitable locations are depicted in light brown.

Table 4.1.   Identified criteria and their respective suitability functions in vertex notation with justifications.

Group	Criteria	Suitability functions	Units	Justifications
Socio-economic	Gross domestic product (GDP)	GDP = [(816,1), (0,0)]	Million dollars per cell	Higher economic development boosts further urban development (Mahtta *et al.*, 2022)
	Population density	Population = [(64161,1), (0,0)]	Inhabitants per cell	New urban development generally occurs closer to densely populated areas (Li & Cao, 2019)
Biophysical	Slope	Slope = [(5,1), (50,0)]	Degrees	Areas with gentle slopes are preferred for urban development (Yan et al., 2020)
	Elevation	Elevation = [(100,1), (4000,0)]	Metres	Areas at lower elevation are more suitable for urban development (Mohamed & Worku, 2020)
Proximity	Proximity to coast & inland water bodies	Water = [(0.99,1), (4.95,0)]	Kilometres	Water bodies provide scenic views and recreational activities (Zhao *et al.*, 2021)
	Proximity to commercial areas	Commercial = [(0.99,1), (9.9,0)]	Kilometres	Proximity to commercial areas provides economic services and opportunities (Musa *et al.*, 2019)
	Proximity to exiting urban areas	Urban = [(0.99,1), (4.95, 0)]	Kilometres	Urban expansion typically occurs in proximity to existing urban development (Rimal *et al.*, 2018)
	Proximity to major roads	Road = [(0.99, 1), (5.94, 0)]	Kilometres	Connection to transportation networks enhances urban development (Yang *et al.*, 2018)

The socio-economic criteria consist of gross domestic product (GDP) and population density. The maximum and minimum values were utilized in developing the GDP and population density suitability functions based on previous studies (Feng et al., 2019; Zhang et al., 2020) that applied socio-economic criteria for analysing urban development suitability. Economic factors are a major determinant of urban development and high GDP is often used as an indicator for high economic activities (He et al., 2014). Areas with high economic activities provide job opportunities as well as financial capital for urban development, thus there is a strong correlation between economic development and urban expansion (Mahtta et al., 2022). The GDP suitability function (Figure 4.2a) is expressed as a linear membership where locations of highest satisfaction are for a value of 816 million dollars per cell which represents the maximum GDP value obtained from the available GDP data. High population density create high

demand for urban development and are often preferred for future development by urban developers (Kim et al., 2020; Wu et al., 2021). These areas also indicate existing support for urban land development. New urban development tends to occur in and around densely populated areas (Bagan & Yamagata, 2015). The population density suitability function utilizes a linear membership based on the obtained maximum value from the available data which is 64,161 inhabitants per hexagonal cell (Figure 4.2b).
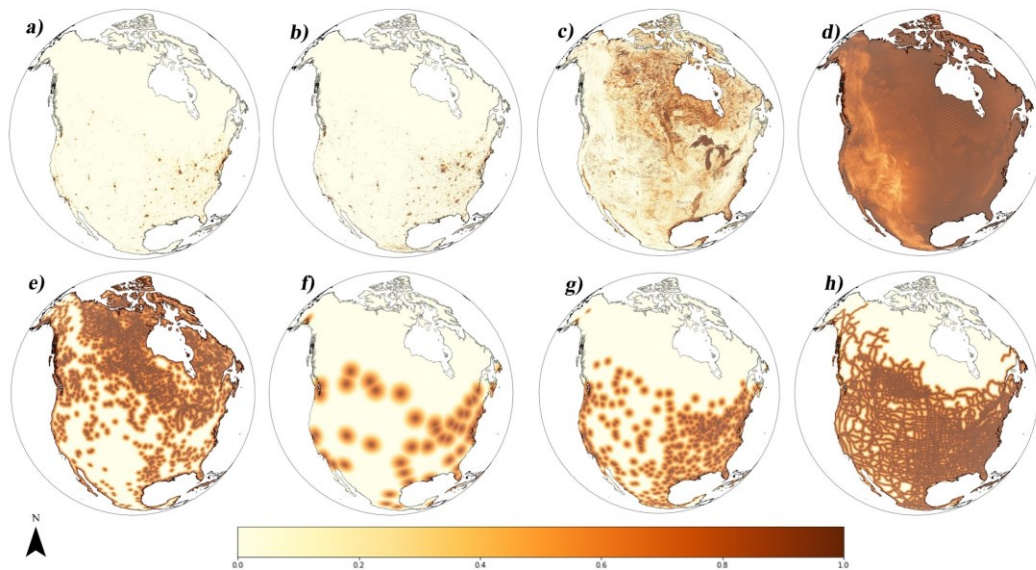
Figure 4.2. **Criterion maps of North America only and based on suitability functions for each criterion: a) GDP, b) Population density, c) Slope, d) Elevation, e) Proximity to coast & inland water bodies, f) Proximity to commercial areas, g) Proximity to exiting urban areas, and h) Proximity to major roads.**

Within the biophysical group are slope and elevation criteria. These two criteria can provide physical limitations to urban development. Generally, flat and gentle slopes are more prone to have urban development as it demands less cost and susceptible to surface run-off and soil erosion (Steiner et al., 2000; Zhou et al., 2021). For the slope suitability function (Figure 4.2c), gradients less than 5º yield maximum satisfaction and slopes steeper than 50º are considered unsuitable. Elevation can influence urban development especially in regions with rugged terrain. Urban development in higher elevation areas increases cost of construction and transportation. Generally, majority of urban development worldwide occurs in areas with lower elevation (Kii & Nakamura, 2017). However, there are selected cities in high elevation for example Calgary, Canada, Denver, US, La Paz, Bolivia, Quito, Ecuador, Bogota, Columbia, and Addis Ababa, Ethiopia, thus they are taken into consideration for the choice of 4,000m as the

maximum elevation. The suitability function (Figure 4.2d) is fully satisfied in locations where elevation is less than 100m and decreases with increasing elevation after 100m with no satisfaction above 4,000m.

The proximity criteria comprise of proximity to coast & inland water bodies, commercial areas, existing urban areas, and major roads. Proximity to coast and inland water bodies provide natural scenery, good views, and opportunities for recreational and sporting activities (Zhao et al., 2021). New urban development typically occurs closer to these areas due to the services they offer (Cai et al., 2018). The approximated distance of 5km was used as research suggest services provided by water bodies decreases significantly after 5km (Baró et al., 2016; Wen et al., 2017). The suitability function proximity to coast & inland water bodies (Figure 4.2e) has no satisfaction in locations within 0.99km of coastline and water bodies due to the risk of flood. This distance is equivalent to one hexagonal cell in the spatial data layer. The suitability function has maximum satisfaction after 0.99km and decreases monotonically with no satisfaction beyond 4.95km which corresponds to five rings of hexagonal cells.

Jobs and employment opportunities are usually concentrated in the commercial areas of cities and also offer agglomeration advantages (Gharaibeh et al., 2020). People prefer to live closer to where they work to reduce the time and cost of commuting. Prior studies indicate compact urban growth is typically concentrated within 10km distance of commercial areas (Cengiz et al., 2022). The proximity to commercial areas suitability function (Figure 4.2f) is fully satisfied in locations within 0.99km of commercial areas and decreases with increasing distance with no satisfaction beyond 9.9km that is represented by 10 hexagonal cells.

Proximity to existing urban areas criterion depict the influence of urban development process as the closer a parcel of land is to urban areas, the easier it is for developers to build new residential areas (Wu & Yeh, 1997). Urban areas provide access to good road networks, already existing amenities, and commercial services among others (Bhatta, 2010). Research confirms urban land develops near existing urban areas and 5km is typically used as the maximum distance for suitability in urban land-use change studies (Rimal et al., 2018). The suitability function for proximity to existing urban areas (Figure 4.2g) is fully satisfied in locations within 0.99km of existing

urban areas and decreases after 0.99km becoming unsuitable beyond 4.95km while considering the size of the hexagons.

Major roads link urban areas together, boost fringe development and provide access to amenities hence, urban development usually occurs in areas with access to major roads (Luo & Wei, 2009). The chosen distance for the suitability function is based on studies by Yang et al. (2018) who indicated no significant change in urban development suitability beyond 6km of major roads. The suitability function proximity to major roads (Figure 4.2h) yields maximum satisfaction in locations within 0.99km of major roads and decreases gradually with no satisfaction after 5.94km, and the distance is equivalent to six hexagonal cells.

4.3.4. Criteria Sensitivity Analysis and Urban Region Clustering

Typically, sensitivity analysis examines the influence of input parameters on the model output variability (Saltelli et al., 2000). To determine the impact of individual criteria on overall suitability in different regions, criteria sensitivity test was performed using global sensitivity analysis (Ligmann-Zielinska & Jankowski, 2014). The technique computes sensitivity and uncertainly from suitability surfaces generated using Monte Carlo simulations and applies variance decomposition methods to allocate model variability to each criterion. Table 4.2 presents results of the global sensitivity analysis for some selected urban regions with distinctive characteristics.

Table 4.2. **Obtained sensitivity values for all criteria in some selected urban regions.**

Criteria	London	Shanghai	Quito	Riyadh	Moscow	New Delhi	Indianapolis
GDP	0.279	0.176	0.333	0.454	0.366	0.208	0.425
Population density	0.196	0.202	0.182	0.294	0.193	0.034	0.305
Slope	0.039	0.076	0.056	0.012	-0.106	-0.069	0.016
Elevation	-0.006	-0.058	0.612	0.044	-0.089	0.092	0.282
Proximity to coast & inland water bodies	0.102	0.114	0.125	-0.049	0.262	-0.103	0.134
Proximity to commercial areas	0.164	0.203	0.676	0.688	0.417	0.218	0.472
Proximity to exiting urban areas	0.209	0.056	0.655	0.705	0.661	0.543	0.470
Proximity to major roads	0.067	0.079	0.347	0.357	0.268	0.136	0.315

While urban development is influenced by similar criteria across different regions, the degree of influence varies. For this reason, there was the need to perform clustering analysis of urban regions to capture the specific similarities within them. The aim is to minimize the differences between urban regions in the same cluster while maximizing differences between the clusters. The world region was divided into 1860 sub areas based on the location of existing cities with population greater than 300,000 inhabitants as per data from 2018 of the United Nations Department of Economic and Social Affairs (UN-DESA)(UN-DESA, 2020). The k-means clustering technique (Jain, 2010) was used due its ability to specify number of clusters (k) suitable for the purpose of this study. Too many or too few clusters would not capture the main characteristics of urban regions. Therefore, four clusters have been chosen to group the sub areas based on similarities related to their biophysical and socioeconomic characteristics. The resulting clusters as global maps are presented in Figure 4.3.
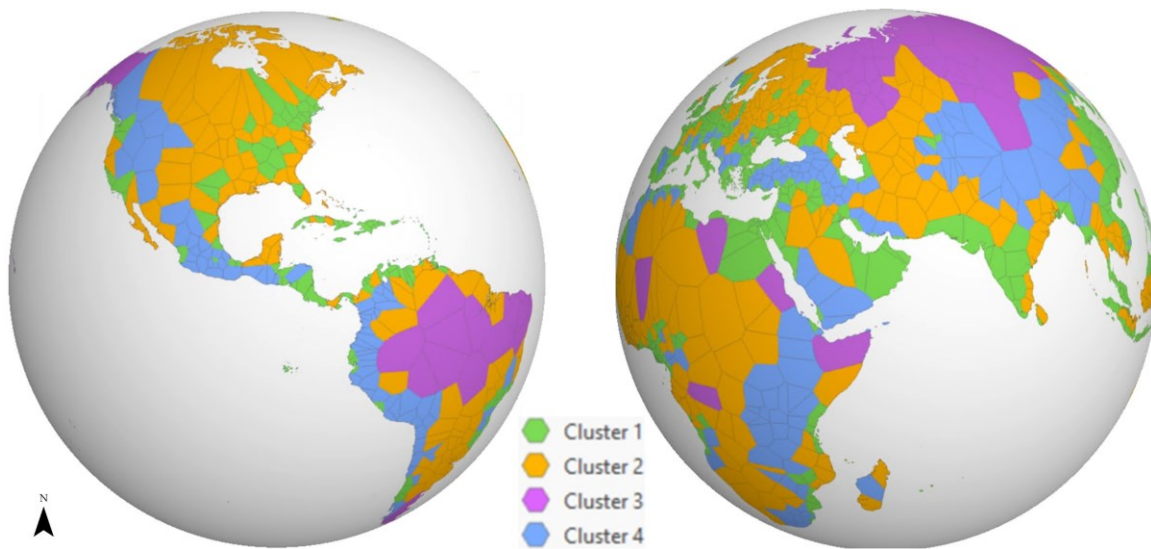
Figure 4.3.   Results of urban region classification into four clusters based on their characteristics.

Cluster 1 consists of urban regions with high population density and GDP, located mainly along the coast or major water bodies consisting of metropolitan areas such as London, New York, Tokyo, Shanghai, Sao Paulo, Los Angeles, and Paris. Cluster 2 represents urban regions with average population density and GDP in low elevation urban regions like Montreal, Houston, Melbourne, Abidjan, and New Orleans. Cluster 3 characterizes urban regions with low population density and GDP in isolated locations such as Brisbane, Anchorage, Manaus, and Niamey. Cluster 4 comprises of

inland urban regions with average population density and GDP in areas with high elevation including Denver, Brasilia, Johannesburg, Riyadh, Calgary, and Quito.

4.3.5. Criterion Weights and GIS-MCE Technique

Criterion weights are generated to reflect the relative influence of each criterion on suitability for urban development. In most GIS-based MCE methods, weights are generally determined by subject experts or stakeholders. Given that this research study addresses the first global MCE-CA urban land-use change model and due to lack of resources, it was however not possible to elicit the opinions of various stakeholders and interest groups. Thus, criterion weights were generated for each urban region cluster using the Automatic Weight Selection technique (Veronesi et al., 2017). The technique uses statistical analysis based on the comparison between randomly sampled cells from spatial data layer representing the selected criteria and urban land-use type cells within each urban region cluster from the land-use data layer. From these two data layers, the Cohen's d (Cohen, 1988) values are computed for each criterion. The generated Cohen's d values are normalized so their sum is equal to 1. This technique is applied to obtain the criterion weights for each urban region cluster and the obtained values are presented in Table 4.3.

Table 4.3.   **Criterion weights based on Cohen's d for the four urban region clusters.**

Criteria	Criteria weight for urban region			
	Cluster 1	Cluster 2	Cluster 3	Cluster 4
GDP	0.1894	0.2554	0.2169	0.2211
Population density	0.1259	0.1108	0.1639	0.1166
Slope	0.0159	0.0135	0.0834	0.0527
Elevation	0.0936	0.0744	0.0870	0.0595
Proximity to coast & inland water bodies	0.0990	0.0984	0.1187	0.0097
Proximity to commercial areas	0.1632	0.0912	0.0099	0.1875
Proximity to existing urban areas	0.2055	0.2213	0.1979	0.2223
Proximity to major roads	0.1074	0.1351	0.1224	0.1308

The final step entails calculating the suitability value of each hexagonal cell using the GIS-MCE method. Overall suitability value for each hexagonal cell at the global level S_{global}^{t} at time t can be calculated as sum of suitability values S_i for each hexagonal cell

of urban region cluster *i (i=1,..., m)* and is based on weighted linear combination (WLC) approach as follows:

$$S_{global}^t = \sum_{i=1}^{m} S_i \qquad (1)$$

$$S_i = \sum_{j=1}^{n} S_{ji}\, w_{ji} \; ; \; 0 < S_i < 1; \; \text{sum of } w_{ji} = 1$$

where S_{ji} is the standardized criterion value based on suitability function transforming the input value of the criterion *j (j=1,..., n)*, *n* denotes number of criteria, *m* is number of urban region clusters and w_{ji} is the weight of importance assigned to criterion *j* and urban region cluster *i*. The generated urban development suitability values are classified using equal interval method into five classes such as: very low (0-0.2), low (0.21-0.4), medium (0.41-0.6), high (0.61-0.8), and very high (0.81-1). Figure 4.4 presents the global suitability output displayed as spherical maps for each part of the Earth.

4.3.6. Spherical CA Model

The spherical cellular automata part of the model (Figure 4.1) is designed to simulate urban land-use change by integrating the GIS-MCE component and the obtained suitability values as model input, and the constrains related to protected areas and national urban demand. The spherical automata *SA* comprises of an array of hexagonal cells *h* covering the Earth surface characterized with their states SA_h^{t+1} at time *t+1* and expressed as:

$$SA_h^{t+1} = \{SA_h^t,\, N_h^t, S_{global}^t, F^t, \Delta T\} \qquad (2)$$

where SA_h^t denotes the state of the hexagonal cell at initial time *t*, N_h^t represents the hexagonal neighbourhood around the central cell, S_{global}^t is the overall suitability value obtained from the GIS-MCE component of the model for each hexagonal cell, F^t is the function of transition rules and ΔT is the time step of one iteration.
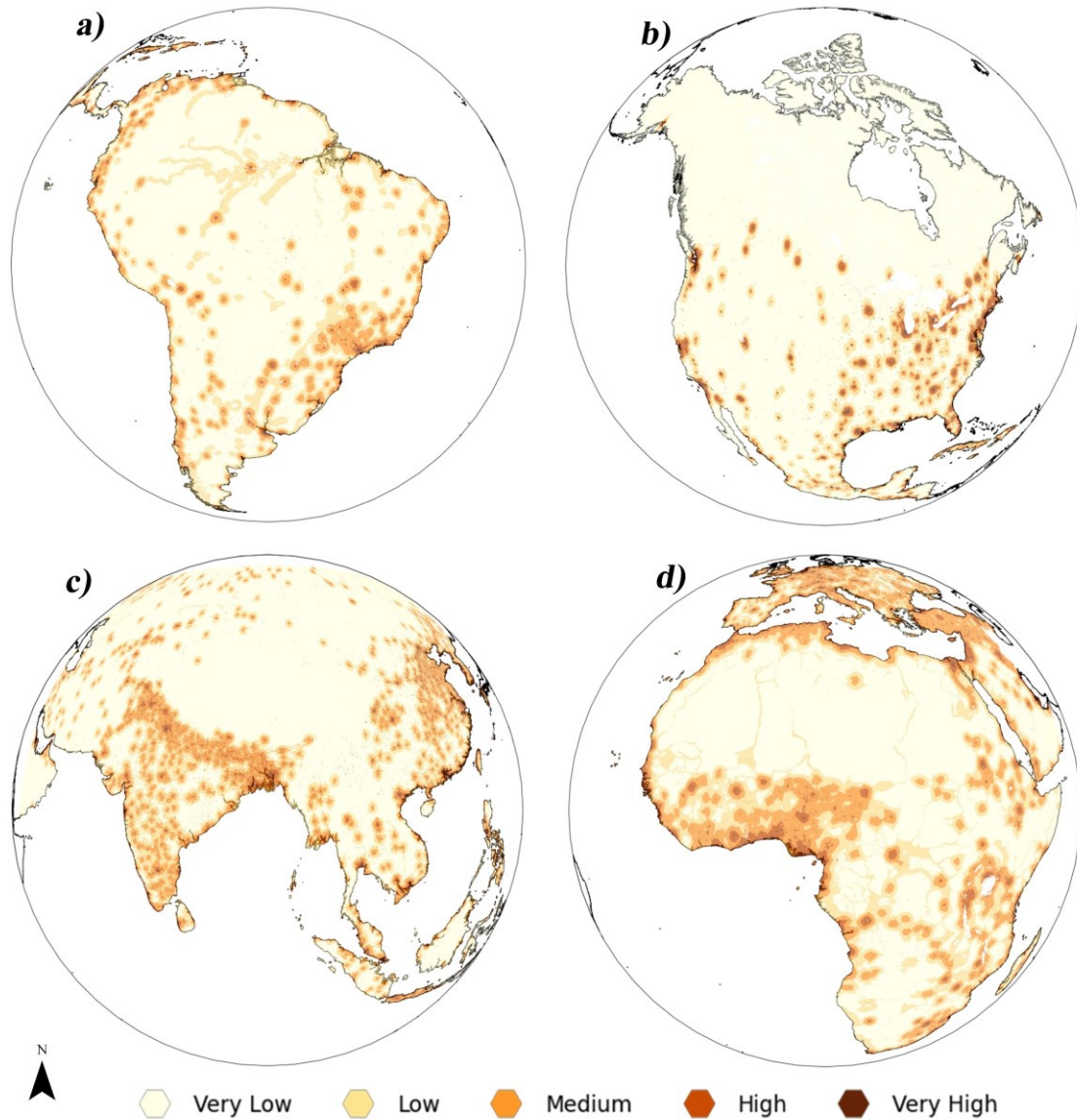
Figure 4.4. Resulting MCE suitability maps at global level for a) South America, b) North America, c) Asia, and d) Europe and Africa.

A total of eight iterations of the model are run to simulate new urban development between 2015 (T_i) and 2095 (T_{i+8}) where each iteration corresponds to a temporal resolution of 10 years. During each iteration, existing urban cells remain unchanged as well as protected areas and water bodies. The MCE-S-CA modelling approach is also constrained by national urban demand. The national urban demand is computed using GDP and population data obtained from UN-DESA (UN-DESA, 2020) (UN-DESA, 2020) and Organization for Economic Co-operation and Development (OECD) (Dellink et al., 2017) respectively. The model iteratively simulates new urban

development until the urban demand for each country has been reached. After each iteration, the S-CA model output becomes the input for the GIS-MCE component of the modelling framework, recalculates the suitability values based on new simulated urban development, and uses the updated information for the next model iteration and application of transition rules. The proposed MCE-S-CA model was programmed in Python (v3.7.7) (Van Rossum & Drake, 2009) using DGGRID and H3 DGGS python libraries that are capable of generating and manipulating hexagonal cells covering the spherical Earth surface.

4.3.7. Model Evaluation

Model evaluation comprises of verification, calibration, and validation. Model verification entails ensuring the model's logic and operations are correct and internally consistent, calibration involves adjusting model parameters whereas model validation often requires comparing the model output with independent datasets not used in building the model (Manson, 2007; Rykiel, 1996). Verification was conducted during the model design and implementation phase to ensure the logic and output of the code used is correct and testing the model after each modification and improvement to ensure it is consistent with the theory of the modelled process. The model was calibrated using historical dataset for the year 1995 and 2005. In the calibration phase, parameters representing transition rules are adjusted to allow for meaningful simulation of urban land-use change process. Model validation was performed using datasets for the year 2015 which represents data that have not been used in the model development and calibration phase. The simulation outputs were compared against actual land-use data using the Figure of Merit (FoM) approach (Pontius et al., 2008) which is the ratio of the intersection of simulated and observed change over the union of simulated and observed change and can be expressed as:

$$FoM = \frac{V}{U + V + W} \tag{3}$$

where *V* is the number of correctly simulated urban cells, *U* denotes the number of actual urban cells simulated as non-urban cells, and *W* is the number of non-urban cells simulated as urban cells. The *FoM* index constitutes three components considering only

one class, urban land-use, was modelled with urban cells remaining unchanged in this research studies.

4.4. Results

4.4.1. Model Testing

For the calibration phase, the FoM value obtained from the MCE-S-CA model was 51.1%, which is better than the 38% obtained for the S-CA model. The integration of MCE into the proposed model increased the FoM value by 13%. Comparison of these two models indicate the significance of operationalizing geosimulation models with MCE to enhance the abilities of function of transition rules. The FoM value for the MCE-S-CA model in the validation phase was 62.3%. The calculated FoM values from the proposed MCE-S-CA model were relatively higher than the values obtained in other global urban land-use change models found in the scientific literature with FoM validation figures ranging between 19% to 43% (Cao et al., 2019; Chen et al., 2020; Li et al., 2017; Li et al., 2021).

4.4.2. Global Overview of Urban Expansion Dynamics

The simulation results indicate urban expansion altogether at the global scale would be rapid and extensive. Figure 4.5 presents the obtained global urban expansion simulation results for 2095 and for different parts of the world as spherical maps. The total global urban extent in 2015 was 747 thousand km^2 and this increased to 2.12 million km^2 in 2095. This corresponds to a global urban expansion of 1.37 million km^2 and an annual growth rate of 1.31% between 2015 and 2095. Although urban expansion is noticeable across all regions, the rate and size of urban growth in developing regions especially in Asia and Africa are relatively higher.
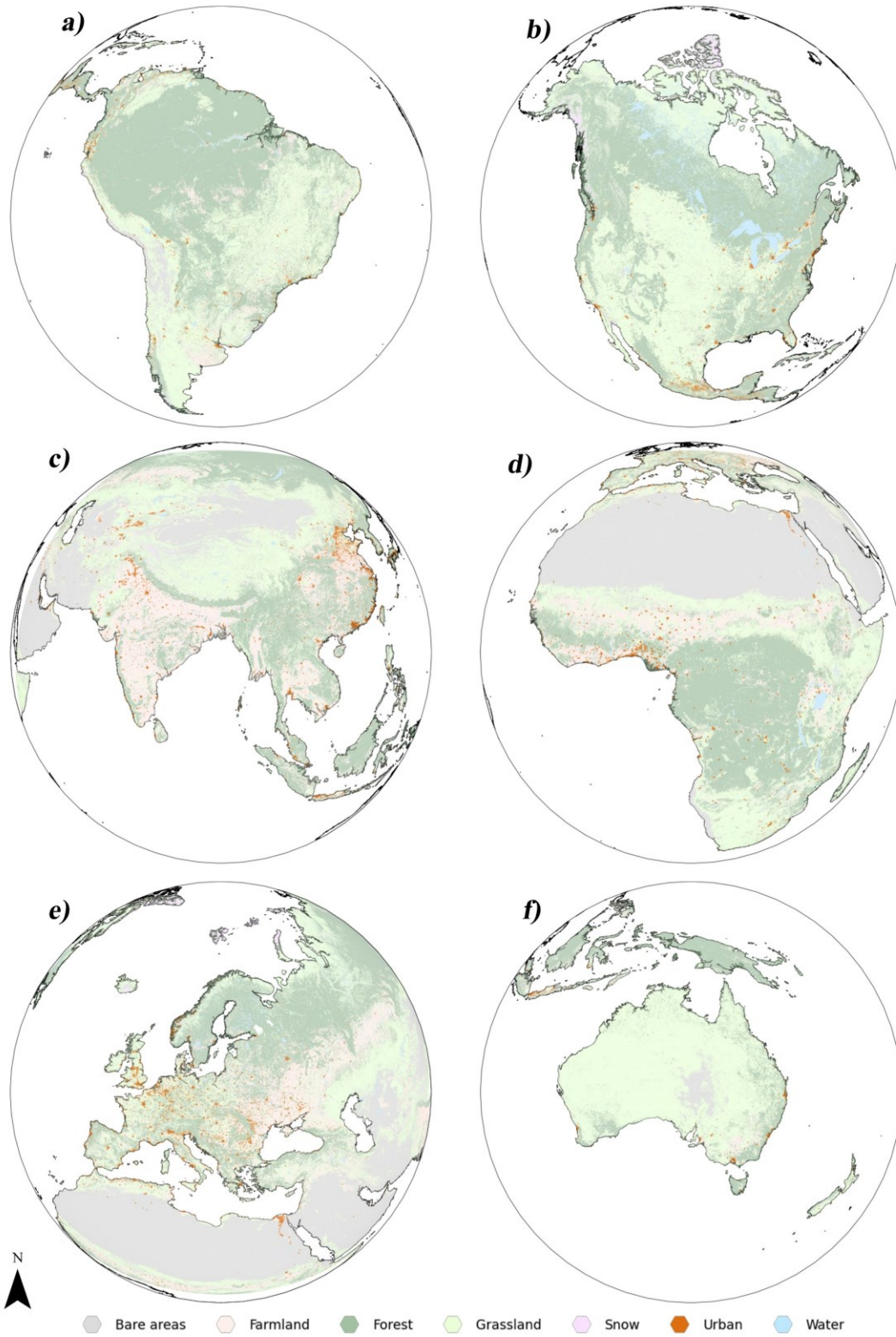
Figure 4.5. Obtained simulation results of global urban expansion for year 2095 in a) South America, b) North America, c) Asia, d) Africa, e) Europe, and f) Australia.

Legend: Bare areas, Farmland, Forest, Grassland, Snow, Urban, Water

4.4.3. Variations in Urban Expansion Across Different Urban Region Clusters

At the metropolitan level, differences in the simulated urban growth patterns can be observed across the four urban region clusters. The simulation results indicate cluster 1 urban regions which typically have high GDP and population density would collectively have the largest urban extent by the end of the century. The urban extent of metropolitan regions in cluster 1 increased from 488 thousand km^2 in 2015 to 1.37 million km^2 in 2095. This value represents an urban expansion of 880 thousand km^2 or 180% of urban growth. The annual growth rate of 1.3% is however slightly lower than the global rate. Urban growth in cluster 2 urban regions characterized by average GDP and population density in low lying regions was also considerable with the total urban extent increasing from 160 thousand km^2 in 2015 to 417 thousand km^2 in 2095. Between 2015 and 2095, the total urban extent in cluster 2 urban regions expanded by 161% with an annual growth rate of 1.21%. The total size of urban areas in metropolitan regions classified as cluster 3 which are in isolated regions with low GDP and population density was 11 thousand km^2 in 2015 and increased to 20 thousand km^2 in 2095. This represents the smallest urban growth rate and extent among the four urban region clusters. Urban areas in cluster 3 regions expanded by 79% with an annual growth rate of 0.73% in the period from 2015 to 2095. On the contrary, metropolitan areas in high elevation areas with average GDP and population density termed cluster 4 urban regions had the highest urban growth rate of 248% and an annual growth rate of 1.57%. The total urban extent of cluster 4 urban regions increased from 89 thousand km^2 in 2015 to 310 thousand km^2 in 2095.

The simulation results of spatial urban expansion between 2015 and 2095 are presented in Figure 4.6 for different metropolitan areas as examples of urban areas that are indicated to have the most rapid urbanization in the four urban region clusters. The simulation results also indicate 64.4% of the total global urban expansion in the period between 2015 and 2095 would occur in cluster 1 metropolitan regions. Further, urban regions in cluster 2 and 4 would account for 18.8% and 16.2% of new urban development respectively. However, less than 1% of the global urban expansion between 2015 and 2095 would occur in cluster 3 urban regions.
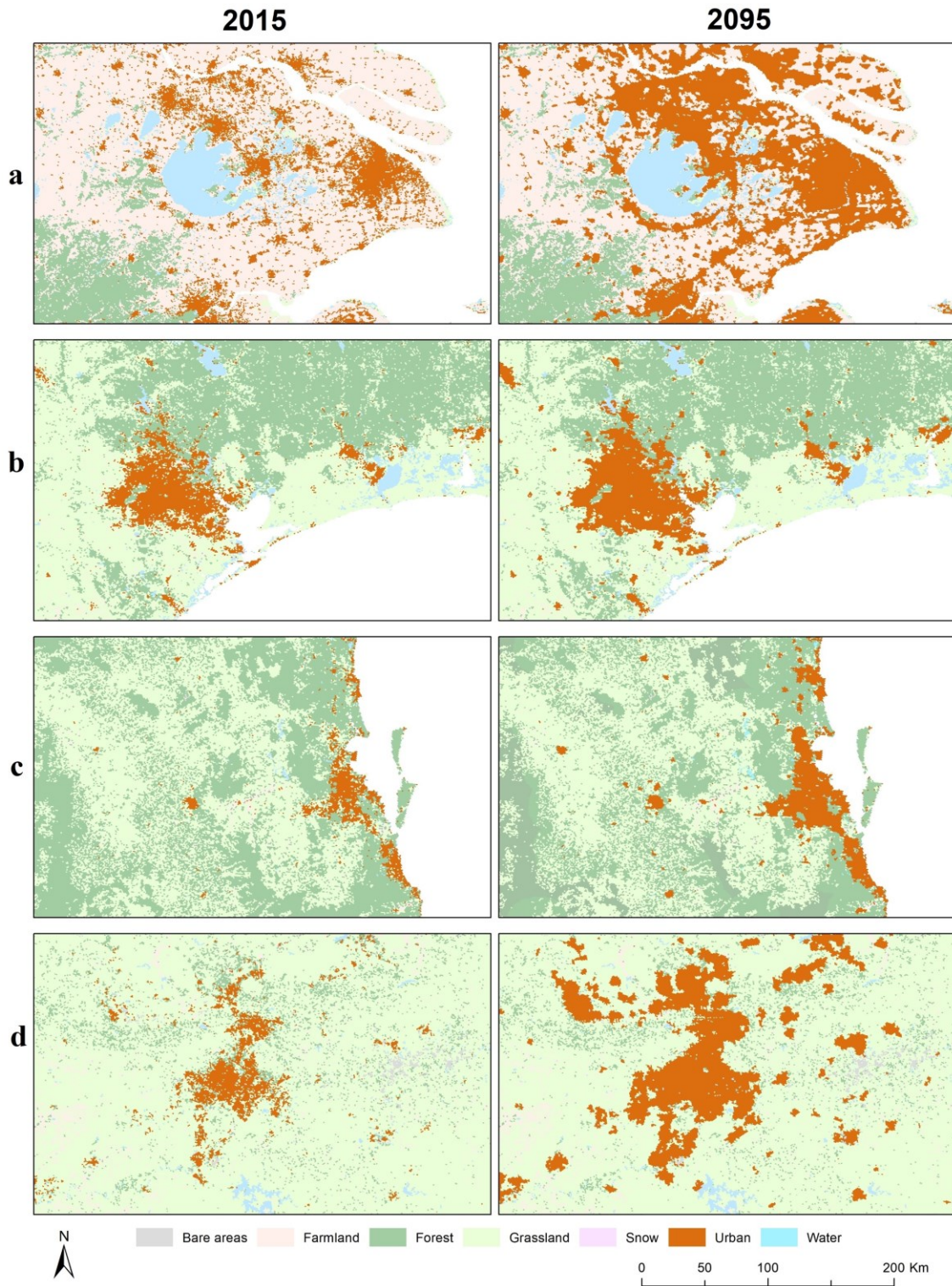
Figure 4.6. Comparison between 2015 urban land extent and obtained simulation results for 2095 for a) Cluster 1, Shanghai, China b), Cluster 2, Houston, USA c) Cluster 3, Brisbane Australia, and d) Cluster 4 Johannesburg, South Africa.

While the simulation results show a general trend of increased urban expansion among the four urban region clusters, differences in growth rates and urban land size can also be observed across continents. For example, the urban extent of cluster 2 metropolitan regions in Africa and Asia expanded by 606% and 395% respectively whiles urban areas in cluster 2 urban regions in Europe and North America increased by 65% and 67% correspondingly. Also, by 2095, Asia would account for 52.7% of the total urban extent in metropolitan areas classified as cluster 1 urban regions. In contrast, Europe and North America would account for 19% and 10.3% respectively of the total urban extent within cluster 1 urban regions. The simulation results also revealed more urban growth would occur in cluster 1 urban regions across all continents albeit different rates. For instance, 72% and 76% of total urban expansion in Asia and Europe would occur in cluster 1 urban regions respectively. In North and South America, 55% and 41% of new urban development between 2015 and 2095 would be in cluster 1 urban regions.

4.5. Discussion and Conclusions

The MCE-S-CA model presented in this research study can realistically represent and capture urban growth dynamics across the globe as indicated by the relatively better *FoM* values obtained during model evaluation. Also, the simulated results from the proposed model are comparable to other global urban land-use change simulations and studies. The simulation outputs indicate the total global urban extent would exceed 2.1 million km^2 by the end of the 21st century. This is consistent with other global land-use change studies such as Li et al. (2019) who projected the total urban extent by the year 2100 to be 2.4 million km^2 in their studies. Africa and Asia would become the frontier of urban expansion and are indicated to have the highest urban expansion rate and largest new urban land size by 2095. The high urban expansion rates observed in developing regions especially in Africa and Asia also correspond to research findings by Li et al. (2021).

Cities are engines of economic growth and human innovation and are expected to play considerable roles in ensuring a globally sustainable future in the coming decades. This is especially true for large global cities that dominate social and economic interactions across the globe. Studies indicate a close correlation between urbanization and economic growth (Chen et al., 2014). The simulation results indicate cluster 1 urban regions which have distinctively high GDP and population density would account for 64%

of the total global urban expansion between 2015 and 2095. This trend is observable across all geographic regions and by the end of the century, cluster 1 urban regions have the largest urban extent within each continent except for Australia and Oceania. Also, by the end of the 21st century, 84.4% of the total global urban extent would be in cluster 1 and 2 urban regions. Metropolitan areas in these two urban clusters are typically located in low lying coastal areas and along major water bodies thus most at risk of the consequences of climate change including sea level rise and flooding. With several developing countries still in the initial phase of urbanization, cities can still shape the future of urbanization in these regions through sustainable urban policies and regional development strategies to limit the negative impacts of rapid urbanization. Cities in Asia and Africa for example would account for 72% of new urban-land development between 2015 and 2095.

The research study has some limitations, and the implemented model can further be enhanced. Firstly, the proposed model does not incorporate random effects for some variables due to lack of data to derive probabilities and computational capacity to run the model at global extent multiple times to examine the convergence. Secondly, the model does not account for the effects of potential human induced changes such as future development of infrastructure of network of new highways or railways, increased economic activities of port cities, deforestation and agricultural land degradation or environmental changes ranging from natural hazards such as earthquakes and forest fires to climate change and sea level rise that can affect urban land use change. Also, the urban development suitability analysis can be improved by including other relevant criteria in the analysis such as local level planning and policies, land value, climate variables or scenarios among others. Incorporating the participation of stakeholders and subject experts would be beneficial to appropriately determine the selection of criteria and importance of criterion weights. This would then require the use of advanced spatial decision technique such as the Logic Scoring of Preference (LSP) method within the CA framework, that are capable of handling larger number of criteria based on soft computing logic. In addition, future research works would focus on representation and comparison of planer and spherical geospatial data to quantify and analyse the source of errors and differences in model outputs. Despite these drawbacks, the proposed geosimulation model is flexible and has the capability to be utilized to explore multiple environmental and urban development scenarios that can be postulated by different

stakeholders, experts, and policy makers within the scope of global urban planning and management procedures.

In conclusion, this research study presents a novel MCE-S-CA geosimulation approach for simulating global urban land-use change by considering the curvature of the global Earth surface. The proposed modelling approach provides decision making capabilities that can represent different urban development criteria and preferences across diverse metropolitan regions at the global level. The model is capable of analysing and identifying suitable locations for urban development and simulating urban land-use change across different global urban regions.

4.6. References

Bagan, H., & Yamagata, Y. (2015). Analysis of urban growth and estimating population density using satellite images of nighttime lights and land-use and population data. *GIScience and Remote Sensing, 52*, 765-780. doi:10.1080/15481603.2015.1072400

Baró, F., Palomo, I., Zulian, G., Vizcaino, P., Haase, D., & Gómez-Baggethun, E. (2016). Mapping ecosystem service capacity, flow and demand for landscape and urban planning: A case study in the Barcelona metropolitan region. *Land Use Policy, 57*, 405-417. doi:10.1016/j.landusepol.2016.06.006

Bhatta, B. (2010). Causes and consequences of urban growth and sprawl. In B. Bhatta (Ed.), *Analysis of urban growth and sprawl from remote sensing data* (pp. 17-36). Berlin, Heidelberg: Springer Berlin Heidelberg.

Cai, Z., Han, G., & Chen, M. (2018). Do water bodies play an important role in the relationship between urban form and land surface temperature? *Sustainable Cities and Society, 39*, 487-498. doi:10.1016/j.scs.2018.02.033

Cao, K., Huang, B., Li, M., & Li, W. (2014). Calibrating a cellular automata model for understanding rural-urban land conversion: A Pareto front-based multi-objective optimization approach. *International Journal of Geographical Information Science, 28*(5), 1028-1046. doi:10.1080/13658816.2013.851793

Cao, M., Zhu, Y., Quan, J., Zhou, S., Lü, G., Chen, M., & Huang, M. (2019). Spatial sequential modeling and predication of global land use and land cover changes by integrating a global change assessment model and cellular automata. *Earth's Future, 7*, 1102-1116. doi:10.1029/2019EF001228

Cengiz, S., Görmüş, S., & Oğuz, D. (2022). Analysis of the urban growth pattern through spatial metrics; Ankara City. *Land Use Policy, 112*. doi:10.1016/j.landusepol.2021.105812

Chen, G., Li, X., & Liu, X. (2022). Global land projection based on plant functional types with a 1-km resolution under socio-climatic scenarios. *Scientific Data, 9*, 1-18. doi:10.1038/s41597-022-01208-6

Chen, G., Li, X., Liu, X., Chen, Y., Liang, X., Leng, J., Xu, X., Liao, W., Qiu, Y. a., Wu, Q., & Huang, K. (2020). Global projections of future urban land expansion under shared socioeconomic pathways. *Nature Communications, 11*, 537. doi:10.1038/s41467-020-14386-x

Cohen, J. (1988). *Statistical power analysis for the behavioral sciences*: Routledge.

de Sousa, L. M., Poggio, L., & Kempen, B. (2019). Comparison of FOSS4G supported equal-area projections ssing discrete distortion indicatrices. *ISPRS International Journal of Geo-Information, 8*(8), 1-13. doi:10.3390/ijgi8080351

Dellink, R., Chateau, J., Lanzi, E., & Magné, B. (2017). Long-term economic growth projections in the Shared Socioeconomic Pathways. *Global Environmental Change, 42*, 200-214. doi:10.1016/j.gloenvcha.2015.06.004

Ellis, E. C., Gauthier, N., Klein Goldewijk, K., Bliege Bird, R., Boivin, N., Díaz, S., Fuller, D. Q., Gill, J. L., Kaplan, J. O., Kingston, N., Locke, H., McMichael, C. N. H., Ranco, D., Rick, T. C., Shaw, M. R., Stephens, L., Svenning, J.-C., & Watson, J. E. M. (2021). People have shaped most of terrestrial nature for at least 12,000 years. *Proceedings of the National Academy of Sciences, 118*(17), e2023483118. doi:doi:10.1073/pnas.2023483118

European Space Agency. (2017). *Land Cover CCI Product User Guide Version 2. Tech. Rep.* Retrieved 10 November 2019 from: http://maps.elie.ucl.ac.be/CCI/viewer/download/ESACCI-LC-Ph2-PUGv2_2.0.pdf

Feng, Y., Wang, J., Tong, X., Shafizadeh-Moghadam, H., Cai, Z., Chen, S., Lei, Z., & Gao, C. (2019). Urban expansion simulation and scenario prediction using cellular automata: comparison between individual and multiple influencing factors. *Environmental Monitoring and Assessment, 191*(5), 291. doi:10.1007/s10661-019-7451-y

Gao, J., & O'Neill, B. C. (2019). Data-driven spatial modeling of global long-term urban land development: The SELECT model. *Environmental Modelling and Software, 119*, 458-471. doi:10.1016/j.envsoft.2019.06.015

Gharaibeh, A., Shaamala, A., Obeidat, R., & Al-Kofahi, S. (2020). Improving land-use change modeling by integrating ANN with Cellular Automata-Markov Chain model. *Heliyon, 6*(9), e05092. doi:10.1016/j.heliyon.2020.e05092

Ghosh, T., Powell, R. L., Elvidge, C. D., Baugh, K. E., Sutton, P. C., & Anderson, S. (2011). Shedding light on the global distribution of economic activity. *The Open Geography Journal, 3*, 148-161. doi:10.2174/1874923201003010147

Hall, J., Wecker, L., Ulmer, B., & Samavati, F. (2020). Disdyakis triacontahedron DGGS. *ISPRS International Journal of Geo-Information, 9*. doi:10.3390/ijgi9050315

He, C., Huang, Z., & Wang, R. (2014). Land use change and economic growth in urban China: A structural equation analysis. *Urban Studies, 51*(13), 2880-2898. doi:10.1177/0042098013513649

Hojati, M., Robertson, C., Roberts, S., & Chaudhuri, C. (2022). GIScience research challenges for realizing discrete global grid systems as a Digital Earth. *Big Earth Data, 00*, 1-22. doi:10.1080/20964471.2021.2012912

Iovine, G., D'Ambrosio, D., & Di Gregorio, S. (2005). Applying genetic algorithms for calibrating a hexagonal cellular automata model for the simulation of debris flows characterised by strong inertial effects. *Geomorphology, 66*(1-4 SPEC. ISS.), 287-303. doi:10.1016/j.geomorph.2004.09.017

Jain, A. K. (2010). Data clustering: 50 years beyond K-means. In *Pattern recognition letters* (Vol. 31, pp. 651-666): Elsevier B.V.

Kiester, A. R., & Sahr, K. (2008). Planar and spherical hierarchical, multi-resolution cellular automata. *Computers, Environment and Urban Systems, 32*, 204-213. doi:10.1016/j.compenvurbsys.2008.03.001

Kii, M., & Nakamura, K. (2017). Development of a suitability model for estimation of global urban land cover. *Transportation Research Procedia, 25*, 3161-3173. doi:10.1016/j.trpro.2017.05.358

Kim, Y., Newman, G., & Güneralp, B. (2020). A review of driving factors, scenarios, and topics in urban land change models. *Land, 9*(8), 246.

Li, M., & Stefanakis, E. (2020). Geospatial Operations of Discrete Global Grid Systems — a Comparison with Traditional GIS. *Journal of Geovisualization and Spatial Analysis, 4*(26).

Li, P., & Cao, H. (2019). Simulating uneven urban spatial expansion under various land protection strategies: Case study on southern Jiangsu urban agglomeration. *ISPRS International Journal of Geo-Information, 8*(11), 521. doi:10.3390/ijgi8110521

Li, X., Chen, G., Liu, X., Liang, X., Wang, S., Chen, Y., Pei, F., & Xu, X. (2017). A new global Land-use and land-Cover change product at a 1-km resolution for 2010 to 2100 based on human–environment interactions. *Annals of the American Association of Geographers, 107*, 1040-1059. doi:10.1080/24694452.2017.1303357

Li, X., Yu, L., Sohl, T., Clinton, N., Li, W., Zhu, Z., Liu, X., & Gong, P. (2016). A cellular automata downscaling based 1 km global land use datasets (2010–2100). *Science Bulletin, 61*, 1651-1661. doi:10.1007/s11434-016-1148-1

Li, X., Zhou, Y., Hejazi, M., Wise, M., Vernon, C., Iyer, G., & Chen, W. (2021). Global urban growth between 1870 and 2100 from integrated high resolution mapped data and urban dynamic modeling. *Communications Earth & Environment, 2*(201), 1-10. doi:10.1038/s43247-021-00273-w

Ligmann-Zielinska, A., & Jankowski, P. (2014). Spatially-explicit integrated uncertainty and sensitivity analysis of criteria weights in multicriteria land suitability evaluation. *Environmental Modelling and Software, 57*(2014), 235-247. doi:10.1016/j.envsoft.2014.03.007

Luo, J., & Wei, Y. H. D. (2009). Modeling spatial variations of urban growth patterns in Chinese cities: The case of Nanjing. *Landscape and Urban Planning, 91*, 51-64. doi:10.1016/j.landurbplan.2008.11.010

Mahtta, R., Fragkias, M., Güneralp, B., Mahendra, A., Reba, M., Wentz, E. A., & Seto, K. C. (2022). Urban land expansion: The role of population and economic growth for 300+ cities. In *npj Urban Sustainability* (Vol. 2): Springer US.

Malczewski, J. (1996). A GIS-based approach to multiple criteria group decision-making. *International Journal of Geographical Information Systems*, 37-41.

Malczewski, J., & Jankowski, P. (2020). Emerging trends and research frontiers in spatial multicriteria analysis. *International Journal of Geographical Information Science, 34*(7), 1257-1282. doi:10.1080/13658816.2020.1712403

Manson, S. M. (2007). Challenges in evaluating models of geographic complexity. *Environment and Planning B: Planning and Design, 34*, 245-260. doi:10.1068/b31179

Masoudi, M., Centeri, C., Jakab, G., Nel, L., & Mojtahedi, M. (2021). GIS-Based Multi-Criteria and Multi-Objective Evaluation for Sustainable Land-Use Planning (Case Study: Qaleh Ganj County, Iran) "Landuse Planning Using MCE and Mola". *International Journal of Environmental Research, 15*(3), 457-474. doi:10.1007/s41742-021-00326-0

Meijer J.R., Huijbegts, M. A. J., Schotten, C. G. J., & Schipper, A. M. (2018). *Global patterns of current and future road infrastructure*. Retrieved from: www.globio.info

Mohamed, A., & Worku, H. (2020). Simulating urban land use and cover dynamics using cellular automata and Markov chain approach in Addis Ababa and the surrounding. *Urban Climate, 31*(2020), 100545. doi:10.1016/j.uclim.2019.100545

Musa, S. I., Hashim, M., & Reba, M. N. M. (2019). Geospatial modelling of urban growth for sustainable development in the Niger Delta Region, Nigeria. *International Journal of Remote Sensing, 40*(8), 3076-3104. doi:10.1080/01431161.2018.1539271

National Research Council. (2014). *Advancing land change modeling: Opportunities and research requirements*. Washington, DC: The National Academies Press.

Nugraha, A. T., Waterson, B. J., Blainey, S. P., & Nash, F. J. (2020). On the consistency of urban cellular automata models based on hexagonal and square cells. *Environment and Planning B: Urban Analytics and City Science*, 1-15. doi:10.1177/2399808319898501

Nuissl, H., & Siedentop, S. (2021). Urbanisation and Land Use Change. In T. Weith, T. Barkmann, N. Gaasch, S. Rogga, C. Strauß, & J. Zscheischler (Eds.), *Sustainable Land Management in a European Context: A Co-Design Approach* (pp. 75-99). Cham: Springer International Publishing.

Pontius, R. G., Boersma, W., Castella, J.-C., Clarke, K., de Nijs, T., Dietzel, C., Duan, Z., Fotsing, E., Goldstein, N., Kok, K., Koomen, E., Lippitt, C. D., McConnell, W., Mohd Sood, A., Pijanowski, B., Pithadia, S., Sweeney, S., Trung, T. N., Veldkamp, A. T., & Verburg, P. H. (2008). Comparing the input, output, and validation maps for several models of land change. *The Annals of Regional Science, 42*(1), 11-37. doi:10.1007/s00168-007-0138-2

Purss, M. B. J., Peterson, P. R., Strobl, P., Dow, C., Sabeur, Z. A., Gibb, R. G., & Ben, J. (2019). DataCubes: a discrete global grid systems perspective. *Cartographica, 53*, 63-71. doi:10.3138/cart.54.1.2018-0017

Rimal, B., Zhang, L., Keshtkar, H., Haack, B. N., Rijal, S., & Zhang, P. (2018). Land use/land cover dynamics and modeling of urban land expansion by the integration of cellular automata and markov chain. *ISPRS International Journal of Geo-Information, 7*(4). doi:10.3390/ijgi7040154

Robertson, C., Chaudhuri, C., Hojati, M., & Roberts, S. A. (2020). An integrated environmental analytics system (IDEAS) based on a DGGS. *ISPRS Journal of Photogrammetry and Remote Sensing, 162*, 214-228. doi:10.1016/j.isprsjprs.2020.02.009

Rose, A. N., McKee, J. J., Sims, K. M., Bright, E. A., Reith, A. E., & Urban, M. L. (2020). *LandScan 2019* [digital raster data]. Retrieved from: https://landscan.ornl.gov/

Rykiel, E. J. (1996). Testing ecological models: The meaning of validation. *Ecological Modelling, 90*, 229-244. doi:10.1016/0304-3800(95)00152-2

Sahr, K. (2011). Hexagonal discrete global GRID systems for geospatial computing. *Archives of Photogrammetry, Cartography and Remote Sensing, 22*, 363-376.

Saltelli, A., Chan, K., & Scott, M. (2000). Sensitivity analysis. In *Probability and statistics series*. New York: John Wiley & Sons.

Seto, K. C., Güneralp, B., & Hutyra, L. R. (2012). Global forecasts of urban expansion to 2030 and direct impacts on biodiversity and carbon pools. *Proceedings of the National Academy of Sciences of the United States of America, 109*, 16083-16088. doi:10.1073/pnas.1211658109

Steiner, F., McSherry, L., & Cohen, J. (2000). Land suitability analysis for the upper Gila River watershed. In *Landscape and Urban Planning* (Vol. 50, pp. 199-214).

Turner, B. L., Lambin, E. F., & Verburg, P. H. (2021). From land-use/land-cover to land system science. *Ambio, 50*(7), 1291-1294. doi:10.1007/s13280-021-01510-4

United Nations - Department of Economic and Social Affairs: Population Division. (2020). *World Population Prospects 2019*. Retrieved 9 November 2020 from: https://population.un.org/wpp/

United State Geological Survey. (2020). *USGS EROS Archive - Digital elevation - shuttle radar topography mission (SRTM) 1 arc-second global*. Retrieved August 2020 from: https://www.usgs.gov/centers/eros/science/usgs-eros-archive-digital-elevation-shuttle-radar-topography-mission-srtm-1-arc?qt-science_center_objects=0#qt-science_center_objects

Van Rossum, G., & Drake, F. (2009). *Python 3 Reference Manual*. Scotts Valley, CA: CreateSpace.

Ventrella, J. (2011). Glider dynamics on the sphere: Exploring cellular automata on geodesic grids. *Journal of Cellular Automata, 6*, 245-256.

Verburg, P. H., Crossman, N., Ellis, E. C., Heinimann, A., Hostert, P., Mertz, O., Nagendra, H., Sikor, T., Erb, K. H., Golubiewski, N., Grau, R., Grove, M., Konaté, S., Meyfroidt, P., Parker, D. C., Chowdhury, R. R., Shibata, H., Thomson, A., & Zhen, L. (2015). Land system science and sustainable development of the earth system: A global land project perspective. *Anthropocene, 12*, 29-41. doi:10.1016/j.ancene.2015.09.004

Veronesi, F., Schito, J., Grassi, S., & Raubal, M. (2017). Automatic selection of weights for GIS-based multicriteria decision analysis: Site selection of transmission towers as a case study. *Applied Geography, 83*, 78-85. doi:10.1016/j.apgeog.2017.04.001

Wen, H., Xiao, Y., & Zhang, L. (2017). Spatial effect of river landscape on housing price: An empirical study on the Grand Canal in Hangzhou, China. *Habitat International, 63*, 34-44. doi:10.1016/j.habitatint.2017.03.007

Winkler, K., Fuchs, R., Rounsevell, M., & Herold, M. (2021). Global land use changes are four times greater than previously estimated. *Nature Communications, 12*(1), 1-10. doi:10.1038/s41467-021-22702-2

World Database on Protected Areas. (2020). *Global database on terrestrial and marine protected areas*. Retrieved 4 March 2020 from: https://www.protectedplanet.net/en/search-areas?filters%5Bdb_type%5D%5B%5D=wdpa&geo_type=region

Wu, F., & Webster, C. J. (1998). Simulation of land development through the integration of cellular automata and multicriteria evaluation. *Environment and Planning B: Planning and Design, 25*, 103-126. doi:10.1068/b250103

Wu, F., & Yeh, A. G. O. (1997). Changing spatial distribution and determinants of land development in Chinese cities in the transition from a centrally planned economy to a socialist market economy: A case study of Guangzhou. *Urban Studies, 34*(11), 1851-1879. doi:10.1080/0042098975286

Wu, R., Li, Z., & Wang, S. (2021). The varying driving forces of urban land expansion in China: Insights from a spatial-temporal analysis. *Science of the Total Environment, 766*, 142591. doi:https://doi.org/10.1016/j.scitotenv.2020.142591

Yang, J., Liu, W., Li, Y., Li, X., & Ge, Q. (2018). Simulating intraurban land use dynamics under multiple scenarios based on fuzzy cellular automata: A case study of Jinzhou district, Dalian. *Complexity, 2018*. doi:10.1155/2018/7202985

Zhai, X., Xiao, Z., & Yin, P. (2010). *Framework of cellular automaton on sphere*. Paper presented at the ICCET 2010 - 2010 2nd International Conference on Computer Engineering and Technology, Proceedings.

Zhang, X., Zhou, J., & Song, W. (2020). Simulating Urban Sprawl in China Based on the Artificial Neural Network-Cellular Automata-Markov Model. *Sustainability, 12*(11). doi:10.3390/su12114341

Zhao, L., Li, G., Yao, X., Ma, Y., & Cao, Q. (2022). An optimized hexagonal quadtree encoding and operation scheme for icosahedral hexagonal discrete global grid systems. *International Journal of Digital Earth*, 1-26. doi:10.1080/17538947.2022.2088871

Zhao, W., Wang, Y., Chen, D., Wang, L., & Tang, X. (2021). Exploring the influencing factors of the recreational utilization and evaluation of urban ecological protection green belts for urban renewal: a case study in Shanghai. *International Journal of Environmental Research and Public Health, 18*. doi:10.3390/ijerph181910244

Zhou, L., Dang, X., Mu, H., Wang, B., & Wang, S. (2021). Cities are going uphill: Slope gradient analysis of urban expansion and its driving factors in China. *Science of the Total Environment, 775*, 145836. doi:10.1016/j.scitotenv.2021.145836

Zhou, Y., Varquez, A. C. G., & Kanda, M. (2019). High-resolution global urban growth projection based on multiple applications of the SLEUTH urban growth model. *Scientific Data, 6*, 1-10. doi:10.1038/s41597-019-0048-z

Chapter 5.

Modelling Global Deforestation using Spherical Geographic Automata Approach[4]

5.1. Abstract

Deforestation as a land-cover change process is linked to several environmental problems including desertification, biodiversity loss and ultimately climate change. Understanding land-cover change process and its relation to human-environment interactions is important for supporting spatial decisions and policy making at the global level. However, current geosimulation model applications mainly focus on characterizing urbanization and agriculture expansion. Existing modelling approaches are also unsuitable for simulating land-cover change processes covering large spatial extents. Thus, the objective of this research is to develop and implement a spherical geographic automata model to simulate deforestation at the global level under different scenarios designed to represent diverse future conditions. Simulation results from the deforestation model indicate the global forest size would decrease by 10.5% under the "business-as-usual" scenario through 2100. The global forest extent would also decline by 15.3% under the accelerated deforestation scenario and 3.7% under the sustainable deforestation scenario by the end of the 21st century. The obtained simulation outputs also revealed the rate of deforestation in protected areas to be considerably lower than the overall forest cover change rate under all scenarios. The proposed model can be utilized by stakeholders to examine forest conservation programs and support sustainable policy making and implementation.

5.2. Introduction

Deforestation as a land-cover change (LCC) process caused by natural and anthropogenic factors further entailing environmental degradation with several negative consequences both at the regional and global scales (Foley et al., 2005; Van Asselen

---

[4] A version of this chapter is published: Addae, B., & Dragićević, S. (2023). Modelling global deforestation using spherical geographic automata approach. *ISPRS International Journal of Geo-Information, 12*(8), 308.

and Verburg (2013). Rates of deforestation especially in developing countries triggered by factors such as agricultural expansion, timber production, forest fire, mining, and urbanization have been increasing over the last century (Curtis et al., 2018; Hoang & Kanemoto, 2021; Lambin & Geist, 2003). These trends of decreasing forest cover and deteriorating conditions has resulted in deforestation becoming a major global environmental issue considering the several critically important ecosystem services and functions forests provide (Brockerhoff et al., 2017; Felipe-Lucia et al., 2018). Forests are important areas for biodiversity with approximately 80% of the world's terrestrial biodiversity found in forest regions (FAO 2020). Further, forests represent the largest terrestrial sink of carbon dioxide (CO_2) and are globally responsible for significant carbon stocks (Keenan & Williams, 2018; Pan et al., 2011). These highlight the important roles forests play in the Earth's biochemical and ecological systems.

Geosimulation modelling has become an important tool for representing land-cover change (LCC) processes and assisting in understanding the interaction between anthropogenic activities and the impact of deforestation on other environmental systems, permitting for spatial analyses of the underlying causes of this dynamic process (Ren et al., 2019). Further, the simulation of possible LCC scenarios provide useful mechanism to inform environmental and forest management policies and decision-making for providing valuable insights for developing appropriate measures to alleviate the negative impacts of deforestation (Vannier et al., 2022). Specifically, data on forest cover and future trajectories provide significant information for estimating carbon stocks, ecosystem service evaluation, and forestry conservation (Sun et al., 2022; Yu et al., 2022). Assessing the performance and effectiveness of environmental policies such as the Reduction in Emissions from Deforestation and Forest Degradation (REDD+) policies requires detailed spatial data on forest cover change and future scenarios (Bos et al., 2019).

Forests can be considered as complex biophysical spatial systems with many components and some considerably depend on human interactions at the local level to give rise to global patterns of deforestation process over time [(Messier et al., 2016)]. Thus, geosimulation modelling approaches are seen as suitable for representing forest change processes. Accordingly, several geosimulation models have been implemented to represent the dynamics of forest changes as a complex spatial process including approaches based on cellular automata (CA) (Kura & Beyene, 2020; Moreno et al.,

2007), and some were enhanced with techniques such as Markov Chain (Adhikari & Southworth, 2012; Vázquez-Quintero et al., 2016), logistics regression (Kucsicsa & Dumitrică, 2019; Miranda-Aragón et al., 2012), multi-criteria evaluation (MCE) (Monjardin-Armenta et al., 2020; Takam Tiamgne et al., 2022), machine learning (Mas et al., 2004), and deep learning (Ball et al., 2022). Several studies have also been incorporating human interactions to represent deforestation processes using agent-based geosimulation models (ABM) (Deadman et al., 2004; Manson & Evans, 2007). However, these modelling approaches are all developed mainly to operate on small spatial extents and implemented to simulate forest cover change dynamics at the local and regional levels.

The use of existing geosimulation models at larger spatial scales presents challenges that are peculiar to spatial modelling at the global level. Primarily, these models do not consider the curvature of the Earth's surface when modelling at larger extents which can lead to errors in spatial and statistical analyses due to spatial distortions caused by planar map projections (Ellis et al., 2021). The limitations of using planar spatial models for analyses and simulations at the global level have been documented in the scientific literature (Cao et al., 2019; Hu et al., 2021; Li et al., 2017), with spherical models proposed as a possible solution. While spatially explicit land-cover change models are becoming prevalent over the last decade, geosimulation models for deforestation are still scarce with existing global applications typically focusing on simulating urbanization (G. Chen et al., 2020; Gao & O'Neill, 2020) and agricultural expansion (Meiyappan et al., 2014). In order to improve simulation results, CA models are often integrated with other techniques such as spatial multi-criteria evaluation (MCE) to identify suitable or susceptible locations for potential occurrence of the geographic phenomena and then guide transitions rules. The MCE technique provides a comprehensive approach that combines several criteria often conflicting based on suitability functions, weights, and their overall aggregation (Malczewski, 1996). The approach has been implemented in several applications including land-cover change (Deribew & Dalacho, 2019; Feng et al., 2014), deforestation (Monjardin-Armenta et al., 2020) and urban growth (Gharaibeh et al., 2020), although all these studies address small spatial extents. Therefore, the main objective of this research study is to develop and implement a spherical geographic automata (SGA) modelling approach by

integrating MCE and cellular automata to simulate the process of deforestation at the global level and considering the curved surface of the Earth.

5.3. Materials and Methods

5.3.1. Spherical Deforestation Model Overview

The methodology extends the theoretical concepts of the spherical geographic automata (SGA) approach (Addae & Dragićević, 2023) and integrates susceptibility analysis for global deforestation modelling. The methodological flow chart of the modelling approach is presented in Figure 5.1.
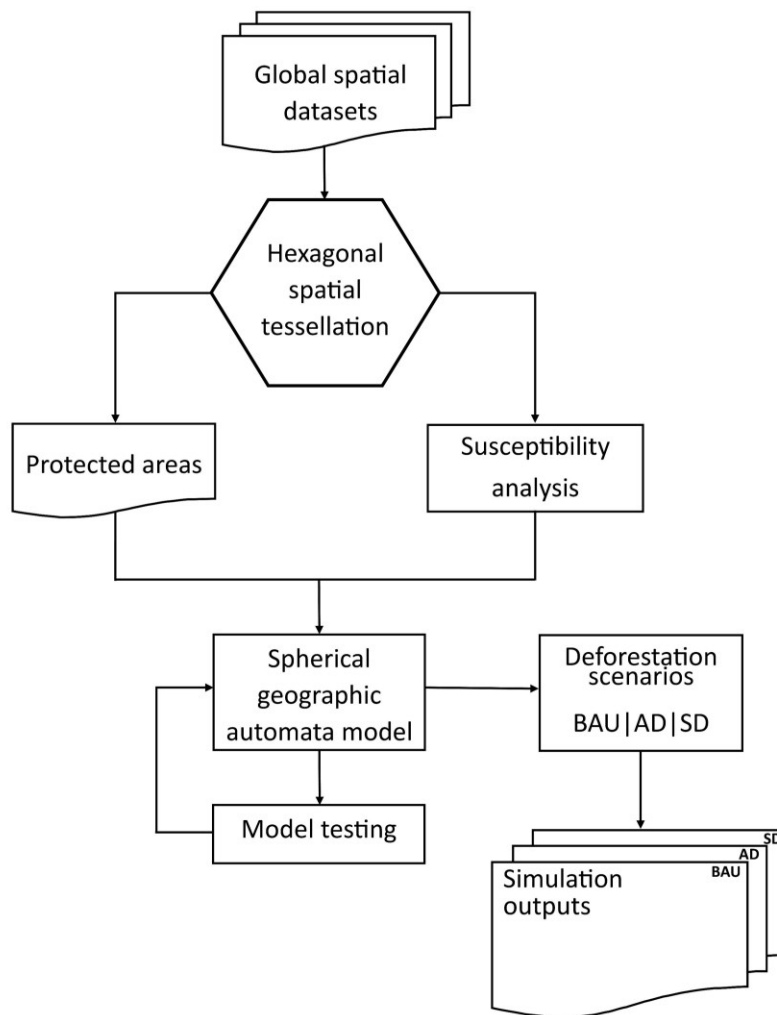
Figure 5.1. **Flowchart of the spherical deforestation model for simulating forest land-cover change at the global level.**

The spherical component of the model is operationalized with the use of discrete global grid system (DGGS) (Sahr et al., 2003) and hexagonal spatial tessellations as a base unit that allows for geospatial data representation at the global level and with consideration of the curvature of the Earth's surface. The MCE technique is used to identify susceptible locations for forest cover loss using several criteria as possible drivers of deforestation. Three scenarios have been developed to represent possible future deforestation processes under different conditions.

5.3.2. Global Deforestation Spherical Geographic Automata

The spherical geographic automata (SGA) component is the central component of the proposed modelling methodology, and it is designed to simulate the process of deforestation at the global level. The SGA utilizes a spherical cell space based on DGGS and comprising of hexagonal tessellation covering the Earth's curved surface. As a geospatial model, DGGS applies a spherical grid framework to partition and represent the curvature of the Earth's surface (Sahr et al., 2003). The DGGS spatial model is based on the icosahedron polyhedron with equal area hexagonal cells. When used to tesselate spherical surfaces, hexagonal cells are the most compact and offer uniform adjacency and neighbouring relationships over other regular polygons such as squares and triangles. The global spatial datasets are transformed into hexagonal spatial tessellations as the model input. The spherical geographic deforestation model extends the previous research study (Addae & Dragićević, 2023) and can be formulated as follows:

$$GA_h^{t+1} = \left[GA_h^t,\ HN_h^t,\ S_{\text{def\_global}}^t, f, \Delta T \right] \tag{1}$$

where GA_h^{t+1} is the state of the hexagonal cell *h* at the next time step *t+1*, GA_h^t denotes the state of hexagonal cell at initial time t, HN_h^t represents the hexagonal neighbourhood of six cells surrounding the central cell, $S_{\text{def\_global}}^t$ is the overall susceptibility value obtained for each hexagonal cell, f is the function of transition rules that determine how the state of cells change over time, and ΔT is the discrete time step representing one iteration of the model. The effects of protected areas on deforestation as constraints and values of susceptibility analysis of deforestation are also considered. The function of transition rules represents the actual dynamics of the deforestation process. During each

iteration, cells representing forest are converted to the dominant non-forest land-cover type based on the cell's neighbourhood, susceptibility value, and constraint parameter.

5.3.3. Datasets

The study area in this research study encompasses the entire global land surface except for Antarctica and several spatial datasets with global extent are acquired to implement the model. Land-cover datasets are obtained from the European space agency (ESA) portal (ESA, 2022), global roads dataset from the Global Roads Inventory Project (GRIP) (Meijer J.R. et al., 2018), protected areas from the World Database on Protected Areas (WDPA) [(WDPA., 2023), past forest disturbance from the Global Wildfire Information System (GWIS) (Artés et al., 2019), population density from the LandScan portal (Rose et al., 2020), and elevation dataset from the United States Geological survey (USGS) portal (USGA, 2022). All spatial datasets are converted into Icosahedral Snyder Equal Area (ISEA) aperture 3 hexagonal cell format (Sahr, 2011) with each cell having an area of 32 km^2 and intercell spacing of 6.1 km. A total of 4,235,365 hexagonal cells were used to tessellate the Earth's land surface which corresponds to an area of 135.5 million km^2. The global land size excluding Antarctica varies between 134.1 million km^2 and 135 million km^2 based on the scientific literature (Dinerstein et al.; Gleeson et al., 2016; Williams et al., 2020). The existing spatial datasets were converted into hexagonal DGGS cells following the approach presented in Robertson et al. (2020). The temporal resolution in the research study was determined to be 10 years and the model was implemented and evaluated using datasets for the years 2000, 2010 and 2020.

5.3.4. Susceptibility Analysis

General multi-criteria evaluation (MCE) approaches (Malczewski, 1996) have been adopted to implement deforestation susceptibility analysis and has been executed at the global level in this research study. The susceptibility analysis assesses the vulnerability of specific areas to the process of deforestation by evaluating the factors and conditions that contribute to forest loss. Driving factors are identified to represent relevant criteria that characterize the process of deforestation and susceptibility functions are derived for each criterion. Susceptibility functions transform criterion values into a normalized range between 0 and 1, where 1 indicate highest satisfaction and 0

denotes no satisfaction for the particular criterion. Moreover, each criterion is normalized with respective suitability function, then weighted and aggregated to obtain the deforestation susceptibility scores for each hexagonal cell. Finally, susceptibility scores can be used to generate global deforestation susceptibility maps that can be one of the inputs that guide the transition rules of the SGA model.

The selected criteria express some of the key drivers of deforestation process at the global level are based on the scientific literature and can be grouped into three categories: socioeconomic (population density), terrain (slope, elevation), and proximity (proximity to urban areas, major roads, water bodies, agriculture, forest edge, past forest disturbances) (Curtis et al., 2018; Monjardin-Armenta et al., 2020; Sharma et al., 2020). Table 5.1 presents the selected criteria and their respective susceptibility functions as graphs.
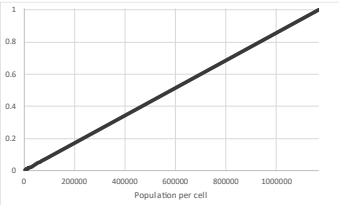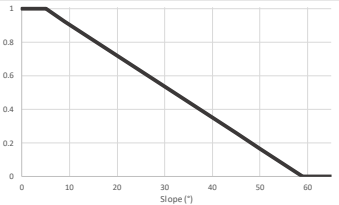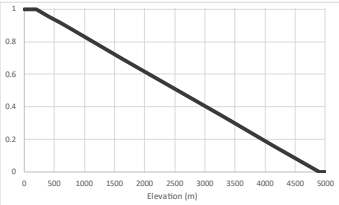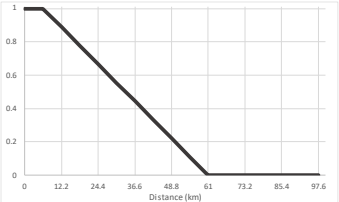
The susceptibility functions are generated for each criterion and are informed from the literature (Grinand et al., 2020; Hyandye & Martz, 2017; Jana et al., 2022; Monjardin-Armenta et al., 2020). Socioeconomic group of criteria rooted in anthropogenic activities are a major determinant of deforestation and population density is often used as an indicator for concentration of urban regions thus human activities (Uusivuori et al., 2002). Increasing population density and urban area expansion causes pressure on nearby forest due to harvesting of wood for construction and fuel, farming, cattle grazing, urban and infrastructure development (Vieilledent et al., 2013). The population density susceptibility function is expressed as a linear membership based on the maximum population density value obtained from the data sets which is 1,168,691 inhabitants per cell. Characteristics of the terrain build another group of criteria. Differences in elevation and slope can represent restrictions to deforestation. Areas with steep slopes are less prone to deforestation as they are unfavourable for other land-use types such as agriculture, infrastructure, and urban development (Adhikari et al., 2017; Sharma et al., 2020). Flat areas however allow for accessibility for clearing of forest for agricultural activities, urban and infrastructure development. For the slope susceptibility function, gradients less than 5° yield maximum satisfaction and slopes steeper than 59° are considered unsuitable for deforestation. The susceptibility function for elevation has maximum satisfaction in locations where altitude is less than 200m and decreases with increasing elevation until 4900m. The maximum elevation is set to 4900m given the highest forest stand is located at this altitude (Georg et al., 2007; Liang et al., 2016).

Proximity based criteria are selected due to different land-use and land-cover features that are driving the deforestation process. Urbanization creates increased demand for land and deforestation is more prone in areas closer to urban centers as forests are more likely to be cleared for urban expansion, wood harvesting for fuel, and agricultural activities. The function uses a linear membership with maximum susceptibility in locations within 6.1km of urban areas, which is equivalent to one hexagonal cell, and no susceptibility beyond 61 km of urban areas, corresponding to 10 hexagonal cells in the spatial dataset. Major roads provide accessibility to areas dominated by forest land-cover for anthropogenic activities such as urbanization, infrastructure development, agriculture and resource extraction (Barber et al., 2014). Several research studies have indicated a strong positive correlation between deforestation rates and proximity to major roads (Bax et al., 2016; Southworth et al., 2011). Prior studies indicate 95% of deforestation can occur with 4.5km of major roads with the influence of roads on deforestation extending as far as 100 km (Barber et al., 2014). The susceptibility function decreases with increasing distance from major roads with no susceptibility beyond 97.6km of roads and equivalent to 16 hexagonal cells in the spatial data layer. Proximity to water bodies can also potentially influence the dynamics of deforestation by increasing accessibility to remote areas, transporting forest resources such as timber and providing water resources for human settlements (González-González et al., 2021). The proximity to water bodies susceptibility function also decreases with increasing distance from water bodies with no susceptibility beyond 42.7km of water bodies that is represented by 7 hexagonal rings. Further, prior studies have indicated agricultural expansion to be another significant driving factor of deforestation (Doggart et al., 2020; Gibbs et al., 2010; Pendrill et al.). Forest areas closer to agricultural lands are more likely to be converted for agricultural purposes to support increasing demand for food, biofuels and animal production. The susceptibility function is based on a decreasing linear function with no susceptibility past 30.5 km, corresponding to 5 hexagonal cells.

Deforestation typically proceeds from the edge of forests into the interior and subsequently leads to the fragmentation of large forest regions into smaller non-contiguous areas (Broadbent et al., 2008; Precinoto et al., 2022). Thus, areas closers to forest edges are more prone to deforestation due to their accessibility by local population. The susceptibility function for proximity to forest edge decrease with distance

until 61 km. Also, past forest disturbance is often seen as a precursor to future forest degradation and several studies have indicated deforestation is more likely to occur in areas that have experienced some form of disturbance including forest fire, logging, mining, etc. (Brown et al., 2007; Hamunyela et al., 2020; Lima et al., 2012). The past disturbance susceptibility function also uses a linear membership where susceptibility decreases with distance until 67.1 km and equal to 11 hexagonal cells.

Table 5.1. **Selected criteria of deforestation with their respective susceptibility functions with rationale and criteria weights.**

Category	Deforestation criteria	Susceptibility functions	Rationale	Criteria weights
Socioeconomic	Population density		Population density is an indicator for the concentration of human activities thus closeness of possible deforestation processes.	0.03418
Terrain	Slope		Areas with gentle slopes are more suitable for land-use/land-cover change	0.04323
	Elevation		Areas at lower elevation are more prone to deforestation as they are more accessible.	0.17615
Proximity	Proximity to urban areas		Urbanization creates demand for land to support urban activities and infrastructure, thus entail deforestation of adjacent forests.	0.00824
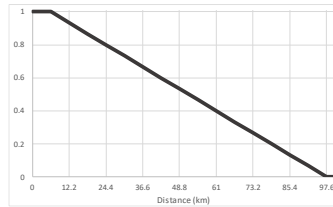
Proximity to major roads		Connection to transportation networks enhances deforestation by providing easy access to forest areas.	0.04777
Proximity to water bodies		Water bodies provide access ways to forest regions and remote areas thus increasing the possibility of deforestation.	0.00645
Proximity to agriculture		Forest areas closer to agricultural land are more prone to deforestation due to expansion of farmlands and agroforestry.	0.12282
Proximity to forest edges		Deforestation typically starts from the edges of existing forest regions as they are much easier to clear.	0.38784
Proximity to past forest disturbances		Past forest disturbance areas are often precursors to future forest degradation or agricultural use.	0.17331
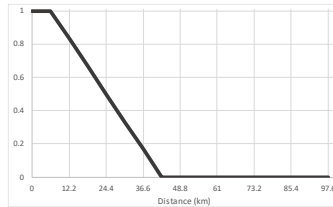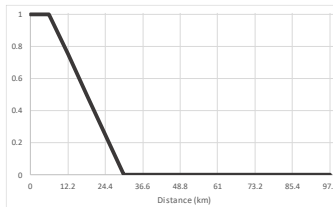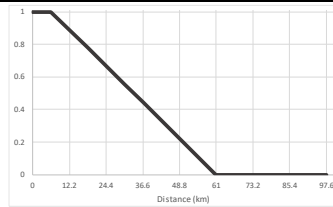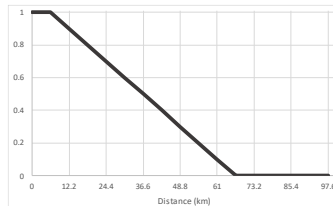
5.3.5. Criterion Weights Generation and Global Susceptibility Maps

Weights are generated for each criterion to reflect the relative importance of the selected criteria in determining deforestation. While criteria weights in most GIS-based MCE methods can be determined by subject experts or stakeholders, this was however not possible in this research study due to the global scope of the model's application and resource limitations. Thus, the Automatic Weight Selection technique (Veronesi et al., 2017) was applied to generate the weights of importance and values are normalized so the sum of all weights is equal to one. The technique is based on the comparison between locations of deforestation and random sampling sites using the Cohen's d metric (Cohen, 1977). The obtained criterion weights are presented in Table 5.1. Based on the normalized criterion values and criterion weights, the Weighted Linear Combination (WLC) technique (Malczewski, 2000) is used to calculate the overall deforestation susceptibility scores for each hexagonal cell for deforestation. The obtained susceptibility scores are classified into five classes using the equal interval method. They are categorized such as: very low (0-0.2), low (0.21-0.4), medium (0.41-0.6), high (0.61-0.8), and very high (0.81-1) susceptibility to deforestation. The equal interval method is chosen to classify the susceptibility values due to its ability to create categories of equal sizes and for easy comparison. Figure 5.2 depicts the obtained global deforestation susceptibility output maps for different parts of the Earth.
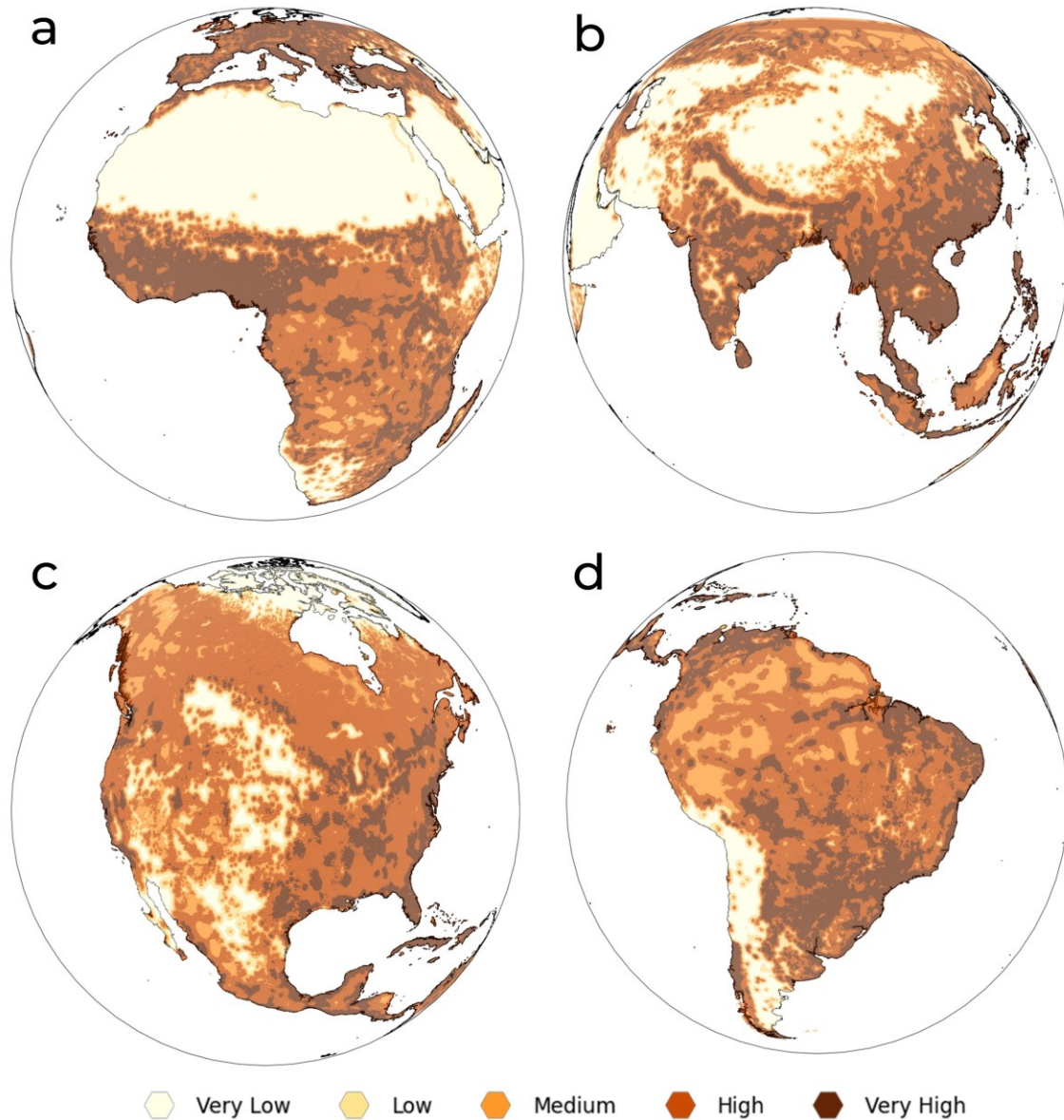
Figure 5.2. **Global deforestation susceptibility maps for, a) Africa, b) Asia, c) North America, and d) South America.**

5.3.6. Deforestation Scenarios

In this research study, three deforestation scenarios are designed and implemented to simulate forest land-cover change under different conditions: Business as Usual (BAU), Accelerated Deforestation (AD), and Sustainable Deforestation (SD) scenarios. The Business as Usual scenario assumes the historical rate of deforestation observed between 2010 and 2020 would continue in the future (Galford et al., 2010). Further, deforestation inside protected areas is allowed due to ineffective implementation

of forest conservation polices in some regions and to allow either for urbanization or agricultural expansion (Prevedello et al., 2019). Research reveals increased demand for forest products and services could amplify rates of deforestation by half in some parts of the world (Ceccherini et al., 2020). Therefore, the Accelerated Deforestation scenario assumes the rate of forest loss would be 50% higher than the current rate as well as loose implementation of environmental conservation policies. This represents a pessimistic deforestation scenario used to represent forest cover change under complete absence of forest management policies and lack of political commitments to reducing deforestation at the local and global levels. The Sustainable Deforestation scenario is the most optimistic and assumes a reduction in the current trend of deforestation by 50% through 2050 and 75% by 2100. Also, it encompasses the strict enforcement of forest conservation policies and programmes, and deforestation is restricted in protected areas under this scenario. Prior studies indicate the effective implementation of forest conservation policies and measures can positively impact global climate change. The research findings indicate reducing rates of deforestation by 50% could potentially reduce carbon emissions from land-cover change by 13 to 50 gigatons of carbon (GtC) (Kindermann et al., 2006; Mollicone et al., 2007).

Under each scenario, the model is constrained by the rate of deforestation at the country level and calculated using the 2010 and 2020 land-cover datasets. Due to lack of adequate data, the conversion of forest cover to water and snow as well as the process of reforestation are however not considered.

5.3.7. Model Implementation and Evaluation

The spherical deforestation model is implemented in the Python programming language (Van Rossum & Drake, 2009) using the DDGRID open-source library [(Sahr, 2022)]. The model is implemented on a workstation with Intel(R) Xeon(R) Gold 6128 CPU @ 3.40GHz 3.39 GHz processor and 32 GB RAM with the processing time for each scenario implementation varying between 81 to 88 hours. The model is run for eight iterations with a temporal resolution of 10 years to simulate global deforestation between 2020 (T^i) and 2100 (T^{i+8}) and for the three scenarios.

Model evaluation was performed using the relative operating characteristic (ROC) technique (Swets, 1988) and the Figure of Merit (*FoM*) (Pontius et al., 2008).

124

ROC entails metrics for assessing the performance of binary classification with continuous output or rank order values (Gilmore Pontius & Pacheco, 2004; Mas et al., 2013). ROC applies thresholds to generate a contingency table with four performance descriptors: true positives (TP), false negatives (FN), false positives (FP), and true negatives (TN) (Camacho Olmedo et al., 2022). True positives (TP) correspond to changed forest cells correctly simulated as change by the model, false negatives (FN) are unchanged forest cells wrongly simulated as changed cells, false positives (FP) are changed forest cells the model was unable to simulate as changed cells and true negatives (TN) are changed forest cells simulated to the wrong class (Pontius & Parmentier, 2014). From the contingency table, the true positive rates (TPR) and false positive rates (FPR) can be calculated as:

$$TPR = \frac{True\ Positives}{True\ Positives + False\ Negatives} \tag{2}$$

$$FPR = \frac{False\ Positives}{False\ Positives + True\ Negatives} \tag{3}$$

By plotting the TPR on the vertical axis and FPR on the horizontal axis of the graph, the ROC curve and Area Under the Curve (AUC) metrics are obtained (Paegelow, 2018). AUC values range between 0 and 1, where a larger value indicates higher model accuracy. Additionally, the simulation outputs are compared with actual land-cover datasets using the Figure of Merit (*FoM*) index which can be expressed as:

$$FoM = \frac{hits}{misses + hits + false\ alarms} \tag{4}$$

where the definition of the term misses is the same as false negative, hits denote true positives, and false alarms is equivalent to false positives.

In this research study, global datasets for the period 2000-2010 were used for model calibration and then 2010-2020 for model validation. The AUC value obtained for the global spherical geographic deforestation model in the calibration phase was 0.9 and 0.87 in the validation phase. Other global geosimulation model applications in the scientific literature report the AUC values ranging between 0.72 and 0.93 (Čengić et al.,

2023; Li et al., 2016; Li et al., 2021). For the *FoM* metric, the value obtained for the model calibration was 36.5 and 29.9% during model validation. *FoM* values obtained in other global geosimulation models range between 19% and 43% (G. Chen et al., 2020; Li et al., 2021). Thus, the evaluation of the proposed modeling methodology yields commensurate values.

5.4. Results

5.4.1. Global and Regional Variations in Forest Cover Change

In 2020, forest covered 48 million km^2 of the terrestrial Earth's surface, corresponding to 35.6% of the global land area. The simulation results of deforestation are presented in Figure 5.3 for North America only as an illustration of detailed model outputs, and for each time step between 2020 and 2100 under the Accelerated Deforestation (AD) scenario. The obtained simulation outputs of deforestation under the different scenarios by the year 2100 compared with the base year 2020 are also presented for different parts of the globe in Figure 5.4.

Under the BAU Scenario, the global forest extent shrinks to 43 million km^2, decreasing by 5 million km^2 between 2020 and 2100 which corresponds to an annual forest loss of 63 thousand km^2 per year, about twice the size of the Netherlands. Approximately 10.5% of the forest extent in 2020 would be lost by the end of the 21st century based on the current trend of deforestation. Under the AD scenario, the global forest extent would decrease by 7.3 million km^2, representing a forest loss of 15.3% by 2100. Conversely, the simulation results indicate 1.8 million km^2 of the global forest area would be deforested by 2100 under the SD scenario, which represents a global forest loss of 3.7%. Figure 5.5 presents the global cumulative deforestation obtained for the three scenarios.
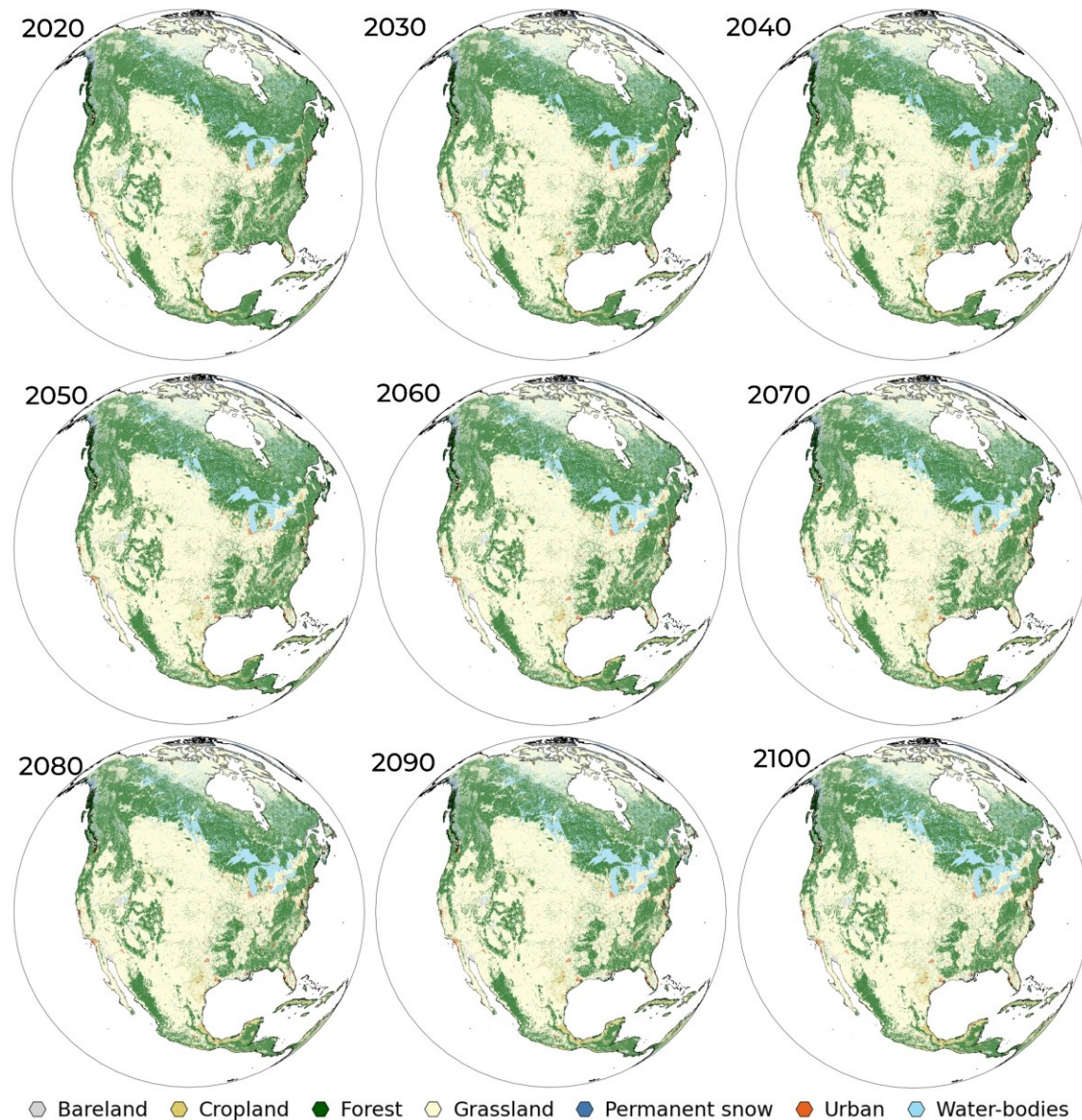
Figure 5.3. Simulated deforestation for North America from 2020 to 2100 for each 10-year iteration under the Accelerated Deforestation (AD) scenario.

The simulation results also revealed marked differences in deforestation dynamics at the continental level. Table 5.2 presents summaries of the simulated forest cover change per continent in the period between 2020 and 2100. At the continental level, Europe had the largest forest cover loss with 1.9 million km^2 and corresponding to 15.5% of the continent's forest extent in 2020 under the BAU scenario. The results further indicate forest loss in Europe would reach 2.7 million km^2 under the AD scenario.

It must however be noted that, the Russian Federation which is considered part of Europe in this research accounts for 81.8% of Europe's forest area in 2020.
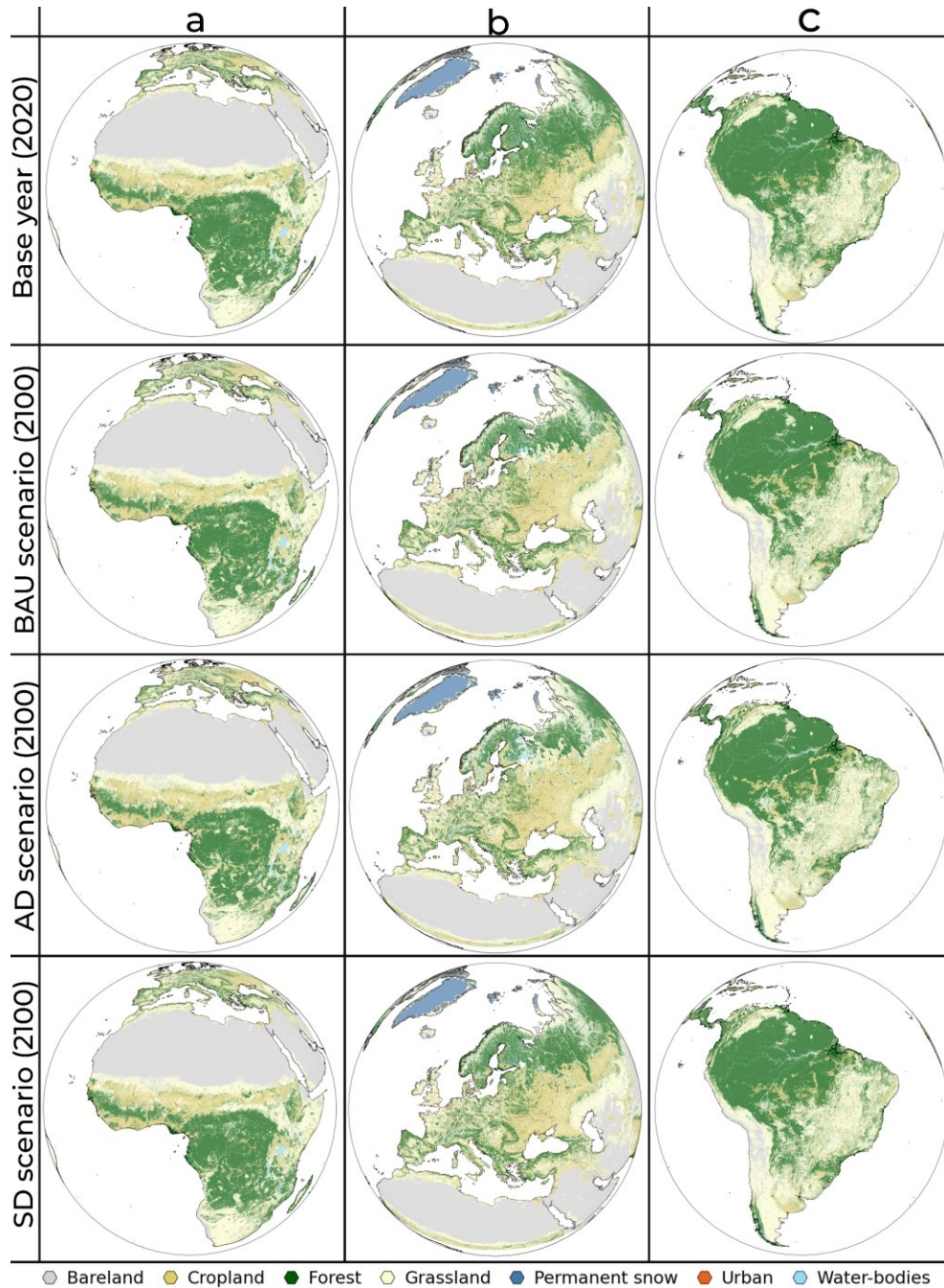
Figure 5.4. **Comparison of initial year 2020 forest cover with obtained simulation results of deforestation under Business as Usual (BAU), Accelerated Deforestation (AD), and Sustainable Deforestation (SD) scenarios for a) Africa, b) Europe, and c) South America**
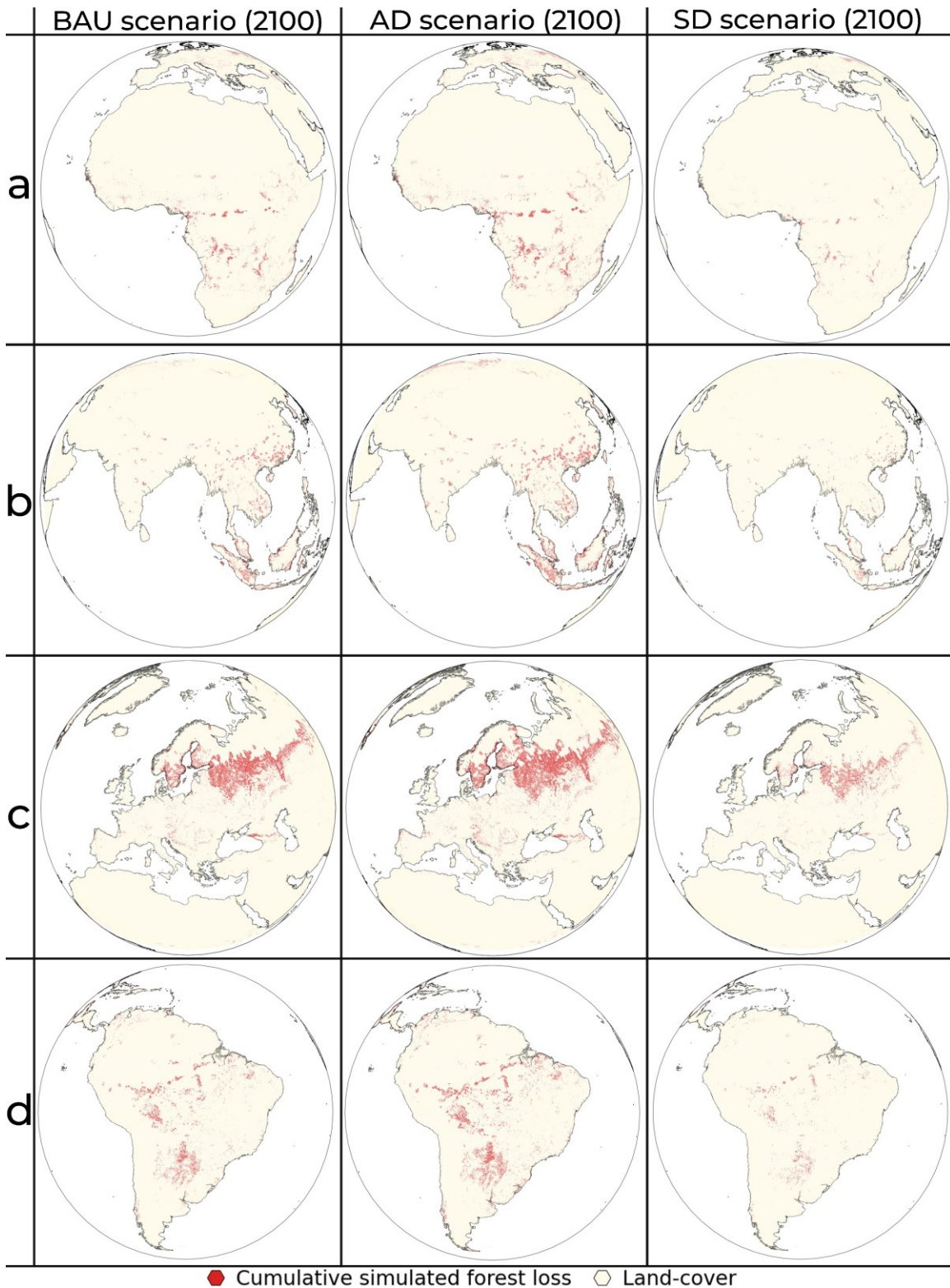
Figure 5.5. Cumulative loss of forest land-cover between 2020 and 2100 based on the obtained simulation results under Business as Usual (BAU), Accelerated Deforestation (AD), and Sustainable Deforestation (SD) scenarios for a) Africa, b) Asia, c) Europe, and d) South America.

The simulation outputs also reveal considerable deforestation in North America with 1.02 million km² of forest lost under the BAU scenario and 1.5 million km² under the AD scenario. Forest loss in Africa, Asia and South America are revealed to be 0.58 million km², 0.66 million km², and 0.76 million km², respectively under the BAU scenario. Figure 5.6 depicts simulated deforestation in 2100 compared to the base year for different forest regions across the globe under the three scenarios. The Amazon Forest, Congo basin, and Eastern USA regions are presented here due to the extensive forest loss revealed by the simulation results.

Table 5.2. **Simulated forest cover extent (in million km²) and percentage of cumulative forest lost (%) by continent between 2020 and 2100 under the Business as Usual (BAU), Accelerated Deforestation (AD), and Sustainable Deforestation (SD) scenarios.**

Continent	2020 [10⁶ km²]	Scenario	2030	2040	2050	2060	2070	2080	2090	2100	Lost [%]
Africa	8.42	BAU	8.34	8.27	8.20	8.12	8.05	7.98	7.91	7.84	**6.85**
		AD	8.31	8.20	8.09	7.98	7.88	7.77	7.67	7.57	**10.08**
		SD	8.38	8.34	8.31	8.29	8.27	8.25	8.23	8.22	**2.40**
Asia	7.28	BAU	7.19	7.11	7.03	6.94	6.86	6.78	6.70	6.62	**9.03**
		AD	7.15	7.02	6.90	6.78	6.66	6.55	6.43	6.32	**13.18**
		SD	7.24	7.20	7.15	7.13	7.11	7.09	7.07	7.05	**3.21**
Australia	1.10	BAU	1.08	1.07	1.05	1.04	1.03	1.01	1.00	0.98	**10.20**
		AD	1.07	1.05	1.03	1.01	0.99	0.97	0.95	0.93	**14.97**
		SD	1.09	1.08	1.07	1.07	1.07	1.06	1.06	1.06	**3.61**
Europe	12.12	BAU	11.88	11.64	11.39	11.15	10.92	10.68	10.46	10.24	**15.48**
		AD	11.75	11.39	11.03	10.68	10.34	10.02	9.70	9.40	**22.45**
		SD	12.00	11.88	11.77	11.71	11.65	11.58	11.52	11.46	**5.41**
North America	7.97	BAU	7.83	7.70	7.57	7.45	7.33	7.20	7.08	6.96	**12.74**
		AD	7.77	7.57	7.38	7.19	7.01	6.84	6.66	6.49	**18.61**
		SD	7.90	7.84	7.77	7.74	7.71	7.67	7.64	7.61	**4.51**
Oceania	0.51	BAU	0.50	0.50	0.49	0.49	0.48	0.48	0.48	0.47	**6.58**
		AD	0.50	0.49	0.49	0.48	0.47	0.47	0.46	0.46	**9.67**
		AD	0.50	0.49	0.49	0.48	0.47	0.47	0.46	0.46	**9.67**
South America	10.40	BAU	10.30	10.20	10.10	10.00	9.91	9.82	9.73	9.64	**7.33**
		AD	10.25	10.10	9.95	9.81	9.68	9.55	9.42	9.30	**10.58**
		SD	10.35	10.30	10.25	10.22	10.20	10.18	10.15	10.13	**2.65**

Considerable differences in forest extent and rates of deforestation can be observed at the country level as well. The simulation results indicate the largest extent of

deforestation would occur in the Russian Federation, Canada, United States, and Brazil. Under the AD scenario for example, 2.3 million km^2, 0.81 million km^2, 0.67 million km^2, and 0.45 million km^2 of forest area were lost in the Russian Federation, Canada, United States, and Brazil, respectively between 2020 and 2100. In relative terms, 17.4% of forest in Canada and 20.3% of forest in the United States would be lost by the end of the 21st century under this scenario. Moreover, there are several countries (over 50) with zero forest loss due these countries having no forest cover, lack of data, or the country being too small to capture the change in forest cover change.
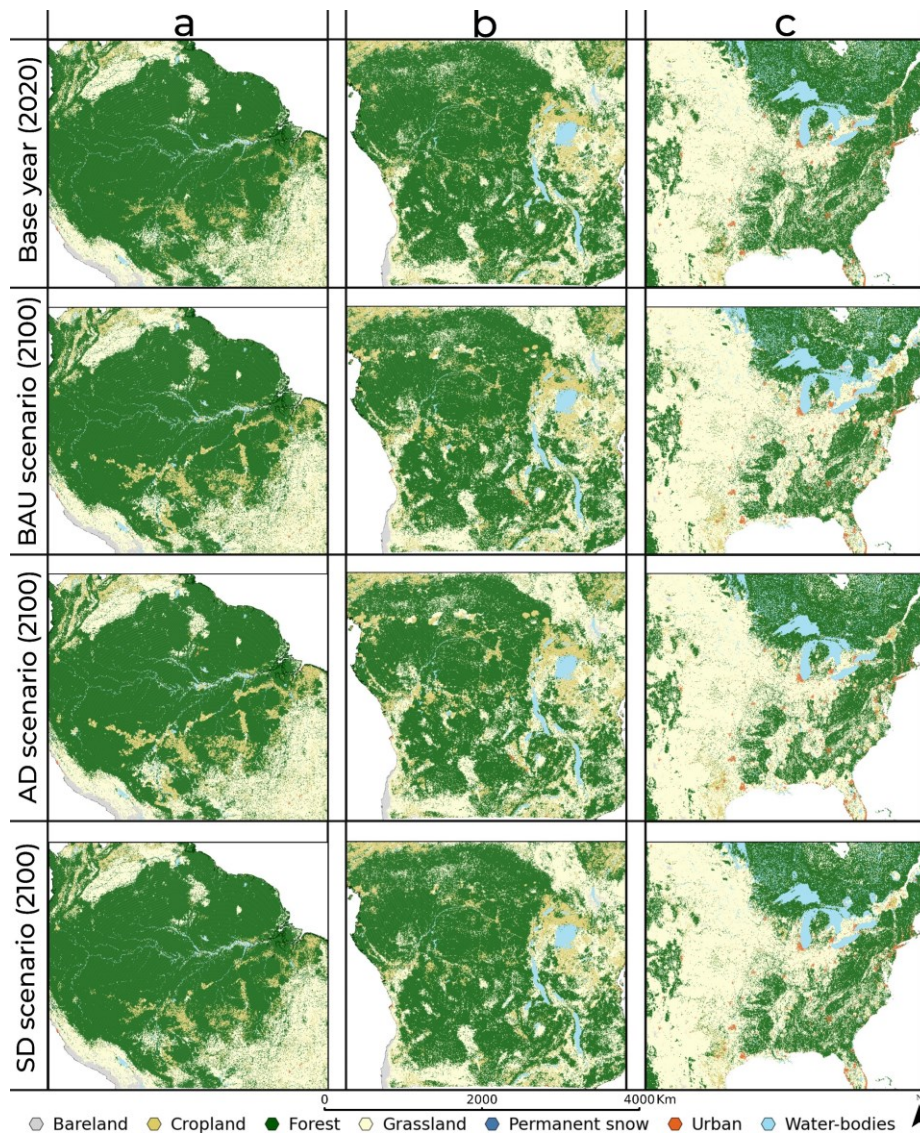
Figure 5.6. Obtained simulation results of deforestation under Business as Usual (BAU), Accelerated Deforestation (AD), and Sustainable Deforestation (SD) scenarios compared to the base year for a) Amazon Forest, b) Congo basin, and c) Eastern USA.

5.4.2. Forest Change in Protected Areas

In 2020, about 9.3 million km^2 of the global forest were in protected areas which corresponds to 19.5% of the global forest extent. Simulation results indicate that this proportion however increases to 21.8%, 23%, and 20.2% by 2100, under the BAU, AD, and SD scenarios, respectively. The rate of deforestation within protected areas was significantly lower than the global rate as well. Between 2020 and 2100, only 0.03% of forests in protected areas were deforested under the BAU scenario and 0.09% under the AD scenario. The forest extent in protected areas under the SD scenario however remained the same over the simulation period with no forest loss due to the restriction of deforestation in these areas. Table 5.3 presents the percentages of the share of forest extent located in protected areas at the continental level by 2100 and compared to the base year under the three scenarios. By 2100, 3.7 million km^2 of forest in South America would be in protected areas under the BAU scenario which represents 38.7% of all forest cover on the continent, representing the largest share of protected forest area at the continental scale. In contrast, Oceania, North America, and Europe have the lowest percentage of protected forests at the continental level under all scenarios.

Table 5.3. **Proportions of forest cover in percentages (%) located in protected areas by 2100 at the continental level under the Business as Usual (BAU), Accelerated Deforestation (AD), and Sustainable Deforestation (SD) scenarios and compared to the base year 2020.**

Scenario [%]	Africa	Asia	Australia	Europe	North America	Oceania	South America
Base year 2020	20.92	11.22	32.53	14.55	10.70	3.91	35.90
BAU 2100	22.44	12.34	36.23	17.21	12.26	4.18	38.73
AD 2100	23.25	12.85	38.26	18.76	13.15	4.33	40.14
SD 2100	21.43	11.60	33.75	15.38	11.21	4.00	36.88

5.5. Discussion

Based on the simulation outputs, the global forest extent is projected to decrease over the coming decades with total forest extent by 2100 ranging between 46 and 40 million km^2. The rate and magnitude of deforestation however differs among the three scenarios and at the regional and country levels. The results indicate that Europe has the largest extent of deforestation by 2100, with 85.4% of the deforested areas in Europe however occurring in the Russian Federation. The results from the model presented in

this research are comparable with other projections found in the literature with range of outcomes varying between 25 million to 50 million km^2 by 2100 under different scenarios (Cao et al., 2019; M. Chen et al., 2020; Li et al., 2017). However, as a caveat, simulation results from the presented model are largely dependent on the quality of the datasets utilized in the research. For instance, the rate of deforestation obtained at the country level for implementing the scenarios are derived from the available ESA-CCI land-cover datasets.

The pattern of forest cover change observed also follows the process of deforestation as reported by prior studies (Broadbent et al., 2008; Precinoto et al., 2022). From the simulation outputs, deforestation initially begins from the fringes of large forest regions and diminishes into the interior. This spatial pattern can be justified where forest regions in proximity to past forest disturbances, urban areas, water bodies and road networks are more prone to deforestation. Over the course of the simulation run, regions initially covered by large forests become fragmented as deforestation spreads into the forest core. This pattern can be observed from the temporal simulation outputs presented in Figure 5.3.

While no forest management polices were explicitly included in the scenario design and implementation, the difference in results among the scenarios indicate the model can be utilized to assess different forest conservation policies. When properly implemented, protected areas can be used as effective forest conservation scheme to reducing deforestation. For instance, in the SD scenario where forest management polices are strictly implemented and deforestation in protected areas is not allowed, the simulation results reveal no loss of forest cover. Such an outcome would however be difficult to achieve due to the financial and human resources required to implement such a policy across large regions. The positive impact of protected areas on deforestation is however proven by other studies in the scientific literature (Barber et al., 2014; d'Annunzio et al., 2015). Research study by Qin et al (2023) indicate that deforestation in protected areas accounted for only 5% of net forest loss between 2000 and 2021 in the Brazilian Amazon. Presently, protected areas are predominantly located in tropical regions of Africa, Asia, and South America in contrary to the small proportion of protected forest areas in Europe and North America as obtained from the simulation results. According to FAO and UNEP (2020), less than 10% of subtropical humid forest,

133

temperate steppe and boreal coniferous forests largely found in Europe and North America are protected.

Despite the model's capabilities in simulating deforestation at the global level and across different regions, the research study has some limitations. The improvements can be made to the model pending on quality and detailed global datasets to simulate land-cover change at finer spatial resolution as well as including more relevant criteria related to deforestation such as soil properties, climate variables or forest type classification. By experimenting with different weighting methods such as Analytic Hierarchy Process (AHP) (Saaty, 1980) or incorporating advanced spatial decision technique such as Ordered Weighted Averaging (OWA) (Yager, 1988) or Logic Scoring of Preference (LSP) (Dujmovic et al., 2010), the deforestation susceptibility analysis can be further improved for the SGA modelling framework. The selection of the relevant drivers of deforestation and generation of criterion weights can also be determined through engagement with subject experts and stakeholders in the model implementation phase of the research study. Considering the spatial heterogeneity and dynamics of the different drivers of deforestation across diverse regions and countries, implementation of region specific economic or climate policies would be beneficial to improve the model. While only homogenous forest was considered in this research, the different forest types such as rainforest, boreal, deciduous, mangrove, to name a few, can also be included in order to incorporate detailed characteristics of the different forest change dynamics. Additionally, the model can further be developed to incorporate multiple land-use/land-cover change types to reflect their different dynamics. This can assist in making informed decisions at country or regional levels and considering REDD+ (Angelsen, 2009) and OECD (OECD, 2018) concepts. Consideration of natural regeneration of forests, reforestation, afforestation, and age of forested areas would be beneficial to enhance the proposed modelling approach. Moreover, with climate being one of the drivers of forest distribution, the inclusion of climate variables and scenarios can enhance the model's ability to characterize future deforestation patterns and considering the effects of climate change. Augmenting computational power with more efficient code for SGA model to run faster or on multiple processors when using global datasets would be another advantage.

5.6. Conclusions

This research study aims to develop and implement a unique spherical geographic automata modelling approach that has been applied to represent and simulate global deforestation process. Compared to existing geosimulation models and applications, the proposed model considers the curvature of the Earth's surface that is often ignored when modelling at the global level. For large scale spatial applications, it is determined that the use of planer spatial models can produce very different results. Further, most global land-cover change models in the literature generally focus on simulating agricultural and urban land-use change with few studies including deforestation.

Results from this research study indicate the spherical deforestation model can be successfully implemented to simulate forest land-cover change process at the global level and under different 'what-if' scenarios. Ultimately, the model is flexible and allows for further enhancements, thus the proposed deforestation modelling approach has a solid foundation to be used by intergovernmental entities, policy makers, ecologist, and researchers to support global forest management and conservation. With the United Nations (UN) Sustainable Development Goal (SDG) 15 set on promoting sustainable use of terrestrial ecosystems, sustainable forest management, and halting biodiversity loss, the spherical geographic deforestation model proposed in this research study can provide valuable insight and spatial decision support tool for achieving these targets.

5.7. References

Addae, B., & Dragićević, S. (2023). Enabling geosimulations for global scale: Spherical geographic automata. *Transactions in GIS, 27*(3), 821–840. doi:10.1111/tgis.13054

Addae, B., & Dragićević, S. (2023). Integrating multi-criteria analysis and spherical cellular automata approach for modelling global urban land-use change. *Geocarto International, 38*(1), 2152498. doi:10.1080/10106049.2022.2152498

Adhikari, S., Fik, T., & Dwivedi, P. (2017). Proximate causes of land-use and land-cover change in Bannerghatta National Park: A spatial statistical model. *Forests, 8*(9). doi:10.3390/f8090342

Adhikari, S., & Southworth, J. (2012). Simulating forest cover changes of Bannerghatta National Park based on a CA-Markov model: A remote sensing approach. *Remote Sensing, 4*(10), 3215-3243. doi:10.3390/rs4103215

Angelsen, A. (2009). Policy options to reduce deforestation. *Realising REDD+: National strategy and policy options*, 125-138.

Artés, T., Oom, D., de Rigo, D., Durrant, T. H., Maianti, P., Libertà, G., & San-Miguel-Ayanz, J. (2019). A global wildfire dataset for the analysis of fire regimes and fire behaviour. *Scientific Data, 6*(1), 296. doi:10.1038/s41597-019-0312-2

Ball, J. G. C., Petrova, K., Coomes, D. A., & Flaxman, S. (2022). Using deep convolutional neural networks to forecast spatial patterns of Amazonian deforestation. *Methods in Ecology and Evolution, 13*(11), 2622-2634. doi:10.1111/2041-210X.13953

Barber, C. P., Cochrane, M. A., Souza, C. M., & Laurance, W. F. (2014). Roads, deforestation, and the mitigating effect of protected areas in the Amazon. *Biological Conservation, 177*, 203-209. doi:10.1016/j.biocon.2014.07.004

Bax, V., Francesconi, W., & Quintero, M. (2016). Spatial modeling of deforestation processes in the Central Peruvian Amazon. *Journal for Nature Conservation, 29*, 79-88. doi:10.1016/j.jnc.2015.12.002

Bos, A. B., De Sy, V., Duchelle, A. E., Herold, M., Martius, C., & Tsendbazar, N.-E. (2019). Global data and tools for local forest cover loss and REDD+ performance assessment: Accuracy, uncertainty, complementarity and impact. *International Journal of Applied Earth Observation and Geoinformation, 80*, 295-311. doi:10.1016/j.jag.2019.04.004

Broadbent, E. N., Asner, G. P., Keller, M., Knapp, D. E., Oliveira, P. J. C., & Silva, J. N. (2008). Forest fragmentation and edge effects from deforestation and selective logging in the Brazilian Amazon. *Biological Conservation, 141*(7), 1745-1757. doi:10.1016/j.biocon.2008.04.024

Brockerhoff, E. G., Barbaro, L., Castagneyrol, B., Forrester, D. I., Gardiner, B., González-Olabarria, J. R., Lyver, P. O. B., Meurisse, N., Oxbrough, A., Taki, H., Thompson, I. D., van der Plas, F., & Jactel, H. (2017). Forest biodiversity, ecosystem functioning and the provision of ecosystem services. *Biodiversity and Conservation, 26*(13), 3005-3035. doi:10.1007/s10531-017-1453-2

Brown, S., Hall, M., Andrasko, K., Ruiz, F., Marzoli, W., Guerrero, G., Masera, O., Dushku, A., DeJong, B., & Cornell, J. (2007). Baselines for land-use change in the tropics: application to avoided deforestation projects. *Mitigation and Adaptation Strategies for Global Change, 12*(6), 1001-1026. doi:10.1007/s11027-006-9062-5

Camacho Olmedo, M. T., Mas, J.-F., & Paegelow, M. (2022). Validation of soft maps produced by a land use cover change model. In *Land use cover datasets and validation tools: Validation practices with QGIS*, (Eds.) D. García-Álvarez, M. T. Camacho Olmedo, M. Paegelow, & J. F. Mas,(pp. 189-203). Cham: Springer International Publishing.

Cao, M., Zhu, Y., Quan, J., Zhou, S., Lü, G., Chen, M., & Huang, M. (2019). Spatial sequential modeling and prediction of global land use and land cover changes by integrating a global change assessment model and cellular automata. *Earth's Future, 7*, 1102-1116. doi:10.1029/2019EF001228

Ceccherini, G., Duveiller, G., Grassi, G., Lemoine, G., Avitabile, V., Pilli, R., & Cescatti, A. (2020). Abrupt increase in harvested forest area over Europe after 2015. *Nature, 583*(7814), 72-77. doi:10.1038/s41586-020-2438-y

Čengić, M., Steinmann, Z. J. N., Defourny, P., Doelman, J. C., Lamarche, C., Stehfest, E., Schipper, A. M., & Huijbregts, M. A. J. (2023). Global maps of agricultural expansion potential at a 300 m resolution. *Land, 12*(3). doi:10.3390/land12030579

Chen, G., Li, X., Liu, X., Chen, Y., Liang, X., Leng, J., Xu, X., Liao, W., Qiu, Y. a., Wu, Q., & Huang, K. (2020). Global projections of future urban land expansion under shared socioeconomic pathways. *Nature Communications, 11*, 537. doi:10.1038/s41467-020-14386-x

Chen, M., Vernon, C. R., Graham, N. T., Hejazi, M., Huang, M., Cheng, Y., & Calvin, K. (2020). Global land use for 2015–2100 at 0.05° resolution under diverse socioeconomic and climate scenarios. *Scientific Data, 7*(1), 320. doi:10.1038/s41597-020-00669-x

Cohen, J. (1977). *Statistical power analysis for the behavioral sciences*: Lawrence Erlbaum Associates.

Curtis, P. G., Slay, C. M., Harris, N. L., Tyukavina, A., & Hansen, M. C. (2018). Classifying drivers of global forest loss. *Science, 361*(6407), 1108-1111. doi:10.1126/science.aau3445

d'Annunzio, R., Sandker, M., Finegold, Y., & Min, Z. (2015). Projecting global forest area towards 2030. *Forest Ecology and Management, 352*, 124-133. doi:10.1016/j.foreco.2015.03.014

Deadman, P., Robinson, D., Moran, E., & Brondizio, E. (2004). Colonist household decisionmaking and land-use change in the Amazon Rainforest: An agent-based simulation. *Environment and Planning B: Planning and Design, 31*(5), 693-709. doi:10.1068/b3098

Deribew, K. T., & Dalacho, D. W. (2019). Land use and forest cover dynamics in the North-eastern Addis Ababa, central highlands of Ethiopia. *Environmental Systems Research, 8*(1), 8. doi:10.1186/s40068-019-0137-1

Dinerstein, E., Joshi, A. R., Vynne, C., Lee, A. T. L., Pharand-Deschênes, F., França, M., Fernando, S., Birch, T., Burkart, K., Asner, G. P., & Olson, D. A "Global Safety Net" to reverse biodiversity loss and stabilize Earth's climate. *Science Advances, 6*(36), eabb2824. doi:10.1126/sciadv.abb2824

Doggart, N., Morgan-Brown, T., Lyimo, E., Mbilinyi, B., Meshack, C. K., Sallu, S. M., & Spracklen, D. V. (2020). Agriculture is the main driver of deforestation in Tanzania. *Environmental Research Letters, 15*(3), 034028. doi:10.1088/1748-9326/ab6b35

Dujmovic, J. J., Tré, G. D., & Weghe, N. V. d. (2010). LSP suitability maps. *Soft Comput., 14*(5), 421-434. doi:10.1007/s00500-009-0455-8

Ellis, E. C., Gauthier, N., Klein Goldewijk, K., Bliege Bird, R., Boivin, N., Díaz, S., Fuller, D. Q., Gill, J. L., Kaplan, J. O., Kingston, N., Locke, H., McMichael, C. N. H., Ranco, D., Rick, T. C., Shaw, M. R., Stephens, L., Svenning, J.-C., & Watson, J. E. M. (2021). People have shaped most of terrestrial nature for at least 12,000 years. *Proceedings of the National Academy of Sciences, 118*(17), e2023483118. doi:doi:10.1073/pnas.2023483118

European Space Agency. (2022). *ESA CCI Land Cover map series 1992-2020*. Retrieved 15 November 2022 from: http://maps.elie.ucl.ac.be/CCI/viewer/index.php

Felipe-Lucia, M. R., Soliveres, S., Penone, C., Manning, P., van der Plas, F., Boch, S., Prati, D., Ammer, C., Schall, P., Gossner, M. M., Bauhus, J., Buscot, F., Blaser, S., Blüthgen, N., de Frutos, A., Ehbrecht, M., Frank, K., Goldmann, K., Hänsel, F., Jung, K., Kahl, T., Nauss, T., Oelmann, Y., Pena, R., Polle, A., Renner, S., Schloter, M., Schöning, I., Schrumpf, M., Schulze, E.-D., Solly, E., Sorkau, E., Stempfhuber, B., Tschapka, M., Weisser, W. W., Wubet, T., Fischer, M., & Allan, E. (2018). Multiple forest attributes underpin the supply of multiple ecosystem services. *Nature Communications, 9*(1), 4839. doi:10.1038/s41467-018-07082-4

Feng, H., Lim, C. W., Chen, L., Zhou, X., Zhou, C., & Lin, Y. (2014). Sustainable deforestation evaluation model and system dynamics analysis. *The Scientific World Journal, 2014*, 106209. doi:10.1155/2014/106209

Foley, J. A., DeFries, R., Asner, G. P., Barford, C., Bonan, G., Carpenter, S. R., Chapin, F. S., Coe, M. T., Daily, G. C., Gibbs, H. K., Helkowski, J. H., Holloway, T., Howard, E. A., Kucharik, C. J., Monfreda, C., Patz, J. A., Prentice, I. C., Ramankutty, N., & Snyder, P. K. (2005). Global consequences of land use. *Science, 309*(5734), 570-574. doi:10.1126/science.1111772

Food and Agriculture Organization and The United Nations Environment Programme. (2020). *The state of the world's forests 2020*. Retrieved from Rome:

Food and Agriculture Organization of the United Nations. (2020). *Global gorest resources assessment 2020: Main report*. Retrieved from Rome:

Galford, G. L., Melillo, J. M., Kicklighter, D. W., Cronin, T. W., Cerri, C. E. P., Mustard, J. F., & Cerri, C. C. (2010). Greenhouse gas emissions from alternative futures of deforestation and agricultural management in the southern Amazon. *Proceedings of the National Academy of Sciences, 107*(46), 19649-19654. doi:10.1073/pnas.1000780107

Gao, J., & O'Neill, B. C. (2020). Mapping global urban land for the 21st century with data-driven simulations and Shared Socioeconomic Pathways. *Nature Communications, 11*(1), 1-12. doi:10.1038/s41467-020-15788-7

Georg, M., Sabine, M., Jonas, V., Sonam, C., & Duo, L. (2007). Highest treeline in the northern hemisphere found in Southern Tibet. *Mountain Research and Development, 27*(2), 169-173. doi:10.1659/mrd.0792

Gharaibeh, A. A., Shaamala, A. H., & Ali, M. H. (2020). Multi-criteria evaluation for sustainable urban growth in An-Nuayyimah, Jordan; post war study. *Procedia Manufacturing, 44*, 156-163. doi:10.1016/j.promfg.2020.02.217

Gibbs, H. K., Ruesch, A. S., Achard, F., Clayton, M. K., Holmgren, P., Ramankutty, N., & Foley, J. A. (2010). Tropical forests were the primary sources of new agricultural land in the 1980s and 1990s. *Proceedings of the National Academy of Sciences, 107*(38), 16732-16737. doi:10.1073/pnas.0910275107

Gilmore Pontius, R., & Pacheco, P. (2004). Calibration and validation of a model of forest disturbancein the Western Ghats, India 1920–1990. *GeoJournal, 61*(4), 325-334. doi:10.1007/s10708-004-5049-5

Gleeson, T., Befus, K. M., Jasechko, S., Luijendijk, E., & Cardenas, M. B. (2016). The global volume and distribution of modern groundwater. *Nature Geoscience, 9*(2), 161-167. doi:10.1038/ngeo2590

González-González, A., Villegas, J. C., Clerici, N., & Salazar, J. F. (2021). Spatial-temporal dynamics of deforestation and its drivers indicate need for locally-adapted environmental governance in Colombia. *Ecological Indicators, 126*, 107695. doi:10.1016/j.ecolind.2021.107695

Grinand, C., Vieilledent, G., Razafimbelo, T., Rakotoarijaona, J.-R., Nourtier, M., & Bernoux, M. (2020). Landscape-scale spatial modelling of deforestation, land degradation, and regeneration using machine learning tools. *Land Degradation & Development, 31*(13), 1699-1712. doi:10.1002/ldr.3526

Hamunyela, E., Brandt, P., Shirima, D., Do, H. T. T., Herold, M., & Roman-Cuesta, R. M. (2020). Space-time detection of deforestation, forest degradation and regeneration in montane forests of Eastern Tanzania. *International Journal of Applied Earth Observation and Geoinformation, 88*, 102063. doi:10.1016/j.jag.2020.102063

Hoang, N. T., & Kanemoto, K. (2021). Mapping the deforestation footprint of nations reveals growing threat to tropical forests. *Nature Ecology & Evolution, 5*(6), 845-853. doi:10.1038/s41559-021-01417-z

Hu, X., Næss, J. S., Iordan, C. M., Huang, B., Zhao, W., & Cherubini, F. (2021). Recent global land cover dynamics and implications for soil erosion and carbon losses from deforestation. *Anthropocene, 34*, 100291. doi:10.1016/j.ancene.2021.100291

Hyandye, C., & Martz, L. W. (2017). A Markovian and cellular automata land-use change predictive model of the Usangu Catchment. *International Journal of Remote Sensing, 38*(1), 64-81. doi:10.1080/01431161.2016.1259675

Jana, A., Jat, M. K., Saxena, A., & Choudhary, M. (2022). Prediction of land use land cover changes of a river basin using the CA-Markov model. *Geocarto International, 37*(26), 14127-14147. doi:10.1080/10106049.2022.2086634

Keenan, T. F., & Williams, C. A. (2018). The terrestrial carbon sink. *Annual Review of Environment and Resources, 43*(1), 219-243. doi:10.1146/annurev-environ-102017-030204

Kindermann, G. E., Obersteiner, M., Rametsteiner, E., & McCallum, I. (2006). Predicting the deforestation-trend under different carbon-prices. *Carbon Balance and Management, 1*(1), 15. doi:10.1186/1750-0680-1-15

Kucsicsa, G., & Dumitrică, C. (2019). Spatial modelling of deforestation in Romanian Carpathian Mountains using GIS and Logistic Regression. *Journal of Mountain Science, 16*(5), 1005-1022. doi:10.1007/s11629-018-5053-8

Kura, A. L., & Beyene, D. L. (2020). Cellular automata Markov chain model based deforestation modelling in the pastoral and agro-pastoral areas of southern Ethiopia. *Remote Sensing Applications: Society and Environment, 18*, 100321. doi:10.1016/j.rsase.2020.100321

Lambin, E. F., & Geist, H. J. (2003). Regional differences in tropical deforestation. *Environment: Science and Policy for Sustainable Development, 45*(6), 22-36. doi:10.1080/00139157.2003.10544695

Li, X., Chen, G., Liu, X., Liang, X., Wang, S., Chen, Y., Pei, F., & Xu, X. (2017). A new global Land-use and land-cover change product at a 1-km resolution for 2010 to 2100 based on human–environment interactions. *Annals of the American Association of Geographers, 107*, 1040-1059. doi:10.1080/24694452.2017.1303357

Li, X., Yu, L., Sohl, T., Clinton, N., Li, W., Zhu, Z., Liu, X., & Gong, P. (2016). A cellular automata downscaling based 1 km global land use datasets (2010–2100). *Science Bulletin, 61*, 1651-1661. doi:10.1007/s11434-016-1148-1

Li, X., Zhou, Y., Hejazi, M., Wise, M., Vernon, C., Iyer, G., & Chen, W. (2021). Global urban growth between 1870 and 2100 from integrated high resolution mapped data and urban dynamic modeling. *Communications Earth & Environment, 2*(201), 1-10. doi:10.1038/s43247-021-00273-w

Liang, E., Wang, Y., Piao, S., Lu, X., Camarero, J. J., Zhu, H., Zhu, L., Ellison, A. M., Ciais, P., & Peñuelas, J. (2016). Species interactions slow warming-induced upward shifts of treelines on the Tibetan Plateau. *Proceedings of the National Academy of Sciences, 113*(16), 4380-4385. doi:10.1073/pnas.1520582113

Lima, A., Silva, T. S. F., Aragão, L. E. O. e. C. d., Feitas, R. M. d., Adami, M., Formaggio, A. R., & Shimabukuro, Y. E. (2012). Land use and land cover changes determine the spatial relationship between fire and deforestation in the Brazilian Amazon. *Applied Geography, 34*, 239-246. doi:10.1016/j.apgeog.2011.10.013

Malczewski, J. (1996). A GIS-based approach to multiple criteria group decision-making. *International Journal of Geographical Information Systems*, 37-41.

Malczewski, J. (2000). On the use of weighted linear combination method in GIS: Common and best practice approaches. *Transactions in GIS, 4*, 5-22. doi:10.1111/1467-9671.00035

Manson, S. M., & Evans, T. (2007). Agent-based modeling of deforestation in southern Yucatán, Mexico, and reforestation in the Midwest United States. *Proceedings of the National Academy of Sciences, 104*(52), 20678-20683. doi:10.1073/pnas.0705802104

Mas, J.-F., Soares Filho, B., Pontius, R. G., Farfán Gutiérrez, M., & Rodrigues, H. (2013). A suite of tools for ROC analysis of spatial models. *ISPRS International Journal of Geo-Information, 2*(3), 869-887. doi:10.3390/ijgi2030869

Mas, J. F., Puig, H., Palacio, J. L., & Sosa-López, A. (2004). Modelling deforestation using GIS and artificial neural networks. *Environmental Modelling & Software, 19*(5), 461-471. doi:10.1016/S1364-8152(03)00161-0

Meijer J.R., Huijbegts, M. A. J., Schotten, C. G. J., & Schipper, A. M. (2018). Global patterns of current and future road infrastructure. *Environmental Research Letters*(15), 064006. doi:10.1088/1748-9326/aabd42

Meiyappan, P., Dalton, M., O'Neill, B. C., & Jain, A. K. (2014). Spatial modeling of agricultural land use change at global scale. *Ecological Modelling, 291*, 152-174. doi:10.1016/j.ecolmodel.2014.07.027

Messier, C., Puettmann, K., Filotas, E., & Coates, D. (2016). Dealing with non-linearity and uncertainty in forest management. *Current Forestry Reports, 2*(2), 150-161. doi:10.1007/s40725-016-0036-x

Miranda-Aragón, L., Treviño-Garza, E. J., Jiménez-Pérez, J., Aguirre-Calderón, O. A., González-Tagle, M. A., Pompa-García, M., & Aguirre-Salado, C. A. (2012). Modeling susceptibility to deforestation of remaining ecosystems in North Central Mexico with logistic regression. *Journal of Forestry Research, 23*(3), 345-354. doi:10.1007/s11676-012-0230-z

Mollicone, D., Freibauer, A., Schulze, E. D., Braatz, S., Grassi, G., & Federici, S. (2007). Elements for the expected mechanisms on 'reduced emissions from deforestation and degradation, REDD' under UNFCCC. *Environmental Research Letters, 2*(4), 045024. doi:10.1088/1748-9326/2/4/045024

Monjardin-Armenta, S. A., Plata-Rocha, W., Pacheco-Angulo, C. E., Franco-Ochoa, C., & Rangel-Peraza, J. G. (2020). Geospatial simulation model of deforestation and reforestation using multicriteria evaluation. *Sustainability, 12*(24). doi:10.3390/su122410387

Moreno, N., Quintero, R., Ablan, M., Barros, R., Dávila, J., Ramírez, H., Tonella, G., & Acevedo, M. F. (2007). Biocomplexity of deforestation in the Caparo tropical forest reserve in Venezuela: An integrated multi-agent and cellular automata model. *Environmental Modelling & Software, 22*(5), 664-673. doi:10.1016/j.envsoft.2005.12.022

Organisation for Economic Co-operation and Development (OECD). (2018). *Rethinking Urban Sprawl: Moving Towards Sustainable Cities*. Retrieved from Paris: https://www.oecd-ilibrary.org/content/publication/9789264189881-en

Paegelow, M. (2018). LUCC based validation indices: figure of merit, producer's accuracy and user's accuracy. In *Geomatic approaches for modeling land change scenarios*, (Eds.) M. T. Camacho Olmedo, M. Paegelow, J.-F. Mas, & F. Escobar,(pp. 433-436). Cham: Springer International Publishing.

Pan, Y., Birdsey, R. A., Fang, J., Houghton, R., Kauppi, P. E., Kurz, W. A., Phillips, O. L., Shvidenko, A., Lewis, S. L., Canadell, J. G., Ciais, P., Jackson, R. B., Pacala, S. W., McGuire, A. D., Piao, S., Rautiainen, A., Sitch, S., & Hayes, D. (2011). A large and persistent carbon sink in the world's forests. *Science, 333*(6045), 988-993. doi:10.1126/science.1201609

Pendrill, F., Gardner, T. A., Meyfroidt, P., Persson, U. M., Adams, J., Azevedo, T., Bastos Lima, M. G., Baumann, M., Curtis, P. G., De Sy, V., Garrett, R., Godar, J., Goldman, E. D., Hansen, M. C., Heilmayr, R., Herold, M., Kuemmerle, T., Lathuillière, M. J., Ribeiro, V., Tyukavina, A., Weisse, M. J., & West, C. Disentangling the numbers behind agriculture-driven tropical deforestation. *Science, 377*(6611), eabm9267. doi:10.1126/science.abm9267

142

Pontius, R. G., Boersma, W., Castella, J.-C., Clarke, K., de Nijs, T., Dietzel, C., Duan, Z., Fotsing, E., Goldstein, N., Kok, K., Koomen, E., Lippitt, C. D., McConnell, W., Mohd Sood, A., Pijanowski, B., Pithadia, S., Sweeney, S., Trung, T. N., Veldkamp, A. T., & Verburg, P. H. (2008). Comparing the input, output, and validation maps for several models of land change. *The Annals of Regional Science, 42*(1), 11-37. doi:10.1007/s00168-007-0138-2

Pontius, R. G., & Parmentier, B. (2014). Recommendations for using the relative operating characteristic (ROC). *Landscape Ecology, 29*(3), 367-382. doi:10.1007/s10980-013-9984-8

Precinoto, R. S., Prieto, P. V., Figueiredo, M. d. S. L., & Lorini, M. L. (2022). Edges as hotspots and drivers of forest cover change in a tropical landscape. *Perspectives in Ecology and Conservation, 20*(4), 314-321. doi:10.1016/j.pecon.2022.07.001

Prevedello, J. A., Winck, G. R., Weber, M. M., Nichols, E., & Sinervo, B. (2019). Impacts of forestation and deforestation on local temperature across the globe. *PLoS ONE, 14*(3), e0213368. doi:10.1371/journal.pone.0213368

Qin, Y., Xiao, X., Liu, F., de Sa e Silva, F., Shimabukuro, Y., Arai, E., & Fearnside, P. M. (2023). Forest conservation in Indigenous territories and protected areas in the Brazilian Amazon. *Nature Sustainability, 6*(3), 295-305. doi:10.1038/s41893-022-01018-z

Ren, Y., Lü, Y., Comber, A., Fu, B., Harris, P., & Wu, L. (2019). Spatially explicit simulation of land use/land cover changes: Current coverage and future prospects. *Earth-Science Reviews, 190*, 398-415. doi:10.1016/j.earscirev.2019.01.001

Robertson, C., Chaudhuri, C., Hojati, M., & Roberts, S. A. (2020). An integrated environmental analytics system (IDEAS) based on a DGGS. *ISPRS Journal of Photogrammetry and Remote Sensing, 162*, 214-228. doi:10.1016/j.isprsjprs.2020.02.009

Rose, A. N., McKee, J. J., Sims, K. M., Bright, E. A., Reith, A. E., & Urban, M. L. (2020). *LandScan 2019* [digital raster data]. Retrieved from: https://landscan.ornl.gov/

Saaty, T. L. (1980). *The analytical hierarchy process*. New York: McGraw-Hill.

Sahr, K. (2011). Hexagonal discrete global GRID systems for geospatial computing. *Archives of Photogrammetry, Cartography and Remote Sensing, 22*, 363-376.

Sahr, K. (2022). DGGRID version 7.5. Retrieved March 2023 from https://github.com/sahrk/DGGRID

Sahr, K., White, D., & Kimerling, A. J. (2003). Geodesic discrete global grid systems. *Cartography and Geographic Information Science, 30*, 121-134. doi:10.1559/152304003100011090

Sharma, P., Thapa, R. B., & Matin, M. A. (2020). Examining forest cover change and deforestation drivers in Taunggyi District, Shan State, Myanmar. *Environment, Development and Sustainability, 22*(6), 5521-5538. doi:10.1007/s10668-019-00436-y

Southworth, J., Marsik, M., Qiu, Y., Perz, S., Cumming, G., Stevens, F., Rocha, K., Duchelle, A., & Barnes, G. (2011). Roads as drivers of change: Trajectories across the Tri-National frontier in MAP, the Southwestern Amazon. *Remote Sensing, 3*(5), 1047-1066. doi:10.3390/rs3051047

Sun, J., Zhang, Y., Qin, W., & Chai, G. (2022). Estimation and simulation of forest carbon stock in Northeast China forestry based on future climate change and LUCC. *Remote Sensing, 14*(15). doi:10.3390/rs14153653

Swets, J. A. (1988). Measuring the accuracy of diagnostic systems. *Science, 240*(4857), 1285-1293. doi:10.1126/science.3287615

Takam Tiamgne, X., Kanungwe Kalaba, F., Raphael Nyirenda, V., & Phiri, D. (2022). Modelling areas for sustainable forest management in a mining and human dominated landscape: A geographical information system (GIS)-multi-criteria decision analysis (MCDA) approach. *Annals of GIS, 28*(3), 343-357. doi:10.1080/19475683.2022.2026469

United State Geological Survey. (2022). *USGS EROS Archive - Digital elevation - shuttle radar topography mission (SRTM) 1 arc-second global*. Retrieved August 2020 from: https://www.usgs.gov/centers/eros/science/usgs-eros-archive-digital-elevation-shuttle-radar-topography-mission-srtm-1-arc?qt-science_center_objects=0#qt-science_center_objects

Uusivuori, J., Lehto, E., & Palo, M. (2002). Population, income and ecological conditions as determinants of forest area variation in the tropics. *Global Environmental Change, 12*(4), 313-323. doi:10.1016/S0959-3780(02)00042-0

Van Asselen, S., & Verburg, P. H. (2013). Land cover change or land-use intensification: Simulating land system change with a global-scale land change model. *Global Change Biology, 19*, 3648-3667. doi:10.1111/gcb.12331

Van Rossum, G., & Drake, F. (2009). Python 3 Reference Manual. Scotts Valley, CA: CreateSpace. Retrieved from https://www.python.org/

Vannier, C., Cochrane, T. A., Zawar Reza, P., & Bellamy, L. (2022). An analysis of agricultural systems modelling approaches and examples to support future policy development under disruptive changes in New Zealand. *Applied Sciences, 12*(5). doi:10.3390/app12052746

Vázquez-Quintero, G., Solís-Moreno, R., Pompa-García, M., Villarreal-Guerrero, F., Pinedo-Alvarez, C., & Pinedo-Alvarez, A. (2016). Detection and projection of forest changes by using the Markov chain model and cellular automata. *Sustainability, 8*(3). doi:10.3390/su8030236

Veronesi, F., Schito, J., Grassi, S., & Raubal, M. (2017). Automatic selection of weights for GIS-based multicriteria decision analysis: Site selection of transmission towers as a case study. *Applied Geography, 83*, 78-85. doi:10.1016/j.apgeog.2017.04.001

Vieilledent, G., Grinand, C., & Vaudry, R. (2013). Forecasting deforestation and carbon emissions in tropical developing countries facing demographic expansion: a case study in Madagascar. *Ecology and Evolution, 3*(6), 1702-1716. doi:https://doi.org/10.1002/ece3.550

Williams, B. A., Venter, O., Allan, J. R., Atkinson, S. C., Rehbein, J. A., Ward, M., Di Marco, M., Grantham, H. S., Ervin, J., Goetz, S. J., Hansen, A. J., Jantz, P., Pillay, R., Rodríguez-Buriticá, S., Supples, C., Virnig, A. L. S., & Watson, J. E. M. (2020). Change in terrestrial human footprint drives continued loss of intact ecosystems. *One Earth, 3*(3), 371-382. doi:https://doi.org/10.1016/j.oneear.2020.08.009

World Database on Protected Areas. (2023). *Global database on terrestrial and marine protected areas*. Retrieved 4 March 2020 from: https://www.protectedplanet.net/en/search-areas?filters%5Bdb_type%5D%5B%5D=wdpa&geo_type=region

Yager, R. R. (1988). On ordered weighted averaging aggregation operators in multicriteria decisionmaking. *IEEE Transactions on Systems, Man, and Cybernetics, 18*(1), 183-190. doi:10.1109/21.87068

Yu, Z., Ciais, P., Piao, S., Houghton, R. A., Lu, C., Tian, H., Agathokleous, E., Kattel, G. R., Sitch, S., Goll, D., Yue, X., Walker, A., Friedlingstein, P., Jain, A. K., Liu, S., & Zhou, G. (2022). Forest expansion dominates China's land carbon sink since 1980. *Nature Communications, 13*(1), 5374. doi:10.1038/s41467-022-32961-2

Chapter 6.

Forecasting scenarios of global multiclass land-use and land-cover change using deep learning and spherical geographic automata model

6.1. Abstract

Modelling land-use/land cover (LULC) change is vital for addressing global environmental and sustainability issues and evaluating various land system scenarios. However, existing geosimulation methodologies for global LULC change are inappropriate as they neglect spatial distortions caused by the Earth's curvature and cannot incorporate multiple LULC change processes. In this research a deep learning (DL) is integrated with spherical geosimulation modelling approach to simulate change of multiple LULC types globally under the shared socioeconomic pathways (SSP) scenarios. Based on the simulation results, the frontiers of urbanization, cropland expansion, and deforestation are indicated to be in developing countries particularly in Asia and Africa. The simulation outputs also reveal 42.5% - 63.2% of new urban development would occur on croplands. The proposed modelling approach can serve as a valuable tool for spatial decision-making and environmental policy formulation at the global level.

6.2. Introduction

Land-use/land-cover (LULC) change characterizes the modification of the Earth's surface through anthropogenic activities and manifested by processes such as urbanization, agricultural intensification and expansion, deforestation, afforestation, desertification, among others (Hu et al., 2021). According to estimates, approximately three quarters of the Earth's terrestrial surface has been altered by human activities (IPCC, 2019; Winkler et al., 2021). LULC change is perceived as a local process but however has several negative consequences at the regional and global level including biodiversity loss, ecosystem fragmentation, soil degradation, altered carbon cycle, and ultimately climate change (Foley et al., 2005; Malek et al., 2019). In recent decades, globalization, growth in human population and its associated increase in consumption,

expansion of bioenergy crops, and economic development have resulted in increased pressure on global land resources (Lambin & Meyfroidt, 2011). Thus, understanding and modelling the dynamics of LULC change at larger spatial scale has become essential for tackling environmental and sustainability issues across the globe (Turner et al., 2021).

Simulations provide spatial data and information for assessing the possible effects of policies under different trajectories and conditions, monitoring sustainable development, and for Earth systems modelling (Verburg et al., 2016). For instance, the shared socioeconomic pathways (SSP) scenarios (O'Neill et al., 2014) offer a consistent framework for exploring different plausible future conditions based on demographic, economic, human development, policies, and environmental factors. Implementing spatially-explicit models for global LULC change simulations in alignment with widely adopted long-term scenario frameworks can significantly enhance contributions to integrated modelling across different fields and facilitate research on large-scale interactions between social and environmental systems. (Gao & O'Neill, 2019). Further, global LULC change models are required for examining the interactions and feedback between LULC change processes and other socioeconomic and environmental systems operating at large spatial extents (Meiyappan et al., 2014).

To characterize different spatial dynamic systems and understand the relationship between LULC change processes and driving factors, spatially explicit modelling approaches are required (Verburg et al., 2016). Geosimulation models particularly cellular automata (CA) have become a preferred modelling choice due to their simplicity, ability to represent the non-linear process of change, and capture the spatiotemporal characteristics of complex systems (Torrens & O'Sullivan, 2001). Over the past decades, hybrid modelling approaches have been developed that integrate CA framework with other techniques including Markov chain (Rimal et al., 2018), multi-criteria evaluation (MCE) (Gharaibeh et al., 2020), logistic regression (Shu et al., 2020), etc. More recently, machine learning (ML) and deep learning (DL) techniques have also been integrated with CA models to simulate different LULC change processes and scenarios at the local and regional scale (Ball et al., 2022; Cao et al., 2019; Wang et al., 2023; Ye et al., 2019). In contrast to conventional ML techniques, DL architecture are able to extract relevant correlation features from numerous geospatial datasets resulting in improved modeling performance (Xiao et al., 2022). DL algorithms are also integrated with geosimulation models to mine transitions rules for simulating different complex

spatial processes (He et al., 2018). These algorithms are often implemented in LULC change models to derive transition probabilities using drivers of LULC change based on biophysical, socio-economic, and proximity factors (Mithun et al., 2022).

Despite the noted importance of large-scale LULC change models for environmental assessment and scenario development, several limitations in global LULC change modelling still persist. Primarily, existing global LULC change modelling approaches are implemented with conventional two-dimensional (2D) spatial data models that do not consider the curvature of the Earth's surface (Hu et al., 2021). This limitation causes distortion of geographic features and can result in spatial and computational errors when these models are utilized for large scale applications (Hall et al., 2020). For raster GIS datasets which are commonly applied in global LULC change modelling, the use of conventional geospatial models for global applications can result in overestimation of computed cell area especially at higher latitudes due to spatial distortions (Kelly & Šavrič, 2021). Further, due to the complexity of modelling interactions between different land systems and representing the spatial heterogeneity of LULC change processes in geosimulation models at the global level, several existing global LULC change applications only consider and simulate the dynamics of only one type of LULC change process such as urbanization (Gao & O'Neill, 2020; Li et al., 2021), agricultural expansion (Cao et al., 2021; Meiyappan et al., 2014), or deforestation (d'Annunzio et al., 2015). These model applications often consider only one land class and on binary representation such as urban and non-urban or forest and non-forest, which over simplifies the represented mechanisms of LULC change. Considering that different LULC change processes occur concurrently, comprehensive multi LULC change simulations are required for determining ensemble of land types to generate more realistic possible outcomes of LULC change patterns (Liu et al., 2017).

Given the advantages of DL techniques in handling large datasets and the gap in representing multi LULC types in geosimulation models at the global level, this research study aims to leverage the capabilities of DL and geosimulation approaches for characterizing the spatio-temporal dynamics of different LULC types. The main objectives are to 1) develop a DL-based geographic automata model for simulating multiple LULC types at the global scale; 2) implement the model on global datasets and considering the SSP scenarios to forecast LULC change across the 21st century.

148

6.3. Materials and Methods

6.3.1. Model Overview

The proposed multi LULC change spherical geographic automata model is based on the integration of the DGGS spatial framework, DL, and geographic automata for simulating multiple LULC change processes at the global level. The schematic representation of the modelling framework utilized in this research study is presented in Figure 6.1. The modelling framework consists of several subcomponents and mechanisms including the spherical spatial framework, DL, LULC conversion matrix, urban rank size, spherical geographic automata (SGA), and land demand model. These subcomponents and mechanisms are all linked together through the SGA component. The spherical spatial component of the model is based on the DGGS framework which provides a suitable spherical spatial medium for representing geospatial datasets at the global level by considering the curvature of the Earth's surface. The DL technique is incorporated to derive transition probabilities and applied for guiding the LULC change transition rules. The conversion matrix characterizes the level of difficulty in converting one LULC type into another. This model component captures the likelihood of a specific land-use or land-cover type changing to another type.

To capture the hierarchical relationship between different cities in an urban system, an urban rank size rule algorithm was implemented. The law highlights the spatial heterogeneity in urban systems, indicating that larger cities exert a bigger impact on urban development (Berry, 1964; Krugman, 1996; Wang et al., 2022). LULC change is simulated by the SGA component based on parameters such as transition rules, neighbourhood, cell state, constraints, LULC conversion weights, and Zipf's law coefficient. A land demand model is utilized to calculate the extent of land change for the different LULC types and consistent with the five SSP baseline scenarios. The following sections describe each component of the proposed model in detail.
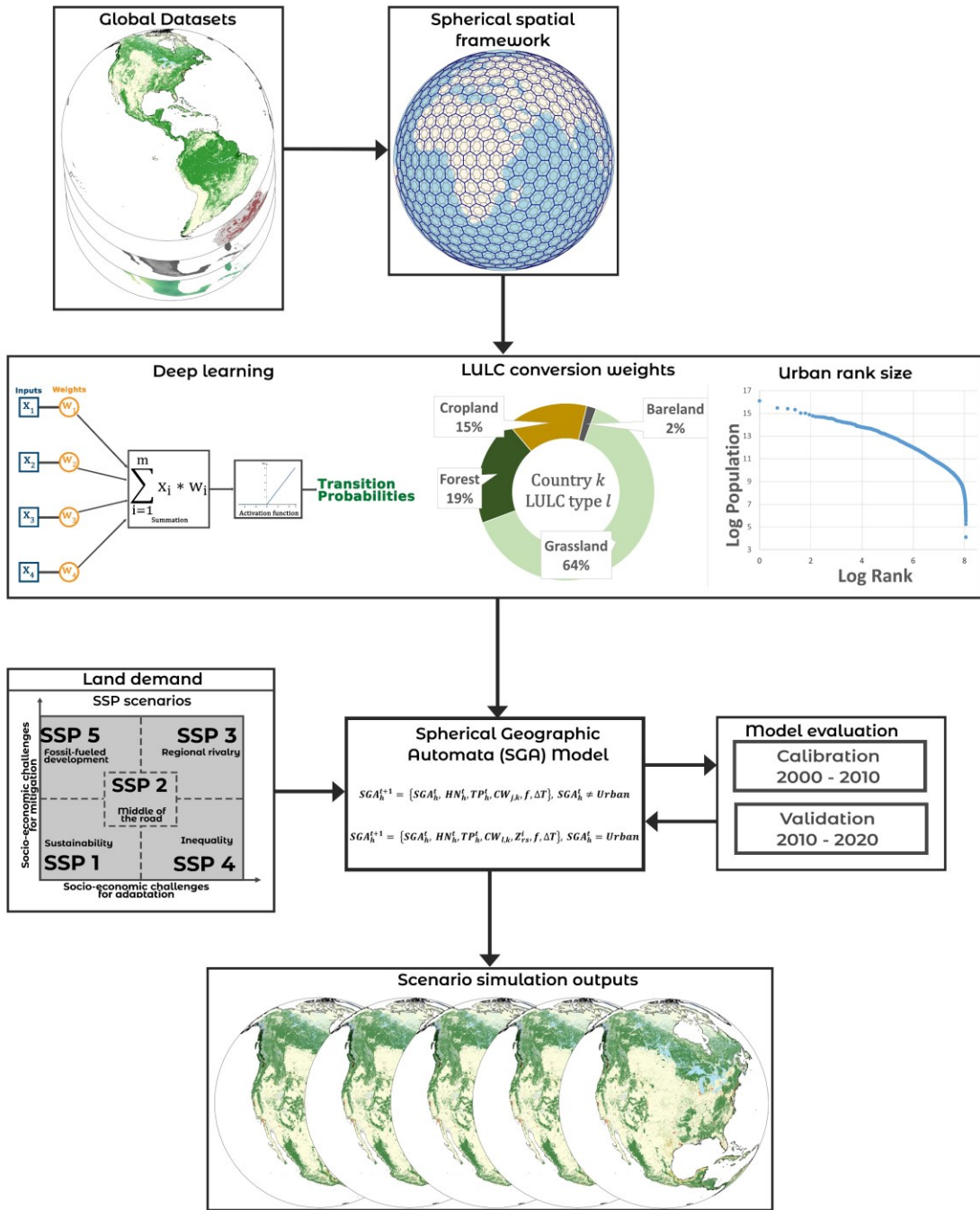
Figure 6.1. Framework of the multiclass DL-based spherical geographic automata modelling approach for simulating LULC change processes at the global level.

Datasets

This research study covers the entire terrestrial surface of the Earth except for Antarctica and employs several available geospatial datasets with global coverage to implement the model. Global land-use/land-cover datasets were obtained from the

European Space Agency (ESA) portal (ESA, 2022). The original 37 LULC classes in the ESA datasets were reclassified into seven main land types: urban, forest, cropland, grassland, bare areas, water bodies, and snow and permanent ice. Gridded population density dataset was acquired from the LandScan database (Sims et al., 2022) and gross domestic product (GDP) from (J. Chen et al., 2022). Global digital elevation model (DEM) was retrieved from the United States Geological Survey (USGS) data portal (USGS, 2022). Bioclimatic variables including temperature and precipitation datasets were acquired from the WorldClim portal (Fick & Hijmans, 2017) and soil properties datasets from the SoilGrids data portal (Hengl et al., 2017). Location of protected areas were obtained from the World Database on Protected Areas (WDPA) online data catalogue (WPDA, 2023). Additionally, global road dataset was sourced from the Global Road Inventory Project (GRIP) portal (Meijer et al., 2018) and past forest disturbance from the Global Wildfire Information System (GWIS) (Artés et al., 2019). Datasets detailing the boundaries of administrative regions were also acquired from the Global Administrative Areas (GADM) data portal (GADM, 2023). Datasets for years 2000, 2010 and 2020 were used to build and evaluate the model, with temporal resolution of 10 years.

Spherical spatial framework component

The spherical spatial framework is based on the icosahedron polyhedron and projected to the WGS84 ellipsoid using the icosahedral Snyder equal-area (ISEA) projection. The utilization of ISEA DGGS cells provide equal-area cells to partition the Earth's surface while also considering its curvature (Goodchild, 2018). Hexagons are utilized to tessellate the spherical surface given its properties and merits over other regular polygons such as squares and triangles. For instance, hexagons offer uniform neighbouring relationships, can be used to approximate circular regions, and tessellate the sphere with the least average error (Sahr, 2011; Zhou et al., 2020). Thus, the proposed modelling framework utilizes geospatial datasets that are mapped to a specified DGGS composed of hexagonal spatial tessellation with each cell encompassing an area of 3.55km2 and intercell spacing of 2.04 km. The quantization of existing spatial datasets into DGGS format follows the method in Robertson et al. (2020), and using the DGGRID library (Sahr, 2022).

DL component

In this study, the DL component is used to estimate transition probabilities for each LULC type and was implemented using several relevant spatial drivers informed from the literature and data availability including socio-economic (population density, gross domestic product (GDP)), proximity-based variables, biophysical (soil properties, elevation, slope), and climate variables (temperature, rainfall). These driver variables are normalized into the range [0-1] and utilized to derive the transition probability for the different LULC types.

The DL component utilizes the deep neural network technique and is constructed with several hyperparameters including activation function, loss function, optimization algorithm, epoch, and batch size. The DL algorithm derives transition probabilities for the different LULC types based on the relationships between LULC change and the associated spatial driving factors. Commonly used activation functions for implementing DL models include the sigmoid function, tanh function, ReLU function, etc. In this research study the ReLU activation function was utilized due to its computational efficiency and also allows the model to easily obtain sparse representation, which can help the model capture patterns and relationships in datasets (Glorot et al., 2011). The binary cross entropy (BCE) is utilized as the loss function and the Adam optimization algorithm applied to update the weight of the DL model after each epoch. The maximum epoch of the DL model was set to 500 with the batch size set to 20. The combination of hyperparameters utilized in this study are determined based on the results of DL model testing. In developing the DL model, 70% of the datasets were used as training set to train the model and the remaining 30% was utilized as testing dataset to assess the performance of the DL technique. The resulting transition probability outputs, derived using data for years 2010 and 2020, are fed to the SGA model component and used as input parameter for guiding the transition rules for the different LULC types. In this study, the DL model is implemented in the Python programming language with the Pytorch deep learning library (Paszke et al., 2019).

LULC conversion weights component

The LULC conversion weights represent the difficulty or desirability associated with converting one LULC type into another. This mechanism represents the economic or environmental constraints linked to the conversion of a particular LULC type into a

different type. In the proposed modelling framework, this characterizes the likelihood of a hexagonal cell with a specific LULC type changing into another type. The LULC conversion weights are derived based on analysis of historical LULC data and in this research study, utilizing the 2010 and 2020 ESA land-use/land-cover datasets. To account for the spatial heterogeneity of LULC change processes across different regions, the LULC conversion weights are calculated separately for each country and for the different LULC types. Conversion weights range between 0 and 1, where 0 indicate conversion to a particular LULC type is not possible and a higher value denote increased likelihood of conversion to that specific LULC type. For instance, in a specific country, the likelihood of converting grassland into urban land-use can be very high whereas the cost of converting cropland into urban is very low. In this context, the higher economic value attributed to croplands in comparison to grasslands may render the conversion from grassland to urban more feasible than the conversion from cropland to urban use. Thus, in the proposed model, cells with state grassland are more likely to be simulated into urban in that specific country.

Urban rank size component

Generally, the size of cities or urban systems is inversely proportional to its rank across a specific geographic space, and this can be explained by the "Rank Size Rule" or Zipf's law (Auerbach & Ciccone, 2023; Zipf, 1949). Zipf's law also reflect the fractal nature of cities and the interconnectedness within a complex urban system (Batty, 2013). Research studies indicate the size and rank of urban systems can remain steady over long periods at the national level and even across larger spatial extents (Jiang et al., 2015; Veneri, 2016). Larger cities tend to grow faster due to factors such as agglomerative economics, urban infrastructure, and human capital (Duranton & Puga, 2014). Thus, to preserve the national urban size distribution in this research study, a rank size rule algorithm was incorporated into the modelling framework. The algorithm is applied at the national level using sub-region as the spatial units, derived from the GADM dataset. Based on the rule, urban areas in sub-regions with larger population have a higher rank coefficient for urban development than urban areas in sub-regions with smaller population. This component of the model is implemented to characterize the rank size effect of cities existing in urban systems at the national level. The rank size rule (Soo, 2005) can be formulated as:

$$\log y_i = \log A - \alpha \log x_i \tag{1}$$

where x is the size of sub-region i in terms of population, y is the number of sub-regions with population greater than sub-region i, α is a constant, and A is the size of the largest sub-region at the national level. Population values for each sub-region were extracted from the Landscan dataset, based on the methodology described in Dobson et al. (2000). In all, a total of 356,508 sub-regions were utilized to calculate the Zipf's rank coefficient.

Spherical geographic automata component

The SGA component is designed to simulate multiple LULC changes based on several parameters. During each iteration, the state of each hexagonal cell changes or remains the same based on the cell's neighbourhood, transition probability from the DL model, LULC conversion weight, constraint parameter, and in the case of urban development, Zipf's law coefficient. The spherical geographic automata transition rules for urban LU type can be expressed as:

$$SGA_h^{t+1} = \{SGA_h^t, HN_h^t, TP_h^t, CW_{l,k}, Z_{rs}^i, f, \Delta T\}, SGA_h^t = Urban \tag{2}$$

and for non-urban LULC types as:

$$SGA_h^{t+1} = \{SGA_h^t, HN_h^t, TP_h^t, CW_{j,k}, f, \Delta T\}, SGA_h^t \neq Urban \tag{3}$$

where SGA_h^{t+1} denotes the state of a hexagonal cell h at the next time step t+1, SGA_h^t is the state of hexagonal cell at initial time t , HN_h^t represents the hexagonal neighbourhood consisting of six cells around the central cell, TP_h^t is the transition probability obtained from the DL component of the model, $CW_{j,k}$ is the LULC conversion weight which indicate the likelihood of LULC type l changing into another type in country k, Z_{rs}^i is the urban rank size rule coefficient obtained for sub-region i, f is the function of transition rules that determine how the state of cells change over time, and ΔT is the discrete time increment representing one iteration of the model. For the urbanization process ($SGA_h^t = Urban$), the additional parameter Z_{rs}^i is implemented to ensure cells in sub-regions with higher coefficient have an increased likelihood of being converted into urban at the next iteration. The LULC types of water bodies and permanent ice and snow remain unchanged. The model iteratively simulate LULC changes based on the different model

parameters until the demand for the different LULC types are reached for each country under the different SSP scenarios. One model iteration is equivalent to a temporal resolution of 10 years.

Land demand component

The shared socioeconomic pathways is a set of five distinctive scenarios of future socio-economic development and challenges to climate change mitigation and adaptation under a consistent set of assumptions over the 21st century (O'Neill et al., 2014). The SSP scenarios do not however incorporate mitigation strategies, adaptation responses, or the impacts of climate change (O'Neill et al., 2017). In addition, the projections of possible future changes in scenario variables and indicators in the SSP database are limited to quantity and lack spatial components (Riahi et al., 2017). This research study is providing the spatial and dynamic component of the LULC change process and connecting with the SSP scenarios. The five scenarios are named SSP1: Sustainability - taking the green road, SSP2: Middle of the road (business as usual), SSP3: Regional rivalry - a rocky road, SSP4: Inequality - a road divided, and SSP5: Fossil-fuelled development - taking the highway. Table 6.1 provides a summary of the land-use characteristics and assumptions across the five SSPs as presented in Pop et al. (2017). The SSP scenario framework and data variables has been widely adopted and often integrated with different models to assess greenhouse gas emissions, energy consumption, LULC change, as well as climate impact and adaptation across different sectors from the local to the global scale (O'Neill et al., 2020).

Table 6.1.   Description of land use characteristics and assumptions for the five SSP scenarios. Source; O'Neill et al., 2017.

Assumptions	SSP1	SSP2	SSP3	SSP4	SSP5
Population Growth	Relatively low	Medium	Low	Relatively high	Relatively low
GDP	High in LICs, MICs; medium in HICs	Medium; Uneven	Slow	Low in LICs, medium in other countries	High
Urbanization	High; well managed	Medium; continuation of historical patterns	Low; poorly managed	High; mixed across and within cities	High; better management. over time, some sprawl
Land-use change regulation	Strong regulation to avoid environmental trade-offs	Medium regulation; slow decline in the rate of deforestation	Limited regulation; continued deforestation	Highly regulated in MICs and HICs; lack of regulation in LICs lead to high deforestation rates	Medium regulation; slow decline in the rate of deforestation
Agriculture productivity	High improvements in agricultural productivity; rapid diffusion of best practices	Medium pace of technological change	Low technology development	Productivity high for large scale industrial farming, low for small-scale farming	Highly managed, resource-intensive; rapid increase in productivity
Environmental Impact of food consumption	Low growth in food consumption, low- meat diets	Material-intensive consumption, medium meat consumption	Resource-intensive consumption	Elites: high consumption lifestyles; Rest: low consumption	Material-intensive consumption, meat-rich diets
Land-based mitigation policies	No delay in international cooperation for climate change mitigation. Full participation of the land use sector	Delayed international cooperation for climate change mitigation. Partial participation of the land use sector	Heavily delayed international cooperation for climate change mitigation. Limited participation of the land use sector	No delay in international cooperation for climate change mitigation. Partial participation of the land use sector	Delayed international cooperation for climate change mitigation. Full participation of the land use sector

In the implementation phase of the proposed multi-class DL-SGA model, the total amount of change required for the different LULC change types are computed with the land demand component using datasets including projected population, GDP, and LULC change from the SSP database (Popp et al., 2017; Riahi et al., 2017). Country level historical data on GDP and population were also obtained from the World Bank (World Bank, 2023) and United Nations (UN) Population Division (UN-DESA, 2023), respectively. The land demand component is designed to compute the magnitude of land change for each LULC type and country at a 10-year temporal interval between 2020 and 2100. Country specific urban change demand is computed based historical data of urban land-use, GDP, and population for years 2010 and 2020 and future projections of population and GDP using a regression function. In this context, data on projected changes in GDP and population are utilized as indicators for future changes in urban extent at the country level. The land demand for forest and cropland are based on the SSP LULC database for the different scenarios. To ensure the total area of the different LULC types in the SSP database is consistent with the ESA LULC dataset utilized in this research, a harmonization function (G. Chen et al., 2022) was implemented and can be expressed as:

$$LD_{l,r}^{t+1} = \frac{ESA_i^t * SSP_i^{t+1}}{SSP_{l,r}^t} \qquad (4)$$

where $LD_{l,r}^{t+1}$ represents the adjusted land demand for LULC type l and for region r at time *t+1*, ESA_i^t denotes the land area for LULC l in region r at time t from the ESA data, SSP_i^{t+1} represents the land area for LULC l in region r at time *t+1* from the SSP database, and $SSP_{l,r}^t$ denotes the land area for LULC l in region r at time t from the SSP database.

6.3.2. Multiclass DL-SGA Model Evaluation and Implementation

Multiclass DL-SGA evaluation, consisting of calibration and validation was executed using different LULC change evaluation metrics such as the relative operating characteristic (ROC), figure of merit (FoM), producer's accuracy (PA), and user's accuracy (UA). ROC (Hanley & McNeil, 1982) is a model evaluation technique that is often used for assessing the performance of binary classification with continuous values (Mas et al., 2013). The ROC curve is derived by plotting the true positive rate against the

false positive rate using different value thresholds. From the ROC curve, the area under the curve (AUC) metric is obtained with values ranging between 0 and 1, where a higher AUC value indicates a more accurate model (Camacho Olmedo et al., 2022). AUC values were calculated for LULC types of cropland, forest, and urban. Additionally, the FoM metric (Pontius et al., 2008) was applied to evaluate the proposed model by comparing the simulation output against observed LULC data. The FoM index is a common measure for determining the accuracy of LULC change models as it focuses on the accuracy of the changed areas, rather than the entire study area. The FoM index is the ratio of the intersection of simulated and observed change over the union of simulated and observed change and expressed as:

$$FoM = \frac{B}{A + B + C + D} \tag{5}$$

where A is the number of observed changed hexagonal cells simulated as non-change, B is the number of observed changed hexagonal cells correctly simulated as change, C is the number of observed changed hexagonal cells simulated as change but to the wrong LULC type, and D is the number of unchanged hexagonal cells simulated as change by the model. From the FoM components, two additional accuracy indices, producer's accuracy (PA) and user's accuracy (UA) can be derived (Paegelow, 2018). Producer accuracy represent the proportion of cells the model corrected simulated as change against observed changed cells and user accuracy is the proportion of cells the model corrected simulated as change against the total simulated change by the model. The producer's accuracy and user's accuracy indices are formulated as:

$$PA = \frac{B}{A + B + C} \tag{6}$$

$$UA = \frac{B}{A + B + D} \tag{7}$$

The model was calibrated using observed datasets for the year 2000 and 2010 and validated using data for year 2020, which represents independent dataset not used in the model building and calibration phases. The obtained values for FoM, PA, and UA

are presented in Table 6.2. The FoM values derived in the model calibration and validation phases were 28.61% and 23.35% respectively. These values are similar to the results of other global LULC change simulations with reported values in the range of 10% and 19% (G. Chen et al., 2022; Li et al., 2017).

Table 6.2. **Obtained model evaluation values for FoM, PA, and UA metrics for the calibration and validation phases.**

Metric	Calibration	Validation
FoM	28.61%	23.35%
PA	33.17%	38.59%
UA	35.66%	42.07%

Validation of the proposed model with the ROC metric reveals the AUC values for all LULC types to be above 0.8 with obtained values ranging between 0.81- 0.94, indicating an overall good performance of the model. Figure 6.2 presents the ROC curves and the AUC values for the different LULC types simulated in this research. The AUC values derived for model evaluation in this research commensurate with values obtain from other global geosimulation models with values from these studies varying between 0.72 and 0.96 (G. Chen et al., 2022; Li et al., 2016; Li et al., 2021).
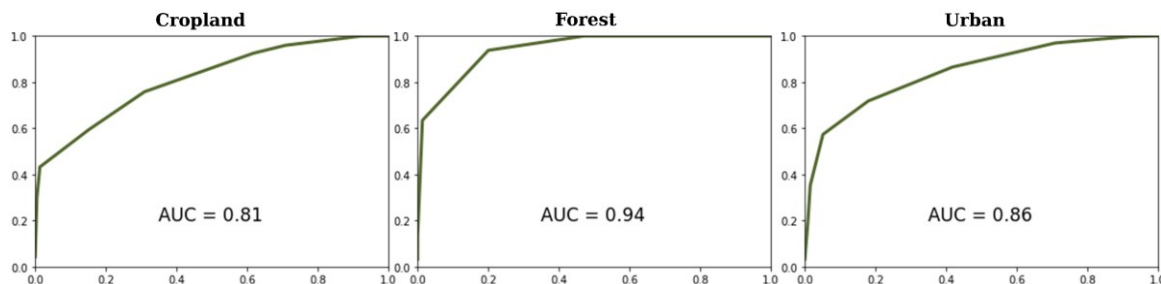
Figure 6.2. **Obtained ROC curves and AUC values for cropland, forest, and urban LULC types.**

Given the evaluation results, the model is then used to simulate various LULC change across the five SSP scenarios. For each scenario, the proposed model is run for eight iterations with a temporal resolution of 10 years to simulate global LULC change between 2020 (T^i) and 2100 (T^{i+8}). The Multiclass DL-SGA model and its components are designed and implemented in the Python programming language (Van Rossum & Drake, 2009).

6.4. Simulation Results

6.4.1. Global Trends of Land-use/Land-cover Change

Although the different LULC types have the same initial extent in 2020 under the five SSP scenarios, the simulated LULC changes over the course of the simulation vary significantly across scenarios. Changes in the extent of the major LULC types modelled in this research study between 2020 and 2100 are presented in Figure 6.3. Based on the obtained simulation results, the global urban extent by 2100 varies between 1.4 million km^2 and 3.08 million km^2 across the five SSP scenarios. The least change in urban extent was observed under the SSP3 (Regional rivalry) scenario with the total global urban extent increasing by 78.7% between 2020 and 2100. In contrast, the global urban extent under the SSP5 (Fossil-fuelled development) scenario increased by 272% within the same time period. Despite the differences in urban growth rates across the five scenarios, similarities can also be observed. For example, both the SSP3 and SSP4 scenarios have noticeably slower rates of urbanization and show similar trends between 2020 and 2100. The SSP1 and SSP2 scenarios can also be classified as having moderate growth trends with the difference in urban extent between the two scenarios by 2100 amounting to only 123 thousand km^2. Urbanization mainly occurs at the expense of cropland with 42.48% - 63.23% of new urban expansion occurring on cropland. The largest conversion of cropland to urban land-use occurs under the SSP5 scenario with a total of 0.96 million km^2 of cropland converted into urban between 2020 and 2100. Grassland is also a key contributor to urban expansion with 25.86% - 42.28% of new urban expansion transitioning from grassland into urban land-use across the five scenarios.

In 2020, 14.5 million km^2 of the Earth's terrestrial surface was covered by cropland. By 2100, the total extent of cropland at the global level obtained from the simulations vary between 15.8 million km^2 and 23.5 million km^2 across the scenarios. Further analysis indicate between 3.44 million km^2 to 9.73 million km^2 of land would be converted into cropland whereas 0.69 million km^2 to 2.07 million km^2 of cropland would transition into other LULC types. This represents a net cropland gain between 1.37 million km^2 and 9.03 million km^2 in the period between 2020 and 2100. The largest net increase in the extent of cropland occurs under the SSP3 scenario whereas SSP1 has the least net gain in cropland. Expansion in cropland mainly comes from forest and

grassland which collectively contribute 85.51% – 98.37% of cropland increase at the global level. On the contrary, the main cause of cropland reduction across the five scenarios is urbanization, accounting for 26.41% to 87.44% of the observed decline in cropland. Conversion of cropland into urban land-use is largest under SSP5 with 0.96 million km^2 of cropland converted into urban whereas the least conversion would occur under SPP3 and SSP4 with 0.41 million km^2 and 0.43 million km^2, respectively. These extents represent 66.6%, 59.05%, and 26.41%, correspondingly of the total cropland loss under these three scenarios.
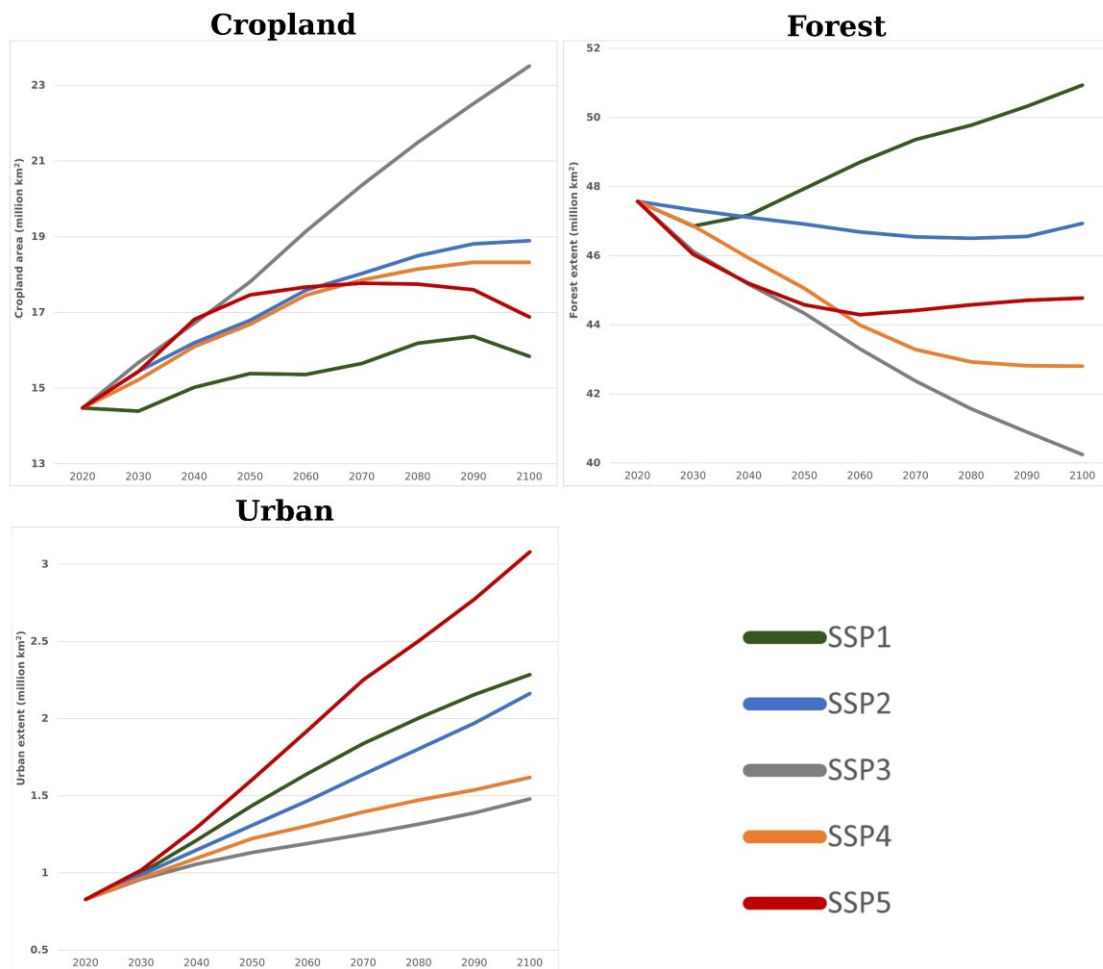
Figure 6.3. Simulated land use change (million km^2) for urban, cropland, and forest LULC types across the five SSP scenarios.

The simulation results also reveal changes in the total global forest land-cover type extent across the SSP scenarios. The global forest extent in 2020 was 47.6 million km^2 and ranges between 40.2 million km^2 and 50.9 million km^2 by 2100. There is a net loss of forest under SSP2, SSP3, SSP4 and SSP5 with the global net forest loss under

these four scenarios ranging between 0.64 million km^2 and 7.33 million km^2. There is however a net gain in forest extent under the SSP1 scenarios with the global net forest gain under this scenarios amounting to 3.36 million km^2. At the global level, gains of forest are typically from grassland (68.53% - 97.88%) and cropland (2.04% - 31.47%). These two land-cover types are also the main contributor to deforestation with 39.41% - 73.18% and 23.6% - 56.47% of forest cover converted into cropland and grassland respectively, across the five scenarios between 2020 and 2100.

6.4.2. Observed LULC Changes at the Continental and Regional Levels

Differences in the rates and extents of LULC changes can be observed at the regional level and among the different scenarios. Based on the simulation results, Asia would have the largest extent of new urban development with 50.16%- 63.54% of the total global urban expansion occurring on the Asian continent. The obtained simulation output also reveal Africa would have the second largest contribution to global urbanization accounting for 9.27%- 19.7% of new urban development at the global level. The extent of new urban development in Europe under SSP4 would however be larger than that of Africa. Collectively, Europe and North America would account for 6.61% - 25.73% of new urban development under the five scenarios. In relative terms, the rate of urbanization is fastest in Africa under all scenarios except for the Inequality scenario (SSP4). For instance, under the SSP1 scenario, the urban extent in Africa increased by 458% whereas the urban area in Asia increased by 258%. On the contrary, the urban extents in Europe and North America increased by only 76% and 67% respectively. Figure 6.4 presents the rate of urban growth between 2020 and 2100 under the SSP2 scenario and across different regions and countries.

In Africa and Asia, urban expansion mainly occurs at the expense of cropland. Across the five scenarios, cropland would account for 35.49% - 61.95% and 54.81% - 76.09% of the total urban expansion on these two continents, respectively. However, on other continents, urban land-use expansion was mainly from grassland. In Europe and North America for example, 51.98% – 72.43% and 93.95% -100% of future urban expansion would occur on grassland. Despite the high transition of grassland into urban land-use in these regions, loss of cropland due to urban expansion is still prominent. For

instance, in Europe, 14.09% - 34.49% of all urban growth would occur on croplands across the five SSP scenarios.
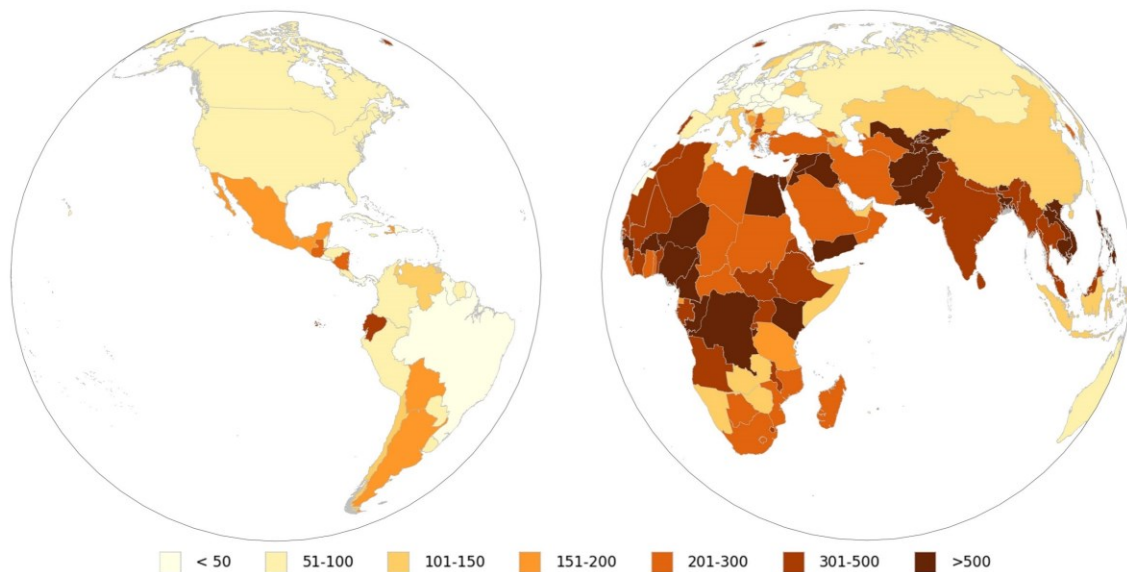
Figure 6.4. **Rates of urban expansion (%) between 2020 and 2100 across different countries and countries under the SSP2 (Middle of the road) scenario.**

Beside the SSP2 and SSP3 scenarios where there is increase in the extent of cropland across all continents, the simulation results revealed varied changes in cropland patterns across different regions. The largest net increase in cropland would be under the SSP3 scenario for all regions except for Eastern Europe which has a net cropland loss of 116.4 thousand km^2. At the regional level, the largest net increase in cropland would be in Africa with the extent increasing by 6.18 million km^2 and 4.53 million km^2 under the SSP3 and SSP4 scenarios respectively. South America is also revealed to have extensive growth in cropland, with the extent of cropland increasing by 1.47 million km^2 and 1.37 million km^2 under the SS1 and SSP3 scenarios respectively. On the contrary, 0.68 million km^2 of cropland would be lost in Asia under the SSP1 scenario. The net decrease in the extent of cropland in Europe would also amount to 0.53 million km^2 and 0.24 million km^2 under SSP1 and SSP5, respectively. The expansion of cropland occurs mainly at the expense of grassland and forest across the different regions. Under SSP3, 26% and 59.1% of cropland expansion in Asia would be from forest and grassland respectively while 70.35% and 29.2% of cropland increase in Europe would transition from forest and grassland, correspondingly. The conversion of cropland into other LULC types differs across regions and the five scenarios as well.

163

However, the conversion of cropland into urban remains consistent across several regions and scenarios. The largest conversion of cropland into urban would be in Asia and Africa with the total area ranging between 315 thousand km^2 - 772 thousand km^2 and 38 thousand km^2 - 164 thousand km^2, respectively. The conversion of cropland into grassland and forest is also prominent especially in Europe, North America, and South America. Under the SSP5 scenario for example, 81.45%, 84.12%, and 88.36% of cropland loss in Europe, North America, and South America, respectively would transition into forest and grassland collectively.

The largest net gain in forest area would be in Asia, Europe and North America. The net forest gain on these three continents under the under SSP1 and SSP4 scenarios could vary between 0.96 million km^2 - 2.51 million km^2, 0.092 million km^2 - 0.8, and 0.042 million km^2 - 0.98 million km^2 respectively. On the contrary, Africa would experience the largest rate of deforestation with the net forest loss across all scenarios varying between 0.35 million km^2 to 6.25 million km^2. The pattern of deforestation in South America vary greatly, with the region experiencing net forest loss under the SSP2 and SSP3. The net forest loss in South America would vary between 0.88 million km^2 and 1.67 million km^2 under these two scenarios. There is however a net gain in forest under the other three scenarios (SSP1, SSP4, and SSP5). The transition of other LULC types into forest is dominated by grassland as well as cropland under the five scenarios. Likewise, loss of forest is mostly to cropland, grassland, and urban. Transition from forest to cropland is prominent in Asia, Europe, and South America whereas forest transition to grassland is prominent in North America. Under the SSP3 scenario for example, 0.42 million km^2 and 0.68 million km^2 of forest in Asia and South America were converted into cropland respectively, corresponding to 71.3% and 76.26% of deforested areas in these two regions.

6.4.3. Trends in LULC Change at the National Level

At the national level, results from the simulation output reveal variations in LULC change across the different scenarios and countries. Figure 6.5 presents the net change in cropland, forest, and urban extents for different countries under the five SSP scenarios. In addition, Figure 6.6 also depicts the obtained simulation outputs of LULC changes in 2100 compared to the base year for different regions across the globe under the different scenarios. In the context of urban development, China, India, and Pakistan

164

are among the top seven countries with the largest extent of new urban development across the five scenarios. The urban extent is largest under the SSP5 scenario for majority of countries and least under the SSP3 scenario. China is revealed to have the largest urban extent by 2100 across all scenarios with the urban extent varying between 0.23 million km^2 and 0.44 million km^2 by 2100. This is followed by the United States with its total urban extent by 2100 ranging between 0.16 million km^2 and 0.37 million km^2.
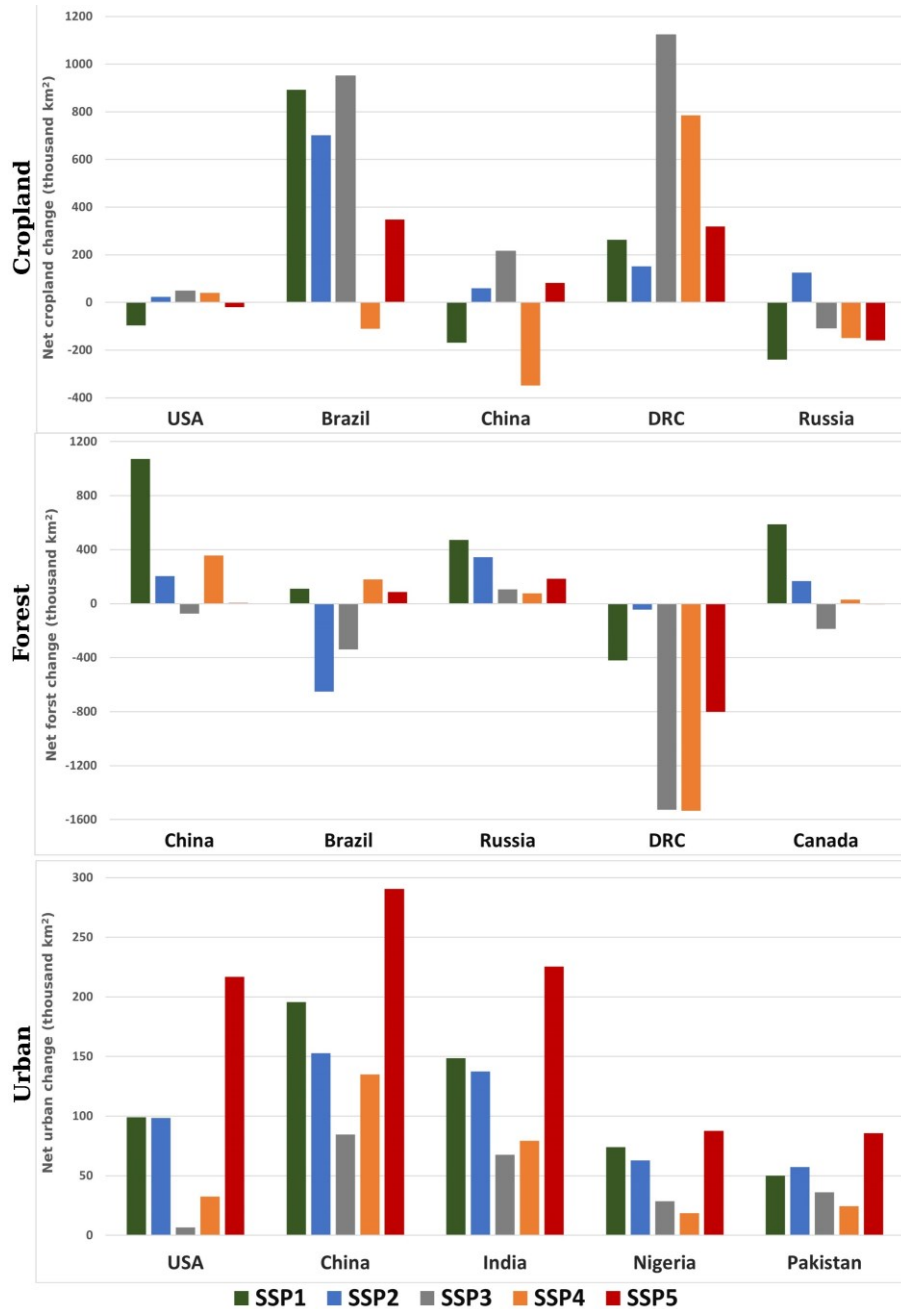

Figure 6.5. Net change in cropland, forest, and urban extent under the five scenarios across different countries.
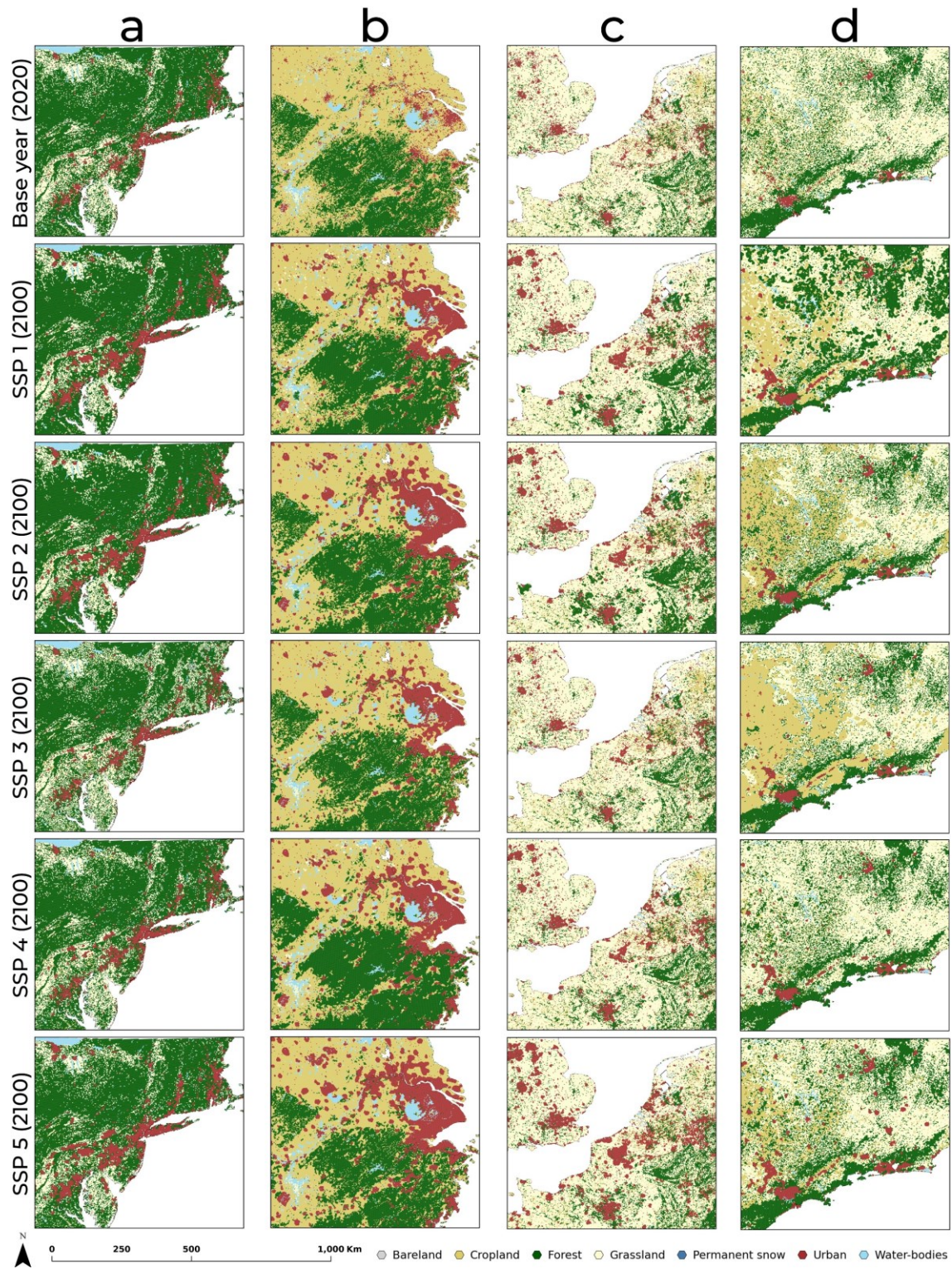
Figure 6.6. Obtained simulation results of LULC change for year 2100 under the five SSP scenarios compared to the base year 2020 for a) Eastern USA, b) Yangtze Delta, China, c) Western Europe, and d) Rio de Janeiro-Sao Paulo Megalopolis; Brazil.

Moreover, the trend of urban expansion varies across countries at different stages of urbanization. Urban expansion is very extensive and rapid in countries in the initial stages of urbanization whereas the rate of expansion is slower in developed and already urbanized countries. Here the United States, China, and India are used as examples of countries at the mature, middle, and initial stages of urbanization respectively. The United States experiences moderate urban growth with the rate of expansion declining towards the end of the 21st century. The extent of new urban development in the United States ranks among the top 5 across all scenarios except for the SSP3 scenario where new urban growth amounts to only 6 thousand km^2. Urbanization in China increases rapidly but begins to plateau and stall after the middle of the 21st century. The extent of new urban development in China would vary between 84 thousand km^2 and 290 thousand km^2 across the five scenarios. Conversely, urban growth in India would expand rapidly with no abatement through 2100. The total urban extent in India would expand between 67 thousand km^2 and 225 thousand km^2 across the five scenarios.

Given the varying socioeconomic conditions under the different scenarios, the simulated change patterns of cropland at the country level are widely diverse. The most distinct pattern of cropland change is the large expansion in South America, Western African and Middle Africa especially in countries such as Brazil, Democratic Republic of Congo (DRC), Nigeria, and Chad. Based on the simulation results, the DRC would have the largest increase in cropland with the net change in cropland varying between 0.15 million km^2 to 1.12 million km^2 across the five scenarios (Fig 6). On the contrary, net loss in cropland is demonstrated to occur mainly across countries in Eastern Europe, China, India, and Pakistan. Under the SSP4 scenario, China is revealed to lose 0.348 million km^2 of cropland, the largest of any country across all scenarios. The Russian Federation would also experience a decrease in the total extent of cropland under all scenarios except for the SSP2 scenario.

Changes in forest at the country level also vary greatly across the SSP scenarios and countries. Based on the results, net gain in forest is demonstrated to occur mainly in China, Russian Federation, Canada, Brazil, and the United States. For instance, under the SSP1 scenario, China, Russian Federation, Canada, and United States collectively are responsible for 79.06% of the global net increase in forest area between 2020 and 2100. The largest net gain in forest area at the country level would occur in China with

the forest extent increasing by 1.07 million km^2 and 0.357 million km^2 under SSP1 and SSP4 respectively (Figure 6.5). The total forest extent of Canada and the Russian Federation would also increase by 0.59 million km^2 and 0.47 million km^2 correspondingly under the SSP1 scenario. On the contrary, hotspots of deforestation are revealed to be in the DRC, Angola, Tanzania, Cameroon, and Brazil. Based on the simulation results, there is a net forest loss of 1.53 million km^2 in the DRC under the SSP4 scenario and 0.65 million km^2 under SSP2 in Brazil. Across SSP3, SSP4, and SSP5, the DRC, Angola, Tanzania, and Cameroon would collectively contribute between 38.08% – 60.24% of the global net forest loss between 2020 and 2100. The DRC alone is revealed to contribute 20.82% - 32.18% of the global net forest loss across these three scenarios. The results also indicate countries in South America especially Brazil could be a source of net forest gain or loss based on scenario.

6.5. Discussions

This research study implements the multiclass DL-SGA model and examines the obtained results of possible future LULC changes under the different SSP scenarios at the global level. The performance of the model, measured by the AUC and *FoM* metrics indicate the proposed model can adequately capture the patterns of different LULC processes at the global level. Results from the studies are logical and consistent with other global LULC change simulations. For example, Li et al. (2019) and Li et al. (2021) estimated the global urban extent in the range of 1.5 million km^2 and 3.1 million km^2 in their studies, which is comparable to the urban growth trends obtained in this research study. Trends in cropland and forest cover changes are also similar with values from the SSP database, albeit exhibiting slight variations given this research applied a different base LULC dataset; the ESA LULC dataset (Estoque et al., 2020).

Variations in the SSP conditions lead to distinct patterns of LULC change at the various levels of analysis. The high urbanization rate under the SSP5 scenario can be attributed to the high levels of economic growth and technological progress across several regions. On the contrary, despite the relatively high population growth under SSP3 and SSP4, the low economic growth results in lower urbanization compared to the other scenarios. Urban growth occurs mainly at the expense of cropland notably in Africa and Asia. Urban expansion in Europe, North America and South America is however mainly from grassland. Under SSP2 for example, about 0.64 million km^2 of cropland,

twice the size of Italy would be converted into urban land-use in Africa and Asia collectively between 2020 and 2100. Globally, loss in the total cropland extent resulting from urban expansion could range between 2.84% to 6.61%. Future urban growth is thus expected to negatively affect food production and security especially in developing countries.

The extent of cropland increases under all scenarios with the largest change being under the SSP3 scenario. This is mainly driven by the burgeoning global population combined with low agricultural intensification especially in Africa. The increasing global population under SSP3 could be a contributing factor to the growing trend in cropland expansion and food demand at the global level between 2020 and 2100 (Popp et al., 2017). Under this scenario, cropland increase is very prominent in Africa, Asia, and South America. Cropland expansion in Africa alone amounts to 6.18 million km^2, corresponding to 68.32% of the global cropland expansion between 2020 and 2100 under the SSP3 scenario. Cropland increase is significantly lower under the SSP1 scenario due to the low demand for agricultural goods and high intensification of agricultural production across several regions of the world (Doelman et al., 2018).

Although cropland shows an increasing trend across all scenarios, analysis of gains and losses reveals the land-use type is highly variable. Sources of cropland expansion are mainly from forest and grassland across all regions. Increasing cropland and food production could thus have implications for deforestation and biodiversity loss across the globe. Loss of cropland mainly transitions into urban, grassland, and forest. Conversion of cropland into grassland and forest could indicate agricultural abandonment and regrowth of the natural vegetation. This process could also be explained by the implementation of afforestation policies to convert unproductive cropland into forest as seen in China's conversion of cropland into forest program (CCFP) (Gutiérrez Rodríguez et al., 2016).

Change in forest extent at the global level is the net result of deforestation in some regions and afforestation in others. For instance, under SSP1 and SSP2, rate of deforestation in Africa is offset by afforestation in Asia, Europe, and North America resulting in a net increase in the global forest extent. The global increase in forest coverage is most significant under the SSP1 scenario due to the low population growth, strong environmental and LULC regulations as well as regrowth of natural vegetation

from abandoned croplands. Although the global forest extent decreases under the other four scenarios, there is afforestation in some regions and countries in Asia, Europe, and North America especially under the SSP2 and SSP4. This can be partially ascribed to the control of land-use alteration in developed nations, particularly within the context of the SSP4 scenario. There is a net decrease in forest extent in Africa across all scenarios and this can be partly attributed to the weak regulation of LULC change in the region. Considering forest represent the largest terrestrial sink of carbon dioxide (CO_2) and a significant proportion of carbon stocks, changes in forest could greatly impact climate change and influence future mitigation policies and actions (Keenan & Williams, 2018). Already, international programs such as the Reducing Emissions from Deforestation and forest Degradation (REDD+) (Agrawal et al., 2011) have been established which focuses on sustainable management of forest and enhancement of forest carbon stocks.

6.6. Conclusions

This research study develops a novel multiclass DL-SGA model for simulating multiple LULC change processes. The modelling framework integrates multiple advancements, incorporating deep learning for generating transition rules, implementing the urban rank-size rule, and LULC conversion matrix. These refinements collectively address the different processes influencing various LULC types and their change dynamics on a global scale. The proposed model was implemented using a spherical spatial framework that accounts for the curvature of the Earth's surface and thus enables improvements to conventional global geosimulation models that often ignore the problem of spatial distortions in large scale spatial models. The use of conventional planer spatial models for global spatial analyses and simulations is demonstrated to produce different results. Also, in comparison to commonly utilized binary global geosimulation models that simulation only one type of LULC, the implemented model in this research study is designed to characterize the dynamics of different LULC types at the global level under the SSP scenarios.

Given the complexity of modelling multiple LULC types at the global scale and across a longer temporal interval, this research has some caveats and limitations. The proposed model can thus be improved to simulate LULC change at a finer resolution of hexagonal cells as well as inclusion of additional driver variables related to the modelled LULC types, depending on data availability. Considering the spatial heterogeneity in

LULC change across various regions, there is potential for enhancing the model through the integration of geospatial agent-based modelling (ABM) within the multiclass DL-SGA modelling framework. ABM can be incorporated to effectively represent and characterize diverse entities involved in the processes of LULC change across different spatial and temporal scales. Random effects can also be integrated into the modelling framework to capture inherent stochasticity and unpredictability associated with real-world land use changes. Incorporating random elements into future iterations of the model could enhance its ability to account for the dynamic and uncertain nature of LULC change. Also, due to computational limitations, only LULC change under the reference SSP marker scenarios were simulated in this research study. However, a comprehensive modelling of LULC change across all the multiple non-marker SSP scenarios can assist in exploring uncertainties in future LULC change across the five SSP scenarios. Further, the impact of climate and environmental change on future LULC change was not considered in this research.

The proposed multiclass DL-SGA model however provides a consistent modelling framework for simulating the different dynamics of multiple LULC types at the global level and can be utilized by intergovernmental entities, policy makers, researcher, and ecologist, for global environmental assessments and formulation of sustainable environmental policies especially related to climate change, biodiversity loss, and sustainable land-use planning.

6.7. References

Agrawal, A., Nepstad, D., & Chhatre, A. (2011). Reducing emissions from deforestation and forest degradation. *Annual Review of Environment and Resources, 36*(1), 373-396. doi:10.1146/annurev-environ-042009-094508

Artés, T., Oom, D., de Rigo, D., Durrant, T. H., Maianti, P., Libertà, G., & San-Miguel-Ayanz, J. (2019). A global wildfire dataset for the analysis of fire regimes and fire behaviour. *Scientific Data, 6*(1), 296. doi:10.1038/s41597-019-0312-2

Auerbach, F., & Ciccone, A. (2023). The law of population concentration. *Environment and Planning B: Urban Analytics and City Science, 50*(2), 290-298. doi:10.1177/23998083221147139

Ball, J. G. C., Petrova, K., Coomes, D. A., & Flaxman, S. (2022). Using deep convolutional neural networks to forecast spatial patterns of Amazonian deforestation. *Methods in Ecology and Evolution, 13*(11), 2622-2634. doi:10.1111/2041-210X.13953

Batty, M. (2013). *The new science of cities*: The MIT Press.

Berry, B. J. L. (1964). Cities as systems within systems of cities. *Papers of the Regional Science Association, 13*(1), 146-163. doi:10.1007/BF01942566

Camacho Olmedo, M. T., Mas, J.-F., & Paegelow, M. (2022). Validation of soft maps produced by a land use cover change model. In *Land use cover datasets and validation tools: Validation practices with QGIS*, (Eds.) D. García-Álvarez, M. T. Camacho Olmedo, M. Paegelow, & J. F. Mas,(pp. 189-203). Cham: Springer International Publishing.

Cao, B., Yu, L., Li, X., Chen, M., Li, X., Hao, P., & Gong, P. (2021). A 1km global cropland dataset from 10000 BCE to 2100 CE. *Earth Syst. Sci. Data, 13*(11), 5403-5421. doi:10.5194/essd-13-5403-2021

Cao, C., Dragićević, S., & Li, S. (2019). Short-term forecasting of land use change using recurrent neural network models. *Sustainability, 11*(19). doi:10.3390/su11195376

Chen, G., Li, X., & Liu, X. (2022). Global land projection based on plant functional types with a 1-km resolution under socio-climatic scenarios. *Scientific Data, 9*, 1-18. doi:10.1038/s41597-022-01208-6

Chen, J., Gao, M., Cheng, S., Hou, W., Song, M., Liu, X., & Liu, Y. (2022). Global 1 km × 1 km gridded revised real gross domestic product and electricity consumption during 1992–2019 based on calibrated nighttime light data. *Scientific Data, 9*(1), 202. doi:10.1038/s41597-022-01322-5

d'Annunzio, R., Sandker, M., Finegold, Y., & Min, Z. (2015). Projecting global forest area towards 2030. *Forest Ecology and Management, 352*, 124-133. doi:10.1016/j.foreco.2015.03.014

Dobson, J., Bright, E., Coleman, P., Durfee, R., & Worley, B. (2000). LandScan: A Global Population Database for Estimating Populations at Risk. *Photogrammetric Engineering and Remote Sensing, 66*, 849-857.

Doelman, J. C., Stehfest, E., Tabeau, A., van Meijl, H., Lassaletta, L., Gernaat, D. E. H. J., Hermans, K., Harmsen, M., Daioglou, V., Biemans, H., van der Sluis, S., & van Vuuren, D. P. (2018). Exploring SSP land-use dynamics using the IMAGE model: Regional and gridded scenarios of land-use change and land-based climate change mitigation. *Global Environmental Change, 48*, 119-135. doi:10.1016/j.gloenvcha.2017.11.014

Duranton, G., & Puga, D. (2014). The growth of cities. In *Handbook of Economic Growth*, (Eds.) P. Aghion & S. N. Durlauf,(Vol. 2, pp. 781-853): Elsevier.

Estoque, R. C., Ooba, M., Togawa, T., & Hijioka, Y. (2020). Projected land-use changes in the Shared Socioeconomic Pathways: Insights and implications. *Ambio, 49*(12), 1972-1981. doi:10.1007/s13280-020-01338-4

European Space Agency. (2022). *ESA CCI Land Cover map series 1992-2020*. Retrieved 15 November 2022 from: http://maps.elie.ucl.ac.be/CCI/viewer/index.php

Fick, S. E., & Hijmans, R. J. (2017). WorldClim 2: New 1-km spatial resolution climate surfaces for global land areas. *International Journal of Climatology, 37*(12), 4302-4315. doi:10.1002/joc.5086

Foley, J. A., DeFries, R., Asner, G. P., Barford, C., Bonan, G., Carpenter, S. R., Chapin, F. S., Coe, M. T., Daily, G. C., Gibbs, H. K., Helkowski, J. H., Holloway, T., Howard, E. A., Kucharik, C. J., Monfreda, C., Patz, J. A., Prentice, I. C., Ramankutty, N., & Snyder, P. K. (2005). Global consequences of land use. *Science, 309*(5734), 570-574. doi:10.1126/science.1111772

Gao, J., & O'Neill, B. C. (2019). Data-driven spatial modeling of global long-term urban land development: The SELECT model. *Environmental Modelling and Software, 119*, 458-471. doi:10.1016/j.envsoft.2019.06.015

Gao, J., & O'Neill, B. C. (2020). Mapping global urban land for the 21st century with data-driven simulations and Shared Socioeconomic Pathways. *Nature Communications, 11*(1), 1-12. doi:10.1038/s41467-020-15788-7

Gharaibeh, A. A., Shaamala, A. H., & Ali, M. H. (2020). Multi-criteria evaluation for sustainable urban growth in An-Nuayyimah, Jordan; post war study. *Procedia Manufacturing, 44*, 156-163. doi:10.1016/j.promfg.2020.02.217

Global Administrative Areas (GADM). (2023). *Database of Global Administrative Areas*. Retrieved May 10, 2023 from: https://gadm.org/

Glorot, X., Bordes, A., & Bengio, Y. (2011). *Deep Sparse Rectifier Neural Networks*. Paper presented at the Proceedings of the Fourteenth International Conference on Artificial Intelligence and Statistics, Proceedings of Machine Learning Research.

Goodchild, M. F. (2018). Reimagining the history of GIS. *Annals of GIS, 24*, 1-8. doi:10.1080/19475683.2018.1424737

Gutiérrez Rodríguez, L., Hogarth, N. J., Zhou, W., Xie, C., Zhang, K., & Putzel, L. (2016). China's conversion of cropland to forest program: a systematic review of the environmental and socioeconomic effects. *Environmental Evidence, 5*(1), 21. doi:10.1186/s13750-016-0071-x

Hall, J., Wecker, L., Ulmer, B., & Samavati, F. (2020). Disdyakis triacontahedron DGGS. *ISPRS International Journal of Geo-Information, 9*. doi:10.3390/ijgi9050315

Hanley, J. A., & McNeil, B. J. (1982). The meaning and use of the area under a receiver operating characteristic (ROC) curve. *Radiology, 143*(1), 29-36. doi:10.1148/radiology.143.1.7063747

He, J., Li, X., Yao, Y., Hong, Y., & Jinbao, Z. (2018). Mining transition rules of cellular automata for simulating urban expansion by using the deep learning techniques. *International Journal of Geographical Information Science, 32*(10), 2076-2097. doi:10.1080/13658816.2018.1480783

Hengl, T., Mendes de Jesus, J., Heuvelink, G. B. M., Ruiperez Gonzalez, M., Kilibarda, M., Blagotić, A., Shangguan, W., Wright, M. N., Geng, X., Bauer-Marschallinger, B., Guevara, M. A., Vargas, R., MacMillan, R. A., Batjes, N. H., Leenaars, J. G. B., Ribeiro, E., Wheeler, I., Mantel, S., & Kempen, B. (2017). SoilGrids250m: Global gridded soil information based on machine learning. *PLoS ONE, 12*(2), e0169748. doi:10.1371/journal.pone.0169748

Hu, X., Næss, J. S., Iordan, C. M., Huang, B., Zhao, W., & Cherubini, F. (2021). Recent global land cover dynamics and implications for soil erosion and carbon losses from deforestation. *Anthropocene, 34*, 100291. doi:10.1016/j.ancene.2021.100291

Intergovernmental Panel on Climate Change (IPCC). (2019). Summary for policymakers. In *Climate Change and Land: an IPCC special report on climate change, desertification, land degradation, sustainable land management, food security, and greenhouse gas fluxes in terrestrial ecosystems*, (Eds.) P. R. Shukla, J. Skea, E. Calvo Buendia, V. Masson-Delmotte, H. O. Pörtner, D. Roberts, P. Zhai, R. Slade, S. Connors, R. Van Diemen, M. Ferrat, E. Haughey, S. Luz, S. Neogi, M. Pathak, J. Petzold, J. Portugal Pereira, P. Vyas, E. Huntley, K. Kissick, M. Belkacemi, & J. Malley.

Jiang, B., Yin, J., & Liu, Q. (2015). Zipf's law for all the natural cities around the world. *International Journal of Geographical Information Science, 29*(3), 498-522. doi:10.1080/13658816.2014.988715

Keenan, T. F., & Williams, C. A. (2018). The terrestrial carbon sink. *Annual Review of Environment and Resources, 43*(1), 219-243. doi:10.1146/annurev-environ-102017-030204

Kelly, K., & Šavrič, B. (2021). Area and volume computation of longitude–latitude grids and three-dimensional meshes. *Transactions in GIS, 25*(1), 6-24. doi:10.1111/tgis.12636

Krugman, P. (1996). Confronting the Mystery of Urban Hierarchy. *Journal of the Japanese and International Economies, 10*(4), 399-418. doi:10.1006/jjie.1996.0023

Lambin, E. F., & Meyfroidt, P. (2011). Global land use change, economic globalization, and the looming land scarcity. *Proceedings of the National Academy of Sciences, 108*(9), 3465-3472. doi:10.1073/pnas.1100480108

174

Li, X., Chen, G., Liu, X., Liang, X., Wang, S., Chen, Y., Pei, F., & Xu, X. (2017). A new global Land-use and land-cover change product at a 1-km resolution for 2010 to 2100 based on human–environment interactions. *Annals of the American Association of Geographers, 107*, 1040-1059. doi:10.1080/24694452.2017.1303357

Li, X., Yu, L., Sohl, T., Clinton, N., Li, W., Zhu, Z., Liu, X., & Gong, P. (2016). A cellular automata downscaling based 1 km global land use datasets (2010–2100). *Science Bulletin, 61*, 1651-1661. doi:10.1007/s11434-016-1148-1

Li, X., Zhou, Y., Eom, J., Yu, S., & Asrar, G. (2019). Projecting global urban area growth through 2100 based on historical time series data and future shared socioeconomic pathways. *Earth's Future, 7*(4), 351-362. doi:10.1029/2019EF001152

Li, X., Zhou, Y., Hejazi, M., Wise, M., Vernon, C., Iyer, G., & Chen, W. (2021). Global urban growth between 1870 and 2100 from integrated high resolution mapped data and urban dynamic modeling. *Communications Earth & Environment, 2*(201), 1-10. doi:10.1038/s43247-021-00273-w

Liu, X., Liang, X., Li, X., Xu, X., Ou, J., Chen, Y., Li, S., Wang, S., & Pei, F. (2017). A future land use simulation model (FLUS) for simulating multiple land use scenarios by coupling human and natural effects. *Landscape and Urban Planning, 168*, 94-116. doi:10.1016/j.landurbplan.2017.09.019

Malek, Ž., Douw, B., Vliet, J. V., Zanden, E. H. V. D., & Verburg, P. H. (2019). Local land-use decision-making in a global context. *Environmental Research Letters, 14*.

Mas, J.-F., Soares Filho, B., Pontius, R. G., Farfán Gutiérrez, M., & Rodrigues, H. (2013). A suite of tools for ROC analysis of spatial models. *ISPRS International Journal of Geo-Information, 2*(3), 869-887. doi:10.3390/ijgi2030869

Meijer, J. R., Huijbregts, M. A. J., Schotten, K. C. G. J., & Schipper, A. M. (2018). Global patterns of current and future road infrastructure. *Environmental Research Letters, 13*(6). doi:10.1088/1748-9326/aabd42

Meiyappan, P., Dalton, M., O'Neill, B. C., & Jain, A. K. (2014). Spatial modeling of agricultural land use change at global scale. *Ecological Modelling, 291*, 152-174. doi:10.1016/j.ecolmodel.2014.07.027

Mithun, S., Sahana, M., Chattopadhyay, S., Chatterjee, S., Islam, J., & Costache, R. (2022). Comparative framework for spatially explicit urban growth modeling for monitoring urban land-use efficiency and sustainable urban development (SDG 11.3.1): a study on Kolkata metropolitan area, India. *Geocarto International, 37*(27), 17933-17970. doi:10.1080/10106049.2022.2136259

O'Neill, B. C., Carter, T. R., Ebi, K., Harrison, P. A., Kemp-Benedict, E., Kok, K., Kriegler, E., Preston, B. L., Riahi, K., Sillmann, J., van Ruijven, B. J., van Vuuren, D., Carlisle, D., Conde, C., Fuglestvedt, J., Green, C., Hasegawa, T., Leininger, J., Monteith, S., & Pichs-Madruga, R. (2020). Achievements and needs for the climate change scenario framework. *Nature Climate Change, 10*(12), 1074-1084. doi:10.1038/s41558-020-00952-0

O'Neill, B. C., Kriegler, E., Ebi, K. L., Kemp-Benedict, E., Riahi, K., Rothman, D. S., van Ruijven, B. J., van Vuuren, D. P., Birkmann, J., Kok, K., Levy, M., & Solecki, W. (2017). The roads ahead: narratives for shared socioeconomic pathways describing world futures in the 21st century. *Global Environmental Change, 42*, 169-180. doi:10.1016/j.gloenvcha.2015.01.004

O'Neill, B. C., Kriegler, E., Riahi, K., Ebi, K. L., Hallegatte, S., Carter, T. R., Mathur, R., & van Vuuren, D. P. (2014). A new scenario framework for climate change research: the concept of shared socioeconomic pathways. *Climatic Change, 122*(3), 387-400. doi:10.1007/s10584-013-0905-2

Paegelow, M. (2018). LUCC based validation indices: figure of merit, producer's accuracy and user's accuracy. In *Geomatic approaches for modeling land change scenarios*, (Eds.) M. T. Camacho Olmedo, M. Paegelow, J.-F. Mas, & F. Escobar,(pp. 433-436). Cham: Springer International Publishing.

Paszke, A., Gross, S., Massa, F., Lerer, A., Bradbury, J., Chanan, G., Killeen, T., Lin, Z., Gimelshein, N., Antiga, L., Desmaison, A., Köpf, A., Yang, E., DeVito, Z., Raison, M., Tejani, A., Chilamkurthy, S., Steiner, B., Fang, L., Bai, J., & Chintala, S. (2019). PyTorch: an imperative style, high-performance deep learning library. In *Proceedings of the 33rd International Conference on Neural Information Processing Systems*, pp. Article 721): Curran Associates Inc.

Pontius, R. G., Boersma, W., Castella, J.-C., Clarke, K., de Nijs, T., Dietzel, C., Duan, Z., Fotsing, E., Goldstein, N., Kok, K., Koomen, E., Lippitt, C. D., McConnell, W., Mohd Sood, A., Pijanowski, B., Pithadia, S., Sweeney, S., Trung, T. N., Veldkamp, A. T., & Verburg, P. H. (2008). Comparing the input, output, and validation maps for several models of land change. *The Annals of Regional Science, 42*(1), 11-37. doi:10.1007/s00168-007-0138-2

Popp, A., Calvin, K., Fujimori, S., Havlik, P., Humpenöder, F., Stehfest, E., Bodirsky, B. L., Dietrich, J. P., Doelmann, J. C., Gusti, M., Hasegawa, T., Kyle, P., Obersteiner, M., Tabeau, A., Takahashi, K., Valin, H., Waldhoff, S., Weindl, I., Wise, M., Kriegler, E., Lotze-Campen, H., Fricko, O., Riahi, K., & van Vuuren, D. P. (2017). Land-use futures in the shared socio-economic pathways. *Global Environmental Change, 42*, 331-345.

Riahi, K., van Vuuren, D. P., Kriegler, E., Edmonds, J., O'Neill, B. C., Fujimori, S., Bauer, N., Calvin, K., Dellink, R., Fricko, O., Lutz, W., Popp, A., Cuaresma, J. C., Samir, K. C., Leimbach, M., Jiang, L., Kram, T., Rao, S., Emmerling, J., Ebi, K., Hasegawa, T., Havlik, P., Humpenöder, F., Silva, L. A. D., Smith, S., Stehfest, E., Bosetti, V., Eom, J., Gernaat, D., Masui, T., Rogelj, J., Strefler, J., Drouet, L., Krey, V., Luderer, G., Harmsen, M., Takahashi, K., Baumstark, L., Doelman, J. C., Kainuma, M., Klimont, Z., Marangoni, G., Lotze-Campen, H., Obersteiner, M., Tabeau, A., & Tavoni, M. (2017). The shared socioeconomic pathways and their energy, land use, and greenhouse gas emissions implications: an overview. *Global Environmental Change, 42*, 153-168.

Rimal, B., Zhang, L., Keshtkar, H., Haack, B. N., Rijal, S., & Zhang, P. (2018). Land use/land cover dynamics and modeling of urban land expansion by the integration of cellular automata and markov chain. *ISPRS International Journal of Geo-Information, 7*(4). doi:10.3390/ijgi7040154

Robertson, C., Chaudhuri, C., Hojati, M., & Roberts, S. A. (2020). An integrated environmental analytics system (IDEAS) based on a DGGS. *ISPRS Journal of Photogrammetry and Remote Sensing, 162*, 214-228. doi:10.1016/j.isprsjprs.2020.02.009

Sahr, K. (2011). Hexagonal discrete global GRID systems for geospatial computing. *Archives of Photogrammetry, Cartography and Remote Sensing, 22*, 363-376.

Sahr, K. (2022). DGGRID version 7.5. Retrieved March 2023 from https://github.com/sahrk/DGGRID

Shu, B., Zhu, S., Qu, Y., Zhang, H., Li, X., & Carsjens, G. J. (2020). Modelling multi-regional urban growth with multilevel logistic cellular automata. *Computers, Environment and Urban Systems, 80*. doi:10.1016/j.compenvurbsys.2019.101457

Sims, K., Reith, A., Bright, E., McKee, J., & Rose, A. (2022). *LandScan Global 2021* [raster digital data]. Retrieved from: landscan.ornl.gov

Soo, K. T. (2005). Zipf's Law for cities: a cross-country investigation. *Regional Science and Urban Economics, 35*(3), 239-263. doi:10.1016/j.regsciurbeco.2004.04.004

The World Bank. (2023). *Gross Dometic Product*. Retrieved May 10, 2023 from: https://databank.worldbank.org/

Torrens, P. M., & O'Sullivan, D. (2001). Cellular automata and urban simulation: where do we go from here? *Environment and Planning B: Planning and Design, 28*, 163-168. doi:10.1068/b2802ed

Turner, B. L., Lambin, E. F., & Verburg, P. H. (2021). From land-use/land-cover to land system science. *Ambio, 50*(7), 1291-1294. doi:10.1007/s13280-021-01510-4

United Nations - Department of Economic and Social Affairs: Population Division. (2023). *World Population Prospects 2022*. Retrieved 9 June 2023 from: https://population.un.org/wpp/

United State Geological Survey. (2022). *USGS EROS Archive - Digital elevation - shuttle radar topography mission (SRTM) 1 arc-second global*. Retrieved August 2020 from: https://www.usgs.gov/centers/eros/science/usgs-eros-archive-digital-elevation-shuttle-radar-topography-mission-srtm-1-arc?qt-science_center_objects=0#qt-science_center_objects

Van Rossum, G., & Drake, F. (2009). Python 3 Reference Manual. Scotts Valley, CA: CreateSpace. Retrieved from https://www.python.org/

Veneri, P. (2016). City size distribution across the OECD: does the definition of cities matter? *Computers, Environment and Urban Systems, 59*, 86-94. doi:10.1016/j.compenvurbsys.2016.05.007

Verburg, P. H., Dearing, J. A., Dyke, J. G., Leeuw, S. v. d., Seitzinger, S., Steffen, W., & Syvitski, J. (2016). Methods and approaches to modelling the Anthropocene. *Global Environmental Change, 39*, 328-340. doi:10.1016/j.gloenvcha.2015.08.007

Wang, J., Yin, X., Liu, S., & Wang, D. (2023). Spatiotemporal change and prediction of land use in Manasi region based on deep learning. *Environmental Science and Pollution Research, 30*(34), 82780-82794. doi:10.1007/s11356-023-27826-0

Wang, Y., Wei, Y. D., & Sun, B. (2022). New economy and national city size distribution. *Habitat International, 127*, 102632. doi:10.1016/j.habitatint.2022.102632

Winkler, K., Fuchs, R., Rounsevell, M., & Herold, M. (2021). Global land use changes are four times greater than previously estimated. *Nature Communications, 12*(1), 1-10. doi:10.1038/s41467-021-22702-2

World Database on Protected Areas. (2023). *Global database on terrestrial and marine protected areas*. Retrieved 4 March 2020 from: https://www.protectedplanet.net/en/search-areas?filters%5Bdb_type%5D%5B%5D=wdpa&geo_type=region

Xiao, B., Liu, J., Jiao, J., Li, Y., Liu, X., & Zhu, W. (2022). Modeling dynamic land use changes in the eastern portion of the hexi corridor, China by cnn-gru hybrid model. *GIScience & Remote Sensing, 59*(1), 501-519. doi:10.1080/15481603.2022.2037888

Ye, L., Gao, L., Marcos-Martinez, R., Mallants, D., & Bryan, B. A. (2019). Projecting Australia's forest cover dynamics and exploring influential factors using deep learning. *Environmental Modelling & Software, 119*, 407-417. doi:10.1016/j.envsoft.2019.07.013

Zhou, J., Ben, J., Wang, R., Zheng, M., & Du, L. (2020). Lattice quad-tree indexing algorithm for a hexagonal discrete global grid system. *ISPRS International Journal of Geo-Information, 9*(2), 83. doi:10.3390/ijgi9020083

Zipf, G. K. (1949). *Human behavior and the principle of least effort: an introduction to human ecology*. Cambridge: Addison-Wesley.

Chapter 7.

Conclusions

7.1. General Conclusions

Land systems constitute the terrestrial component of the Earth system and comprise all processes and activities associated with the human use of land. LULC changes are results of human interaction with the natural environment and therefore are often characterized as complex systems, leading to the utilization of geographic automata modelling approaches to represent and simulate their spatio-temporal dynamics. While these methodologies have proven successful in simulating diverse complex spatial systems at the local level and smaller spatial extents, they are considered unsuitable for global applications. Existing geographic automata approaches are based on two-dimensional planar spatial models that neglect the spherical and curved properties of the Earth and are inadequate to represent geospatial dynamic phenomena at the global scale. For these reasons this dissertation research extends the concepts of planar geosimulation methods to operate on a spherical surface.

The spherical geographic automata approaches proposed and developed in this research study are successfully applied to represent different complex spatial systems at the global level and under diverse possible future scenarios. The proposed suite of modelling approaches is well-suited for characterizing and simulating LULC change processes operating at the global level such as urbanization and deforestation. This research also represents a departure from the use of traditional two-dimensional planar GIS to a spherical spatial framework, that is more appropriate for global applications. Furthermore, the methodology offers a foundational framework for further development of advanced spatio-temporal modelling techniques and analysis of processes on a spherical surface.

7.2. Summary of Findings

The proposed methodology utilizes the theory of complex systems, geographic automata, and spherical geodesic grid for the representation, conceptualization, and

analysis of complex spatial systems on a spherical surface. In Chapter 2, an overview of spherical geodesic grids is presented as well as comparison with existing traditional spatial reference systems. The chapter also proposes, designs, and implements the spherical geographic automata (SGA) modelling approach, by integrating the techniques of geographic automata and spherical geodesic grid for representing complex spatial systems on curved surfaces. The approach also departs from the classical square grid cellular space commonly used in geosimulation applications by utilizing a hexagonal spatial tessellation. The developed approach is general and adaptable, allowing its application for representing and analysing various real-world complex systems, such as social-economic, ecological, and biogeographical. Comparative analysis with planar models indicates that spherical geodesic grids provide a more accurate representation of geographic features at the global level. Conversely, traditional geospatial models demonstrate different forms of spatial distortions when used for applications with global coverage. The research revealed that the use of traditional spatial models to represent global datasets could result in overestimation of the total global urban extent by almost 20%. This findings reinforces the potential implications of using traditional raster based spatial models for global applications. In this chapter, the SGA model is applied as proof-of-concept to characterize different complex spatial processes including population change dynamics, global urban expansion, and global deforestation at a courser spatial scales with hexagonal cell size of 287 km^2. The application of the Game of Life global population model indicates an overall trend of population growth while maintaining equilibrium between the proportions of alive cell types. Simulation results obtained from the global urban growth model also indicate the global urban extent could increase by 77% and 118% under the Stalled Development and Sustainable Development scenarios respectively. Further, the deforestation model indicates the global forest cover to shrink by 38% between 2020 and 2100. Successful implementations of the proposed methodology in the three case studies indicate the proposed SGA methodology can be utilized to characterize and simulate different real-world complex spatial systems at the global level. Nonetheless, the used hexagonal spatial tessellation were course and the more refined spatial resolutions have been used for developed models in subsequent chapters.

In chapter 3, the SGA model is implemented with the use of real-world geospatial datasets to simulate the spatial processes of global urban land-use change across 235

countries with improved model parameters between 2015 and 2095 with each hexagon encompassing an area of 4.5 km^2. The SGA framework design is capable of representing different "what-if' scenarios and the global urban land-use change model application reveals the approach can be applied to represent different possible future urban land-use change conditions. Obtained simulation results from the model also indicate the proposed SGA approach can be utilized to capture the growth and dynamics of urban regions across different regions at the global scale. Based on the model outputs, the rate and magnitude of urban growth is extensive in Africa and Asia with these two continents together contributing between 65% to 68% of new urban development at the global level under the two scenarios. In some regions in Africa, the rate of urbanization would be as high as 600% across the constant fertility scenario. Cities in Africa and Asia therefore present several challenges and opportunities for achieving global sustainable goals. Evaluation of results from the proposed model and a traditional raster-based planar CA model with the same model parameters indicates the SGA model performs better than the conventional geosimulation modelling approach in simulating urban growth dynamics. The Figure of Merit (*FoM*) metric obtained for the proposed SGA model during the calibration and validation phases was 7.1% and 10.2% higher, respectively, compared to the planar CA model.

Chapters 4 and 5 extend the SGA model to incorporate the multi-criteria evaluation (MCE) technique, and the MCE-SGA model is implemented to characterize two real-world complex spatial processes. The MCE technique is integrated to enable a systematic approach to decision-making, while also incorporating the inherent complexity and multiplicity of land-use planning. This is achieved by taking into account input from diverse stakeholders associated with the choice of criteria and wights related to the factors influencing the LULC change. It must however be noted that, given the global scope of the model application and limited resources, in this dissertation research, opinions of stakeholders were not incorporated in the two MCE-SGA model applications. Instead, a statistical method was applied to obtain the weight of importance for each criterion. In chapter 4, the model is implemented to simulate the spatial processes of urbanization at the global level and at a finer spatial scale, utilizing hexagonal cells encompassing an area of 0.63 km^2. Findings from the global urban land-use change model implementation indicate the inclusion of the MCE component in the modelling framework improves the model's capability for simulating LULC changes. Also, the

spatial pattern and dynamics of urban growth varies across sub-region clusters, revealing the difference in the urbanization process across the globe. The simulation results reveal 64% of the total global urban expansion is anticipated to occur in urban region clusters characterized by high economic development and population density, while cities in isolated locations would have relatively lower rates of urban development. This underscores the significance of major cities with substantial economic resources in the future development of urban areas and in the context of global urbanization. Furthermore, 84.4% of the total global urban extent would be in cities located in low lying coastal areas and along major water bodies. Considering their location, these cities are particularly vulnerable to the potential impacts of possible extreme climate change events such as flooding, erosion, rising sea levels, and saltwater intrusion.

The second model application, presented in Chapter 5 simulates global forest land-cover change under three scenarios: business-as-usual, accelerated deforestation, and sustainable deforestation scenario. The obtained results and model evaluation metric indicate the MCE-SGA approach was able to appropriately capture the dynamics of deforestation while also considering diverse conservation strategies. Results from the model reveal the extent of global deforestation between 2020 and 2100 ranges between 1.8 million km^2 and 7.3 million km^2 based on different forest conversation scenarios. The simulation outputs additionally indicated that the rate of deforestation in protected areas was significantly less than the overall rate of forest cover change across all scenarios.

Chapter 6 of the dissertation focuses on the enhancement of the already developed MCE-SGA modelling framework to be capable of characterizing multiple complex spatial processes related to different LULC change types considered as part of overall change process. A deep learning model is also incorporated into the modelling framework to better capture the relationship between the change processes and their driving factors. The model is implemented to simulate LULC change across the five shared socioeconomic pathways (SSP) scenarios in the period between 2020 and 2100. The SSP comprises of five scenarios outlining future socio-economic development and challenges to climate change mitigation and adaptation based on a consistent set of assumptions. The five scenarios are labelled as follows: SSP1- Sustainability, taking the green road; SSP2- Middle of the road (business as usual); SSP3- Regional rivalry, a rocky road; SSP4- Inequality, a road divided; and SSP5- Fossil-fuelled development, taking the highway. Obtained simulation results reveal varying rates and extent of LULC

change under the different scenarios and regions. Under all five SSP scenarios, there is a notable expansion of cropland at the global level, with the most significant changes occurring in Africa and Asia and under the SSP3 scenario. This can partially be attributed to the increasing population coupled with limited agricultural intensification in parts of Africa and Asia. The largest rate of urbanization would occur under the SSP5 scenarios while SSP3 would have the least change in urban extent. Future urban development would have negative consequences for food production, particularly in developing countries, with cropland being the primary contributor to urban growth. The results also reveal a net loss of forest (deforestation) under SSP3, SSP4, and SSP5 while afforestation would occur under the SSP1 and SSP2 scenarios. Extensive deforestation rates are projected for Africa, while afforestation is anticipated predominantly in Asia, Europe, and North America. The successful implementation of the multi-LULC change SGA modelling framework demonstrates the model's capability for representing different LULC change processes and interaction at the global level. This enhanced multi-LULC change SGA modelling approach can therefore be useful for exploring wider varieties of LULC change processes and scenarios at the global level with potential application in policy formulation and environmental assessment.

7.3. Addressing Limitations of the Current Work and Linking with Future Research Directions

Despite the obtained results demonstrating the model's capabilities in simulating LULC change processes, there are some limitations to the developed approach. Advancements in the model could be achieved through the integration of finer hexagonal resolution and high-quality global datasets, enabling a more detailed simulation of LULC change. Improvement of the model could also involve incorporating a broader array of relevant criteria related to ecological, socioeconomic, and climatic factors. For instance, more detailed data can be used to represent and characterize different LULC types such high-rise, mid-rise, and low-rise urban areas, or different forest classifications. By incorporating a more comprehensive set of variables, the model could better capture the complexities of LULC change processes, thereby offering a better representation of the dynamics of land systems at the global scale. Advancement in remote sensing has led to increased availability of geospatial datasets with global coverage (Zhu et al., 2022), providing the opportunity to incorporate diverse datasets into the modelling framework.

Such improvements would however require leveraging high-performance computing (HPC) facilities, given the increased computational demands associated with enhanced spatial resolution of hexagons, increased datasets, and complexity inherent in the modelled system.

Furthermore, the proposed suite of SGA models does not consider the potential impacts of human-induced changes such as potential expansion of transportation infrastructure that would entail increased economic activities among urban regions and port cities, and a variety of environmental changes including wildfires, climate change and possible sea level rise. The consideration of such events in the model is however contingent on the availability of datasets to represent these factors as well as interdisciplinary research with other related fields such as environmental and climate sciences. However, the flexibility of the proposed SGA models means the framework can be easily extended to characterize these mechanisms, thereby rendering them endogenous to the model. Future works would focus on advancing the modelling approach to properly represent and account for factors stemming from human and environment interactions that influence LULC change at the global level.

The results of the proposed models may be influenced by a range of errors and uncertainties stemming from both data sources and model components. Data source errors encompass LULC type misclassifications, data transformation, and topological inaccuracies. Additionally, uncertainties emanate from various aspects of the CA model parameters such as choice of neighbourhood type and size, spatial and temporal resolutions, and choice of the transition rules. Other model components such as MCE criteria and weights, DL hyperparameters, LULC conversion weights, and Zipf's law coefficient also contribute to uncertainty. While Chapter 3 of the dissertation delves into aspects of model sensitivity and uncertainty, there is a need for a more comprehensive analysis of model sensitivity which involves the identification and quantification of model uncertainty. This expanded analysis would encompass a broader spectrum of model parameters, including but not limited to transition rules, hexagonal neighborhood configuration, randomization, and stochasticity, as well as use of different spatial and temporal resolution. A crucial aspect to also prioritize is addressing uncertainly arising from simulated model outputs especially across multiple scenarios. However, this endeavour could be a dissertation per se, considering the complexity of geosimulation procedure and the model itself, as well as long computational time required to run only

one full simulation that included all iterations (Crooks et al., 2008; Kang et al., 2022; Ligmann-Zielinska & Jankowski, 2014). To statistically evaluate the model with random effects, a minimum of 30 simulation runs would be necessary. However, due to the extensive computational time required, particularly given the size of the dataset and the global scale of the research study, this poses a significant challenge. By addressing these aspects of sensitivity and uncertainty, the proposed suite of models could offer a better understanding of the proposed models' capabilities and limitations. This, in turn, could enhance utility and applicability of the proposed models.

Additionally, the proposed modelling framework can be enhanced by incorporating human decision-making mechanisms. This presents the opportunity to incorporate geospatial agent-based modelling (ABM) into the proposed modelling framework for representing the spatial heterogeneity of diverse entities involved in the processes of LULC change at different spatial and temporal scales. Changes in land-use and land-cover are often the outcome of decisions of individuals and collective entities in response to their socio-economic and natural environment. Thus, the integration of agent-based modelling approaches into the proposed model could be very beneficial especially for representing spatial heterogeneity of land systems and specifics of different regions on the globe (An et al., 2023; Vaz, 2016). This would also allow for improved characterization of different environmental and socio-economic policies implemented in different land systems across different regions as well as response of different decision-making processes and entities. Agent-based models have been applied for LULC change simulations for specific case studies especially at very local levels. However, global scale LULC change models do not yet incorporate explicit human decision-making and are largely based on economic theories and biophysical suitability-based assumptions, which limits their realism (Turner et al., 2021). Such an approach would however require the adoption of a data driven geosimulation methodology and increased computational power (Ravaioli et al., 2023; Venkatramanan et al., 2018).

7.4. Research Contributions

In general, this study contributes to the representation, modelling, analysis, and visualization of LULC change processes at the global level. The research builds on conventional geosimulation modelling approaches by integrating geographic automata

and spherical spatial models with hexagonal spatial tessellation to develop a novel modelling framework, termed spherical geographic automata (SGA) for characterizing different spatio-temporal processes. The developed suite of modelling approaches is implemented to represent different LULC change processes in this dissertation to demonstrate the capabilities of the proposed models in characterizing and analyzing spatial dynamic systems operating on spherical Earth surface. This new modelling approaches provide an appropriate modelling framework that can be extended to represent other complex systems at the global level such as ecological, socio-economic, and epidemiological systems.

Specifically, the research dissertation contributes to the field of Geographic Information Science (GIScience) and extends existing methodological approaches in geographic automata systems by proposing and implementing a suite of novel spherical modelling approaches for simulating complex dynamic spatial systems at the global level. The developed SGA modelling approaches are designed to leverage the capabilities of geographic automata in characterizing the spatial and temporal dynamics of complex systems and spherical geodesic grids in representing geographic features on a sphere. Unlike conventional geosimulation models which are based on planar spatial models, the SGA modelling approach adopts a spherical spatial model to appropriately represent geographic features at the global scale and considering the curvature of the Earth's surface. The SGA modelling approach thus focuses on the representation, simulation, and analysis of complex spatial systems on a curved surface.

The SGA approaches contribute to longstanding research endeavours aimed at developing new spatial frameworks that effectively capture the curved surface of the Earth and addressing the limitations of traditional two-dimensional models used in GIS dating back to the works of Dutton (1984) and Tobler and Chen (1986) in the mid 80's. Despite progress in this research direction including research works by scholars such as Kimerling et al. (1999), Sahr et al. (2003), Chrisman (2017), and Goodchild (2018) studies in the field of spherical GIS have mainly focused on theoretical and grid design specifications with limited abilities to incorporate real data and operationalize for practical applications (Hojati et al., 2022). The proposed SGA modelling approaches also provide an alternative geosimulation model with a distinct cell typology, suitable for applications that require the properties of hexagonal tessellation.

In addition, this dissertation contributes to the field of Land Use Science and methodological approaches for LULC change modelling through the advancement and development of new techniques for characterizing and simulating the dynamics of LULC change over large spatial extents and long time periods. This capability allows for a thorough understanding, quantification, and projection of changes in various land-use change processes at the global level. The proposed suite of SGA models is adept in identifying hot/cold spots and spatial patterns related to LULC change, particularly in the contexts of urbanization, agricultural intensification, and deforestation. Analyzing the outcomes of these models across diverse regions contributes to a comprehensive understanding of global patterns and variations in LULC change. The modelling approach proposed in this research is flexible and can be parametrized for different case studies as well as accommodating for diverse "what-if" scenarios to characterize different complex system conditions. This flexibility enables for the construction of plausible and coherent narratives about potential LULC future conditions based on different assumptions and driving forces. The models offer a systematic approach for exploring a range of plausible futures to understand the implications of different scenarios including the pathways of socio-economic development. The proposed methodology can be used as a tool for global spatial decision making by different stakeholders in land-use science and related field of environmental science such as intergovernmental agencies for global policy development, planning, conservation, and environmental assessment.

Last but not least, this thesis research contributes to wider research endeavours that utilize simulated outcomes from global LULC change models as input data for modelling including integrated assessment models and Earth System models, employed in the fields of climate modelling and environmental conservation. Besides its application in the field of land-use science, the modelling framework is flexible and can be adapted to characterize different complex spatial systems and processes including global ecological, socio-economic, biogeographical, and epidemiological systems.

7.5. References

An, L., Grimm, V., Bai, Y., Sullivan, A., Turner, B. L., Malleson, N., Heppenstall, A., Vincenot, C., Robinson, D., Ye, X., Liu, J., Lindkvist, E., & Tang, W. (2023). Modeling agent decision and behavior in the light of data science and artificial intelligence. *Environmental Modelling & Software, 166*, 105713. doi:10.1016/j.envsoft.2023.105713

Chrisman, N. R. (2017). Calculating on a round planet. *International Journal of Geographical Information Science, 31*(4), 637-657. doi:10.1080/13658816.2016.1215466

Crooks, A., Castle, C., & Batty, M. (2008). Key challenges in agent-based modelling for geo-spatial simulation. *Computers, Environment and Urban Systems, 32*, 417-430. doi:10.1016/j.compenvurbsys.2008.09.004

Dutton, G. (1984). Geodesic modelling of planetary relief. *Cartographica: Int. J. Geogr. Inf. Geovisualization, 21*(2-3), 188-207. doi:10.3138/R613-191U-7255-082N

Goodchild, M. F. (2018). Reimagining the history of GIS. *Annals of GIS, 24*, 1-8. doi:10.1080/19475683.2018.1424737

Hojati, M., Robertson, C., Roberts, S., & Chaudhuri, C. (2022). GIScience research challenges for realizing discrete global grid systems as a Digital Earth. *Big Earth Data, 6*(3), 358-379. doi:10.1080/20964471.2021.2012912

Kang, J.-Y., Michels, A., Crooks, A., Aldstadt, J., & Wang, S. (2022). An integrated framework of global sensitivity analysis and calibration for spatially explicit agent-based models. *Transactions in GIS, 26*(1), 100-128. doi:10.1111/tgis.12837

Kimerling, J. A., Sahr, K., White, D., & Song, L. (1999). Comparing geometrical properties of global grids. *Cartography and Geographic Information Science, 26*(4), 271-288. doi:10.1559/152304099782294186

Ligmann-Zielinska, A., & Jankowski, P. (2014). Spatially-explicit integrated uncertainty and sensitivity analysis of criteria weights in multicriteria land suitability evaluation. *Environmental Modelling and Software, 57*(2014), 235-247. doi:10.1016/j.envsoft.2014.03.007

Ravaioli, G., Domingos, T., & Teixeira, R. F. M. (2023). A framework for data-driven agent-based modelling of agricultural land use. *Land, 12*(4). doi:10.3390/land12040756

Sahr, K., White, D., & Kimerling, A. J. (2003). Geodesic discrete global grid systems. *Cartography and Geographic Information Science, 30*, 121-134. doi:10.1559/152304003100011090

Tobler, W., & Chen, Z.-t. (1986). A quadtree for global information storage. *Geographical Analysis, 18*(4), 360-371. doi:10.1111/j.1538-4632.1986.tb00108.x

Turner, B. L., Lambin, E. F., & Verburg, P. H. (2021). From land-use/land-cover to land system science. *Ambio, 50*(7), 1291-1294. doi:10.1007/s13280-021-01510-4

Vaz, E. (2016). The future of landscapes and habitats: The regional science contribution to the understanding of geographical space. *Habitat International, 51*, 70-78. doi:10.1016/j.habitatint.2015.10.004

Venkatramanan, S., Lewis, B., Chen, J., Higdon, D., Vullikanti, A., & Marathe, M. (2018). Using data-driven agent-based models for forecasting emerging infectious diseases. *Epidemics, 22*, 43-49. doi:10.1016/j.epidem.2017.02.010

Zhu, Z., Qiu, S., & Ye, S. (2022). Remote sensing of land change: A multifaceted perspective. *Remote Sensing of Environment, 282*, 113266. doi:doi.org/10.1016/j.rse.2022.113266